UNIVERSITÉ DE GRENOBLE

THÈSE

Pour obtenir le grade de

DOCTEUR DE L'UNIVERSITÉ DE GRENOBLE

Spécialité : **Physique de la matière condensée et du rayonnement**

Arrêté ministériel : 7 août 2006

Présentée par

Daniel HERNANGÓMEZ PÉREZ

Thèse dirigée par **Thierry CHAMPEL**

préparée au sein du **Laboratoire de Physique et Modélisation des Milieux Condensés (CNRS / Université Joseph Fourier - Grenoble 1)** et dans l'**École Doctorale de Physique de Grenoble**

Spin-Orbit Coupling and Strong Interactions in the Quantum Hall Regime

Thèse soutenue publiquement le **20 novembre 2014**,
devant le jury composé de :

M. Mark Oliver GOERBIG
Chargé de recherche, Laboratoire de Physique des Solides (CNRS / Université Paris Sud XI), Rapporteur

M. Stéphane NONNENMACHER
Ingénieur-Chercheur, Institut de Physique Théorique, (CEA Saclay), Rapporteur

M. Benoît DOUÇOT
Directeur de recherche, Laboratoire de Physique Théorique et Hautes Énergies (CNRS / Université Pierre et Marie Curie - Paris VI), Examinateur

M. Markus MORGENSTERN
Professeur des Universités, II. Physikalisches Institut B, RWTH Aachen (Germany), Examinateur

M. Sergey SKIPETROV
Directeur de recherche, Laboratoire de Physique et Modélisation des Milieux Condensés, Examinateur

Mme. Julia MEYER
Professeur des Universités, Université Joseph Fourier - Grenoble 1, Présidente

M. Serge FLORENS
Chargé de recherche, Institut Néel (CNRS / Université Joseph Fourier - Grenoble 1), Co-Encadrant

M. Thierry CHAMPEL
Chargé de recherche, Laboratoire de Physique et Modélisation des Milieux Condensés, Directeur de thèse

Dédicace

A María, mi Sambo Sol.

Ora tutto è a posto.

La vie me surprend chaque jour.

Contents

General Introduction IX

I Rashba Spin-Orbit Coupling in the Integer Quantum Hall Regime 1

1. The Integer Quantum Hall Effect 3
1.1. Phenomenology . . . 3
1.1.1. (Non-relativistic) integer quantum Hall effect . . . 3
1.1.2. Relativistic integer quantum Hall effect . . . 6
1.1.3. Two-dimensional electron gases . . . 7
1.2. Classical Hall Effect . . . 10
1.3. Landau Levels . . . 12
1.3.1. Non-relativistic Landau levels . . . 12
1.3.2. Relativistic Landau levels . . . 16
1.4. Drift Effects in a Disorder Potential . . . 17
1.4.1. Edge states . . . 17
1.4.2. Bulk states . . . 19
1.5. Vortex Theory of the Integer Quantum Hall Effect . . . 24
1.5.1. Vortex states . . . 24
1.5.2. The gradient expansion . . . 27
1.5.3. Mixed phase-space formulation at high magnetic fields . . . 30
1.5.4. General solution for closed and open quantum systems . . . 31

2. Rashba Spin-Orbit Interaction in Two-Dimensional Electron Gases 35
2.1. Why Consider Spin-Orbit Interaction? . . . 35
2.2. Rashba Spin-Orbit Coupling in Low Dimensional Semiconductors . . . 36
2.2.1. Physical origin of the spin-orbit interaction . . . 36
2.2.2. Rashba and Dresselhaus Hamiltonians . . . 38
2.2.3. Rashba spin-orbit interaction in two-dimensional electron gases under perpendicular magnetic fields . . . 43
2.3. Spin Dynamics in Spin-Orbit Coupled Systems . . . 47
2.3.1. Spin Hall effect . . . 47
2.3.2. Spin Hall effect in a two-dimensional electron gas in the presence of perpendicular magnetic fields . . . 50

3. Local Spectral Properties in Generalized Disordered Potential Landscapes 53
3.1. Motivation . . . 54
3.2. Spin-Orbit Vortex States . . . 55
3.3. Green's Function Formalism . . . 59
3.3.1. Disorder and fluctuations of the spin-orbit interaction . . . 59
3.3.2. Dyson equation in the spin-orbit vortex representation . . . 60
3.3.3. Reduced matrix elements of the generalized disorder potential . . . 62
3.4. Energy Spectrum in Locally Flat Generalized Potentials . . . 64
3.4.1. Projection into a single Rashba-Landau energy level . . . 64
3.4.2. Quantum spin-orbit drift states . . . 65
3.4.3. Interplay between disorder and spin-orbit fluctuations . . . 66
3.5. Local Density of States . . . 70
3.5.1. General formula in locally flat disorder potentials . . . 70
3.5.2. Approximation for potentials smooth on the cyclotron radius . . . 72
3.5.3. Interpretation of STS experiments in InSb surface gases . . . 73

4. High-Field Local Equilibrium Properties 77
4.1. Motivation . . . 78
4.2. Spin-Orbit Vortex Green's Functions at High Magnetic Fields . . . 79
4.2.1. The high magnetic field expansion . . . 79
4.2.2. Discussion of the high-field expansion . . . 81
4.3. Electron Density and Spin Polarization . . . 82
4.3.1. Quantum expression . . . 82
4.3.2. Semiclassical expression . . . 84
4.3.3. Analysis of the functionals for a one-dimensional parabolic confinement model . . . 85
4.4. Electron Current Density . . . 87
4.4.1. General expression . . . 87
4.4.2. Density-gradient current . . . 89
4.4.3. Drift current . . . 91
4.5. Transport Properties . . . 93
4.5.1. Local Hall conductivity . . . 93
4.5.2. Hall conductivity in a disordered topological insulator surface . . . 94
4.5.3. Spin Hall conductivity in the quantum Hall regime . . . 96
4.5.4. Macroscopic transport . . . 99

II Bicomplex Representation for the Fractional Quantum Hall Effect 101

5. Fractional Quantum Hall Effect in a Nutshell 103
5.1. Phenomenology of Many-Body Effects . . . 103
5.2. Review of Standard Theoretical Approaches . . . 106
5.2.1. Exact numerical diagonalization . . . 108
5.2.2. Trial wave functions . . . 109
5.2.3. Edge state theory . . . 116
5.2.4. Composite fermion flavors . . . 118

6. Bicomplex Vortex Representation for the Generalized Two-Body Problem 125
6.1. Motivation . . . 126
6.2. Bicomplex Numbers . . . 130
6.2.1. Generalities . . . 130
6.2.2. Representations . . . 132
6.2.3. Bicomplex rings and modules . . . 138
6.2.4. Bicomplex functional analysis . . . 139
6.3. Two-Body Vortex States . . . 145
6.3.1. Hamiltonian operator in the bicomplex vortex representation . . . 145
6.3.2. Bicomplex vortex eigenstates . . . 147
6.3.3. Properties of the bicomplex vortex eigenstates . . . 148
6.4. Matrix Elements of the Generalized Potential . . . 149
6.4.1. General expression . . . 149
6.4.2. Overlap . . . 151
6.5. Green's Function Formalism . . . 152
6.5.1. Dyson equation in the bicomplex vortex representation . . . 152
6.5.2. Consistency of the Green's function formalism: proof of the closure relation of the bicomplex vortex states . . . 157

Conclusions and Outlook 161

Appendices 173

A. Overlap and Completeness Relation of the Vortex Representation 173
A.1. Notation . . . 173
A.2. Overlap . . . 173
A.3. Closure Relation . . . 174
A.3.1. Two-dimensional Dirac delta distribution function . . . 176

B. Calculation of the Spin Hall Conductance from Ref. [112] 179
B.1. General Considerations . . . 179
B.2. Hall Conductance . . . 181
B.3. Equilibrium Spin Hall Conductance . . . 182
B.4. Nonequilibrium Spin Hall Conductance . . . 182

C. Contribution to the electron current density from $g^{(1)}(\mathbf{R};\omega)$ 185

D. Dictionary of Abstract Algebra 187
D.1. Rings and Ideals . . . 187
D.1.1. Rings . . . 187
D.1.2. Ideals . . . 189
D.2. Modules and Algebras . . . 190
D.2.1. Modules . . . 190
D.2.2. Algebras . . . 192

E. Coordinate Transformations in the Bicomplex Vortex Representation 195
E.1. Jacobian to Polar Coordinates . . . 195
E.2. Laplacian Operator . . . 196

F. Proof of Relation (6.41) **199**

Bibliography **201**

List of Publications **213**

General Introduction

Context

More than thirty years after its discovery, the quantum Hall effects still constitute a remarkable source of surprises for the condensed matter physics community. This research field presently draws a considerable amount of attention thanks to new experimental findings (*i.e.* zero resistance microwave-induced states [1]), the development of new probes that allow the access to local spatial and spectral properties (such as the real space structure of the electronic wave functions [2]) or the identification of novel experimental systems exhibiting new physical features (single-layer graphene [3] or topological insulators [4] to cite some).

The quantum Hall effects can be roughly classified as being part of a set of phenomena related to orbital magnetism in low dimensional electronic systems. Concretely, when a disordered two-dimensional electron gas (2DEG) is subjected to a strong perpendicular magnetic field and low temperatures, quantum mechanics affects the orbital motion of the electron whose energy becomes discrete. The discrete energy levels in the 2DEG, so-called Landau levels, become apparent in the density of states and are at the ultimate origin of the magnetic quantum oscillations in thermodynamic and transport macroscopic physical quantities. In addition, it is reasonable to accept that a full understanding of quantum Hall systems must also rely on the adequate consideration of disorder (due to impurities and imperfections in the two-dimensional sample) and electron-electron interactions affecting the charged particles that *dance* under the influence of the Lorentz force in the presence of a random electrostatic potential energy. On one hand, at the single particle level and for not too low temperatures (so-called integer quantum Hall regime) disorder affects transport properties by producing both delocalized and localized electronic states, which are responsible for the spectacularly precise quantization of the Hall conductance in beautiful large plateaus proportional to the quantum of conductance, e^2/h (which is inversely proportional to the von Klitzing's constant, $R_{\mathrm{K}} \equiv h/e^2$ with $e = -|e|$ being the electron charge and h Planck's constant). This quantization appears accompanied of a simultaneous brutal oscillation of the longitudinal magnetoresistance, which drops several orders of magnitude within the plateau to values close to zero for a wide range of magnetic field strength. This strong reduction of the dissipation points to the existence of quasi-ballistic electronic states in the sample and also makes compulsory to consider in depth the topology of the potential energy landscape in order to fully understand the behaviour of the transport coefficients. On the other hand, interactions begin to play a crucial role when temperatures are even lower and mobilities are higher, with the kinetic energy related to orbital motion completely quenched. This is the so-called fractional quantum Hall regime characterized by fractional quantization of the Hall plateaus, fractional statistics

and fractionalization of the charge of the quasiparticle excitations.

Despite the one-body nature of the integer quantum Hall effect, a quantitative microscopic description is still a quite challenging theoretical problem. Indeed, one needs to know how to simultaneously consider the smooth disorder potential originated by the impurities (and which broadens the Landau levels) and the confinement potential at the edges of the sample, the external nonequilibrium electric fields driving the macroscopic current or other dissipative mechanisms (phonons, electron-electron interactions ...) starting from a macroscopically degenerate "reference state". Moreover, this problem is also intrinsically non-perturbative at high magnetic fields after projection onto a single Landau level since only a single energy scale (related to the smooth potential energy) is present. The non-perturbative nature manifests itself then, for instance, in the diagrammatic calculations where it is necessary to include more and more diagrams when increasing the magnetic field [5, 6]. Part of the obstacles can be overcome by using a Green's function framework developed in recent years and based on a coherent-state representation of the Landau level states [7]. This approach overcomes the previous shortcomings and does not need averaging over impurity configurations, questionable for strong magnetic fields, where the electron motion is no longer chaotic due to collision with impurities, but becomes quasi-integrable or regular.

When, in addition to the disorder potential, the spin of the electron and its coupling to the cyclotron (orbital) motion of the electron are taken into account, interesting new physics in quantum Hall systems appears. The coupling between these two degrees of freedom is necessarily present in every semiconductor heterostructure lacking structure inversion symmetry, where standard 2DEGs are created, in the form of Rashba spin-orbit (SO) interaction [8]. This kind of SO coupling is peculiar since it depends on potential gradients perpendicular to the 2DEG and, therefore, can be tuned by using an external voltage gate. For this reason, it has been suggested that 2DEGs with Rashba SO coupling could be the natural playground to build spintronic nanodevices, where the spin of the electron is controlled by electrical means (see, for instance Ref. [9]). From a more fundamental point of view, it is also interesting to understand what is the concrete effect of the SO interaction in the quantum Hall states, both in the spectral and transport properties. It is in this context that we can situate part of the work realized in this thesis, which contains the first analytical treatment of Rashba-coupled 2DEGs in the integer quantum Hall regime.

In the case of the fractional quantum Hall effect, the not yet achieved *Grail* in the area is to have a microscopic theory capable to embrace both the effect of the one-body disorder potentials and the strong long-range Coulomb interactions between the electrons in the presence of strong perpendicular magnetic fields. Nevertheless, until now, these two effects have been considered separately, mostly focusing in the two-body interaction, even though the smooth disorder is crucial to explain the characteristic transport properties such as formation of the Hall plateaus at fractional values of the quantum of conductance, e^2/h. This can hardly be done with current theories, which either heavily rely on numerical computations (so that studying the effect of disorder at finite temperatures and in the thermodynamic limit is out of question), or phenomenologically attach flux quanta to electrons in order to get a reduced effective interaction between them [10]. We would like to stress here that, from the theoretical point of view, our goal is clearly ambitious as it is well-known that, in the absence of disorder potential, again a unique energy scale is present in the Hamiltonian, preventing any kind of perturbative expansion. As a consequence,

standard many-body perturbative approaches fail (in particular, mean-field or Hartree-Fock methods) resulting in the need of developing new theoretical tools to gain deeper comprehension and analytical insight both into the spectral and transport properties of disordered fractional quantum Hall liquids. We shall consider this problem in the second part of the thesis where we present a new look to a generalized two-body problem in the fractional quantum Hall regime by proposing an extension of the Green's function formalism developed for the (one-body) integer quantum Hall regime.

Plan of this thesis

As introduced previously, this thesis is organized into two parts.

In the first part we study the effects of Rashba SO coupling in the integer quantum Hall regime, considering both local spectral properties and transport phenomena. We shall first present all the basic concepts which allow us to extend the current theoretical tools to accommodate the influence of the spin degree of freedom and its interaction with the orbital motion in disordered 2DEGs under strong perpendicular magnetic fields. In **chapter one** we review the phenomenology of the integer quantum Hall effect and describe theoretically the origin of its amazing transport features. We also throw spotlight onto the recent coherent-state vortex theory [of the integer quantum Hall effect], which is able to take into account at finite temperatures the peculiar role played by the smooth disorder in this regime. In **chapter two** we include another ingredient to be added to the mix: SO interaction of the Rashba type. We learn about its origin, the form of the Rashba Hamiltonian in two dimensions and focus our attention onto the spectral and spin properties of clean 2DEGs under perpendicular magnetic fields, which present the combined influence of Rashba SO interaction and Zeeman couplings. In **chapter three**, we introduce a smooth electrostatic potential energy into our system (which can represent both confinement and bulk disorder) and random Rashba fields in the integer quantum Hall regime. We extend the quantum-mechanical vortex formalism to incorporate both Rashba SO and Zeeman interactions and obtain analytical nonperturbative expressions for the energy spectrum and the local density of states (LDoS) at high magnetic fields. The obtained formulas are then used to examine the puzzling correlations between the energy spin-splitting of the LDoS peaks and the critical points of the potential landscape noticed in recent scanning tunneling spectroscopy measurements [11]. In **chapter four** we microscopically describe the influence of Rashba SO interaction into the charge and spin properties at high magnetic fields, where a local (hydrodynamic) equilibrium regime sets in. We derive analytical expressions for the density-gradient and drift current densities; the former allows us to analyze the spatial dispersion of the edge states, while the latter can be used to extract a formula for the local Hall conductivity combining the peculiar non-relativistic and relativistic hallmarks of Rashba coupled 2DEGs. Using this expression, we also define a physically relevant spin Hall conductivity that describes dissipationless flow of angular momentum and that could be useful to address the nature of the spin transport in the quantum Hall regime. Finally, we explore the consequences of having a non-zero Rashba SO parameter into the macroscopic transport coefficients at strong magnetic fields.

In the second part of the manuscript, we investigate strong correlations in the 2D electron liquid at very low temperatures. In **chapter five**, we try to survey and summarize part of the vast body of literature that exists on the fractional quantum Hall effect. First we compare the signatures of the many-body effects to the single-particle counterpart (integer

quantum Hall regime) as it is seen in magnetotransport measurements. Next, we shortly discuss the most important theoretical approaches used to study the fractional quantum Hall regime by computing the energy gaps, response and correlation functions in the more stable odd-denominator fractions appearing within the lowest Landau level. In particular, we shall revisit the inner workings of the exact numerical diagonalization, the trial wave functions, the edge state theory and the Chern-Simons approaches (both a reformulated and simplified version of the field theory and the Hamiltonian formalism). Finally, in **chapter six**, we present the first step on the microscopic understanding of this effect by a novel look to a generalized two-body problem in the presence of disorder potentials. To that purpose, we introduce a new coherent-state vortex representation of the two-particle states that naturally encodes topological long-range correlations between the electrons by the means of a non-Euclidean metric. This change of metric from the Euclidean (standard) one makes necessary to preliminary extend a considerable quantity of mathematical notions, which are deeply studied in the first portion of the chapter. Afterwards, we show that this representation forms an overcomplete semiorthogonal basis in an extended Hilbert space and we obtain the equation of motion for the electron pair composite in this representation. Finally, we explain why one has to go beyond the semiclassical equations to recover the expected energy gaps and demonstrate the consistency of our approach within any Landau level for the pair by proving the closure relation of the two-body vortex states using a non-trivial polynomial identity.

Plus de trente ans après sa découverte, les effets Hall quantiques constituent toujours une boîte à surprises remarquable pour la communauté de la physique de la matière condensée. Ce domaine de la recherche attire aujourd'hui une attention importante grâce aux découvertes inattendues (i.e. états de résistance nulle induits par le rayonnement micro-ondes [1]), au développement de nouvelles sondes qui permettent accéder aux propriétés locales spatiales ainsi que spectrales (telles que la structure dans l'espace réel des fonctions d'onde électroniques [2]) ou l'identification de systèmes expérimentales inhabituels qui présentent quelques attributs physiques inusités (pour faire référence à certains de ces systèmes nous pouvons citer, par exemple, les couches individuelles de graphène [3] et les isolants topologiques [4]).

Les effets Hall quantiques peuvent être classifiés grossièrement comme appartenant à l'ensemble de phénomènes reliés au magnétisme orbital dans les systèmes électroniques de basse dimension. Concrètement, lorsqu'un gaz d'électrons bidimensionnel (GE2D) désordonné est soumis a un fort champ magnétique perpendiculaire et a basses températures, la mécanique quantique affecte le mouvement orbital de l'électron dont l'énergie devient discrète (et pas continue). Les niveaux d'énergie résultants du GE2D sont appelés niveaux de Landau et se manifestent dans la densité d'états ainsi que dans les oscillations quantiques magnétiques de certaines quantités physiques thermodynamiques et de transport macroscopiques. En plus, il est raisonnable d'admettre qu'une compréhension complète de l'effet Hall quantique a besoin d'un étude approprié du désordre (causé par les impuretés et les défauts dans l'échantillon quasi-bidimensionnel) et des interactions électron-électron qui affectent aux particules chargées soumises à l'influence de la force de Lorentz en présence d'une énergie potentiel électrostatique aléatoire. D'un côté, pour le problème à une particule et des tempéra-

tures pas trop basses (i.e. le régime de l'effet Hall quantique entier) le désordre affecte aux propriétés de transport et entraîne l'apparition des états électroniques localisés et délocalisés. Ces états sont les responsables de la quantification spectaculaire de la conductance de Hall en très jolis et larges plateaux, qui se manifestent à valeurs entiers du quantum de conductance, e^2/h (inversement proportionnel à la constante de von Klitzing, $R_K \equiv h/e^2$ avec $e = -|e|$ la charge de l'électron et h la constante de Planck). La quantification de la composante transverse du tenseur de conductance est accompagnée des oscillations brutales de la composante longitudinale, qui chute plusieurs ordres de grandeur et à travers de chaque plateau (pour un intervalle important du champ magnétique) présente des valeurs presque nulles. Cette forte réduction de la dissipation suggère l'existence d'états électroniques quasi-ballistiques dans l'échantillon et, par conséquent, il est nécessaire de prendre en considération la topologie du paysage d'énergie potentielle pour comprendre pleinement le comportement spatiale des coefficients de transport. De l'autre côté, les interactions commencent à jouer un rôle crucial pour des températures plus basses et mobilités plus élevées avec en plus, l'énergie cinétique liée au mouvement orbital maintenue constante. Ceci est le régime de l'effet Hall quantique fractionnaire caractérisé par la quantification fractionnaire de la conductance de Hall et la charge et statistique fractionnaires des excitations.

Malgré le fait que l'effet Hall quantique entier peut être compris comme un phénomène à un corps, une description microscopique et quantitative complète est toujours une problème théorique très extrêmement compliqué. En fait, il est nécessaire de considérer au même temps le potentiel de désordre lisse produit par les impuretés (et, qui élargisse les niveaux de Landau), le potentiel de confinement près des bords de l'échantillon, les champs électriques appliqués qui créent un courant macroscopique hors-équilibre ou autres mécanismes dissipatifs (phonons, interaction électron-électron ...) à partir d'un état "de référence" dégénéré macroscopiquement. En plus, ce problème dégénéré macroscopiquement est intrinsèquement non-perturbatif après projection dans un niveau de Landau à très fort champ magnétique car il n'y a qu'une seule échelle d'énergie (qui vient de l'énergie potentiel lisse). La nature non-perturbative s'exprime, par exemple, dans les calculs diagrammatiques où il est nécessaire d'inclure de plus en plus de diagrammes quand le champ magnétique est augmenté [5, 6]. Une partie importante de ces problèmes peuvent être réglés avec un formalisme de fonctions de Green développé récemment et basé sur une représentation cohérente des états de Landau [7]. Cet approche aide à surmonter les défauts des théories précédentes et n'a pas besoin de faire appel au moyennage sur les positions des impuretés, procédure de validité discutable à fort champ magnétique, quand le mouvement de l'électron n'est plus chaotique à cause des collisions avec les impuretés mais quasi-integrable ou régulier.

Quand, additionnellement au potentiel de désordre, le spin de l'électron et son couplage au mouvement cyclotron (orbital) sont prises en compte, nous rencontrons de la nouvelle (et intéressante) physique dans les systèmes à effet Hall quantique. Le couplage entre les deux degrés de liberté susmentionnés est présent de manière nécessaire dans toutes les heterostructures semiconductrices (où les GE2D standards sont crées) manquant une symétrie d'inversion structurale, ce qui produit une interaction spin-orbite (SO) de type Rashba. Le couplage SO Rashba est assez particulier car il est dépendent des gradients de potentiel appliqués perpendiculairement au GE2D.

Par conséquent, il peut être modifié en utilisant une grille métallique qui contrôle une source de tension extérieure. En effet, c'est pour cette raison que les GE2D présentant un fort couplage SO de type Rashba ont été proposés comme le terrain de jeu idéal pour la construction de dispositifs spintroniques à l'échelle nanométrique, dans lesquels le spin de l'électron est manipulé par le biais de moyens exclusivement électriques (cf. Réf. [9], par exemple). D'un point de vue plus fondamental, c'est aussi intéressant de comprendre quelles sont la véritable conséquences microscopiques de l'interaction SO Rashba sur les états quantiques d'un système à effet Hall, à la fois dans les propriétés spectrales et de transport. À cet égard, nous pouvons situer dans ce contexte une partie du travail original de cette thèse où nous présentons une théorie analytique pour un GE2D avec couplage SO Rashba dans le régime de l'effet Hall quantique entier.

Dans le cas de l'effet Hall quantique fractionnaire, le graal dans le domaine, qui n'est pas encore accompli, c'est de développer une théorie microscopique de ce régime capable d'embrasser simultanément le potentiel de désordre à un corps et la forte interaction coulombienne (à longue portée) entre les électrons, tout en présence d'un fort champ magnétique perpendiculaire au GE2D. Néanmoins, l'effet du désordre et des interactions à été considéré séparément jusqu'aujourd'hui, les théories existantes étant focalisées plutôt sur l'interaction à deux corps - même si la présence du désordre lisse est cruciale pour expliquer les propriétés de transport caractéristiques (par exemple, la formation de plateaux de Hall pour des valeurs fractionnaires du quantum de conductance, e^2/h). Cela peut être accompli très difficilement avec les théories connues actuellement, qui dépendent fortement bien de lourdes simulations numériques (donc, l'étude de l'effet du désordre à température finie et dans la limite thermodynamique est hors de question) ou bien d'une vision purement phénoménologique qui introduit l'attachement de flux magnétique aux électrons pour diminuer l'interaction effective parmi eux [10]. Nous voudrions anticiper déjà ici que, sur le plan théorique, notre objective reste énormément ambitieux car nous avons entre nos mains un problème à N-corps non-perturbatif (en absence de désordre il n'y a qu'une seule échelle d'énergie présent dans l'Hamiltonien, ce qui interdit tout type d'expansion perturbative dans l'énergie). Par conséquent, les méthodes perturbatifs standards de la physique à N-corps échouent (concrètement, des méthodes de champ moyen type Hartree-Fock) ce qui appelle à la nécessité de développer de nouveaux outils pour obtenir une compréhension analytique plus profonde des propriétés spectrales et de transport des liquides électroniques désordonnés dans le régime de l'effet Hall fractionnaire. Nous considérons ce problème dans la deuxième partie de cette thèse dans laquelle nous jetons un nouveau coup d'oeil à un problème à deux particules généralisé dans le régime fractionnaire en proposant une extension du formalisme des fonctions de Green développé pour le régime de l'effet Hall quantique entier.

Part I

Rashba Spin-Orbit Coupling in the Integer Quantum Hall Regime

Chapter 1

The Integer Quantum Hall Effect

In this chapter, we review the phenomenological and theoretical aspects proper to the integer quantum Hall effect. First, we succinctly reconsider the well-known experimental facts that motivated the subsequent vast amount of theoretical research. We briefly revisit the classical theory of the Hall effect as a starting point in order to understand why the discovery and comprehension of the (integer) quantum version is nowadays considered such an important progress by the condensed matter community. We also introduce the concepts of Landau levels and disorder-induced classical localization which allow to get an intuitive picture for the origin of the peculiar quantum transport properties at low temperatures. Finally, we discuss a more sophisticated analytical theory capable of taking into account in a controlled way the effect of two-dimensional disorder in the integer quantum Hall regime.

Dans ce chapitre, nous revisitons les aspects phénoménologiques et théoriques plus remarquables relatifs à l'effet Hall quantique entier. D'abord, nous reconsidérons succinctement les résultats expérimentaux bien connus qui ont motivé l'immense quantité de recherche théorique ultérieure dans ce domaine. Ensuite, nous rappelons quelques notions utiles de la théorie de l'effet Hall classique, qui servira comme point de départ pour comprendre pourquoi la découverte et la compréhension de l'effet Hall quantique entier est aujourd'hui considérée comme un événement majeur dans la communauté de la physique de la matière condensée. Puis, nous présentons les concepts de niveaux de Landau et localisation classique induite par le désordre qui permettent d'avoir une image intuitive de l'origine des propriétés particulières de transport quantique à très basse température. Finalement, nous discutons une théorie analytique beaucoup plus sophistiquée, capable d'inclure de manière controllée l'effet du désordre bidimensionnel dans le régime de l'effet Hall quantique entier.

1.1. Phenomenology

1.1.1. (Non-relativistic) integer quantum Hall effect

The integer quantum Hall effect is one of the most remarkable phenomena discovered in the field of condensed matter physics in the 20th century. Together with superconduc-

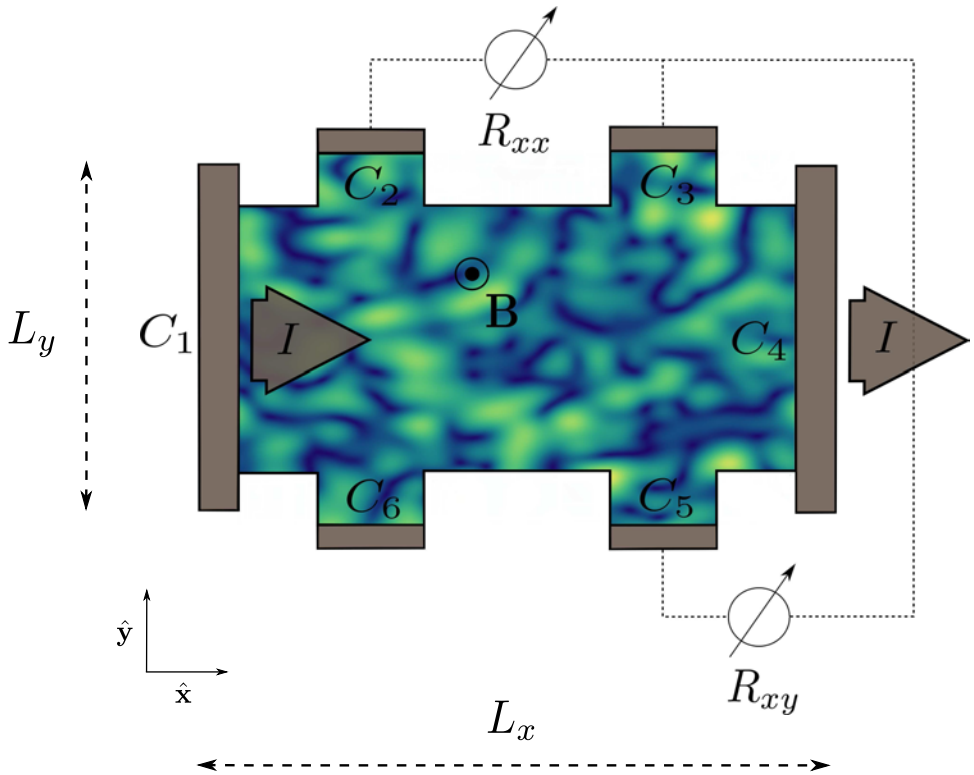

Figure 1.1 – Scheme of a six-terminal Hall bar experimental setup. A source-drain current I is set up through the system from left to right in the presence of a perpendicular magnetic field $\mathbf{B} = B\hat{\mathbf{z}}$ and a disordered potential landscape (represented by the color background). Resistance can be measured using the contact probes C_i where $i \in \{2, 3, 5, 6\}$. L_x and L_y give the length of the device in the $\hat{\mathbf{x}}$ and $\hat{\mathbf{y}}$ directions.

tivity and superfluidity, it constitutes a clear manifestation of quantum mechanics at the macroscopic scale in a non-trivial (disordered) physical system. Its discovery can be dated very precisely: the night of 4th to 5th February 1980, K. von Klitzing was performing systematic electronic transport measurements in two-dimensional electron gases (2DEGs) confined in the inversion layer of a silicon MOSFET (metal-oxide-semiconductor field effect transistor) at the High Magnetic Field Laboratory in Grenoble [12, 13]. Relatively clean samples had been provided by G. Dorda and M. Pepper with a particular configuration that allows to directly measure the full 2D resistance tensor. This configuration, known as six-terminal Hall bar, is shown in Fig. 1.1. In a typical transport experiment, a current is driven between the contacts C_1 and C_4 as a result of a macroscopic voltage drop. The longitudinal resistance, $R_{xx} \equiv R_L$, can be probed by a direct measurement of the voltage drop, V_L, between the contacts C_2 and C_3 since $R_L = V_L/I$. The transverse resistance (with respect to the direction of the current), noted R_{xy} and defined to be the opposite of the Hall resistance, $R_{\text{H}} \equiv -R_{xy}$, can be measured from the (Hall) voltage drop V_{H} between the contacts C_3 and C_5 through the simple relation $R_{\text{H}} = V_{\text{H}}/I$. The components of the resistance tensor therefore read, assuming an isotropic system,

$$\bar{R} = \begin{pmatrix} R_L & R_{\text{H}} \\ -R_{\text{H}} & R_L \end{pmatrix}. \tag{1.1}$$

The macroscopic conductance (tensor)[1], which is defined as $\bar{G} \equiv \bar{R}^{-1}$, is given by

$$\bar{G} = \begin{pmatrix} G_L & -G_{\text{H}} \\ G_{\text{H}} & G_L \end{pmatrix} = \frac{1}{R_L^2 + R_{\text{H}}^2} \begin{pmatrix} R_L & -R_{\text{H}} \\ R_{\text{H}} & R_L \end{pmatrix}. \tag{1.2}$$

Note that when the longitudinal resistance vanishes one gets $G_{\text{H}} = R_{\text{H}}^{-1}$.

K. von Klitzing, who was interested in the experimental determination of the scattering mechanisms that affect the electron mobility in semiconductor devices, performed transport measurements at high perpendicular magnetic fields ($B = 18$ T) and low temperatures ($T = 1.5$ K). To his surprise, he observed (see Fig. 1.2) that the transverse resistance was quantized in very precise values proportional to h/e^2 (where h is the Planck's constant and $e = -|e|$ is the electron charge) and formed plateaus of finite width when represented as a function of the magnetic field. Simultaneously, the longitudinal resistance dropped exponentially by several orders of magnitude and almost vanished, pointing towards the existence of dissipationless electronic states. Only at the transitions between the different plateaus the longitudinal resistance increased again (exponentially due to thermal activation mechanisms) vanishing as soon as we attained the next plateau.

The quantized Hall resistance was therefore found to satisfy $R_{\text{H}} = R_{\text{K}}/\nu_f$ with $\nu_f \in \mathbb{N}_{>0}$ an integer and $R_{\text{K}} = h/e^2$ the so-called von Klitzing's constant ($R_{\text{K}} \simeq 25812.807\,\Omega$). R_{K}, which depends exclusively on fundamental constants, is insensitive to the geometry of the device, the material used to fabricate the 2DEG or microscopic details of the sample such as the in-plane disorder or interfaces. Furthermore, the quantization is completely unexpected from a classical point of view (see Sec. 1.2) justifying the 1985 Nobel Prize given to K. von Klitzing for the now dubbed (non-relativistic) integer quantum Hall effect [14].

Almost immediately, K. von Klitzing realized that the quantized Hall resistance could be used to get an extremely accurate value of the fine structure constant $\alpha_0 = e^2/\hbar c \simeq$

[1] This quantity cannot be directly probed in the Hall bar configuration but it can be measured in the disk or Corbino geometry [14].

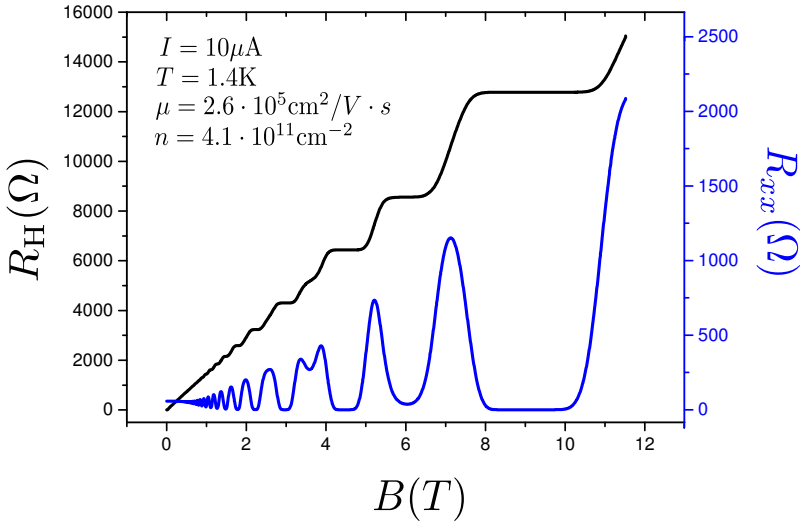

Figure 1.2 – Typical shape of the Hall resistance, R_{H}, and the longitudinal resistance, R_{xx}, both measured in ohms (Ω) as a function of the magnetic field, B, measured in teslas (T). The GaAs/$\mathrm{Al}_x\mathrm{Ga}_{1-x}$As sample is characterized by the experimental parameters detailed in the upper left corner. The large Hall plateau at $\nu_f = 2$ located at magnetic fields between $B \simeq (8-10)$ T is typically used for metrological purposes (calibration and universality tests). Reprinted by permission from Cambridge University Press: MRS Bulletin [17], copyright 2012.

1/137 (here $\hbar = h/2\pi$) characterizing the electromagnetic interactions [12]. Indeed, already in 1980 follow up measurements [15] R_{K} was obtained with a relative uncertainty of one part in 10^6, of the same order of magnitude than the uncertainty for α_0 known through other methods at that moment (nowadays von Klitzing's constant can be obtained with relative uncertainty of the order of one part in 10^9 [16]). Furthermore, if the fine structure constant is known from other physical quantities (such as the magnetic moment of the electron or the gyromagnetic ratio of the proton) the robustness and reproducibility of the integer quantum Hall effect could allow to set up a new accurate (and international) standard of resistance[2] by a top-bottom approach. The effect thus has obvious applications to metrology since other capabilities are possible such as a precise determination of the Planck's constant thanks to the watt balance experiment or of the electron charge by closing the metrological triangle [16].

1.1.2. Relativistic integer quantum Hall effect

Recently, experimental advances in material science have also allowed to observe the relativistic counterpart of the integer quantum Hall effect described in the previous section for standard 2DEGs. This unconventional integer quantum Hall effect has been directly measured in graphene [3, 18], even at room temperature [19], and in the surface states of 3D topological insulators [4]. These condensed matter systems are quite particular since, as it will be presented in Sec. 1.3.2, low energy electrons are described as massless relativistic-

[2]This standard was adopted in 1990 which is why in metrology we denote R_{K} by $R_{\mathrm{K}-90}$. Before that date the resistance standard was maintained nationally with a set of resistors whose resistance was deduced from other derived SI units [16].

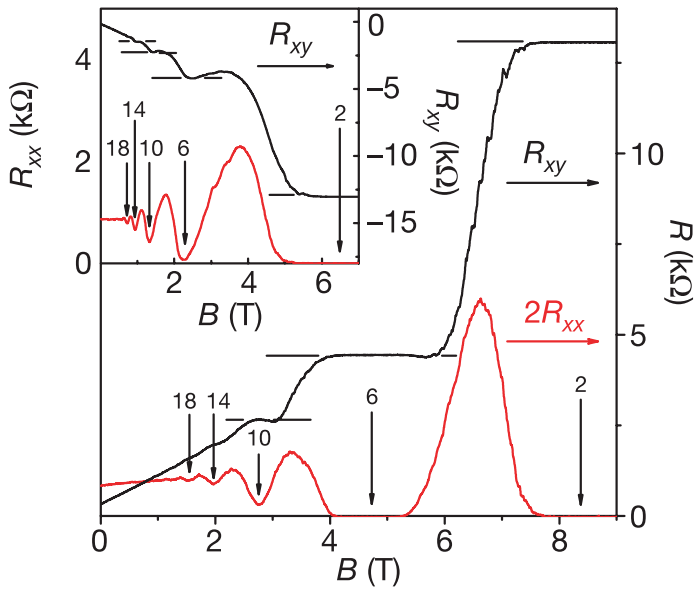

Figure 1.3 – Longitudinal resistance (red solid line) and Hall resistance (black solid line), measured in kilo-ohms (kΩ), as a function of the external magnetic field (in teslas, T) for a monolayer electronic graphene sheet subjected to very low temperatures. The inset shows the same quantities but obtained in the hole side of the spectrum (below the Dirac or neutrality point). The sequence of plateaus at $\nu_f = \pm 2, \pm 6, \pm 10$ is clearly resolved in both cases. Reprinted by permission from Macmillan Publishers Ltd.: Nature [18], copyright 2005.

like particles when the chemical is close to the neutrality point(s) in the Brillouin zone (*i.e.* points where the electron and hole bands touch each other), mimicking high-energy quantum electrodynamics in a small-scale experimental setup.

Graphene (or monolayer graphite) is a quasi-2D single layer of carbon atoms arranged in a hexagonal (honeycomb) lattice due to sp^2 hybridization of the atomic orbitals. It naturally presents a 2DEG near the surface, and as shown in Fig. 1.3, exhibits Hall plateaus at high magnetic fields but not at the expected (integer) sequence. Instead, the Hall resistance appears to satisfy $R_{\mathrm{H}} = R_{\mathrm{K}}/\nu_f$ where $\nu_f = \pm 4(n + 1/2)$ and $n \in \mathbb{N}$ [the $\pm$ sign points out to the existence of two types of carriers, electrons (+) and holes (−), while the factor of four is related to the spin and Brillouin zone - valley - degeneracies]. In the case of 3D topological insulators, such as strained bulk HgTe, the plateaus are also expected to appear for very particular values $\nu_f = \pm 2(n + 1/2)$ [here, the factor of two comes from the fact that both the top and bottom surfaces seem to contribute to transport]. Since part of this thesis deals with Rashba spin-orbit (SO) interaction in 2DEGs, which are systems that present features of both conventional and relativistic 2DEGs, we present in the next sections the main peculiarities and differences between both of them.

1.1.3. Two-dimensional electron gases

Before entering into more technical details, we would like to briefly review how experimentalists are able to create 2DEGs where the quantum Hall effect has been seen[3]. In particular, we discuss commonly used systems, such as silicon MOSFETs and semiconductor heterostructures, together with graphene and 3D topological insulators, both of which have recently attracted a considerable amount of attraction. Amazingly, all of these systems, with the single exception of topological insulators, present as a common denominator that the driving force in their discovery has been not the theoretical input but the technological development in the fabrication of 2DEGs.

[3] "Trapping" 2DEGs is easier and safer for a pencil-paper theoretician, of course!

The silicon MOSFET was the kind of device originally used in the discovery of the quantum Hall effect [12]. The traditional structure is made from three layers: a p-doped silicon substrate, an oxide intermediate film (typically SiO_2) and a top aluminum gate. Application of a positive voltage on the metallic side bends the semiconductor electron bands downwards and creates, first, a (positively charged) hole depletion layer in the valence band and, after a threshold voltage, a (negatively charged) electron inversion layer in the conduction band. The inversion layer confines electrons in the lowest energy subband of a triangular potential well situated in the proximity of the interface between the semiconductor and the insulator. As a consequence, one can effectively obtain a 2DEG located in a narrow spatial region ($3-5$ nm) whose density can be controlled by an external voltage source [22].

Although in silicon MOSFETs it is possible to obtain 2DEGs of relatively high mobilities $\mu_e \sim 10^6$ cm^2/V$\cdot$s (with surface densities of the order of $n_s \sim 10^{11}$ cm^{-2}), these mobilities are limited due to the roughness (*i.e.* disorder, crystal discontinuities) of the semiconductor-oxide interface. Nevertheless, new techniques such as molecular beam epitaxy (MBE) yield possible the fabrication of extremely clean interfaces with a regularity close to the atomic size. At these interfaces, high-quality 2DEGs can be obtained and the improved mobilities allow for the observation of finer effects such as the fractional quantum Hall effect [23] which will be the main theme of the second half of this thesis.

MBE is commonly used to grow the popular modulation-doped semiconductor heterostructures GaAs/$Al_xGa_{1-x}As$ (with Al molar fraction $x \simeq 0.3$) layer-by-layer with a smooth spatial transition between both compounds, as they present almost the same lattice constant [22, 24]. Essentially, the heterostructures consist of two different semiconductors with different band gap (larger for $Al_xGa_{1-x}As$ than for GaAs). The $Al_xGa_{1-x}As$ is n-doped, with all the donors concentrated in a thin plane called δ-doping layer. This layer is spatially separated from the GaAs by an undoped $Al_xGa_{1-x}As$ spacer. Since the conduction band of the GaAs compound in the heterojunction has lower energy than the conduction band of the $Al_xGa_{1-x}As$ (the energy difference is of the order of 0.3 eV), it is energetically favorable for the donor electrons to populate the conduction band on the GaAs side. This leaves a region of positively charged holes close to the interface which plays a similar role to the metallic gate of the silicon MOSFET, bending the valence and conduction bands of the GaAs downwards to create an electron inversion layer close to the interface. The 2DEG gets then trapped in the lowest energy subband of a triangular potential well since the electrons cannot scatter to the conduction band of the $Al_xGa_{1-x}As$ that is energetically much higher, as shown in Fig. 1.4. Note that, contrary to the silicon MOSFET, the properties of the inversion layer of the GaAs/$Al_xGa_{1-x}As$ heterostructure are determined by the fixed dopant density. These heterostructures, however, present an important advantage: the δ-doping layer is located relatively far from the effective 2DEG strongly reducing the disorder potential fluctuations at the interface. As a consequence, an increase in the carrier mobility of two orders of magnitude with respect to the MOSFET can be attained[4] (see also Refs. [20, 22]).

Furthermore, the 2DEGs that can be created in a MOSFET or a semiconductor heterostructure are located far from the device boundaries and, therefore, they are inaccessible to local probes such as scanning tunneling microscopy (STM). The former technique gives interesting insights into the microscopic mechanisms at play in the integer quantum Hall

[4]Mobility in GaAs/$Al_xGa_{1-x}As$ heterostructures is also higher due to the reduced electronic effective mass of GaAs, $m^* = 0.067m_0$ where m_0 is the bare electron mass [24].

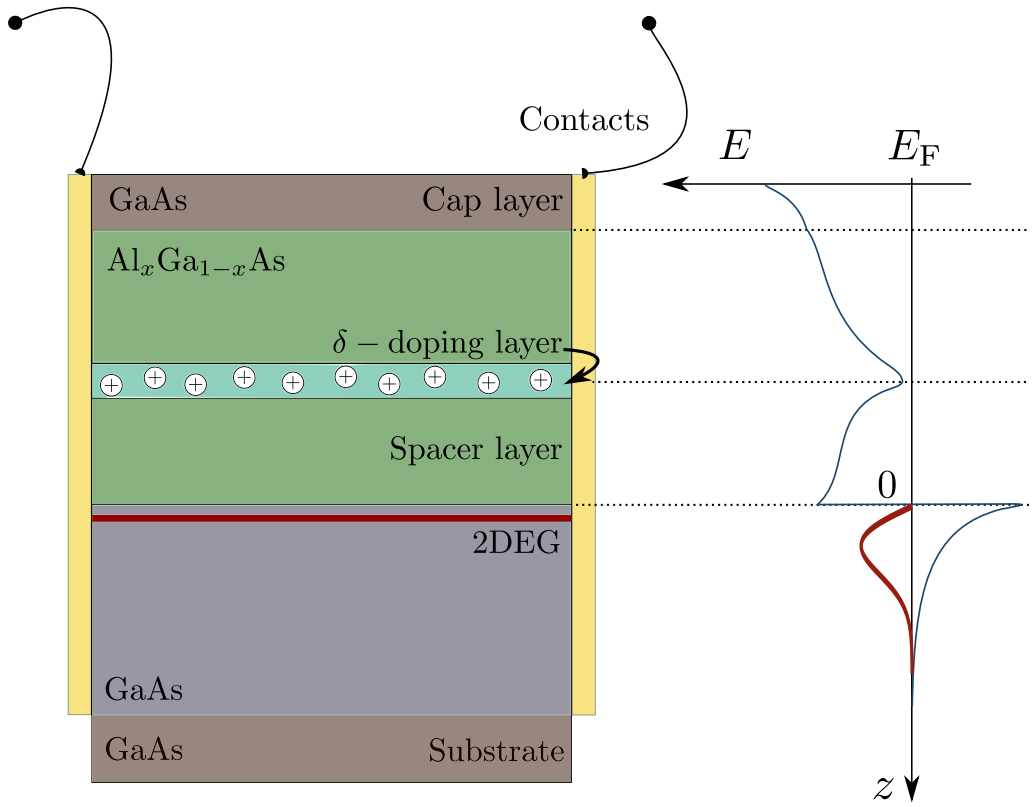

Figure 1.4 – Illustration of a cross section in a GaAs/$Al_xGa_{1-x}As$ heterostructure where confined 2DEGs can be experimentally created, together with an scheme of the energy (E) in the conduction band measured with respect to the Fermi energy. The energy scheme also shows the localized electronic wave function in the perpendicular ($\hat{\mathbf{z}}$) direction. The wave function (here plotted in arbitrary units) gets trapped in the triangular well formed at the interface between the semiconductors GaAs and $Al_xGa_{1-x}As$.

effect which cannot be detected by macroscopic transport measurements. Remarkably, it has recently been possible to experimentally realize surface 2DEGs which can be studied by these methods. Three main types can be distinguished: surface 2DEGs created at the boundaries of bulk semiconductors by deposition of alkali ad-atoms, graphene and surface states of 3D topological insulators. The last two, which were introduced in Sec. 1.1.2, will be briefly reviewed in the next paragraph while leaving the discussion of semiconductor surface 2DEGs for chapter 3.

As described above, graphene is a monolayer of carbon atoms which naturally presents a 2DEG at the surface. This material constitutes a zero-gap semiconductor (or semimetal) with a linear dispersion relation at low energies that strongly affects transport properties [25]. In the absence of doping, the graphene Fermi energy is located at special doubly degenerated points (Dirac points) in the Brillouin zone where the linear valence and conduction bands touch. The degeneracy of the zero energy state is called valley degeneracy [26]. We would like to note that research in graphene has recently been boosted (even if graphite was known for centuries) after its first experimental isolation almost ten years ago by the mechanical exfoliation technique at ambient temperatures [27], which allows the obtention of irregular graphene flakes in a random spatial orientation. As a consequence of

the strong disorder (whose origin are the atomic vacancies, impurities or the spatial distortion of the graphene flakes), electron mobilities in exfoliated graphene can be much lower than in semiconductor heterostructures[5], $\mu_e \sim 10^4 - 10^5$ cm^2/ V $\cdot$ s [20, 21]. The electronic mobilities can be vastly improved (and also the size, orientation and growing kinetics of the graphene sheet) by large-scale synthesis techniques such as chemical vapor deposition on the surface of metallic wafers or graphitization of SiC crystals under appropriate annealing conditions [28].

Finally, surface 2DEGs have also been obtained on the surface of 3D topological insulators. These materials are states of matter topologically different from conventional semiconductors and insulators and presenting strong spin-orbit (SO) interaction. SO coupling typically creates a band inversion which produces Dirac-type (linear) energy bands at the boundaries of the bulk material. As in graphene, peculiar relativistic-like properties at low energies have been observed both in the transport coefficients under magnetic fields[6] (*e.g.* in strained bulk HgTe [4]) and in local properties (*e.g.* scanning tunneling spectroscopy experiments in Bi_2Se_3 [29] and Bi_2Se_3 [30]).

1.2. Classical Hall Effect

I shall devote this section to briefly describe the well-known physical phenomenon of the classical Hall effect, following Refs. [20, 32], in order to get a more precise and quantitative insight of why the integer quantum version is considered such an important breakthrough.

The classical Hall effect was discovered by E. Hall in 1879 [33] who, intrigued after reading a passage of Maxwell's *magnum opus* "A Treatise on Electricity and Magnetism", decided to check experimentally whether the force acting on a conductor carrying a current under an external (perpendicular) magnetic field acted on the whole metallic sample or only on the current flowing through it. Since he believed that the latter case was indeed true, he expected to find an increase of the transverse resistance due to the deflection of the current by the external magnetic field (which should create a so-called Hall voltage drop, perpendicular to the current due to the Lorentz force). He found that the Hall resistance related to this transverse voltage drop was given by the relation

$$R_{\mathrm{H}} = \frac{B}{n_s e c}, \tag{1.3}$$

where n_s is a spatially constant surface particle density and c is the speed of light. The classical Hall resistance only depends on the particle density and carrier charge as intrinsic material-dependent parameters and, unlike the quantum version described in Sec. 1.1, grows linearly with the external applied magnetic field. As a result, formula (1.3) is customary used to experimentally determine the density and type of carrier (given by the sign of the Hall resistance) in bulk conductors.

Additionally, we also note that in 2D the Hall resistance R_{H} does not depend on the geometry of the sample. One may understand this fact from a simple scaling argument: for a d-dimensional conductor the relation between the resistance and the resistivity is given by $R = \rho(L/A)$ where L is the length over which the voltage drops and A is the cross

[5] Extremely nice plateaus in the Hall resistance can still be measured due to the larger gap between energy levels, see Sec. 1.3.2

[6] This a difficult and controversial experiment since topological insulators usually present quite low mobilities and bulk contributions to surface transport.

section orthogonal to the current. As it can be seen in Fig. 1.1, for the Hall component we immediately get $R_{\rm H} = \rho_{\rm H}$ since the current is driven orthogonally to the resistance bridge and the cross section is one-dimensional (L_x). On the other hand, the longitudinal term gives $R_L = \rho_L(L_y/L_x)$, still containing geometrical sample dependent parameters (and so must do the longitudinal conductance, as a difference to the Hall conductance in a plateau for the quantum regime, see Sec. 1.1).

Therefore, as a result of the argument in the previous paragraph, we arrive at the conclusion that in Hall systems[7] resistance (what is measured) and resistivity (what is usually computed) have to present the same dimensions, in agreement with the scaling theory of localization[8]. We will therefore not distinguish between macroscopic resistance and effective (global) resistivity tensors, the latter satisfying Ohm's law $\boldsymbol{\mathcal{E}} = \bar{\rho}\mathbf{j}$ with $\mathbf{j}$ a (spatially averaged) current density and $\boldsymbol{\mathcal{E}}$ a spatially constant macroscopic electric field.

We come now for good to a simple theoretical derivation of Eq. (1.3). The classical Hall result can be understood using the Drude-Lorentz theory of electronic diffusive magnetotransport in metals. Within this theory, we consider 2D non-interacting electrons of effective mass m^* and velocity $\mathbf{v}(t) \equiv \mathbf{v} = (v_x, v_y)$ which move under the influence of mutually perpendicular electric, $\boldsymbol{\mathcal{E}} = (\mathcal{E}_x, \mathcal{E}_y)$, and magnetic fields, $\mathbf{B} = B\hat{\mathbf{z}}$. The particle at position $\mathbf{r}(t) \equiv \mathbf{r} = (x, y)$ in the plane is also assumed to feel the presence of a random disorder potential $V(\mathbf{r})$ which will be taken into account in a pure phenomenological way within the relaxation time approximation. The equation of motion for each electron is then given by

$$m^* \left(\frac{d\mathbf{v}}{dt} + \frac{\mathbf{v}}{\tau} \right) = e \left(\boldsymbol{\mathcal{E}} + \frac{\mathbf{v}}{c} \times \mathbf{B} \right), \tag{1.4}$$

where τ is the transport time (determined by the random potential and which accounts for momentum relaxation mechanisms such as collision with impurities or phonon scattering). The Lorentz force on the right-hand side reflects the deflection of the electron trajectory orthogonally to the initial direction of the motion by the magnetic field (*e.g.* the particle describes an in-plane circular or cyclotron motion). In the steady state where, $d\mathbf{v}/dt = \mathbf{0}$, Eq. (1.4) translates into the condition

$$\sigma_0 \boldsymbol{\mathcal{E}} = n_s e \left(\mathbf{v} + \omega_c \tau \, \hat{\mathbf{z}} \times \mathbf{v} \right), \tag{1.5}$$

where we have introduced the Drude conductivity in the absence of external magnetic field

$$\sigma_0 = \frac{n_s e^2 \tau}{m^*}, \tag{1.6}$$

and the cyclotron frequency

$$\omega_c = \frac{|e|B}{m^* c}. \tag{1.7}$$

Using the definition of the current density, $\mathbf{j} = n_s e \mathbf{v}$, and Ohm's law, $\boldsymbol{\mathcal{E}} = \bar{\rho}\mathbf{j}$, we obtain the following expression for the resistivity tensor $\bar{\rho}$

$$\bar{\rho} = \frac{1}{\sigma_0} \begin{pmatrix} 1 & \omega_c \tau \\ -\omega_c \tau & 1 \end{pmatrix}, \tag{1.8}$$

[7] This is a general argument that applies to both the classical and quantum counterparts.

[8] This theory states than in a hypercube of dimension d and side length L, resistance scales as $R = \rho L^{2-d}$ [31].

whose off-diagonal components yield the Hall resistivity/ resistance (1.3). The conductivity tensor $\bar{\sigma}$ can be easily computed from the inversion of the resistivity tensor, $\bar{\sigma} = \bar{\rho}^{-1}$,

$$\bar{\sigma} = \frac{\sigma_0}{1 + (\omega_c \tau)^2} \begin{pmatrix} 1 & -\omega_c \tau \\ \omega_c \tau & 1 \end{pmatrix}. \tag{1.9}$$

At this point, it is interesting to consider the limit $\omega_c \tau \to +\infty$ which accounts for large relaxation times due to strong (infinite) magnetic fields or extremely long relaxation times that appear in quasi-clean systems. In this situation, it is straightforward to see that the resistivity (1.8) and conductivity (1.9) tensors are purely off-diagonal with

$$\sigma_{\mathrm{H}} = \frac{n_s e c}{B}, \tag{1.10}$$

and $\rho_{\mathrm{H}} = \sigma_{\mathrm{H}}^{-1}$ in agreement with Eq. (1.3). Note that, as expected, we have lost track of the relaxation time that appears as a consequence of the random potential. Moreover, it can be shown that this result exclusively relies on Galilean invariance (*i.e.* translational symmetry is not broken), also surviving in the presence of interactions [36]. For finite magnetic fields, the longitudinal conductivity can also be seen to decrease as $\sigma_{xx} \sim B^{-2}$. Importantly, it is known that this is true for not too high magnetic fields when the electron motion is still chaotic and the center of the cyclotron orbit performs a random walk of characteristic step equal to its radius. The break-down of Drude-Lorentz theory occurs whenever the correlation length of the long-range random disorder potential is much smaller than the length scale related to the circular motion of the electron produced by the Lorentz force. At this moment, the electronic motion is no longer chaotic but regular with the trajectories of the particles localized on certain constant energy contours of the disordered potential landscape [34, 35]. We note that, theoretically, it is also known that this breakdown of the Drude-Lorentz law (1.9) is correlated with the onset of the integer quantum Hall regime at much lower temperatures.

To conclude this section, we must mention that the Hall conductivity tensor does not show the characteristic features of the integer quantum Hall regime discussed in Sec. 1.1. First, we obtain a linear dependence with the electron density n_s in Eq. (1.10), which is a continuous function and therefore there are *a priori* no plateaus. The longitudinal conductance / resistance also does not show any hint of the spectacular (thermally activated) oscillations which were seen in Fig. 1.2. This is because at low temperatures, the description of the quantum regime needs to consider the quantization of the cyclotron motion together with the quasiclassical drift of the center of the cyclotron orbit. Discussion of these aspects will be the main content of the next two sections.

1.3. Landau Levels

1.3.1. Non-relativistic Landau levels

Let us consider now the much simpler problem of a single spinless electron confined in a 2D plane (xy) in the presence of a perpendicular magnetic field $\mathbf{B} = B\hat{\mathbf{z}}$ roughly following [20, 36]. The Hamiltonian, containing only the kinetic energy (in the absence of disorder potential), is given by

$$\mathcal{H}_{\mathrm{2DEG}} = \frac{\mathbf{\Pi}^2}{2m^*} = \frac{1}{2m^*} \left[\mathbf{p} - \frac{e}{c} \mathbf{A}(\mathbf{r}) \right]^2, \tag{1.11}$$

where $\mathbf{\Pi} = (\Pi_x, \Pi_y)$ is the gauge invariant / kinetic momentum, $\mathbf{p} = (p_x, p_y)$ is the canonical momentum and $\mathbf{A}(\mathbf{r})$ the electromagnetic vector potential. We also remind that we note by m^* the effective mass, $e = -|e|$ the electron charge and c the speed of light. This Hamiltonian can be obtained from the Hamiltonian for a non-relativistic free particle and the application of the minimal coupling rule $\mathbf{p} \to \mathbf{\Pi}$. Alternatively, we can derive Eq. (1.11) applying Hamilton's principle to the action

$$S_{\text{2DEG}} = \int_{t_1}^{t_2} dt \left[\frac{m^*}{2} \left(\frac{d\mathbf{r}}{dt} \right)^2 + \frac{e}{c} \mathbf{A}(\mathbf{r}) \cdot \frac{d\mathbf{r}}{dt} \right], \tag{1.12}$$

with $\mathbf{v} = d\mathbf{r}/dt$. The electromagnetic vector potential appearing in Eqs. (1.11) and (1.12) is related to the external applied magnetic field by the constitutive relation $\mathbf{B} = \boldsymbol{\nabla}_{\mathbf{r}} \times \mathbf{A}(\mathbf{r})$. Note that the vector potential is not uniquely determined but defined up to a local gauge factor. This is because the gauge transformation $\mathbf{A}(\mathbf{r}) \to \mathbf{A}'(\mathbf{r}) = \mathbf{A}(\mathbf{r}) + \boldsymbol{\nabla}_{\mathbf{r}} \Lambda(\mathbf{r})$ with $\Lambda(\mathbf{r}) \in C^\infty$ [*i.e.* $\Lambda(\mathbf{r})$ is continuous and infinitely derivable] leaves unchanged the observable magnetic field as the rotational of a gradient always vanishes. Consequently, the action (1.12) is not gauge invariant since under a (gauge) transformation of the electromagnetic field yields

$$S_{\text{2DEG}} \to S'_{\text{2DEG}} = S_{\text{2DEG}} + \frac{e}{c} \left[\Lambda(\mathbf{r}_2) - \Lambda(\mathbf{r}_1) \right]. \tag{1.13}$$

Note that, as expected, the Hamiltonian and the classical equations of motion are unaffected by the gauge transformation since the change only involves the (fixed) end points of the electron path and adds a constant term to the action (extremals of S and S' are the same).

The gauge invariant momentum components satisfy the commutation relation

$$\{\Pi_j, \Pi_k\} = \epsilon_{jk} \frac{eB}{c} \equiv -\epsilon_{jk} \frac{\hbar}{l_B^2}, \tag{1.14}$$

where $\{\,\cdot\,,\,\cdot\,\}$ are the Poisson brackets[9], ϵ_{jk} is the antisymmetric tensor ($\epsilon_{xy} = -\epsilon_{yx} = 1$ and zero otherwise) and

$$l_B = \sqrt{\frac{\hbar c}{|e|B}}, \tag{1.17}$$

is the so-called *magnetic length* which represents the fundamental length scale of the problem. The commutation relation encapsulates the particularity introduced by the magnetic field: the physical momentum $\mathbf{\Pi} = m^* \mathbf{v}$ does not correspond to the canonical momentum and has components which are mutually conjugate within the gauge invariant Poisson brackets[10].

[9] The Poisson brackets of two smooth phase space functions $A, B : \mathbb{R}^n \times \mathbb{R}^n \to \mathbb{R}$ of canonical coordinates $\mathbf{r} = (r_1, \ldots, r_n)$ and $\mathbf{p} = (p_1, \ldots, p_n)$ are defined as

$$\{A, B\} \equiv A \sum_{j=1}^{n} \left(\overleftarrow{\partial}_{r_j} \overrightarrow{\partial}_{p_j} - \overleftarrow{\partial}_{p_j} \overrightarrow{\partial}_{r_j} \right) B, \tag{1.15}$$

where the arrows above the partial derivatives gives the factor to which the derivative has to be applied. Consequently,

$$\{r_j, r_k\} = \{p_j, p_k\} = 0 \quad \text{and} \quad \{r_j, p_k\} = \delta_{jk}. \tag{1.16}$$

The phase space variables $\mathbf{r}$ and $\mathbf{p}$ are said to be *canonically conjugate*.

[10] Note, however, that we still have $\{r_j, \Pi_k\} = \delta_{jk}$.

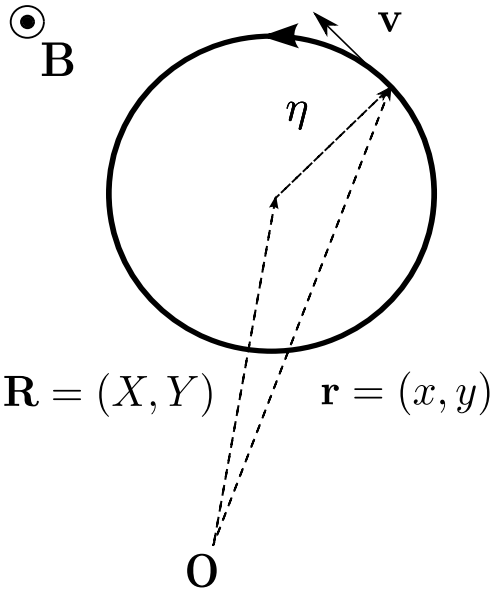

Figure 1.5 – Decomposition of the electronic motion $\mathbf{r}$ into the combination of slow and fast motions labeled by the guiding center $\mathbf{R}$ and cyclotron $\boldsymbol{\eta}$ coordinates, *i.e.* $\mathbf{r} = \mathbf{R} + \boldsymbol{\eta}$. The solid circle represents the electronic cyclotron orbit described by the electron due to the Lorentz force, with linear velocity $\mathbf{v}$ and angular velocity ω_c.

Additionally, it is possible to define a new set of canonical coordinates which commute with the kinetic momenta

$$\mathbf{R} = \mathbf{r} - \boldsymbol{\Pi} \times \hat{\mathbf{z}} \frac{\hbar}{l_B^2} \equiv \mathbf{r} - \boldsymbol{\eta}, \tag{1.18}$$

with Poisson brackets

$$\{R_j, R_k\} = \epsilon_{jk} \frac{l_B^2}{\hbar}. \tag{1.19}$$

Therefore, we see that the phase space symplectic structure forces a geometrical decomposition of the electronic motion at high magnetic fields, given by the coordinate $\mathbf{r}$, into two degrees of freedom characterized by the guiding center $\mathbf{R}$ and relative $\boldsymbol{\eta} = \mathbf{v} \times \hat{\mathbf{z}}/\omega_c$ coordinates respectively. Moreover, one clearly sees from the Poisson brackets (1.14) and (1.19) that 2DEGs will present two very different kind of limits: weak magnetic fields, $l_B \to +\infty$, and strong magnetic fields, $l_B \to 0$. At high magnetic fields, which is the regime we are interested in, the components of the guiding coordinate $\mathbf{R}$ commute classically (1.19) and describe a slow degree of freedom compared to the relative coordinate $\boldsymbol{\eta}$ that characterizes (fast) rotation of the electron around the arbitrary position $\mathbf{R}$ [see Eq. (1.18)]. The previously described decomposition is shown schematically in Fig. 1.5.

We turn at this point to the quantum mechanical problem by following Dirac's canonical quantization method [37] which amounts to replace the Poisson brackets by commutators[11] and phase space functions by (Hermitian) operators according to the rule

$$\{A, B\} \to \frac{1}{i\hbar}[\hat{A}, \hat{B}]. \tag{1.20}$$

[11] The commutator of two operators $\hat{A}$ and $\hat{B}$ is defined by $[\hat{A}, \hat{B}] \equiv \hat{A}\hat{B} - \hat{B}\hat{A}$.

Using this procedure, the quantization and diagonalization of the Hamiltonian (1.11) are trivial operations. In fact, we define the (mutually Hermitian) ladder operators

$$\hat{a}_{\pm} = \frac{1}{\sqrt{2}} \frac{l_B}{\hbar} \left(\hat{\Pi}_x \pm i \hat{\Pi}_y \right), \tag{1.21}$$

which obey the commutation relation[12]

$$[\hat{a}_-, \hat{a}_+] = \mathbb{1}, \tag{1.22}$$

and rewrite the quantum operator obtained from Eq. (1.11) as

$$\hat{\mathcal{H}}_{\text{2DEG}} = \hbar\omega_c \left(\hat{a}_+ \hat{a}_- + \frac{1}{2} \right). \tag{1.23}$$

This is the Hamiltonian of a harmonic oscillator with characteristic energy scale given by the cyclotron energy $\hbar\omega_c$. The eigenvalue problem for this Hamiltonian, $\hat{\mathcal{H}}_{\text{2DEG}}\Psi = E\Psi$, yields an energy spectrum characterized by discrete energy levels, called Landau levels,

$$E_n = \hbar\omega_c \left(n + \frac{1}{2} \right), \tag{1.24}$$

with $n \geq 0$ an integer denominated Landau level index. Landau levels are macroscopically degenerate since the motion of the electron in the 2D plane has two degrees of freedom but Eq. (1.24) presents a single quantum number (while two are required to fully represent the quantum states). This degeneracy is related to the fact that the quantum guiding center coordinates $\hat{\mathbf{R}}$ are a constant of the motion and therefore can present an arbitrary location in the 2D plane. This can be proved since Eq. (1.23) can be rewritten as

$$\hat{\mathcal{H}}_{\text{2DEG}} = \frac{1}{2} m^* \omega_c^2 \left(\hat{\eta}_x^2 + \hat{\eta}_y^2 \right), \tag{1.25}$$

which, together with the commutators $[\hat{R}_j, \hat{\eta}_k] = 0$, yields $[\hat{R}_j, \hat{\mathcal{H}}_{\text{2DEG}}] = 0$ for $j, k \in \{x, y\}$.

We note that, although the classical problem was determined by two Poisson brackets, (1.14) and (1.19), and two degrees of freedom, $\boldsymbol{\eta}$ and $\mathbf{R}$, up to the present moment we have only introduced a single pair of operators $\hat{a}_{\pm}$ (related to the relative motion). We can now proceed to define a new set of mutually Hermitian ladder operators related to the guiding center coordinates [38]

$$\hat{b}_{\pm} = \frac{1}{\sqrt{2} l_B} (\hat{X} \pm i\hat{Y}), \tag{1.26}$$

which obey $[\hat{b}_-, \hat{b}_+] = \mathbb{1}$ and $[\hat{a}_+, \hat{b}_{\pm}] = [\hat{a}_-, \hat{b}_{\pm}] = 0$, where the latter commutators follow from $[\hat{R}_j, \hat{\eta}_k] = 0$. These operators describe the structure inside the Landau levels (the degeneracy) and, therefore, do not present any related energy scale. As such, they are typically used to generate the single-particle states that appear as building blocks in the many-body wavefunction for the lowest Landau level, $|0, q\rangle \propto \hat{b}_+^q |\text{vacuum}\rangle$, with the vacuum state satisfying $\hat{a}_- |\text{vacuum}\rangle = \hat{b}_- |\text{vacuum}\rangle = 0$ (see also Sec. 5.2.2).

Let us finish this section by an estimation of the level degeneracy [20]. First, we note that Eq. (1.19) induces the quantum-mechanical commutation relation $[\hat{R}_j, \hat{R}_k] = i\epsilon_{jk} l_B^2 =$

[12] For a proof, we simply apply the result $[\hat{\Pi}_j, \hat{\Pi}_k] = -i\epsilon_{jk}\hbar^2/l_B^2$ which follows from Eq. (1.14) and canonical quantization rules.

$-[\hat{\eta}_j, \hat{\eta}_k]$. This commutator also defines the particularity of the magnetic field in 2DEGs; the position operators *do not* commute. The non-commutativity, as well as the quantum commutators, are already fixed by the symplectic structure of the phase space present at the classical level. Non-commutativity of the guiding center coordinates also allows to consider a "real" phase space where the minimal surface is determined by the squared magnetic length (which plays the role of a magnetic field dependent effective reduced Planck's constant). Particularly, the phase space area associated to each state is equal to $2\pi|[\hat{R}_x, \hat{R}_y]| = 2\pi l_B^2$ (it can, indeed, be proved that in this case the Heisenberg inequality $\Delta R_x \Delta R_y \geq 2\pi l_B^2$ becomes an equality. This minimal phase space surface is associated to Heisenberg smearing of the guiding center position $\mathbf{R}$ related to each quantum state. In this sense, we can think that electrons acquire a finite size due the applied magnetic field dividing the 2D plane into disjoint quantum cells. We can compute then the number of states available per unit area in a given Landau level by

$$n_B = \frac{1}{2\pi l_B^2} = \frac{B}{\Phi_0}, \tag{1.27}$$

where we have introduced the flux quantum $\Phi_0 = hc/|e|$. The degeneracy of each Landau level is therefore equal to the ratio between the magnetic flux per unit area across the 2D sample and the natural unit of (magnetic) flux. From Eq. (1.27) we now define the single-particle filling factor, denoted ν_f, as the ratio between the surface electron density n_s and the number of states per Landau level n_B

$$\nu_f = \frac{n_s}{n_B} = \frac{n_s}{B}\Phi_0. \tag{1.28}$$

The integer part of the filling factor, $[\nu_f]$, gives the number of completely filled Landau levels below the Fermi energy and is related to the quantization of the Hall resistance. Note that ν_f may be experimentally varied by a changing of the electron density (*e.g.* thanks to external voltage gates) or modifying the occupation of the energy levels by means of the applied magnetic field.

1.3.2. Relativistic Landau levels

To complete this section, we shall discuss the energy spectrum of clean relativistic-like 2D systems placed under external perpendicular magnetic fields. The typical system to be considered here is a single graphene valley or a topological insulator surface decoupled from the bulk of the 3D material. Both are characterized by a single Dirac cone at low energies and can be described by a 2D Weyl Hamiltonian (or some variant such as the Rashba Hamiltonian - to be introduced in chapter 2 - related to the former by a unitary transformation) [26, 39]. Therefore, the Hamiltonian operator for the relativistic 2DEG is

$$\hat{\mathcal{H}}_{\text{2DEGr}} = v_{\text{F}}\hat{\mathbf{\Pi}} \cdot \boldsymbol{\sigma}, \tag{1.29}$$

where v_{F} is the Fermi velocity and $\boldsymbol{\sigma} = (\sigma_x, \sigma_y, \sigma_z)$ is a vector whose components are the Pauli matrices [we implicitly assume here and elsewhere that $\mathbf{\Pi} = (\Pi_x, \Pi_y, 0)$]. From the condensed matter perspective, the Hamiltonian can be obtained by performing an expansion at lowest order in the momentum within a tight-binding framework for graphene or a topological insulator crystal and then using the minimal coupling rule as in Eq. (1.11).

Introducing the ladder operators (1.21) as for the non-relativistic case, we can rewrite the previous Hamiltonian as

$$\hat{\mathcal{H}}_{\text{2DEGr}} = \hbar\Omega_c \begin{pmatrix} 0 & \hat{a}_- \\ \hat{a}_+ & 0 \end{pmatrix}, \tag{1.30}$$

with $\Omega_c = v_{\text{F}}\sqrt{2}/l_B$ the characteristic frequency that defines the typical energy in the problem. Diagonalization $\hat{\mathcal{H}}_{\text{2DEGr}}\tilde{\Psi} = E\tilde{\Psi}$ is straightforward by using as an ansatz a two-component spinor $\tilde{\Psi}$ and we get, as a result [26] the so-called relativistic Landau energy spectrum

$$E_{n,\lambda} = -\lambda\sqrt{n}\hbar\Omega_c, \tag{1.31}$$

where $n \geq 0$ is the Landau level index and $\lambda \equiv \lambda(n)$ is a band index that takes the values $\lambda = \pm$ for $n \geq 1$ and $\lambda = -$ if $n = 0$. The quantum number λ defines the hole / electron character of the eigenvalues and appears as an additional degree of freedom with respect to the non-relativistic Landau levels.

The peculiar energy spectrum of the relativistic 2DEGs merits a detailed discussion. First, note that the characteristic frequency is independent of the mass of the charge carriers which, indeed, is equal to zero for the case of a material whose band structure is a gapless Dirac cone. Next, we remark that the relativistic Landau levels present a square-root dependence on the level index n and the external magnetic field B as a difference to the non-relativistic Landau levels (1.24), where dependence is linear. As a consequence, the spectrum (1.31) does not exhibit equidistant energy levels. Finally, the $n = 0$ Landau level is special in these systems since the band index takes only a single value (it presents half of the weight compared to the $n > 0$ energy levels[13]) and sits exactly at zero energy. The existence of this electron-hole symmetric Landau level is guaranteed by the supersymmetric structure of the Hamiltonian (1.30) and can be related to half-integer quantization of the Hall conductance [40, 142] (see also Sec. 4.5).

1.4. Drift Effects in a Disorder Potential

1.4.1. Edge states

We now move on to briefly discuss transport properties in quantum Hall systems. A very simple scheme that allows us to understand transport in this regime is the so-called edge state picture initiated by B. I. Halperin [44] and later generalized by M. Büttiker in his seminal paper [49]. This theory relies on the formation of chiral edge states due to the confinement potential while disorder in the bulk of the system creates a population of localized states that do not contribute to transport. Quantum mechanically, the edge states become the counterparts of the quasi-classical skipping orbits created by the magnetic field at the sample boundaries, where the chiral electron trajectory imposed by the Lorentz force gets reflected by the strong confinement region (see Fig. 1.6).

At zero temperature, the number of edge channels below the Fermi energy is given by the integer part of the filling factor, $[\nu_f]$, which, equivalently, yields the number of bulk Landau levels below the Fermi energy. The spatial location of the corresponding edge channel is obtained from the intersection of the Landau band with the Fermi level. We note that the disorder potential does not affect the edge states, whose velocity is always

[13] The discussion of the degeneracy per Landau level made in Sec. 1.3.1 still holds for the relativistic levels since it only depends on the symplectic structure of the phase space and is therefore equal to n_B.

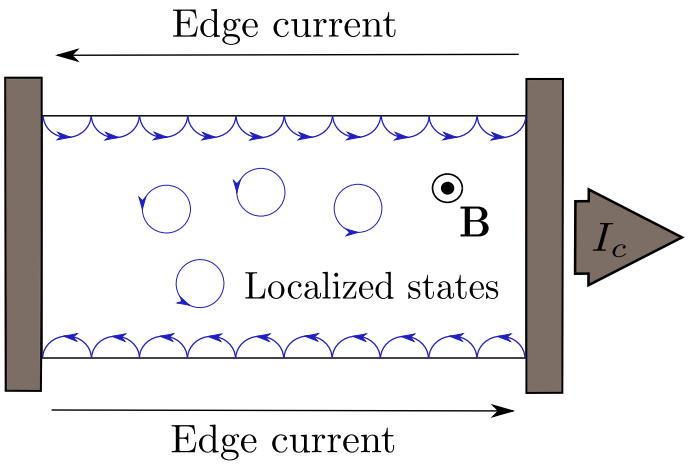

Figure 1.6 – Semiclassical picture of a two-terminal Hall bar (here charge current is labeled by I_c) under a perpendicular magnetic field $\mathbf{B}$. In the bulk of the system, the cyclotron motion is fully periodic and creates a reservoir of localized states. Next to the boundaries, confinement produces a reflection of the electron trajectories and creates counterpropagating edge channels characterized by open skipping orbits connecting the two contacts.

proportional to the derivative of the energy function and therefore, at each side of the sample, they give a current always flowing in the same direction. Within this approach, the current and the Hall conductance are computed using the S-matrix and the calculation of the transmission coefficient for each channel, which carries a current proportional to e/h, shows that each of them contributes to the (Hall) conductance with a weight proportional to e^2/h [24].The transverse resistance, which appears as a response to the Hall voltage drop, is understood as a consequence of the difference in the population between the two edges with respect to the equilibrium values. The vanishing longitudinal resistance is then explained by the absence of backscattering between the two populations of counterpropagating edge states due to a macroscopic spatial separation[14]. A nonzero longitudinal resistance can only occur if selective scattering between edge channels is possible through available states in the center of the Landau band.

The existence of edge states can be related to the bulk incompressibility of the disorder-free 2DEGs at zero temperature. This is just a consequence of the bulk-boundary correspondence [50]. The compressibility, κ, is the coefficient that measures how the area changes as a response to a variation in the pressure (for fixed particle number). It can be expressed by means of simple thermodynamic relations as a derivative of the chemical potential μ [41, 51]

$$\kappa^{-1} \equiv -S\frac{\partial P}{\partial S}\bigg|_N = n_s^2\frac{\partial \mu}{\partial n_s}. \tag{1.32}$$

The system is incompressible, $\kappa = 0$, if the electron density is a discontinuous function of the chemical potential; that is, if the spectrum presents energy gaps. As such, any type of excitation has to involve the promotion of the electron from an energy level to another and costs a finite amount of energy[15] (at least $\hbar\omega_c$ in the integer quantum Hall

[14]In addition, note that scattering between edge channels within the same edge does not affect the transmission coefficient for each channel since all states are chiral and unaffected by impurities.

[15]In a compressible system, an infinitesimal compression has an infinitesimal cost of energy.

regime), even in the thermodynamic limit. Therefore, incompressibility can be related to quasi-constant regions in the particle density and, consequently, in the Hall conductance (at least semiclassically, see Sec. 4.5). Note that the addition of smooth disorder is not expected to modify this picture qualitatively in any way.

As we have briefly seen, the edge state theory of the quantum Hall effect seems to be a natural framework to explain the quantization of the transverse resistance in this regime. It accounts for the universality of the Hall plateaus (when considering the scaling arguments that relate resistance and resistivity presented in Sec. 1.2), it is also conceptually simple and appealing (since it relies on the counting of conduction channels below the Fermi energy) and allows us to consider the role of the (possibly disordered) contacts that are present in real experiments. However, it is an incomplete theory since it must rely on the input given by microscopic calculations of the bulk properties to fully understand what happens at the transition between the Hall plateaus or the possible deviations of the perfect quantization in the Hall resistance. Moreover, the explanation of the quantization in terms of edge states does not actually imply that current must necessarily and exclusively flow only at the edges of the sample when the chemical potential is pinned between two Landau levels [52] (this is related to the arbitrariness in the choice of an origin of energies and can also be seen as a hint of the existence of an equilibrium bulk current). In addition, the analytical S-matrix approach, which is used in this form in Ref. [49], is also limited to 1D geometries with the problem becoming solvable only numerically when 2D arbitrary disorder potentials are considered. In this sense, this approach also misses the intrinsic 2D character of the longitudinal resistance when the diffusive propagation sets in at the plateaus transition. The edge state picture also misses the intrinsic topological character of the Hall conductance since in all the calculations the same arguments used in the obtention of the conductance quantization through a quantum point contact - the latter having a pure geometrical origin related to strong confinement - are considered. Finally, it is also clearly unnatural to treat, at different levels, the bulk disorder which localizes the electrons and the confining potential creating the edge channels. A unified analytical framework - the vortex formalism - that considers all the types of potential energy as a single entity and which can be used to develop an alternative theory of transport is presented in Sec. 1.5.

1.4.2. Bulk states

In Sec. 1.3.1, we saw the importance of classical mechanics to understand the motion of a particle in a 2D plane in the presence of a perpendicular magnetic field. Now, we want to get a deeper insight in the way random disorder affects the electron dynamics in 2DEGs following Refs. [36, 41].

The classical equation of motion for an electron in a plane subjected to the presence of mutually perpendicular electric $\boldsymbol{\mathcal{E}}$ and magnetic $\mathbf{B}$ fields was given in Eq. (1.4). For negligible scattering events caused by point-like impurities, *i.e.* $\omega_c\tau \to +\infty$, this equation simply describes the Lorentz force $\mathbf{f} = e[\boldsymbol{\mathcal{E}} + (\mathbf{v}/c) \times \mathbf{B}]$ acting on a charge e located at position $\mathbf{r} = (x, y)$ and time t. Using complex notation, $z = x + iy$ and $\mathcal{E} = \mathcal{E}_x + i\mathcal{E}_y \equiv |\mathcal{E}| \exp(i\phi)$, we rewrite the equation of motion as

$$\frac{d^2}{dt^2} z = i\omega_c \frac{d}{dt} z + \frac{e|\mathcal{E}|}{m^*} \exp(i\phi). \tag{1.33}$$

Performing the following change of variables, which amounts to making a Galilean trans-

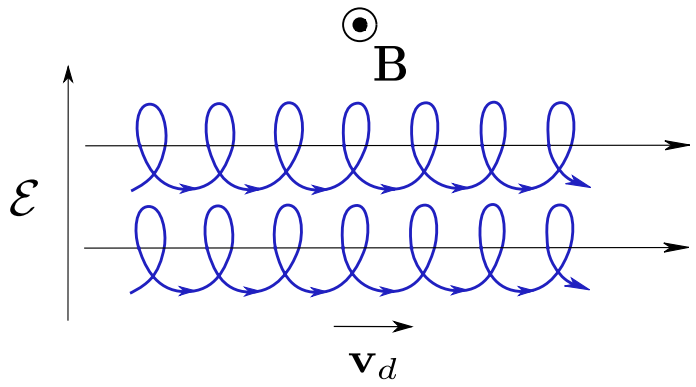

Figure 1.7 – Classical electron trajectory in the presence of mutually orthogonal electric and magnetic fields. The guiding center of the cyclotron orbit moves with drift velocity $|\mathbf{v}_d| = c|\boldsymbol{\mathcal{E}}|/B$; the resulting motion describes a helix in the 2D plane.

formation to the reference frame where the electric field vanishes,

$$z \to z' = z - i\frac{c|\mathcal{E}|}{B}\exp(i\phi)t, \tag{1.34}$$

we can easily obtain the general solution to Eq. (1.33)

$$z = \underbrace{Z_0 - i\frac{c|\mathcal{E}|}{B}\exp(i\phi)t}_{\text{Guiding center}} + \underbrace{R_c\exp(i\omega_c t)}_{\text{Cyclotron}}, \tag{1.35}$$

where $Z_0 = X_0 + iY_0$ is a constant of the motion and $R_c = |\mathbf{v}|/\omega_c$ can be fixed by the initial conditions (we assume a linear velocity $\mathbf{v} = \boldsymbol{\Pi}/m^*$ at $t = 0$). The solution has a more intuitive form written in terms of a 2D vector

$$\mathbf{r} = \mathbf{R} + R_c(\cos\omega_c t, \sin\omega_c t) \equiv \mathbf{R} + \boldsymbol{\eta}, \tag{1.36}$$

where the guiding center coordinate is given by

$$\mathbf{R} = \mathbf{R}_0 + \mathbf{v}_d t, \tag{1.37}$$

with $\mathbf{R}_0 = (X_0, Y_0)$ the initial position of the guiding center, and the Hall drift velocity

$$\mathbf{v}_d = \frac{c}{B^2}\boldsymbol{\mathcal{E}} \times \mathbf{B}. \tag{1.38}$$

Therefore, we obtain the same decomposition of the electronic motion into a slow guiding center drift, characterized by the drift velocity $\mathbf{v}_d$ orthogonal to the applied electric and magnetic fields, and a fast cyclotron rotation around the guiding center position $\mathbf{R}$, with angular velocity ω_c and (classical) cyclotron radius R_c, related to $\boldsymbol{\eta}$. The described situation was already discussed in the canonical (Poisson bracket) approach from Sec. 1.3.1 and represented pictorially in Fig. 1.5.

If the electron is placed in a slowly varying potential $V(\mathbf{r}) = e\Phi(\mathbf{r})$ such as $\boldsymbol{\mathcal{E}}(\mathbf{r}) = -\boldsymbol{\nabla}_{\mathbf{r}}\Phi(\mathbf{r})$ (where "slowly varying" means that $|\partial_j\partial_k V| \ll m^*\omega_c^2$ with $j,k \in \{x,y\}$), the decomposition (1.36) still holds. Additionally, at high magnetic fields one also has the

condition $l_B \boldsymbol{\nabla}_{\mathbf{R}} V(\mathbf{R}) \ll \hbar\omega_c$ which guarantees the ineffective energy exchange between the cyclotron and guiding center degrees of freedom. The equation of motion for the guiding center coordinate therefore reads

$$\mathbf{v}_d(\mathbf{R}) = \frac{d}{dt}\mathbf{R} = \frac{c}{eB}\hat{\mathbf{z}} \times \boldsymbol{\nabla}_{\mathbf{R}} V(\mathbf{R}). \tag{1.39}$$

Consequently, the classical guiding center is constrained to follow the equipotential lines of the (arbitrary) potential $V(\mathbf{r})$ and the motion of the electron becomes quasi-integrable. For an arbitrary potential, we can distinguish two types of equipotential lines and, as a consequence, two different kinds of electronic motion. On the one hand, at closed equipotential lines around maxima / minima of the potential, the electron is trapped and cannot contribute to macroscopic transport (it cannot move from one contact to another). Thus, the electron is said to be *localized*[16]. On the other hand, open equipotential lines contribute to transport since the electron can percolate (at a single critical energy) through the whole macroscopic sample. In this case, the electron is said to be *delocalized*. The imaginary frontier between the two types of states in energy space is called the *mobility edge*.

The former decomposition also holds at the quantum level. Indeed, it is easy to compute the equations of motion for the operator $\hat{\mathbf{R}}$ in the Heisenberg picture to get

$$\frac{d}{dt}\hat{X} = \frac{l_B^2}{\hbar}\partial_Y V(\hat{\mathbf{R}} + \hat{\boldsymbol{\eta}}) \qquad \text{and} \qquad \frac{d}{dt}\hat{Y} = -\frac{l_B^2}{\hbar}\partial_X V(\hat{\mathbf{R}} + \hat{\boldsymbol{\eta}}), \tag{1.40}$$

which amounts to the same kind of localized / delocalized[17] splitting in the motion for the (quantum) electronic states if the Landau level remains a good quantum number, *i.e.* $l_B\langle \boldsymbol{\nabla}_{\mathbf{R}} V(\mathbf{R})\rangle \ll \hbar\omega_c$ where $\langle \cdots \rangle$ refers here to the quantum average [20]. This also means that transport properties have to be described in terms of the topology of the percolation network of equipotential lines where the states, denominated *drift* states, are spatially located.

Furthermore, disorder also affects the spectral properties of the Landau levels as it was realized very soon after the discovery of the integer quantum Hall effect. Indeed, simple toy models [43, 44] already suggested that the clean Landau levels get broadened due to the potential energy (for $T = 0$), with localized states appearing at the tails of the Landau levels separated by a mobility edge from a very narrow band of delocalized states close to the center (a very visual example of this is given in Fig. 1.8 that describes a LDoS experiment). The broadening of the Landau levels can be mostly related to the energy scale coming from the motion of the drift states [45], which is typically smaller than the cyclotron energy in the case of smooth long-range potentials at high magnetic fields.

The previous semiclassical picture has obtained beautiful experimental confirmation in relatively recent high-resolution scanning tunneling spectroscopy measurements performed in surface 2DEGs in the quantum Hall regime [42]. Measurement of the local density of states (LDoS) in this system across the quantum Hall transition within the spin-split lowest Landau level shows clear experimental signatures of the existence of two types of states (see Fig. 1.8): extended (percolating) drift states lying close to the center of the disorder broadened Landau levels and energy-spread localized drift states sitting at the tails of the former (trapped either at the minima or maxima of the potential landscape).

[16] Note that this is a purely classical effect unrelated to other types of localization (Anderson localization, weak localization, Wigner localization ...).

[17] Delocalized states are also known as *extended* states.

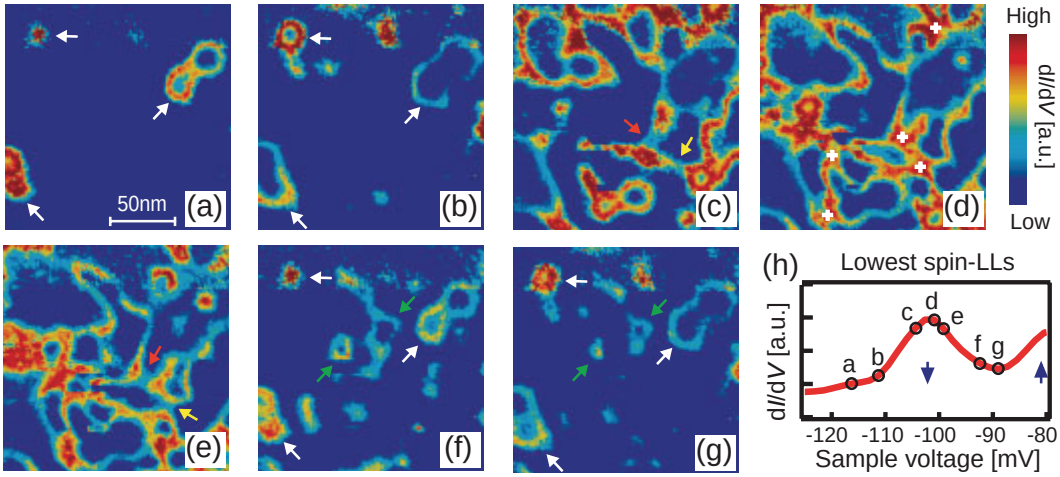

Figure 1.8 – Spatial distribution of the LDoS in the quantum Hall regime ($B = 12$ T and $T = 0.3$ K). The LDoS is mapped at various energies across the spin-split $n = 0$ Landau level as shown from (a) to (g). The color code corresponds to the different probability density of the electronic drift states (warm colors for high and cold colors for low probabilities respectively). Panel (h) gives the density of states (spatially averaged LDoS) with circles marking the energies at which the spatial maps (a)-(g) have been taken. For low energies, (a) - (b), the electron follows closed paths trapped in the equipotentials around valleys of the disorder potential. As energy is increased [close to the center of the Landau level (c) - (e)] a percolation network of extended states develops, with states getting localized again at higher energies around the maxima of the disorder potential, (f) - (g). Reprinted figure with permission from [42]. Copyright 2008 by the American Physical Society.

A localization / delocalization / localization transition driven by the disorder appears to be the mechanism that can explain the peculiar transport features of the integer quantum Hall regime. As a consequence, macroscopic transport across the sample can only appear through the quasiballistic edge channels when the chemical potential sits far from the disorder-broadened center of the Landau levels or at the percolation threshold where a diffusive electronic propagation sets in via the bulk percolation network.

A crucial final ingredient affecting the percolation image of the quantum Hall effect is the presence of saddle points in the percolation network. Going back to Eq. (1.38) which describes the Hall drift velocity, it is clear that the velocity vanishes, $\mathbf{v}_d \simeq \mathbf{0}$, for $\boldsymbol{\nabla}_{\mathbf{r}} V(\mathbf{r}) \simeq \mathbf{0}$, *i.e.* in the vicinity of saddle points of the potential landscape where two equipotential lines cross. These (rare) points are marked by yellow / red arrows and white crosses in Fig. 1.8 [panels (c) to (e)]. Saddle points are important topological points in the percolation network because they connect different sets of equipotential lines. Understanding the competition of the different mechanisms at finite temperature [45] that allow the electron to pass through these points through the whole macroscopic sample, such as quantum tunneling (also present at $T = 0$), electron-phonon scattering or thermal smearing, is very important since they seem to affect critical properties of the Hall transition like the localization exponent [42]. In particular, tunneling at finite temperature can explain why the delocalized states seem to be located in a narrow band of finite width centered around the (clean) Landau level even if they are expected to appear at a precise critical energy (or, equivalently, why the transition between the Hall plateaus is smooth at finite temperature). Moreover, saddle points form the elementary building block of percolation models [46, 47], which try to capture the dissipative features of the quantum Hall regime, or appear as the electronic analog of optical beam-splitters in mesoscopic transport experiments [48].

Finally, bulk LDoS spatial maps also confirm experimentally the intuition that in quantum Hall systems macroscopic (global) resistivities can be very different from microscopic (local) ones. This point, which is crucial and frequently poorly understood, mainly arises because 2DEGs are strongly inhomogeneous and charge transport under perpendicular magnetic fields is dominated by long-range spatial disorder correlations. As a result, the microscopic resistivity tensor, $\bar{\rho}(\mathbf{r})$, is usually very different from the effective one related to the macroscopic resistance, $\bar{\rho}$, due to the clear separation between the relevant length scales caused by the percolation features characterizing the fractal nature of the transport network[18]. This is equivalent to the fact that, at high magnetic fields, quasi-ballistic transport is determined by disorder across the whole sample instead of being smeared out in extended simple potential structures, as for purely diffusive systems (where typically one encounters self-averaging of physical properties). As a consequence, finding a microscopic description of transport in this regime requires the use of a new *palette* of theoretical methods. We shall come back to this aspect in Sec. 4.5.4 dedicated to transport properties in the presence of Rashba SO and Zeeman couplings in quantum Hall systems.

[18] Clearly, this distinction does not make any sense in clean systems but only in disordered 2DEGs in which the effective length scale characterizing average quantities is very different from the microscopic one.

1.5. Vortex Theory of the Integer Quantum Hall Effect

1.5.1. Vortex states

As we hinted in previous sections, the explanation of the (integer) quantum Hall effect has created an important body of theoretical work in the last three decades, with many concepts that have passed to nearby research topics in condensed matter physics. However, there is not, up to the present moment, a complete analytical microscopic theory of disordered quantum Hall systems which can be applied to all ranges of temperature and magnetic fields and that can be used to get insight into the local transport properties. This may seem surprising since the integer quantum Hall effect can be understood as being mainly a one-body effect. However, one should bear in mind that the quantum Hall regime is a very particular, regular and non-chaotic regime where the usual theoretical tools that are commonly used to compute transport coefficients fail. The so-called vortex theory of the quantum Hall effect offers a serious and successful attempt in the search of a fully analytical microscopic explanation of the integer quantum Hall effect [7]. We review this theory in the present chapter as a warm-up for chapters 3 and 4 where other subtle effects related to Rashba SO and Zeeman interactions in this regime are discussed.

As we have seen in Sec. 1.3, the degeneracy of the Landau levels is related to the fact that in a clean system, the position of the classical guiding center of the electronic motion can be arbitrarily chosen in the 2D plane. Quantum-mechanically, this means that there is a great liberty in the choice of a basis which diagonalizes the Hamiltonian (1.11), $\hat{\mathcal{H}}_{\text{2DEG}}\Psi = E_n\Psi$, the particular choice depending on the symmetry of the gauge invariant probability density $|\Psi|^2$. The selection of an appropriate basis for the degenerate Landau problem seems then crucial if one wants to be able to microscopically describe and understand the lifting of the quantum degeneracy by the presence of an arbitrary potential energy $V(\mathbf{r})$. In addition, the problem of lifting the energy degeneracy by an external potential energy is a subtle one since it is intrinsically nonperturbative at high magnetic fields. This is a simple consequence of the fact that, after projection onto a given Landau level, only the single energy scale related to the potential energy remains (assuming that interactions are negligible or can be treated at the mean-field level), so that perturbation theory approaches for smooth long-range potentials are doomed to fail [7].

The desired family of quantum states must also encode in some way that the Landau levels index n has a topological origin related to the quantization of the cyclotron orbit followed by the electric charge (or correspondingly, the quantization of the magnetic flux enclosed by the cyclotron orbits). We can understand this point from a semiclassical perspective: indeed, the kinetic energy may be expressed as

$$E = \frac{1}{2}m^*v^2 = \frac{1}{2}m^*(R_c\omega_c)^2, \tag{1.41}$$

and using the result for the quantum cyclotron radius resulting from the semiclassical Bohr-Sommerfeld quantization rule[19] $R_c \equiv R_n = l_B\sqrt{2n+1}$ we immediately obtain the Landau energy levels (1.24). The topological nature of the Landau levels necessarily has

[19] Computing

$$\oint_{\partial\Omega}\left[\mathbf{p} - \frac{e}{c}\mathbf{A}(\mathbf{r})\right]\cdot d\mathbf{r} = h\left[n + \gamma(\partial\Omega)\right], \tag{1.42}$$

where $\partial\Omega$ is a circular orbit of radius R_c, the term in brackets is the gauge invariant momentum, $n \in \mathbb{N}$ and γ is a generalized Maslov index. This index takes into account both the number of caustics and the Berry phase along the closed path being equal to $\gamma(\partial\Omega) = 1/2$ for the simple harmonic oscillator problem

to be reflected in the wave functions too, by a non-trivial (complex) phase[20]. Indeed, a dependence of the phase of the wave function on the Landau level index is also expected when Eq. (1.41) is written as $E = \hbar\omega_c(\Phi_c/\Phi_0)$ with $\Phi_c = \pi R_c^2 B$ the magnetic flux encircled by the cyclotron trajectory. Accordingly, n is understood as a winding number which gives the number of magnetic flux quanta Φ_0 enclosed by the cyclotron trajectory (the constant phase shift of $1/2$ is interpreted both as the signature of the quantum vacuum zero-point energy of the oscillators or, equivalently, as a trace of the Heisenberg uncertainty principle; clearly it can be anticipated to be an unimportant pure global phase factor which does not play any physical role).

The quantum states that fulfill the previous conditions can be found from the Schrödinger equation imposing the probability density to be a function of $|\mathbf{r}-\mathbf{R}|$ only, so that it reflects the classical orbital motion of the electron around a guiding-center $\mathbf{R}$. In the symmetrical gauge, $\mathbf{A}(\mathbf{r}) = \mathbf{B}\times\mathbf{r}/2$, these so-called vortex states [54, 55] read

$$\Psi_{n,\mathbf{R}}(\mathbf{r}) = \frac{1}{\sqrt{2\pi l_B^2 n!}}\left(\frac{z-Z}{\sqrt{2}l_B}\right)^n \exp\left(-\frac{|z|^2+|Z|^2-2Zz^*}{4l_B^2}\right), \tag{1.43}$$

where $z = x+iy$ and $Z = X+iY$ are complex numbers whose real and imaginary part represents the coordinates of the position of the electron and the center of the vortex respectively[21]. Note that the constraint $n \geq 0$ automatically excludes the states with negative vorticity (with polynomial part antianalytic in the complex variable) which have no semiclassical counterpart (they would represent electrons rotating in the opposite sense to that imposed by Lorentz force).

The vortex states, written as $\Psi_{n,\mathbf{R}}(\mathbf{r}) = \langle\mathbf{r}|n,\mathbf{R}\rangle$ within the Dirac notation, are labeled by the collection of quantum numbers $\nu = \{n,\mathbf{R}\}$ where $\mathbf{R} = (X,Y)$ is a doubly continuous quantum number that characterizes the position of the zeros of the wave function (vortex-like phase singularities) in the 2D plane. These vortices also appear associated to the winding number n. Note that the states associated to the lowest Landau level $n = 0$ are special since, as a difference to the states in excited Landau levels $n > 0$, they do not present any phase singularity, *i.e.* they are not a vortex. In addition, it is also important to stress that the continuous quantum number corresponds to a *unique degree of freedom* and not two, as we could have naïvely assumed when it is written in vector notation. This is because the vortex wave function is an object with image in the complex space, $\Psi : \mathbb{R} \to \mathbb{C}$ where the guiding center coordinates X and Y are not independent due to the commutation relation $[\hat{X},\hat{Y}] = il_B^2$.

An important property of the vortex states is that they form a semiorthogonal over-complete basis with overlap

$$\langle n_1,\mathbf{R}_1|n_2,\mathbf{R}_2\rangle = \delta_{n_1,n_2}\langle\mathbf{R}_1|\mathbf{R}_2\rangle, \tag{1.44}$$

[53]. The left-hand side integral can be easily shown to be equal to $R_c^2 h/(2l_B^2)$ so that $R_c = l_B\sqrt{2n+1}$. Alternatively, one can verify that the quantum average of the operator $\hat{\mathbf{R}}^2$ by the eigenstates of Eq. (1.23) is equal to $l_B^2(2n+1)$ and define $R_c \equiv \langle\hat{\mathbf{R}}^2\rangle^{1/2}$ [52].

[20] This is logical because the Hamiltonian $\hat{\mathcal{H}}_{2\mathrm{DEG}}$ obtained from Eq. (1.11) with the canonical momentum operator substituted by its representation in real space $\hat{\mathbf{p}} \to -i\hbar\boldsymbol{\nabla}_{\mathbf{r}}$ is also complex.

[21] We identify the two-dimensional physical space with the complex plane and define the usual bijection between the vectors $(x,y) \in \mathbb{R}^2$ [resp. $(X,Y) \in \mathbb{R}^2$] and the complex numbers $z = x+iy \in \mathbb{C}$ [resp. $Z = X+iY \in \mathbb{C}$].

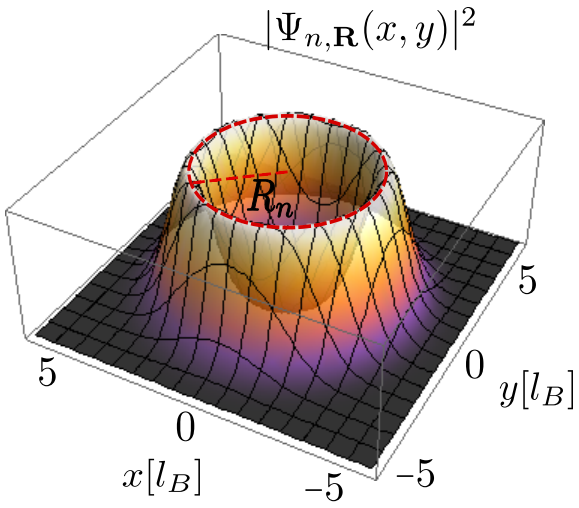

Figure 1.9 – Probability density $|\Psi_{n,\mathbf{R}}(\mathbf{r})|^2$ of a vortex state (here shown for $n = 5$ and $\mathbf{R} = \mathbf{0}$). Lengths are measured in units of l_B which also gives the typical transverse spread of the wave function around the maximum (the average position of this maximum coincides with the quantum cyclotron radius $R_n = l_B\sqrt{2n+1}$). The vortex state presents, for $n \geq 1$, a phase singularity or topological defect around the arbitrary guiding center position $\mathbf{R}$. Since they do not impose any particular symmetry in the degeneracy space, vortex states are expected to be the preferred basis to properly incorporate, in the theoretical description of the quantum Hall regime, arbitrary disorder potentials.

where

$$\langle \mathbf{R}_1|\mathbf{R}_2\rangle = \exp\left[-\frac{(\mathbf{R}_1-\mathbf{R}_2)^2 - 2i\hat{\mathbf{z}}\cdot(\mathbf{R}_1\times\mathbf{R}_2)}{4l_B^2}\right]. \tag{1.45}$$

This overlap defines the coherent states algebra with respect to the continuous quantum number $\mathbf{R}$ [56]. Accordingly, the overlap is almost zero when the two vortex states are spatially separated by a distance larger than a few magnetic lengths, and with a probability density that decreases with the typical Gaussian shape of the coherent states

$$|\langle \mathbf{R}_1|\mathbf{R}_2\rangle|^2 = \exp\left[-\left|\frac{\mathbf{R}_1-\mathbf{R}_2}{2l_B}\right|^2\right]. \tag{1.46}$$

Indeed, the fact that the guiding center presents the coherent states algebra is not surprising as Eq. (1.43) can be obtained both by using the guiding center displacement operator [57] or from the eigenstates of the operator[22] $\hat{b}_-$ [38]. The two methods are commonly used in quantum optics to generate the coherent states of the radiation field.

Therefore, the vortex states are orthogonal with respect to the discrete quantum number n which characterizes the eigenenergies while they remain non-orthogonal with respect to the quantum number describing the degeneracy of the Landau levels. Importantly, we must note that they obey a completeness relation,

$$\int \frac{d^2\mathbf{R}}{2\pi l_B^2}\sum_{n=0}^{+\infty}|n,\mathbf{R}\rangle\langle n,\mathbf{R}| = \mathbb{1}_{\text{orb}}, \tag{1.47}$$

[22] We have $\hat{b}_-|n,\mathbf{R}\rangle = \frac{Z}{\sqrt{2}l_B}|n,\mathbf{R}\rangle$

which allows us to project the 2D electron dynamics (equation of motion) onto this representation. Relations (1.44) and (1.47) are proved in Appendix A.

The vortex basis provides considerable advantages for the description of the lifting of the macroscopic degeneracy of the Landau levels by an arbitrary (smooth) potential landscape $V(\mathbf{r})$. The fundamental reason is that the degeneracy quantum number $\mathbf{R}$ does not result from a particular symmetry imposed to the wave functions[23], in contrast to the commonly used Landau basis or circular basis, where it can be obtained by imposing translational or rotational invariance respectively. Instead, the degeneracy in the vortex representation is incorporated locally through the continuous vortex position $\mathbf{R}$ without the need of specifying the shape of the quantum cell [note that the degeneracy per quantum state (1.27) follows immediately from the phase space volume in the closure relation, Eq. (1.47)]. As a consequence, we expect the vortex states to be the preferred set of states for a realistic description of disordered quantum Hall systems since they should be characterized by certain robustness with respect to random spatial variations of the potential energy together with the fact that they encode the peculiar nature of the Landau level index in the form of a topological defect. Finally, they should also be preferentially selected for the development of a controlled theory built on a gradient expansion of the potential energy (as opposed to a perturbation expansion in the amplitude of the potential) presented in the next section, where the degeneracy is treated from the perspective of differential geometry, thanks to the continuous character of the quantum number $\mathbf{R}$.

1.5.2. The gradient expansion

We now consider that the single spinless electron feels, in addition to the external magnetic field, the presence of a potential energy $V(\mathbf{r})$ so that the full Hamiltonian reads

$$\hat{\mathcal{H}} = \hat{\mathcal{H}}_{\mathrm{2DEG}} + \hat{V}, \tag{1.48}$$

with $\hat{V} \equiv V(\hat{\mathbf{r}})$. The most natural approach, in the physicist mindset, is to consider the diagonalization of Eq. (1.48) and further computation of transport coefficients using the perturbation theory toolbox. This framework can be used either for a single disorder realization or, by performing disorder averaging, for many possible disorder configurations.

Nevertheless this way of considering the current theoretical problem presents several inconvinients. First, the vortex basis introduced previously cannot be used within a stationary perturbation theory framework due to the lack of orthogonality of the unperturbed states. Second, we have also mentioned in the previous section that the lifting of the energy degeneracy within a single Landau level is an intrinsically nonperturbative problem since there is only a single energy scale related to the fluctuations of the arbitrary smooth potential energy. The lack of a small parameter for the energies and the macroscopic degeneracy makes extremely difficult the control of perturbation theory. Finally, regular motion of the guiding center at the constant energy contours of the potential energy landscape yields the procedure of averaging over the disorder configurations questionable at high magnetic fields, at least at the microscopic level.

We can nevertheless use the vortex representation, thanks to Eq. (1.47), within a Green's function formalism which we briefly describe now. Within this framework, we can circumvent the problem of the absence of any small parameter for perturbation theory by the use of a nonperturbative gradient expansion in the potential energy. The gradient

[23] Note, however, that $\hat{\mathbf{R}}$ *is* a symmetry from the point of view of the constants of motion.

expansion relies on the simple fact that our high magnetic field problem, in the presence of disorder potential (1.48), presents two different length scales: the magnetic length l_B and the typical correlation length of the potential ξ. At high magnetic fields, the magnetic length is the smallest length scale compared to ξ, *i.e.* $l_B \ll \xi$. In particular, $l_B \simeq 8$ nm at $B = 10$ T to be compared to $\xi \simeq 100$ nm for typical smooth disorder potentials affecting 2DEGs. As a consequence, one sees the appearance of a hierarchy of quasi-local energy scales

$$V(\mathbf{r}) \gg l_B \partial_j V(\mathbf{r}) \gg l_B^2 \partial_j \partial_k V(\mathbf{r}) \dots \tag{1.49}$$

for $j, k \in \{x, y\}$. This hierarchy, controlled by the magnetic length, naturally orders the contributions of the potential systematically by their magnitude as a function of the magnetic field. This also gives a controlled approximation scheme in which a quantitatively accurate description of the electron dynamics can be obtained by a finite number of contributions from Eq. (1.49) (note that this is so since experiments always take place at finite temperature, which sets a cut-off to the series expansion). The first term in the series is responsible of the lifting of the Landau level degeneracy while the rest contributes either to Landau level mixing or to different subtle quantum effects which become visible only at very low temperatures.

Let us now outline the more technical details of the formalism. The Green's operators associated to the (time-independent) Hamiltonian (1.48) are defined by the operator equation

$$(\omega - \hat{\mathcal{H}} \pm i0^+)\hat{G}^{R,A}(\omega) = \mathbb{1}, \tag{1.50}$$

where the plus (minus) sign corresponds to the retarded (advanced) components, 0^+ is a positive infinitesimal quantity which encodes the information about the boundary conditions for time evolution and $\mathbb{1}$ is the identity operator. Here ω indicates the energy resulting from the Fourier transformation of the relative time dependence $\tau = t_1 - t_2$ in the Dyson equation[24]. The kernel of the Green's operator is the so-called Green's function which can be written in terms of the field operators $\hat{\psi}(x)$ [evaluated at a given point of the space-time $x = (\mathbf{r}, t)$] expressed in the electronic representation

$$G^{R,A}(x_1; x_2) = \mp i\Theta\left[\pm(t_1 - t_2)\right] \langle [\hat{\psi}(x_1), \hat{\psi}^\dagger(x_2)]_+ \rangle, \tag{1.51}$$

with $\Theta(t)$ is the Heaviside step function [$\Theta(t) = 0$ if $t < 0$ and $\Theta(t) = 1$ if $t \geq 0$], $[\,\cdot\,,\,\cdot\,]_+$ represents the anticommutator[25] and the brackets $\langle \cdots \rangle$ represent the thermodynamic average in the grand-canonical ensemble.

A change of basis can be easily performed using Eq. (1.47) at the level of the operator equation (1.50) in order to obtain the equation of motion for the Green's function in the vortex representation

$$\begin{aligned}(\omega - E_{n_1} \pm i0^+)G^{R,A}(n_1, \mathbf{R}_1; n_2, \mathbf{R}_2; \omega) &= \langle n_1, \mathbf{R}_1 | n_2, \mathbf{R}_2 \rangle \\ &+ \int \frac{d^2\mathbf{R}_3}{2\pi l_B^2} \sum_{n_3=0}^{+\infty} \langle n_1, \mathbf{R}_1 | \hat{V} | n_3, \mathbf{R}_3 \rangle G^{R,A}(n_3, \mathbf{R}_3; n_2, \mathbf{R}_2; \omega).\end{aligned} \tag{1.52}$$

[24] Because we consider a time-independent Hamiltonian, the energy is conserved and the Green's operators must only depend on the time difference τ.

[25] The anticommutator of two arbitrary operators $\hat{A}$ and $\hat{B}$ is defined by $[\hat{A}, \hat{B}]_+ \equiv \hat{A}\hat{B} + \hat{B}\hat{A}$.

with $G^{R,A}(n_1,\mathbf{R}_1;n_2,\mathbf{R}_2;\omega)=\langle n_1,\mathbf{R}_1|\hat{G}^{R,A}(\omega)|n_2,\mathbf{R}_2\rangle$. The matrix elements of the potential can be written in the vortex basis as

$$\langle n_1,\mathbf{R}_1|\hat{V}|n_2,\mathbf{R}_2\rangle=\int d^2\mathbf{r}\,\Psi^*_{n_1,\mathbf{R}_1}(\mathbf{r})V(\mathbf{r})\Psi_{n_2,\mathbf{R}_2}(\mathbf{r}), \tag{1.53}$$

$$=\langle\mathbf{R}_1|\mathbf{R}_2\rangle\tilde{v}_{n_1;n_2}(\mathbf{R}_1;\mathbf{R}_2), \tag{1.54}$$

where in the last line we transferred all the non-analytic dependence on the magnetic length to the vortex overlap (1.45). The function $\tilde{v}_{n_1,n_2}(\mathbf{R}_1;\mathbf{R}_2)$ can then be expanded as a series of powers of the magnetic length l_B provided that the potential energy $V(\mathbf{r})$ is smooth. This strategy is used in chapter 4 to consider quantum transport properties of 2DEGs with Rashba SO and Zeeman interactions at high magnetic fields. We can also easily check that it is possible to express the full Green's function self-consistently as

$$G^{R,A}(n_1,\mathbf{R}_1;n_2,\mathbf{R}_2;\omega)=\langle\mathbf{R}_1|\mathbf{R}_2\rangle\tilde{g}^{R,A}_{n_1;n_2}(\mathbf{R}_1;\mathbf{R}_2;\omega), \tag{1.55}$$

so that the Green's function is determined if, and only if, the vortex Green's function $\tilde{g}(\mathbf{R}_1;\mathbf{R}_2;\omega)$ is known. Eq. (1.52) then reads

$$(\omega-E_{n_1}\pm i0^+)\tilde{g}^{R,A}_{n_1;n_2}(\mathbf{R}_1;\mathbf{R}_2;\omega)=\delta_{n_1,n_2}$$
$$+\int\frac{d^2\mathbf{R}_3}{2\pi l_B^2}\sum_{n_3=0}^{+\infty}\tilde{v}_{n_1;n_3}(\mathbf{R}_1;\mathbf{R}_3)\frac{\langle\mathbf{R}_1|\mathbf{R}_3\rangle\langle\mathbf{R}_3|\mathbf{R}_2\rangle}{\langle\mathbf{R}_1|\mathbf{R}_2\rangle}\tilde{g}^{R,A}_{n_3;n_2}(\mathbf{R}_3;\mathbf{R}_2;\omega). \tag{1.56}$$

where

$$\frac{\langle\mathbf{R}_1|\mathbf{R}_3\rangle\langle\mathbf{R}_3|\mathbf{R}_2\rangle}{\langle\mathbf{R}_1|\mathbf{R}_2\rangle}=\exp\left[-\frac{1}{2l_B^2}\left(\mathbf{R}_3-\mathbf{R}_{12}\right)^2\right]. \tag{1.57}$$

with $\mathbf{R}_{12}=[\mathbf{R}_1+\mathbf{R}_2+i(\mathbf{R}_1-\mathbf{R}_2)\times\hat{\mathbf{z}}]/2$ a particular (complex) combination of the center of mass and relative coordinates of two vortex positions. We can now perform the change of variables $\mathbf{r}=\sqrt{2}l_B\mathbf{r}'+\mathbf{R}_{12}$ in Eq. (1.53) so that the potential matrix elements are actually functions of $\mathbf{R}_{12}$, *i.e.* $\tilde{v}_{n_1;n_2}(\mathbf{R}_1;\mathbf{R}_2)\equiv\tilde{v}_{n_1;n_2}(\mathbf{R}_{12})$. This functional form implies in turn that the vortex Green's function must also depend on the vortex coordinates through the same combination[26]. In addition, it also implies that the full nonlocal Green's function is completely specified once the vortex Green's function $\tilde{g}_{n_1;n_2}(\mathbf{R}_{12},\omega)$ is known at coinciding vortex positions $\mathbf{R}_1=\mathbf{R}_2\equiv\mathbf{R}$. This diagonal representation is a well-known property of the coherent states [58].

Using this information in Eq. (1.56), the integral over the vortex position $\mathbf{R}_3$ can be performed analytically [130] and we get a closed equation for the vortex Green's function $\tilde{g}(\mathbf{R},\omega)$

$$(\omega-E_{n_1}\pm i0^+)\tilde{g}^{R,A}_{n_1;n_2}(\mathbf{R};\omega)=\delta_{n_1,n_2}+\sum_{n_3}\tilde{v}_{n_1;n_3}(\mathbf{R})\bowtie\tilde{g}^{R,A}_{n_3;n_2}(\mathbf{R};\omega), \tag{1.58}$$

where we the symbol $\bowtie$ represents the bidifferential infinite order operator

$$\bowtie=\exp\left(\frac{l_B^2}{2}\overleftarrow{\partial}_-\overrightarrow{\partial}_+\right). \tag{1.59}$$

[26]This can be proved using that $(\partial_{X_1}-i\partial_{Y_1})f(\mathbf{R}_{12})=(\partial_{X_2}+i\partial_{Y_2})f(\mathbf{R}_{12})=0$ where f is any arbitrary smooth differentiable function of the vortex coordinates.

Here $\partial_\pm \equiv \partial_X \pm i\partial_Y$ and the arrow above each of the partial derivatives points out to which of the factors (left/right) the partial derivative has to be applied. The operator (1.59) couples the partial derivatives of the matrix elements of the potential and the local vortex Green's function in a non-trivial way. However, they can be decoupled by performing a rotation in phase space

$$v_{n_1;n_2}(\mathbf{R}) = T_{\mathbf{R}}^{-1}\tilde{v}_{n_1;n_2}(\mathbf{R}), \tag{1.60a}$$

$$g_{n_1;n_2}(\mathbf{R};\omega) = T_{\mathbf{R}}^{-1}\tilde{g}_{n_1;n_2}(\mathbf{R};\omega), \tag{1.60b}$$

where $T_{\mathbf{R}}$ represents the differential Gaussian operator

$$T_{\mathbf{R}} \equiv \exp\left(\frac{l_B^2}{4}\Delta_{\mathbf{R}}\right), \tag{1.61}$$

with $\Delta_{\mathbf{R}}$ the Laplacian taken with respect to the vortex position. This transformation, which can be seen as an infinite order resummation of a whole class of l_B dependent terms, maps the Dyson equation (1.59) to

$$(\omega - E_{n_1} \pm i0^+)g^{R,A}_{n_1;n_2}(\mathbf{R};\omega) = \delta_{n_1,n_2} + \sum_{n_3} v_{n_1;n_3}(\mathbf{R}) \star g^{R,A}_{n_3;n_2}(\mathbf{R};\omega), \tag{1.62}$$

where now the symbol $\star$ denotes the bidifferential infinite order symplectic operator defined as

$$\star \equiv \exp\left[i\frac{l_B^2}{2}(\overleftarrow{\partial}_X\overrightarrow{\partial}_Y - \overleftarrow{\partial}_Y\overrightarrow{\partial}_X)\right]. \tag{1.63}$$

Under this form, Dyson equation is now trivial for 1D potentials since the coupled pairs of partial derivatives now always act in orthogonal directions in phase space.

1.5.3. Mixed phase-space formulation at high magnetic fields

The $\star$ product defined in Eq. (1.63) [and the $\bowtie$ product appearing in Eq. (1.59)] can be related to the so-called deformation quantization approach to quantum mechanics [59, 60]. This is a third independent formulation of quantum mechanics, set up in phase space and alternative to the standard Hilbert space and path integral frameworks, where the central object is the Wigner function instead of the wave function. Pioneered by Wigner, Weyl, Moyal and Groenewold seventy years ago, this formalism was recognized as an autonomous theory after the mathematical works of Bayen *et al.* [61]. For 2DEGs under perpendicular magnetic fields, we are dealing more precisely with a mixed phase space deformation quantization theory that combines discrete Landau levels with a (continuous) phase space for the guiding center coordinates $\mathbf{R} = (X, Y)$. The latter is characterized by the commutator $[\hat{X}, \hat{Y}] = il_B^2$ where we can clearly see that the 1D conjugated variables (x, p_x) have been replaced by (X, Y) and that the role of Planck's constant is played by the magnetic field dependent quantity l_B^2.

In the deformation quantization theory, the quantum algebra for non-commuting operators is expressed in terms of phase space functions with the noncommutativity being instead transferred to the particular product between them. The product between the functions is said to be deformed with respect to the usual product, with l_B^2 (or $\hbar$ in the conventional deformation quantization theory) being the deformation parameter. As such, classical and semiclassical limits can be retrieved rather transparently compared to the

usual operator approach since classical mechanics is obtained smoothly by a continuous and controlled limit of the deformation parameter, avoiding any singular correspondence between classical and quantum mechanics as in the Dirac's rule (1.20). For our Green's function theory the semiclassical limit, $l_B \to 0$, corresponds to the limit of infinite magnetic field $B \to +\infty$ where the guiding center dynamics is completely classical, *i.e.* $[\hat{X}, \hat{Y}] = 0$, with the vortex and electronic coordinates fully equivalent.

The $\star$ product can also be understood in this context as a magnetic version of the so-called Moyal-Groenewold $\star$ product while $\bowtie$ is the equivalent to the Wick-Voros product. Both products have been widely used in string theory, spin field theory and, in general, in noncommutative field theory [62]. They originate from a generalized Weyl map [63, 64] which associates phase space functions to operators according to certain quantization rules (Weyl or symmetric and Wick or normal order, respectively). As a consequence, the Groenewold-Moyal and Wick-Voros products control the dynamics of different kind of mathematical objects. Wick-Voros $\bowtie$ product drives the dynamics of Husimi functions[27] while Groenewold-Moyal $\star$ product can be related to Wigner functions [63].

In the framework of deformation quantization, the operator $T_{\mathbf{R}}$ defined in Eq. (1.61) has also a very precise meaning. First, it is the (invertible) transition operator which dresses the Wick-Voros product into the Groenewold-Moyal product. This passage, although mathematically a trivial rotation in phase space, has highly non-trivial consequences since it allows to easily consider the edge states problem [quasi-1D potentials $V(\mathbf{r})$]. Second, the action of the operator onto the Green's function and the potential (1.60a)-(1.60b) can be physically understood as the delocalization of the vortex states (which are initially localized in any direction) along the equipotential lines of the potential, $\boldsymbol{\nabla}_{\mathbf{r}} V(\mathbf{r}) = \mathbf{0}$. As a final remark, it is worth mentioning that in the $\star$ representation of the Green's function we are actually dealing with a peculiar Green's function instead of Wigner functions. The difference can be seen at the level of the equation of motion: Wigner functions satisfy a homogeneous $\star$-value equation, $\mathcal{H} \star f = Ef$ [59], completely analog to the Schrödinger equation for the wave functions; on the other hand the vortex Green's functions $g(\mathbf{R}; \omega)$ verify an inhomogeneous Dyson equation (1.62) which, in addition, incorporates the causality principle (boundary conditions for time evolution) that is missing in the definition of the wave function or the Wigner function.

1.5.4. General solution for closed and open quantum systems

At high magnetic fields, the energy exchange between the vortex and cyclotron motion becomes extremely ineffective due to their very different timescales. This is similar to the Born-Oppenheimer approximation in molecular physics where the energy exchange between the nuclear and electronic degrees of freedom in a molecule can be strongly reduced due to the fact that the quantum electron motion in the atomic shells is much faster than that of the nucleus within the atomic core. There is, however, a crucial difference between both situations: in 2DEGs under perpendicular magnetic fields the kinetic energy is quantized into Landau levels and, therefore, energy exchange is possible only if the latter (topological) index is modified (that would correspond to a deformation of the classical cyclotron orbit) which is forbidden due to the large cyclotron gap $\hbar\omega_c$. Therefore, we can consider that in this situation Landau level mixing becomes negligible [or the projection into a single

[27] The Husimi function is defined as the trace of the density matrix over the basis of coherent states and turns out to be a Gaussian-smoothed Wigner function.

Landau level is allowed, $v_n(\mathbf{R}) \equiv v_{n;n}(\mathbf{R})$ and similarly for the vortex Green's function, $g_n^{R,A}(\mathbf{R};\omega) \equiv g_{n;n}^{R,A}(\mathbf{R};\omega)$] with vortex motion reduced to quasi-1D ballistic dynamics along the equipotential energy contours. Mathematically, this regime can be characterized by $\omega_c \to +\infty$ while keeping l_B finite. The consideration of a finite magnetic length allows us to account for quantum effects within the vortex dynamics.

The vortex formalism is even more powerful in this sense since it allows to find a general analytical solution for any 2D potentials, the solution being exact for all the 2D quadratic potentials. These toy models present more than simple academic interest since they are a valuable approximation for any random smooth potentials near critical points. Moreover, they show that the chosen vortex representation is characterized by a stable set of quantum numbers $\nu = \{n, \mathbf{R}\}$. To be concrete, a potential $V(\mathbf{R})$ can be generally defined by its Taylor expansion around $\mathbf{R}_c$, which is chosen to be the point where the potential gradient vanishes. Assuming that only the terms up to second order in the Taylor expansion are relevant, we can expand the $\star$ product operator (1.63) and use the symmetrized form of Dyson equation (1.62) to get a second order partial differential equation defining the vortex Green's function

$$\left\{\omega_n + \frac{l_B^4}{8}\left[(\partial_Y^2 v_n)\partial_X^2 + (\partial_X^2 v_n)\partial_Y^2 - 2(\partial_X\partial_Y v_n)\partial_X\partial_Y\right]\right\} g_n^{R,A}(\mathbf{R};\omega) = 1, \tag{1.64}$$

where $\omega_n = \omega - E_n - v_n(\mathbf{R}) \pm i0^+$ and $v_n \equiv v_n(\mathbf{R})$ is equal to the (exact) expression[28] [132]

$$v_n(\mathbf{R}) = V(\mathbf{R}) + \frac{l_B^2}{2}\left(n + \frac{1}{2}\right)\Delta_{\mathbf{R}} V(\mathbf{R})\Big|_{\mathbf{R}=\mathbf{R}_c}. \tag{1.65}$$

The antisymmetric form yields the constraint $[\boldsymbol{\nabla}_{\mathbf{R}} v_n(\mathbf{R}) \times \boldsymbol{\nabla}_{\mathbf{R}}\, g_n^{R,A}(\mathbf{R};\omega)] \cdot \hat{\mathbf{z}} = \mathbf{0}$ from which we can deduce that, at this order, the 2D vortex Green's function has the same equipotential lines as the potential $V(\mathbf{R})$. Eq. (1.64) then can be reduced to an ordinary differential equation characterized by the geometrical parameters

$$\gamma = \frac{l_B^4}{4}\left[\partial_X^2 v_n\, \partial_Y^2 v_n - (\partial_X\partial_Y v_n)^2\right]_{\mathbf{R}=\mathbf{R}_c}, \tag{1.66}$$

$$\eta = \frac{l_B^4}{8}\left[\partial_X^2 v_n\, (\partial_Y v_n)^2 + \partial_Y^2 v_n\, (\partial_X v_n)^2 - 2\partial_X v_n\, \partial_Y v_n\, \partial_X\partial_Y v_n\right]_{\mathbf{R}=\mathbf{R}_c}. \tag{1.67}$$

For global quadratic potentials, γ is independent of the choice of the critical point and both coefficients are related by the identity $\boldsymbol{\nabla}_{\mathbf{R}}\eta(\mathbf{R}) = \gamma\boldsymbol{\nabla}_{\mathbf{R}} v_n(\mathbf{R})$ for $\mathbf{R} = \mathbf{R}_c$. Moreover, the coefficient γ can be straightforwardly linked to the determinant of the Hessian matrix for the potential energy function, namely $[H_V]_{jk}(\mathbf{R}) = \partial_j\partial_k v_n(\mathbf{R})$ with $j, k \in \{X, Y\}$. Its value defines a natural energy scale related to the Gaussian curvature of the potential landscape, $E_{\text{curvature}} = \sqrt{|\gamma|}$ while its sign determines the particular nature of the critical point $\mathbf{R}_c$ at which the gradient of the potential vanishes. Positive values, $\gamma > 0$, characterize confining parabolic potentials (with a global maximum or minimum) while negative ones, $\gamma < 0$, are particular of open hyperbolic potentials (saddle-points). The transition between both situations is achieved at $\gamma = 0$ (absence of Gaussian curvature) which corresponds to the particular case of a quadratic 1D potential[29].

[28] See also Sec. 4.2.1

[29] Actually, we have $\gamma = \eta = 0$ for *all* 1D potentials, not only the purely quadratic.

The general solution to Eq. (1.64) whose derivation can be found in Ref. [132], has a very simple form in the time representation

$$g_n^{R,A}(\mathbf{R};\tau) = \mp i\Theta(\pm\tau)\frac{\exp\left[-i\frac{\eta}{\gamma^{3/2}}\tan(\sqrt{\gamma}t)\right]}{\cos(\sqrt{\gamma}\tau)}\exp\left\{i\tau\left[\frac{\eta}{\gamma} - v_n(\mathbf{R}) \pm i0^+\right]\right\}. \quad (1.68)$$

This vortex Green's function embraces all the possible dynamical solutions depending on the values of the geometrical invariants (1.66)-(1.67) characterizing the potential energy landscape. Indeed, for $\gamma > 0$, the vortex Green's function is periodic in time (with period $2\pi/\sqrt{\gamma}$) and displays a discrete set of real poles related to the quantized energy levels in a (local) parabolic potential typical of quantum dots. For $\gamma < 0$, *i.e.* saddle point that models a quantum point contact, the trigonometric functions can be substituted by their hyperbolic counterparts through analytic continuation using $\sqrt{\gamma} = i\sqrt{|\gamma|}$. This introduces lifetime effects characteristic of tunneling processes defined by a time scale of order $\hbar/\sqrt{|\gamma|}$.

As a final remark, one can wonder when the subtleties related to curvature energy (or even smaller energy scales related to higher order derivatives of the potential energy) have to be considered. In this case, we may easily be convinced that temperature sets a cut-off energy k_BT that allows us to disregard fine structure effects in the gradient expansion of the potentials. In the particular case of curvature (second order derivatives taken with respect to orthogonal directions), we can neglect these effects as long as $k_BT > E_{\text{curv}}$ and assume directly that the coefficient $\gamma = 0$. This approximation tantamount to replace the $\star$ product by the simple product between functions and can be used to characterize the drift states moving in a weakly curved potential landscape (in this form, we shall use it throughout chapter 3 when SO interaction is also taken into account).

Chapter 2

Rashba Spin-Orbit Interaction in Two-Dimensional Electron Gases

In this chapter, we gently introduce the second of the two main ingredients needed in the first part of this thesis manuscript, namely Rashba spin-orbit (SO) interaction. We first discuss the physical origin of this type of SO coupling, how it appears in low dimensional semiconductors and the most important features of the Rashba model Hamiltonian. We then break time-reversal symmetry and study the influence of a perpendicular magnetic field in clean 2DEGs that present this Rashba SO and Zeeman interactions, focusing our attention on the peculiar spectral properties presenting a mixed non-relativistic / relativistic character. Finally, we move on to discuss the influence of Rashba SO coupling in the spin dynamical properties, considering in particular the spin currents and the so-called spin Hall effect, both in the absence and the presence of perpendicular magnetic fields.

Dans ce chapitre, nous introduisons doucement le deuxième ingrédient requis dans la première partie de ce manuscrit : le couplage spin-orbite (SO) de type Rashba. Primo, nous discutons son origine physique, comment ce type de couplage apparaît-il dans les semiconducteurs de basse dimensionalité et les propriétés les plus importantes de l'Hamiltonien du modèle de Rashba. Ensuite, nous brisons la symétrie par renversement du temps et étudions l'influence d'un champ magnétique perpendiculaire dans les gaz d'électrons bidimensionnels qui présentent l'effet simultané du couplage SO Rashba et l'interaction Zeeman en absence de désordre. Concrètement, nous nous focalisons dans les propriétés spectrales de ces gaz qui manifestent un caractère composé d'éléments non-relativistes / relativistes. Finalement, nous continuons avec une discussion des effets du couplage SO Rashba dans les propriétés dynamiques du spin de l'électron, en considérant les courants de spin et l'effet Hall de spin en absence et en présence de champs magnétiques perpendiculaires au plan 2D.

2.1. Why Consider Spin-Orbit Interaction?

During the last two decades, the study of SO interaction in semiconductor heterostructures has attracted a considerable amount of attention from the condensed matter commu-

nity. One the main reasons for this keen interest comes from the success of spin electronics or *spintronics* in metallic and semiconductor nanostructures, where the spin degree of freedom of the charge carriers can be manipulated in a controllable way with the objective of generating spin-polarized currents [65]. From this point of view, semiconductor spintronics has also evolved into a rich research subfield [of spintronics] both from the theoretical and experimental sides. On the one hand, this is due to the interesting fundamental physics involved (part of which to be discussed in this chapter) while on the other hand, also because of the numerous potential applications and devices whose utility spans from information processing to quantum computation[1] (see, for example, Ref. [66]). In this context, SO coupling has been recognized as a very well adapted tool to locally inject, transfer or detect the spin in a coherent way. Moreover, one hopes to control the electronic spin by local electric fields created by external voltage gates once the charge and spin degrees of freedom become coupled. In this situation, an implementation of spintronic devices in 2DEGs such as the famous spin field effect transistor [67] or its counterpart in the quantum Hall regime [68, 69], both considered for the type of SO interaction in which we are interested in this thesis, could be possible.

2.2. Rashba Spin-Orbit Coupling in Low Dimensional Semiconductors

2.2.1. Physical origin of the spin-orbit interaction

The spin degree of freedom of the electron is an internal parameter whose existence was proposed in order to explain the astonishing experimental results obtained by Stern and Gerlach in 1922. At that time, these researchers wanted to corroborate the atomic theory of Bohr-Sommerfeld and observed the deflection of neutral silver atoms when they where sent through an inhomogeneous magnetic field [70]. Subsequent detailed studies by Uhlenbeck and Goudsmit [71] suggested that the electron has an intrinsic magnetic moment due to an internal degree of freedom with dimensions of angular momentum: spin $\mathbf{S} = (\hbar/2)\boldsymbol{\sigma}$ [we remind that we note by $\boldsymbol{\sigma} = (\sigma_x, \sigma_y, \sigma_z)$ the vector whose components are the Pauli matrices]. An electronic intrinsic magnetic moment can be written as $\boldsymbol{\mu}_s = g_s \mu_B \mathbf{S}/\hbar$ where g_s is the spin g-factor and $\mu_B = |e|\hbar/(2m_0c)$ the Bohr's magneton with m_0 the bare electron mass. Here, the value $g_s = 2$ explains the experimental data obtained by Stern and Gerlach for the quantization of the intrinsic electronic magnetic moment if one also assumes a coupling with the external magnetic field of the form $\boldsymbol{\mu}_s \cdot \mathbf{B}$. Importantly, the electronic wave function has to be represented by a two component *spinor*

$$\tilde{\Psi}(\mathbf{r}) = \begin{bmatrix} \Psi_+(\mathbf{r}) \\ \Psi_-(\mathbf{r}) \end{bmatrix} = \sum_{\sigma=\pm} \Psi_\sigma(\mathbf{r}) \otimes |\sigma\rangle, \tag{2.1}$$

where $\sigma = \pm$ are the two possible spin projections, $\Psi_\sigma(\mathbf{r})$ is the spatial part of the spinor wave function, $|\sigma\rangle$ are the spin states which span a two-dimensional Hilbert space and $\otimes$ is the tensor product symbol. Once we have accepted that the electron possesses a spin, the physical origin of the SO interaction can be very easily understood [72]. If the

[1] In quantum computation, the spin is viewed as the quantum version of a bit or *qu*bit. The two spin projections correspond to the 0 and 1 of classical computation; in addition all possible linear combinations between the up and down states are also allowed.

electron moves with velocity $\mathbf{v}$ in the presence of an external electric field $\boldsymbol{\mathcal{E}}$ (which can be also spatially varying), a Galilean transformation to the inertial reference frame where the particle is at rest shows that the electron also *feels* an effective magnetic field, $\mathbf{B}_{\text{eff}}$,

$$\mathbf{B}_{\text{eff}} = \boldsymbol{\mathcal{E}} \times \frac{\mathbf{v}}{c}. \tag{2.2}$$

This effective magnetic field acts on the electronic spin (as the Zeeman interaction would do for the orbital motion) coupling to the intrinsic magnetic moment. We therefore obtain the simple SO Hamiltonian

$$\mathcal{H}_{\text{SO}} = \mu_s \mathbf{B}_{\text{eff}} \cdot \mathbf{S}, \tag{2.3}$$

where we defined $\mu_s \equiv g_s \mu_B/\hbar$. The relation with the orbital motion can be made crystal clear when taking into account that the effective magnetic field is orthogonal to the plane formed by the vectors $\mathbf{v}$ and $\boldsymbol{\mathcal{E}}$, and, as a consequence, $\mathbf{B}_{\text{eff}}$ is parallel to the orbital angular momentum $\mathbf{L}$. Indeed, one can rewrite the SO Hamiltonian in a slightly different way

$$\mathcal{H}_{\text{SO}} = \frac{e\lambda_c^2}{2\hbar} \boldsymbol{\sigma} \cdot \mathbf{p} \times \boldsymbol{\mathcal{E}}, \tag{2.4}$$

where $\lambda_c = \hbar/(m^* c)$ is the Compton wave length divided by 2π. This Hamiltonian looks like the standard atomic physics SO interaction term, *i.e.* $\mathcal{H}_{\text{SO}} \propto \mathbf{L} \cdot \mathbf{S}$ since $\boldsymbol{\mathcal{E}}$ should be parallel to the electron position $\mathbf{r}$. The only difference with the atomic physics case is that in Eq. (2.4) the proportionality constant does not depend on the electron state of the atom. Note that the "naïve" approach used obtain Eq. (2.4) also explains why the SO interaction is expected to be more important in compounds formed by heavy elements (such as InSb or the topological insulator HgTe) since, if the electron possesses a large atomic number, then the valence electrons are subjected to a stronger electric field close to the unscreened positively charged nucleus.

Importantly, unlike commonly done in textbooks [73], the derivation of Eq. (2.4) did not involve, apart from the spin degree of freedom, any quantum mechanical effects. To deduce this formula no relativistic argument was needed too so that one can understand the SO interaction as having a quasiclassical origin. Nevertheless, it is also true that a SO Hamiltonian (in an atomic physics context) can be obtained when performing a power expansion of the Dirac equation up to second order in the ratio v/c, for the sake of getting rid of the states with negative energy. This expansion, which allows to mathematically derive the well-known Pauli equation, is important to get the correct prefactors in front of the $\mathbf{L} \cdot \mathbf{S}$ term. Indeed, we must also take into account that the SO interaction presents also a contribution related to the hyperbolic nature of Minkoswki space-time and which manifests as a kinematic effect when performing a circular motion (as, in this case, the electronic reference frame is not inertial). This effect, so-called Thomas precession, yields a contribution that has exactly the same functional form of Eq. (2.4) but with opposite sign and divided by 2. Combining the Eq. (2.4) and the Thomas precession term, we obtain the following Hamiltonian

$$\mathcal{H}_{\text{SO}}^{\text{at}} = \frac{e\lambda_c^2}{4\hbar} \boldsymbol{\sigma} \cdot \mathbf{p} \times \boldsymbol{\mathcal{E}}, \tag{2.5}$$

which serves as a starting point to analyze SO interaction in solid-state systems.

2.2.2. Rashba and Dresselhaus Hamiltonians

The situation in semiconductors is slightly more complicated than that described in Sec. 2.2.1, since the SO coupling depends both on the velocity of the electron in a given energy band [with energies labeled by a band index and the crystal momentum $\mathbf{p} = \hbar\mathbf{k}$, *i.e.* $E_n(\mathbf{p})$] and the Bloch wave functions of the charge carriers in the periodic crystal lattice potential. However, from previous considerations, we shall therefore expect the contribution of each band to the SO Hamiltonian to have the form

$$\mathcal{H}_{\mathrm{SO}}(n,\mathbf{k}) \propto \mathbf{B}_{\mathrm{eff}}(n,\mathbf{k}) \cdot \mathbf{S}, \tag{2.6}$$

where now the effective magnetic field includes the effect of the crystal lattice, interactions and / or possible external (gate) potentials. Microscopically, one is therefore left with the complex task of solving the Schrödinger equation for the Bloch electrons in the presence of SO interaction (which enters in the matrix elements of the Hamiltonian). A popular approach to do it is to use the so-called $\mathbf{k}\cdot\mathbf{p}$ theory and the envelope function approximations [73]. Combined, these two methods are basically perturbation theory together with the assumption that the electromagnetic fields *enjoyed* by the electron are slowly varying on the length scale of the lattice parameter. We also usually account for the crystal lattice potential using the effective mass approximation and replaces the electron g_s-factor by the Landé g-factor[2].

Within the previous context of $\mathbf{k}\cdot\mathbf{p}$ theory, the Hilbert space is infinite-dimensional. However, in this thesis we are mainly interested by 2DEGs created at the interface of III-V semiconductors with zinc-blende crystal structure (such as GaAs, InSb or InAs). These semiconductors present a direct band gap close to the Γ point ($\mathbf{k} = \mathbf{0}$) in the Brillouin zone. Their bulk band structure can be approximated using the so-called Kane model in which the Hilbert space is truncated in order to write an effective Hamiltonian that couples only a finite number of semiconductor energy bands. A common truncation yields a 8×8 Hamiltonian, where the conduction band Γ_6 and the valence bands Γ_7 and Γ_8 (doubly degenerated) are coupled. The valence bands Γ_7 and Γ_8 are separated by an energy gap, which has its origin in the atomic SO interaction (2.5). This situation is depicted schematically in Fig. 2.1.

Focusing in 2DEGs and considering the SO interaction term only, expansion of the 8×8 Hamiltonian at lowest order in the momentum shows [73] that there are two main contributions to this quantity: Rashba [8, 74] and Dresselhaus [75] characterized, respectively, by SO coupling parameters α and β with distinct physical origins. Both terms share nevertheless the fact that they appear as a result of broken inversion symmetry[3]. The quantum-mechanical Rashba Hamiltonian has the following functional form

$$\hat{\mathcal{H}}_{\mathrm{R}} = \alpha \left[\hat{\mathbf{p}} \times \boldsymbol{\sigma}\right]_z = \alpha[\hat{p}_x \otimes \sigma_y - \hat{p}_y \otimes \sigma_x], \tag{2.7}$$

where the coupling constant $\alpha \propto \langle \mathcal{E}_z \rangle$ [here the average for the electric field is taken over the lowest subband in the quantum well that confines the 2DEG in the perpendicular ($\hat{\mathbf{z}}$)

[2]Note that, as it depends on the band structure, the Landé g-factor can also be affected by the SO interaction. A complete self-consistent treatment of the full electronic problem is extremely difficult and will not be considered here.

[3]From Eq. (2.6), we see that if the system presents time reversal symmetry then $\mathbf{B}_{\mathrm{eff}}(n,\mathbf{k}) = -\mathbf{B}_{\mathrm{eff}}(n,-\mathbf{k})$. If it also has inversion symmetry $\mathbf{B}_{\mathrm{eff}}(n,\mathbf{k}) = \mathbf{B}_{\mathrm{eff}}(n,-\mathbf{k})$, which implies a vanishing effective magnetic field. As a consequence, in the absence of external magnetic field the system must present a lack of inversion symmetry.

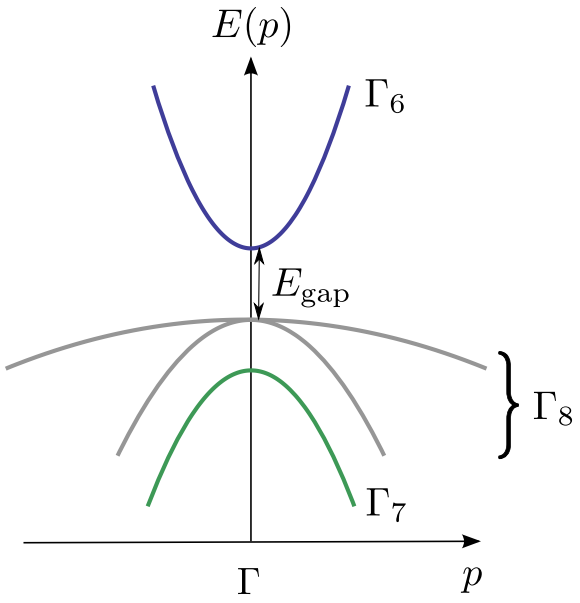

Figure 2.1 – Schematic band structure for the 8×8 Kane Hamiltonian. Defined for momenta close to the Γ point in the Brillouin zone, this Hamiltonian takes exclusively into account the coupling between the conduction band Γ_6 and the valence bands Γ_7, corresponding to light and heavy holes, and Γ_8, split-off by the SO interaction. The figure was inspired by Ref. [73].

direction]. This Hamiltonian is clearly reminescent of Eq. (2.5) and can be mapped to the low energy gapless graphene / two-dimensional Weyl Hamiltonian (1.29) by means of a unitary transformation that rotates the spin by $\varphi = \pi/2$ in the azimuthal plane of the Bloch sphere (*i.e.* $\sigma_x \to -\sigma_y$ and $\sigma_y \to \sigma_x$). A few comments about Rashba SO coupling are now in order. First, this type of SO interaction appears as a consequence of broken *structure* inversion symmetry and is characterized by a SO parameter which can be tuned by external voltage gates [76] (up to ±50% of its average value), since it depends on potential gradients applied in the perpendicular direction. Second, it is a natural consequence of the tunability of the Rashba coupling to admit that the value of this parameter can change spatially, *i.e.* $\alpha(\mathbf{r}) = \alpha + \delta\alpha(\mathbf{r})$ with $\alpha \equiv \langle \alpha(\mathbf{r}) \rangle$ the spatially averaged Rashba SO parameter. Therefore, in addition to Eq. (2.7), the full Rashba Hamiltonian should also have a fluctuating part

$$\delta\hat{\mathcal{H}}_{\mathrm{R}} = \frac{1}{2}\Big[\delta\alpha(\hat{\mathbf{r}}), [\hat{\mathbf{p}} \times \boldsymbol{\sigma}]_z\Big]_+ . \tag{2.8}$$

Here, we remind that $[\,\cdot\,,\,\cdot\,]_+$ represents the anticommutator which guarantees the hermiticity of the fluctuating Rashba Hamiltonian operator. The presence of this commutator is a simple consequence of the lack of commutativity between the spatial fluctuations of the Rashba SO parameter, $\delta\alpha(\mathbf{r})$ and the canonical momentum $\mathbf{p}$. From a physical point of view, this random Rashba SO parameter $\delta\alpha(\mathbf{r})$ can have its origin in the stochastic spatial fluctuations of the local electric fields associated to the confinement in the perpendicular direction to the 2DEG, randomness in the spatial distribution or concentration of the donor ions and fluctuations in the growth direction of the crystal lattice (due to local strain or inhomogeneous growth) [77, 78, 79]. Moreover, we shall assume that the fluctuations have a vanishing spatial average, $\langle \delta\alpha(\mathbf{r}) \rangle = 0$, and their correlations $\langle \delta\alpha(\mathbf{r})\delta\alpha(\mathbf{r}') \rangle$ are described

by a smooth function which depends on the difference between the two electronic positions $\mathbf{r}-\mathbf{r}'$. The spatial correlation function characterizing the fluctuations is, *a priori* different from the correlation function describing the spatial fluctuations of the in-plane disorder potential in the 2D plane (see also discussion in Sec. 3.1). This kind of SO coupling disorder has been very successful in a realistic description of the spin relaxation rate at low magnetic fields where the spin dynamics can be strongly affected by memory effects [79]. Finally, we shall mention that the energy scale associated to the Rashba SO interaction, $E_{\rm SO} = m^*\alpha^2$, can be proved to be of the order of $0.1 - 1.0$ meV [80]. This induces non-negligible SO splitting of the energy levels which can compete with other spin-dependent effects such as the Zeeman energy (see below).

As mentioned previously, the other type of SO interaction is described by the so-called Dresselhaus Hamiltonian. This term, related to *bulk* inversion asymmetry, only depends on the crystal lattice structure [80] and it can be written for 2DEGs as

$$\hat{\mathcal{H}}_{\rm D} = \beta[\hat{p}_x \otimes \sigma_x - \hat{p}_y \otimes \sigma_y], \tag{2.9}$$

with $\beta = \gamma\langle k_z^2\rangle$ (here γ is a material dependent parameter and k_z the wave vector of the lowest energy subband in the quantum well). As such, the Dresselhaus SO interaction is only sensitive to deep changes affecting the crystal lattice structure of the compound. Note that, mathematically, Eqs. (2.7) and (2.9) can both be related by a rotation in spin space described by the map $\sigma_x \leftrightarrow \sigma_y$. This means that a system which presents (spatially constant) Rashba SO interaction can be easily mapped to other characterized by the Dresselhaus SO coupling only.

As a general rule, we must always keep in mind that both Rashba and Dresselhaus SO contributions can be present in a given semiconductor heterostructure, so that a simple single-particle Hamiltonian that describes these systems in the absence of potential energy term can be written as

$$\hat{\mathcal{H}}_0(\alpha,\beta) = \frac{\hat{\mathbf{p}}^2}{2m^*} \otimes \mathbb{1}_{\rm s} + \hat{\mathcal{H}}_{\rm R} + \hat{\mathcal{H}}_{\rm D}, \tag{2.10}$$

to which we eventually may add the fluctuations of the Rashba SO parameter $\delta\hat{\mathcal{H}}_{\rm R}$. Now, which of the SO interactions dominates depends on specific material parameters and / or the perpendicular potential gradients applied to the sample [82]. For example, in GaAs the Rashba contribution is usually negligible and we can safely assume the Dresselhaus coupling to be the only relevant. As a comparison, InSb can be considered to be a compound with pure Rashba SO interaction while InAs presents an intermediate situation where both couplings are present. In this thesis, we consider only the Rashba SO interaction term as the experiments at high magnetic fields are performed in compounds where Dresselhaus SO coupling is negligible. From the experimental point of view, the particular case of a given semiconductor heterostructure can be determined using the transition from weak localization to antilocalization [83] or photocurrent measurements of the angular distribution of the spin density [84]. For pure Rashba SO interaction, the Rashba parameter has also been studied from an analysis of the nodes of the Shubnikov-de Haas oscillations of the longitudinal resistance for low perpendicular magnetic fields [76]. Quite recently, also scanning tunneling spectroscopy measurements have been performed in 2DEGs created at the surface of bulk p-doped InSb. The coupling constant α is extracted in this case from the positions of the nodes in the density of states (DoS) [11, 86]. Local observables, such as the local density of states, have also been studied in this system at high magnetic fields and will be an important point of discussion in chapter 3.

The spectrum of the Hamiltonian given in Eq. (2.10) can be computed straightforwardly and reads [80, 81]

$$E_s(\mathbf{p}) = \frac{\mathbf{p}^2}{2m^*} + s\Delta_{\mathbf{p}}, \tag{2.11}$$

where $s = \pm$ and the gap between the SO-split energies is given by the quantity $\Delta_{\mathbf{p}}$ defined as $\Delta_{\mathbf{p}} \equiv |\mathbf{p}|\sqrt{\alpha^2 + \beta^2 - 2\alpha\beta\sin(2\phi_{\mathbf{p}})}$ with $\tan\phi_{\mathbf{p}} = p_y/p_x$. The eigenstates corresponding to the eigenenergies $E_\pm(\mathbf{p})$ are entangled spinors combined with plane waves that can be written as

$$\tilde{\Psi}_{\mathbf{p},s}(\mathbf{r}) = \langle \mathbf{r}|\mathbf{p}, s\rangle = \frac{1}{\sqrt{2\Omega}} \begin{pmatrix} \mathrm{e}^{i\frac{\theta_{\mathbf{p}}}{2}} \\ s\mathrm{e}^{-i\frac{\theta_{\mathbf{p}}}{2}} \end{pmatrix} \mathrm{e}^{i\mathbf{p}\cdot\mathbf{r}/\hbar}, \tag{2.12}$$

with Ω the normalization area for the plane wave and $\theta_{\mathbf{p}}$ equal to

$$\tan\theta_{\mathbf{p}} = \frac{\alpha p_x + \beta p_y}{\alpha p_y + \beta p_x}. \tag{2.13}$$

We note that for arbitrary Rashba and Dresselhaus SO coupling, α and β, the Hamiltonian (2.10) presents broken spin rotation symmetry, with the spinor part of the eigenstates (2.12) depending on the momentum $\mathbf{p}$ via the nontrivial phases $\theta_{\mathbf{p}}$. At the special degeneracy points where $\alpha = \pm\beta$, $\theta \neq \theta_{\mathbf{p}}$ (so that the spin state is independent of the momentum) and one can prove the manifestation of a global SU(2) symmetry[4], associated to a conserved spin quantity $(\sigma_x \pm \sigma_y)/2$ [80]. Performing a rotation to the new basis, it is possible to show that the system generates spin edge helices that strongly increase the relaxation time of the spin vector [85].

Considering the case of pure Rashba SO interaction, the eigenenergies of the Hamiltonian $\hat{\mathcal{H}}_0(\alpha) \equiv \hat{\mathcal{H}}_0(\alpha, \beta = 0)$ are easily obtained from Eq. (2.11) and have the form

$$E_s^{\mathrm{R}}(\mathbf{p}) = \frac{\mathbf{p}^2}{2m^*} + s\alpha|\mathbf{p}|. \tag{2.14}$$

We plot these energies in Fig. 2.2 as a function of the normalized momentum $p/p_{\mathrm{SO}} = |\mathbf{p}|/p_{\mathrm{SO}}$ and compare them to the eigenenergies of the free 2DEG in the presence of a weak classical magnetic field pointing towards the $\hat{\mathbf{z}}$ direction (see Sec. 2.2.1), which induces a Zeeman spin-splitting

$$E_\sigma^{\mathrm{Z}}(\mathbf{p}) = \frac{\mathbf{p}^2}{2m^*} + \frac{\sigma}{2} g^* \mu_{\mathrm{B}} B. \tag{2.15}$$

In both situations, the Fermi surface (for fixed energy, E_{F}) is constituted by two concentric circles as it can be inferred from the invariance under rotations around the origin in Eqs. (2.14) and (2.15). The main difference between the two physical cases lies in the lifting of the spin degeneracy with respect to the spin-degenerate free 2DEG characterized by a parabolic dispersion relation [see Eq. (1.11) with $\mathbf{A}(\mathbf{r}) = \mathbf{0}$]: in the presence of Rashba SO interaction Eq. (2.14) shows that the parabolas are shifted horizontally while in Eq. (2.15) the Zeeman splitting term shifts both parabolas vertically (*i.e.* it opens a gap). As a consequence, in the Rashba case the degeneracy is still present for $\mathbf{p} = \mathbf{0}$ and one can jump continuously from a given band to the other.

Another important difference between the Rashba and Zeeman couplings appears at the level of the eigenstates. For the Rashba case, the eigenstates of $\hat{\mathcal{H}}(\alpha)$ are given by Eq.

[4] SU(2) is the group of 2×2 unitary matrices with determinant equal to unity.

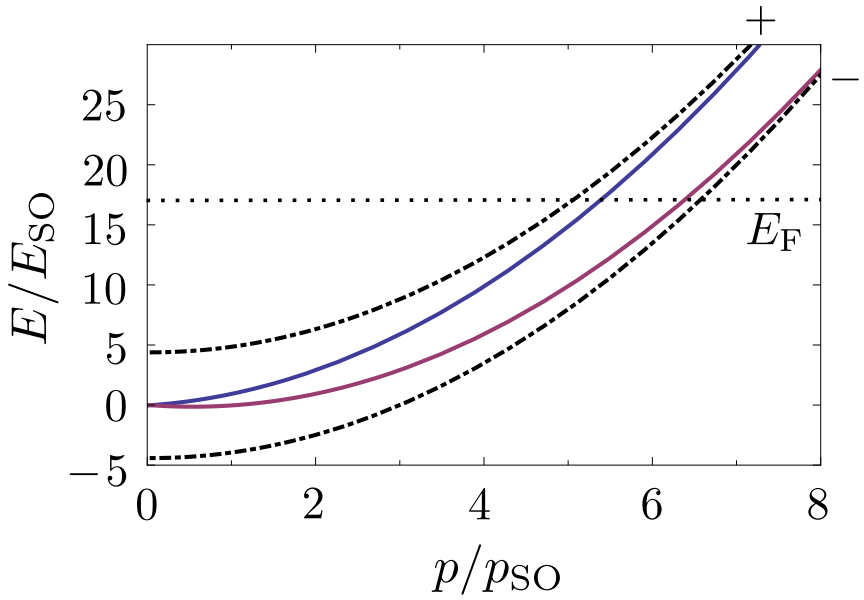

Figure 2.2 – Energy spectrum for the Rashba-split (2.14) (solid curves) and Zeeman-split (2.15) (dashed-dotted curves) energy levels, both in units of the Rashba characteristic energy $m^*\alpha^2$, as a function of the momentum $p = |\mathbf{p}|$ measured in units of $p_{\mathrm{SO}} = m^*\alpha$. We choose for the material parameter values compatible with InAs [96], *i.e.* $m^* = 0.04m_0$, $g = -8$, $\hbar\alpha = 1 \cdot 10^{-11}$ eV m together with a magnetic field of $B = 0.5$ T. The horizontal dotted line marks the Fermi energy E_{F} fixed by the density. The + and − label the two branches in Eqs. (2.14) and (2.20) which correspond to the two possible states (of spin + and spin −). Note that in both cases the energies converge for large momenta where the quadratic term in the spectrum dominates.

(2.12) and Eq. (2.13) with $\theta_{\mathbf{p}}^{\mathrm{R}} = \arctan(p_x/p_y)$

$$\tilde{\Psi}_{\mathbf{p},s}^{\mathrm{R}}(\mathbf{r}) = \langle \mathbf{r}|\mathbf{p},s\rangle_{\mathrm{R}} = \frac{1}{\sqrt{2\Omega}} \begin{pmatrix} 1 \\ s\mathrm{e}^{-i\theta_{\mathbf{p}}^{\mathrm{R}}} \end{pmatrix} \mathrm{e}^{i\mathbf{p}\cdot\mathbf{r}/\hbar}, \tag{2.16}$$

which intertwines the momentum, spin and SO quantum numbers. In the situation of a weak Zeeman effect we simply have the trivial product states $|\mathbf{p},\sigma\rangle_{\mathrm{Z}} = |\mathbf{p}\rangle \otimes |\sigma\rangle$. The topological difference (in the reciprocal space) between the two families of quantum states appears at the level of the spin properties: for the Rashba Hamiltonian it can be easily shown that for each SO projection the eigenstates are helical (spin and momentum are locked) with an average spin polarization

$$_{\mathrm{R}}\langle \mathbf{p},s|\hat{\mathbf{S}}|\mathbf{p},s\rangle_{\mathrm{R}} = \frac{\hbar}{2}(s\cos\theta_{\mathbf{p}}, -s\sin\theta_{\mathbf{p}}, 0). \tag{2.17}$$

As a consequence, the spin is always perpendicular to the momentum along the Fermi surface (with opposite direction in each of the two concentric Fermi circles) and the spin polarization vanishes, consistently with time-reversal symmetry in the SO Hamiltonian [87].

Finally, we may note that the features of the Rashba model described previously can be familiar to our readers since they appear in the description of the surface states of a topological insulator [88]. These systems present gapless surface Dirac fermions topologically protected from perturbations by time-reversal symmetry while the bulk behaves as an ordinary insulator. Indeed, $\hat{\mathcal{H}}(\alpha)$ is a simple model Hamiltonian for the surface of a three-dimensional topological insulator at low energies and belonging to the Wigner-Dyson symplectic class AII (see, for example, [89]). The ground state manifold of this class is partitioned in non-equivalent topological sectors labeled by the topological index $\mathbb{Z}_2$ that can be related to the SO quantum number $s = \pm$. As we shall not pursue this point of view here, we direct the readers to the nice reviews [50] and [90].

2.2.3. Rashba spin-orbit interaction in two-dimensional electron gases under perpendicular magnetic fields

Up to the present moment, several theoretical works have already considered the spectral properties of 2DEGs in the presence of uniform Rashba SO interaction and strong quantizing perpendicular magnetic fields. Note that, under the previous conditions, it is necessary to include in the description the Zeeman interaction which describes the coupling between the electron's intrinsic magnetic moment and the external magnetic field. Therefore, we consider a single-particle Hamiltonian that describes electrons with spin $s = 1/2$, effective mass m^* and charge $e = -|e|$ confined in a two-dimensional plane under a uniform magnetic field $\mathbf{B} = B\hat{\mathbf{z}}$ and in the presence of Rashba SO and Zeeman interactions given by

$$\hat{\mathcal{H}}_0 = \hat{\mathcal{H}}_{\mathrm{2DEG}} \otimes \mathbb{1}_{\mathrm{s}} + \hat{\mathcal{H}}_{\mathrm{R}} + \hat{\mathcal{H}}_{\mathrm{Z}}. \tag{2.18}$$

Here, the first term $\hat{\mathcal{H}}_{\mathrm{2DEG}}$ is the Hamiltonian of a free spinless electron defined in Eq. (1.11) (we remind that $\otimes$ is the tensor product and write as $\mathbb{1}_{\mathrm{s}}$ the 2×2 identity matrix that represents the identity operator in spin space). The second term $\hat{\mathcal{H}}_{\mathrm{R}}$ is the Rashba Hamiltonian [8, 74] given in Eq. (2.7) and to which we have applied the minimal coupling

rule, $\mathbf{p} \to \mathbf{\Pi}$, where the canonical momentum is substituted by the gauge invariant momentum (we point out that we do not consider at this point random spatial fluctuations of the Rashba field)

$$\hat{\mathcal{H}}_{\mathrm{R}} = \alpha[\hat{\mathbf{\Pi}} \times \boldsymbol{\sigma}]_z = \alpha[\hat{\Pi}_x \otimes \sigma_y - \hat{\Pi}_y \otimes \sigma_x], \tag{2.19}$$

This Hamiltonian takes into account the non-trivial coupling between the orbital and the spin degrees of freedom. Finally, the last term describes the Zeeman coupling between the spin and the applied magnetic field

$$\hat{\mathcal{H}}_{\mathrm{Z}} = \frac{1}{2} g \mu_B B \otimes \sigma_z, \tag{2.20}$$

with g the Landé g-factor that replaces the spin g factor when we take also into account the particle's angular momentum.

Diagonalization of the Hamiltonian is straightforward and yields the following energy spectrum for the clean system

$$E_{n,\lambda} = \hbar\omega_c \left(n - \frac{\lambda}{2} \Delta_n \right). \tag{2.21}$$

This spectrum has been known for almost thirty years [8, 74] and describes the set of discrete SO-split Rashba-Landau levels labeled by $n \in \mathbb{N}$, a positive integer, and $\lambda \equiv \lambda(n)$, the SO quantum number which is a function of the former and takes the values $\lambda = \pm$ if $n \neq 0$ and $\lambda = -$ otherwise (this index corresponds to the two possible projections along the Rashba dependent spin precession axis). The corresponding eigenstates, which together with the disordered equivalent of Eq. (2.21) is deeply discussed in chapter 3, are characterized by a spinorial structure composed out of adjacent spinless Landau level states that can be related to the quantization of two different cyclotron orbits in the external magnetic field.

As in Eq. (1.24), the dominant energy scale of the energy levels at high magnetic fields is the cyclotron energy $\hbar\omega_c$, where we remind that $\omega_c = |e|B/(m^*c)$ is the cyclotron pulsation, and $\Delta_n = \sqrt{(1-Z)^2 + nS^2}$ is a dimensionless quantity that defines the gap between the SO-split energy levels in units of the cyclotron energy $\hbar\omega_c$. Note that the dependence of the eigenenergies on the SO interaction always comes through the SO index λ and is related to two other energy scales appearing in Eq. (2.21) via the dimensionless quantities S and Z characterizing the Rashba SO coupling and the Zeeman interaction, respectively[5]. These parameters measure the relative strength of the Rashba SO coupling (per magnetic length) and the Zeeman interaction relative to the cyclotron energy and are defined by the following relations

$$S \equiv \frac{\alpha 2\sqrt{2}}{\omega_c l_B}, \tag{2.22}$$

$$Z \equiv \frac{g\mu_B}{\hbar|e|} m^* c = \frac{g}{2} \frac{m^*}{m_0}. \tag{2.23}$$

In this thesis, we shall assume without loss of generality that $1 - Z > 0$ (the academic case $1 - Z < 0$, which does not correspond to any realistic values of the Landé g factor for

[5]Since we are interested in the integer quantum Hall regime, we safely assume that the energy scale related to disorder and interactions is largely smaller than the cyclotron energy.

the considered semiconductors can be studied in a similar way). Note that, in the absence of electron-electron interaction, S decreases with the magnetic field as $S \sim l_B \sim 1/\sqrt{B}$ while Z is constant; however, since $S \sim Z$ even for high magnetic fields understanding the interplay between both couplings is crucial to explain the observed trends in scanning tunneling spectroscopy (STS) experiments.

It is also particular to the Rashba-Landau energy levels that they formally interpolate between the non-relativistic Landau spectrum in the absence of (magnetic field renormalized) SO interaction[6], $S = 0$, and the relativistic-like (Weyl) spectrum in the limit $|S| \to +\infty$ (one may also consider in this case the simultaneous formal limits $m^* \to +\infty$ and $g \to 0$). The former spin-polarized Landau levels present the typical form, $E_{n,\pm} = \hbar\omega_c(n + 1/2 \pm Z/2)$, with linear dependence on the Landau level index while the latter show a square-root dependence on n expected for massless Dirac fermions, $E_{n,\lambda} = -\lambda\hbar\Omega\sqrt{n}$ (here $\Omega = \alpha\sqrt{2}/l_B$ can be identified with the graphene characteristic frequency after identification of the Rashba SO parameter α with the Fermi velocity v_{F}). Interestingly, we may note that for finite values of the SO parameter S the spectral structure of the Rashba-Landau energy levels still shows some similarities to the relativistic-like Landau levels, in the sense that for $n = 0$ only one of the projections of the SO quantum number is allowed (in contrast to the Zeeman-split Landau levels). There are, however, two important differences: first, due to the presence of the quadratic Hamiltonian (1.11) there is always a zero point energy (or constant mass term); second, the energy spectrum is always bounded from below. This difference will turn out to be crucial in the next chapter for the calculation of the local Hall conductivity at high magnetic fields, see Sec. 4.5.

From a physical point of view, it is also interesting to estimate the energy scales involved in the Rashba problem under perpendicular magnetic fields. As a general rule, the characteristic Rashba energy E_{SO} is one order of magnitude smaller than the typical energy scale related to cyclotron motion (for $B = 1$ T). However, in 2D heterostructures where the SO coupling is strong due to heavy elements such as in InSb, both energies can be of similar order of magnitude. For example, considering the values of the effective mass and the Rashba coupling parameter taken from Ref. [86] and used in Fig. 2.3, the Rashba characteristic energy is of the order of $E_{\mathrm{SO}} \simeq 3$ meV, which is the same order of magnitude of the cyclotron energy at $B = 1$ T used as a benchmark ($\hbar\omega_c \simeq 3$ meV). Note also that in the clean spectrum (2.21), the relevant quantities are the Rashba and Zeeman dimensionless parameters S and Z given by Eqs. (2.22) and (2.23), which take the values $S \simeq 2.33$ and $Z \simeq -0.37$ for $B = 1$ T. Since even for high magnetic fields of several teslas $S \sim 1$, the understanding of the interplay between Zeeman and Rashba couplings in a given energy level n is crucial.

Additionally, we can see that the SO coupling generates non-equidistant energy levels and due to the competition between the terms in the Hamiltonian quadratic and linear in the momentum, two levels with opposite SO index λ can become arbitrarily close and give an accidental double degeneracy. Consequently, the energy spectrum (2.21) presents a rich structure with multiple level crossings controlled by the dimensionless parameters S and Z (therefore, the Rashba SO coupling strength α and / or the applied magnetic field B). We show these crossings in Fig. 2.3 where we plot the normalized energy levels as a function of S for realistic values of the parameters extracted from the experiments. We

[6]The limit $|S| \to 0$, in which the SO and the spin quantum numbers can be identified $\lambda \equiv \sigma$ requires a relabeling of the energy level index according to $n_{-\sigma} + 1 \to n$, in order to reintroduce the picture of the splitting of each Landau level into two spin-polarized sublevels due to the Zeeman interaction only.

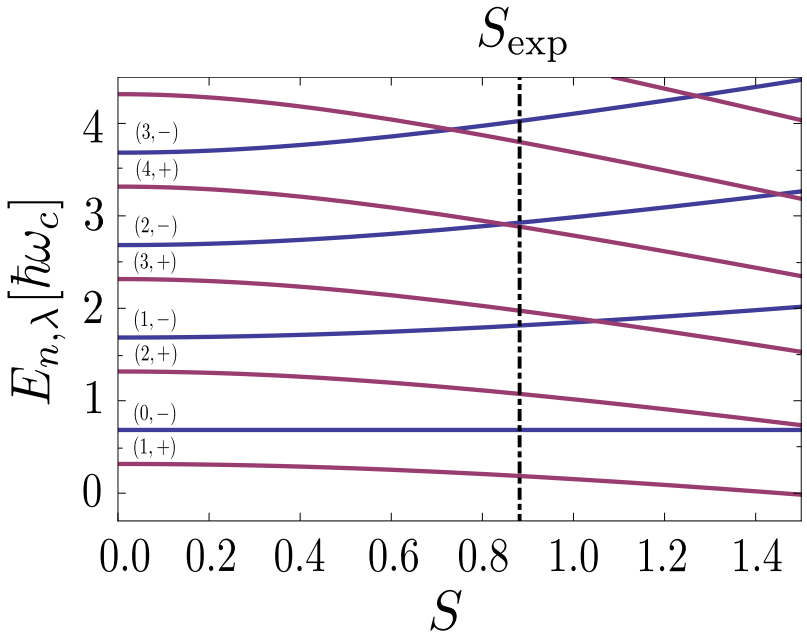

Figure 2.3 – Energy spectrum (in units of the cyclotron energy $\hbar\omega_c$) given in Eq. (2.21) as a function of the dimensionless Rashba parameter S. Values for the parameters are compatible with the STS measurements [11, 86] in InSb surface 2DEGs: $m^* = 0.035m_0$, $g = -21$, $\hbar\alpha = 7 \cdot 10^{-11}$ eV m. The vertical dashed-dotted line shows the particular value $S_{\mathrm{exp}} \simeq 0.88$ (obtained for $B = 7$ T) at which important spatial dispersion in the LDoS spin-splitting has been seen experimentally (see the discussion in Sec. 3.1). Note that the energy level $(0, -)$ does not depend on the parameter S.

can also easily obtain an analytical formula for the level intersections in the energy space which occur for $E_{n_1,\lambda_1} = E_{n_2,\lambda_2}$ with $n_1 \neq n_2$ and necessarily $\lambda_1 = -\lambda_2$. This yields a biquadratic equation in the Rashba SO parameter S whose solution is

$$S_c = 2\sqrt{(n_1 + n_2) - \sqrt{4n_1n_2 + (1 - Z)^2}}. \tag{2.24}$$

From the special values S_c we deduce that level crossings involve different energy levels such that $|n_1 - n_2| > 1 - Z$. The degeneracies associated to each value of S_c have been related to the beating pattern of the DoS [86] or to resonances in spin-related observables [112, 113, 114], to be discussed in Sec 2.3.

All the degeneracies within the energy spectrum are expected to be lifted in the presence of a smooth random potential energy and Landau level mixing. Note that, in that sense, toy models with simple spatial dependence have already been considered in the literature. Unfortunately, most of the used models are not tractable analytically in the quantum regime so that often it is compulsory to resort to numerical simulations to get some physical insight. For the hard-wall potential, there exist theoretical studies using either a wave function formalism [91, 92] or semiclassical approaches based on SU(2) (spin) coherent states [93], the rest of the studies being purely numerical [93, 94, 95]. One-dimensional parabolic confinement models (*quantum wires*) also appear to be not fully analytically tractable in the presence of an external magnetic field and both Rashba and Zeeman interactions. Indeed, this toy model which can be used to describe the edge states of the integer quantum Hall effect has mainly been studied numerically [96] or analytically but without controlled approximations [97]. Finally, two-dimensional confinement potentials, which are considered as toy models that describe semiconductor quantum dots in a magnetic field, have also been investigated but only numerically [82, 98, 99, 100, 101].

To end up this section, we would like to mention that, unfortunately, none of the above theoretical works address the quantum Hall regime described in chapter 1 in which smooth disorder plays a crucial role by producing both localized and delocalized electronic states. These disorder effects can be well captured in a semiclassical picture (guiding center approach) [34, 102, 103, 104, 105] where the electronic motion is described in terms of a fast cyclotron motion and a slow guiding center drift. These two motions decouple at high magnetic fields and (energy conservation) constrains the guiding center to follow the equipotential lines of the disorder electrostatic potential landscape. A throughout analysis, which includes the effect of smooth random fluctuations in the SO coupling parameter will be performed in chapter 3 based on Ref. [121].

2.3. Spin Dynamics in Spin-Orbit Coupled Systems

2.3.1. Spin Hall effect

The spin Hall effect is the analogue of the (charge) Hall effect described in Sec. 1.2 but for the spin degree of freedom, all in the presence of SO interaction. This phenomenon is very easily understood as the generation of a transverse spin current that appears as a response to a longitudinal electric current leading to a spin accumulation at the boundaries of the sample (typically with the spin polarization directed perpendicular to the plane formed by the two previous currents) [106]. This situation is sketched in Fig. 2.4 where we also show the semiclassical skipping orbits representing the Hall edge channels. Historically,

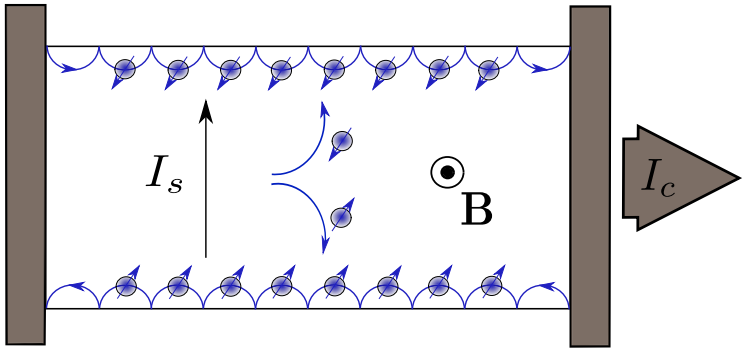

Figure 2.4 – Semiclassical picture of the direct spin Hall effect in a two-terminal Hall bar under a perpendicular magnetic field **B**. In the presence of SO interaction the system generates a transverse spin current I_s as a response to a longitudinal electric current I_c. As a result, we get spin accumulation of different spin projections in opposite edges of the macroscopic sample. Note that,in principle, the spin current cannot be measured directly (as it does not couple to experimental probes) but indirectly either through the previously described difference in the spin densities, thanks the inverse spin Hall effect [111] (where spin current yields a voltage difference) or by optical methods.

research in the spin Hall effect gained a considerable amount of *momentum* within the spintronics community after the seminal article of J. Sinova *et al.* [107] where the theoretical prediction of dissipationless intrinsic[7] spin currents for clean 2DEGs with uniform Rashba SO coupling in the absence of external magnetic fields was realized. Astonishingly, this effect shows that the $\hat{\mathbf{z}}$ component of the spin Hall conductivity at $T = 0$ has a universal value independent of the Rashba parameter α and the electron density

$$\sigma_{\mathrm{H}}^{s} = \frac{e}{8\pi}, \tag{2.25}$$

when both energy bands (for the projections $s = \pm$) are occupied. The remarkable result (2.25) for the transport coefficient associated to the spin current density, defined as $\mathbf{j}_{\gamma}^{s} \equiv \bar{\sigma}_{\gamma}^{s}\boldsymbol{\mathcal{E}}$, can be explained by the peculiar spin-momentum locking relation induced by the Rashba SO interaction [8, 87, 107]. Here, we have noted $\bar{\sigma}_{\gamma}^{s}$ the effective spin Hall conductivity tensor and used the label $\gamma \in \{x, y, z\}$ to account for the three different spin projections [this third order tensor is defined analogously to the conductance tensor given in Eq. (1.2)]. It is noted that the value of the spin Hall conductivity has not at all a topological origin, as it happens with the (quantized) Hall conductivity and, as a result, the effect does not survive to the presence of disorder in the diffusive regime [80]. This is not surprising and can be proved in very general terms [108] to be related to the form of the current density operator for the $\hat{\mathbf{z}}$ spin component to be introduced now.

In general, the spin current density, $\mathbf{j}_{\gamma}^{s} = \mathbf{j}_{\gamma}^{s}(\mathbf{r})$ is computed from the following quantum spin current density operator for each spin component

$$\hat{\mathbf{j}}_{\gamma}^{s} = \frac{1}{2}[\hat{S}_{\gamma}, \hat{\mathbf{v}}]_{+} = \frac{\hbar}{4}\left[\sigma_{\gamma}, \hat{\mathbf{v}}\right]_{+}, \tag{2.26}$$

with $\hat{\mathbf{v}}$ the velocity operator. This operator is given by the Heisenberg equation of motion

[7] The effect is called *intrinsic* because it is exclusively related to the energy spectrum and not to anisotropic spin dependent scattering. The latter is dubbed, in opposition, *extrinsic*.

applied to the Hamiltonian[8] $\hat{\mathcal{H}}_0(\alpha)$

$$\hat{\mathbf{v}} = \frac{i}{\hbar}[\hat{\mathcal{H}}_0(\alpha), \hat{\mathbf{r}}]. \tag{2.27}$$

For the $\hat{\mathbf{z}}$ component, we have[9]

$$\hat{\mathbf{j}}_z^s = \frac{\hbar}{2}\frac{\hat{\mathbf{p}}}{m^*} \otimes \sigma_z. \tag{2.28}$$

It is interesting to note that this operator remains the same both in the presence and the absence of SO interaction. In addition, its functional form suggests that the local current density can be understood as being the difference between the currents carried by the spin-up and spin-down electrons

$$\mathbf{j}_z^s(\mathbf{r}) = \frac{\hbar}{2e}\left[\mathbf{j}_+(\mathbf{r}) - \mathbf{j}_-(\mathbf{r})\right]. \tag{2.29}$$

However, we would like to point out that the definition of the spin density current operator in Eq. (2.26) together with the interpretation given in Eq. (2.29) present important theoretical caveats. First, one can easily check that the spin current density derived from the operator (2.26) does not satisfy a continuity equation [109]. This implies that the spin polarization is no longer conserved[10] and yields fundamental difficulties, since observables such as the macroscopic spin current are not well defined in a realistic system. In addition, one may show that this definition, although somehow "natural", also predicts a non-zero spin current density for localized systems and a violation of the Onsager relations in the thermodynamic limit [109]. Another important fact was also soon realized by Rashba [157] who, previously to all the considerable amount of work done in the spin Hall effect, had noticed that the spin current operator defined by Eq. (2.26) in the presence of SO interaction generates non-vanishing equilibrium spin currents. These persistent currents do not satisfy Ohm's law as they do not appear as a response to an external voltage drop and therefore, cannot describe non-equilibrium spin transport nor spin accumulation can result from the currents.

One possibility to overcome this obstacle which was soon explored after J. Sinova's work [109, 110] is to introduce in the continuity equation a torque dipole term in order to account for the "generation" of spin due to SO interaction. Again, this is nothing else than a consequence of the fact that, in the presence of SO coupling the spin is not a good quantum number so that the interpretation given in Eq. (2.29) is problematic. Consideration of the torque term, which can be derived microscopically from the Schrödinger equation (and allows to take into account the required conservation of the norm of the spin vector) establishes that Eq. (2.28) must be substituted by a tensor product operator, so-called

[8] We recall that this Hamiltonian is obtained from (2.10) taking $\beta = 0$. Additionally, we note that the inclusion of a Zeeman energy term in the Hamiltonian (2.20) does not modify this picture.

[9] We remind that the Pauli matrices satisfy the relation $\sigma_j\sigma_k = i\sum_l \varepsilon_{jkl}\sigma_l + \delta_{jk}\mathbb{1}$ where ε_{jkl} is the Levi-Civita antisymmetric tensor and δ_{jk} is the Kronecker delta. Hence $[\sigma_x, \sigma_z]_+ = [\sigma_y, \sigma_z]_+ = 0$ and the result follows.

[10] Without the continuity equation it is not possible to relate the microscopic, possibly inhomogeneous, current density $\mathbf{j}(\mathbf{r})$ to a macroscopic flux I of a certain quantity (charge, mass, spin) since

$$I \neq \int_{\partial\Omega} \mathbf{j}(\mathbf{r}) \cdot d^2\mathbf{r}.$$

displacement operator,[11]

$$\hat{\mathcal{J}}_z^s = \frac{\hbar}{2}\frac{d(\hat{\mathbf{r}} \otimes \sigma_z)}{dt}. \tag{2.30}$$

The displacement operator contains, in addition to the conventional spin current operator shown in Eq. (2.28), an extra contribution from the spin torque current density [operator]

$$\hat{\mathbf{P}}_z^\tau = \frac{\hbar}{2}\hat{\mathbf{r}} \otimes \frac{d\sigma_z}{dt}. \tag{2.31}$$

The corresponding spin torque current density is related to the spin torque density, $\mathcal{T}_z^s(\mathbf{r})$, by the relation $\mathcal{T}_z^s(\mathbf{r}) = -\boldsymbol{\nabla}_\mathbf{r} \cdot \mathbf{P}_z^\tau(\mathbf{r})$ which holds whenever the average spin torque density vanishes in the bulk of the system. An interpretation of this term as a source in the continuity equation is straightforward since, typically,

$$\boldsymbol{\nabla}_\mathbf{r} \cdot \mathbf{j}_z^s(\mathbf{r}) = -\boldsymbol{\nabla}_\mathbf{r} \cdot \mathbf{P}_z^\tau(\mathbf{r}) = \mathcal{T}_z^s(\mathbf{r}) \neq 0. \tag{2.32}$$

Integration of this equation and use of the Stokes' theorem yields

$$\oint_{\partial\Omega} \mathbf{j}_z^s(\mathbf{r}) \cdot d^2\mathbf{r} = \int_\Omega \mathcal{T}_z^s(\mathbf{r})\, d^3\mathbf{r}, \tag{2.33}$$

and allows for another interpretation of Eq. (2.31). Indeed, we can easily see that the total linear spin current which flows through a closed surface $\partial\Omega$ is equal to the variation of the spin torque in the volume Ω enclosed by the surface. In this sense, one may consider that the total angular momentum vector flow is conserved while there is a transfer of angular momentum between the translational and the rotational degrees of freedom.

Finally, it is also worthwhile to comment another peculiar issue related to the spin current discussed in this section. This is related to a certain freedom in the definition of the spin current density: it can be arbitrarily redefined by adding to it any current $\mathbf{j}_z^s(\mathbf{r}) \to \mathbf{j}_z^s(\mathbf{r}) + \tilde{\mathbf{j}}_z^s(\mathbf{r})$ as long as the spin torque density is equally redefined by $\mathcal{T}_z^s(\mathbf{r}) \to \mathcal{T}_z^s(\mathbf{r}) + \boldsymbol{\nabla}_\mathbf{r} \cdot \tilde{\mathbf{j}}_z^s(\mathbf{r})$. Or, one may note that the spin torque current density $\mathbf{P}_z^\tau(\mathbf{r})$ is not uniquely defined since we can add to it the rotational of any function $\Lambda(\mathbf{r}) \in C^\infty$ without changing the spin torque density (*i.e.* the actual observable that enters in the continuity equation). This, which looks as a purely formal ambiguity in the definition of the spin current density, means that the definition of the former is only complete if we fix simultaneously the spin torque density. In principle, this must not lead to any differences in the physical predictions for a certain choice of boundary conditions at equilibrium. Nevertheless to have this freedom, that appears as a consequence of not selecting the proper spin polarization axis, is conceptually and theoretically dissatisfying. A more natural approach would be to define the spin current with respect to the spin polarization axis which changes in spin space as a result of Rashba SO interaction. This approach, non-standard in diffusive systems, will be considered in chapter 4 for the quantum Hall regime where the motion of the SO-dependent axis is expected to be adiabatic and slow compared to the (fast) cyclotron motion of the electron.

2.3.2. Spin Hall effect in a two-dimensional electron gas in the presence of perpendicular magnetic fields

Spin transport properties of 2DEGs in the presence of Rashba or Dresselhaus SO interaction under external perpendicular magnetic fields $\mathbf{B}$ were theoretically studied by S.

[11] We warn here that this operator must be symmetrized if we want to proceed with any calculation.

Q. Shen *et al.* in a series of papers [112, 113, 114] focused in clean 2DEGs. These authors showed that, using the definition given in Eq. (2.28) in the presence of an external perpendicular magnetic field, it is possible to obtain a resonant spin Hall conductance for very particular values of the SO parameter S. These resonances were quickly related to the crossings (accidental degeneracies) of the energy levels that appear in the Landau spectrum in the presence of Rashba or Dresselhaus SO interaction. The degeneracies are also present in other spin related observables such as the electric spin susceptibility [115] computed for the same physical system using a similar formalism.

Apart from mistakes in the calculations (see, concretely, the discussion in Appendix B) and the use of an incomplete definition (non-conserved) of the spin current density operator as discussed in the previous section, this work pretends to use advanced perturbation theory for the case of 2DEGs under perpendicular magnetic fields in the presence of a spatially constant electric field. To that purpose, the authors consider that the static electric field at equilibrium can both lift the huge degeneracy of the clean energy levels and, at the same time, be responsible for the macroscopic transport properties. Albeit showing some similarity to the vortex method described in Sec. 1.5, this approach presents several problems. First, we have seen that the problem of lifting the level degeneracy at high magnetic fields is intrinsically nonperturbative (only one energy scale is present) where equilibrium and nonequilibrium electric fields need to be treated on equal footing. Second, the theory seems to be inconsistent since in the linear response regime where $|\boldsymbol{\mathcal{E}}| \to 0$ the energy levels become macroscopically degenerate. This is because, *de facto* this theory is implicitly considering two different types of electric field (equilibrium and nonequilibrium) but the observables that are obtained in Refs. [112, 113, 114] are only computed at equilibrium. As such, they cannot describe transport of charge or spin as a response to a non-equilibrium electric field which is the experimental situation occurring in the quantum Hall regime. Therefore, it is perfectly licit to doubt about the physical meaning of the obtained results and the validity of a pure perturbative approach in the field amplitude to compute the macroscopic transport coefficients.

It is also interesting to note that other calculations performed using the Kubo formalism [135] also present these divergences in the spin transport coefficients for clean systems (in particular, for the spin Hall conductance discussed here). Again, we can suspect that these resonances are a pure artifact of the perturbative treatment which is known to be problematic for realistic quantum Hall systems, *i.e.* with disorder. In addition, we can also argue that the Kubo formulation for transport crucially relies on the hypothesis of ergodicity[12] for the given phase space shell [159]. As such, one expects this formula to be valid for diffusive quantum systems where the collision with random impurities provides a mechanism of chaoticity in phase space so that the electron explores all the possible regions allowed by the energy conservation laws. However, in quantum Hall systems where smooth disorder is particularly important at high magnetic fields, transport becomes quasi-ballistic and shows percolation features. In some sense, the quantum Hall regime shows a certain

[12] An observable is said to be ergodic [117] if its time average is equal to its ensemble average, that is,

$$\langle \hat{A} \rangle = \lim_{n \to +\infty} \frac{1}{n} \sum_{k=0}^{n-1} A(T^k),$$

in the $L_2(\mathbb{R})$ sense [here k counts the number of iterations in the time average]. This is the well-known mean-ergodic theorem by Birkhoff. The theorem simply states that, as time evolves, a particle will explore all the region of phase space entirely accessible (with microstates which have the same energy).

kind of ergodicity breaking due to the loss of translational invariance in real space [which, we remind, is the real space for the guiding center coordinates $\mathbf{R} = (X, Y)$ due to the commutator $[\hat{X}, \hat{Y}] = il_B^2$]. As a result, it will not be surprising to see that the result of our calculations for the spin Hall conductance using an extension of the vortex formalism (semiclassical nonperturbative theory discussed in chapter 4) is different to that obtained within the perturbatively based transport theory mentioned here and detailed in Appendix B.

Chapter 3

Local Spectral Properties in Generalized Disordered Potential Landscapes

Our goal in this chapter, based on Ref. [121], is to show how the vortex technique sketched in Sec. 1.5 can be generalized to take into account quantum-mechanically the simultaneous presence of smooth electrostatic disorder, random Rashba SO interaction and Zeeman coupling in the integer quantum Hall regime. The developed formalism allows us to obtain analytical and controlled nonperturbative expressions of the energy spectrum and the local density of states (LDoS) for different temperature regimes. We present a mechanism that explains the experimentally-noticed spatial correlations between the dispersion of the energy spin-splitting and the disorder potential, which otherwise could be naïvely attributed to spatial fluctuations of the Rashba fields. In this sense, we point out that our theoretical analysis of the spatial dispersion of the energy spin-splitting in InSb 2D surface gases suggests that the contribution coming from the fluctuations of Rashba SO coupling is seemingly less important than the effect of spatial fluctuations of the electrostatic potential landscape.

L'objective de ce chapitre, basé sur la Réf. [121], est de montrer comment la technique vortex esquissée dans la Sec. 1.5 peut être généralisée pour tenir compte, de manière quantique et dans le régime de l'effet Hall quantique entier, de la présence simultanée du désordre lisse d'origine électrostatique, de l'interaction SO Rashba (ainsi comme ses fluctuations désordonnées) et du couplage Zeeman. Le formalisme décrit nous permet d'obtenir des fonctionnelles (spectre énergétique et densité d'états locale) analytiques, controllées et non-perturbatives valables dans différents régimes de température. Nous présentons aussi un mécanisme qui explique les corrélations entre la dépendance spatiale du splitting de spin et le potentiel de désordre. Ces correlations spatiales avaient été remarquées expérimentalement auparavant par des mesures locales et pouvaient être attribuées naïvement aux fluctuations spatiales des champs de Rashba. À ce propos, nous signalons que notre analyse théorique de la dispersion spatiale du splitting de spin dans les gaz de surface sur InSb semble indiquer que la contribution des fluctuations du couplage SO Rashba est moins important que l'effet des fluctuations spatiales du potentiel de désordre électrostatique.

3.1. Motivation

In spite of the intense research that has been made to investigate macroscopic transport properties of 2DEGs in the quantum Hall regime during the last two decades, the experimental study of local properties in these systems has remained somehow elusive. The main reason is that, in semiconductor heterostructures, the 2DEG is deeply confined into the lowest energy state of a triangular-like shaped potential, well below the surface (at a distance of about 100 nm from the surface layer [11, 118]). This presents the advantage of avoiding scattering with surface impurities so that high sample mobilities (of the order of 10^7 cm^2 / V $\cdot$ s) can be obtained at low temperatures together with an important electron elastic mean free path (of the order of 0.1 mm) [118, 119]. Unfortunately, this prevents the study of these systems using surface oriented local probe techniques such as scanning tunneling spectroscopy (STS). This fact can be checked by a simple estimation of the tunneling current within the triangular barrier approximation which yields an undetectable current for up-to-date amplifiers.

One possibility to overcome this experimental difficulty is to confine 2DEGs close to the surface of small bandgap semiconductors by chemical deposition of alkali ad-atoms. As a result of the deposition of adsorbate atoms, even at low densities [120], it is energetically favorable for the donors to move from the adsorbate towards the acceptor impurities in the semiconductor, if the latter is p-doped, or to go into the conduction band, if the semiconductor is n-doped. This produces a strong band bending with the chemical potential pinned above the minimum of the conduction band and effectively traps the 2DEG directly below the surface boundary [11, 86]. Having a 2DEG next to the surface opens a window to perform high resolution STS studies[1] which directly gives the real space local density of states from the measurement of the local differential conductivity $\partial I/\partial V$ at position $\mathbf{r} = (x, y)$. This experimental situation is sketched in Fig. 3.1. The technique has been applied to study, in the integer quantum Hall regime, the magnetic field driven delocalization-to-localization Hall transition [42] or to map in real space the quantum mechanical wave functions of the Landau level, revealing their nodal structure produced by the self-interference of the quantum cyclotron orbits [2].

The STS technique can also provide the opportunity of probing locally spatial fluctuations of the Rashba parameter $\alpha(\mathbf{r})$. These fluctuations are to be expected in surface 2DEGs since the concentration of dopant ions in the bulk semiconductor and adsorbate atoms at the surface fluctuates spatially, which in turns gives a random electric field in the direction perpendicular to the potential well [77]. The electron motion in the 2DEG is therefore affected by two different types of disorder that are *a priori* uncorrelated: the in-plane electrostatic disorder potential $V(\mathbf{r})$ and the fluctuating Rashba SO interaction characterized by $\alpha(\mathbf{r})$. As mentioned in chapter 2, fluctuations of the Rashba parameter are also known to influence the spin dynamics under weak magnetic fields [78, 79], and can, via the Rashba coupling to the electric charge have an effect in the electron dynamics.

Recently performed STS measurements [11, 86] at high perpendicular magnetic fields in disordered p-doped InSb 2D surface gases (that present strong Rashba SO interaction) have also shown that the LDoS energy spin-splitting depends on the tip position (see, in particular, Fig. 3.2). Concretely, the spin-split LDoS presents well resolved peaks whenever

[1] However, a disadvantage of the present systems with respect to other surface 2DEGs such as graphene is that potential fluctuations can be very strong, in addition to having more complicated non-parabolic conduction bands.

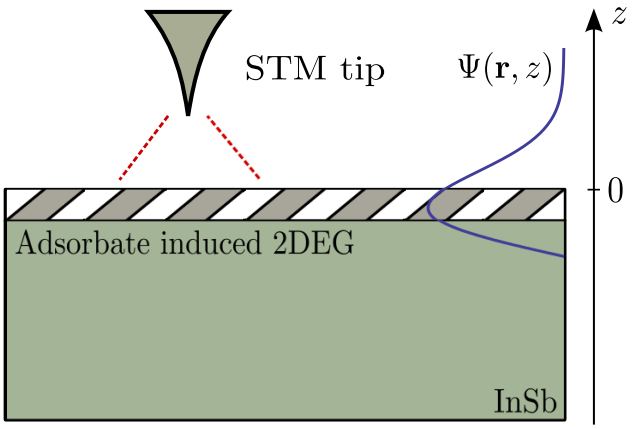

Figure 3.1 – Schematic illustration of the adsorbate-induced 2DEG created by deposition of Cs atoms on top of InSb, together with the STS tip used to measure the tunneling current. The localized (in the perpendicular direction) wave function of the confined electron in the lowest energy subband is also sketched.

the STS tip is located close to local extrema of the disorder potential landscape $V(\mathbf{r})$, with the spin-splitting being larger close to maxima ["hills", where typically $\Delta_{\mathbf{r}} V(\mathbf{r}) < 0$] while being smaller next to minima ["valleys", where $\Delta_{\mathbf{r}} V(\mathbf{r}) > 0$]. When the tip is placed in a region characterized by strong potential gradients, the spin-split peaks can no longer be resolved due to the broadening of the linewidth of the LDoS. We shall give an explanation to this puzzle from a theoretical point of view using a well-suited extension of the vortex Green's function theory which considers the coupling between the charge and spin degrees of freedom. This Green's function formalism will allow to properly interpret the characteristic LDoS features carefully taking into consideration the nonperturbative aspects peculiar to the quantum Hall regime.

3.2. Spin-Orbit Vortex States

The first necessary ingredient to extend the vortex Green's function formalism described in chapter 1 is the knowledge of the energy spectrum for the clean system and a proper choice of the eigenstates which diagonalize the Landau problem. To that purpose, we recall (see Sec. 2.2.3) that the energy spectrum for the single-particle Hamiltonian (2.18), which described an electron of spin $s = 1/2$, effective mass m^* and charge $e = -|e|$ in the presence of Rashba SO and Zeeman interactions confined to a two-dimensional plane and placed under a homogeneous perpendicular magnetic field, $\mathbf{B} = B\hat{\mathbf{z}}$, was given by the expression

$$E_{n,\lambda} = \hbar\omega_c \left(n - \frac{\lambda}{2}\Delta_n \right), \tag{3.1}$$

where $\Delta_n = \sqrt{(1-Z)^2 + nS^2}$ and S and Z are defined respectively in Eqs. (2.22) and (2.23).

As it happened with the standard spinless Landau levels, the energy levels in Eq. (3.1) are macroscopically degenerate with respect to the guiding center position because they depend on only two quantum numbers (while three are needed to fully represent the eigenstates): the positive integer $n \geq 0$, the Rashba-Landau level index - analog to the

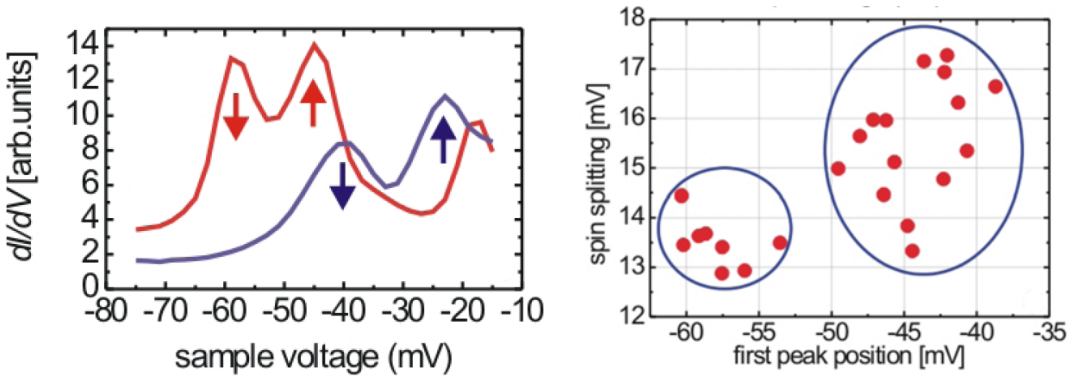

(a) (b)

Figure 3.2 – (a) LDoS (in arbitrary units) as a function of voltage (in mV) measured for two different tip positions in the 2D sample (up and down arrows represent the spin states). The red curve corresponds to the LDoS obtained in a region characterized by a local minimum while the blue curve corresponds to the tip being close to a local maximum. (b) The average energy spin-splitting seems to verify the pattern mentioned in Fig. 3.2 (a) as seen when the energy spin-splitting is plotted as a function of the position of the first LDoS peak. Reprinted from Ref. [11], Copyright 2012 with permission from Elsevier.

spinless Landau level index, and the SO quantum number $\lambda \equiv \lambda(n)$ (that, remember, took the values $\lambda = \pm$ if $n \geq 1$ and $\lambda = -$ if $n = 0$). Note that the macroscopic energy degeneracy of the Rashba-Landau levels with respect to the center of the cyclotron orbit is independent of the strengths of the Rashba and Zeeman interactions. The choice of a basis diagonalizing Eq. (2.18) (that takes into account the great freedom of choice of basis characteristic of the Landau problem) and which allows a proper treatment of the lifting of the degeneracy of the energy levels by a random potential energy seems therefore crucial.

Inspired by the success of the vortex formalism, we shall look for the eigenfunctions of the matrix Hamiltonian (2.18) satisfying the eigenvalue equation $\hat{\mathcal{H}}_0\tilde{\Psi} = E\tilde{\Psi}$ with the following functional form

$$\tilde{\Psi}_{n,\mathbf{R}}(\mathbf{r}) = \sum_{\sigma=\pm} f_\sigma(\theta)\Psi_{n_\sigma,\mathbf{R}}(\mathbf{r}) \otimes |\sigma\rangle. \tag{3.2}$$

This spinor[2] corresponds to a very peculiar combination of the eigenstates of the Pauli matrix σ_z, *i.e.*, $\sigma_z|\sigma\rangle = \sigma|\sigma\rangle$ together with a spatial part characterized by the spinless vortex wavefunctions $\Psi_{n_\sigma,\mathbf{R}}(\mathbf{r})$ [see Eq. (1.43)]. Each of the components $\sigma = \pm$ of the spinor (3.2) presents vortex wave functions characterized by a spin-dependent Landau level quantum number defined by $n_\sigma \equiv n - (1+\sigma)/2$ and weighted by the function

$$f_\sigma(\theta) = \begin{cases} \sin(\theta) & \sigma = +, \\ \cos(\theta) & \sigma = -, \end{cases} \tag{3.3}$$

[2]The form of the spinor wave function can be traced back to the Rashba Hamiltonian (2.19) which written in terms of the matrices $\sigma_\pm = (\sigma_x \pm i\sigma_y)/2$ can be seen to couple (spinless) Landau levels which differ in just one unit. An analogous situation arises when studying the Landau levels of graphene under perpendicular magnetic field [122] since it presents the same Hamiltonian up to a unitary transformation. For this reason, both the graphene spinor wave functions (under perpendicular magnetic field) and the states (3.2) considered here share a common structure.

where the angular parameters are still to be determined. These angles $\theta = \theta_n^\lambda$ get fixed by the diagonalization procedure and are defined by[3]

$$\theta_n^\lambda = \arctan\left[\frac{(1-Z)+\lambda\Delta_n}{S\sqrt{n}}\right]. \tag{3.4}$$

For $n \geq 1$, we also have the relation

$$\theta_n^+ = \theta_n^- + \pi/2, \tag{3.5}$$

between the two projections along the Rashba dependent spin axis. This identity ensures the orthogonality of the SO vortex states within the same Rashba-Landau level n but opposite SO quantum number.

Let us now discuss the properties of the eigenfunctions of the Hamiltonian (2.18) and related to the ansatz (3.2). The eigenstates, dubbed SO vortex eigenstates, are written in Dirac notation as

$$|\nu\rangle \equiv |n, \mathbf{R}, \lambda\rangle = \sum_{\sigma=\pm} f_\sigma(\theta_n^\lambda)|n_\sigma, \mathbf{R}\rangle \otimes |\sigma\rangle, \tag{3.6}$$

where we introduced the multi-index $\nu = \{n, \mathbf{R}, \lambda\}$ for the collection of quantum numbers [therefore the set of normalized SO vortex states[4] is given by $\{|\nu\rangle\} = \{|n, \mathbf{R}, \lambda\rangle\}$] and, as usual, $\tilde{\Psi}_\nu(\mathbf{r}) \equiv \langle \mathbf{r}|\nu\rangle$. Here, we recall that $\mathbf{R} = (X, Y)$ is a continuous quantum number corresponding to the position in the 2D plane of the (guiding) center of the localized vortex wave function.

The SO vortex states inherit many of the properties of their spinless counterparts. First, the SO vortex states are semiorthogonal

$$\langle \nu_1|\nu_2\rangle = \delta_{n_1,n_2}\langle \mathbf{R}_1|\mathbf{R}_2\rangle\delta_{\lambda_1,\lambda_2}, \tag{3.7}$$

as it can be readily checked using the orthogonality relation satisfied by the spin states $\langle\sigma_1|\sigma_2\rangle = \delta_{\sigma_1,\sigma_2}$ and Eq. (3.10a). Therefore, two SO vortex states with same Rashba-Landau level index n and equal SO quantum number λ but different vortex positions $\mathbf{R}$ will present a non-zero overlap characteristic of the coherent states algebra (1.45). More importantly, we can also easily verify that the set of SO vortex states form a basis since they satisfy a completeness relation

$$\begin{aligned}\sum_\nu |\nu\rangle\langle\nu| &= \int \frac{d^2\mathbf{R}}{2\pi l_B^2}\sum_{n=0}^{+\infty}|n, \mathbf{R}\rangle\langle n, \mathbf{R}| \otimes \sum_{\sigma=\pm}|\sigma\rangle\langle\sigma|, \\ &= \mathbb{1}_{\text{orb}} \otimes \mathbb{1}_{\text{s}} \equiv \mathbb{1},\end{aligned} \tag{3.8}$$

where we used the short-hand notation

$$\sum_\nu = \int \frac{d^2\mathbf{R}}{2\pi l_B^2}\sum_{n=0}^{+\infty}\sum_{\lambda=\pm}, \tag{3.9}$$

[3] We note that for the energy level $n = 0$ we have $\lim_{n\to 0}\theta_n^- = 0$.

[4] We have also set $\Psi_{-1,\mathbf{R}}(\mathbf{r}) = \langle \mathbf{r}| - 1, \mathbf{R}\rangle \equiv 0$ so that Eq. (3.6) also holds for the particular Rashba-Landau level $n = 0$.

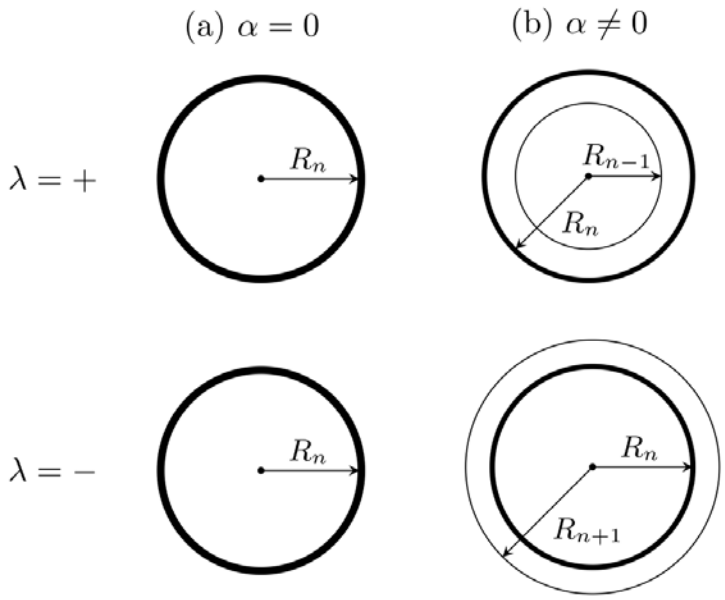

Figure 3.3 – Sketch of the quantum cyclotron orbits for the spin vortex states in column (a) and the SO vortex states in column (b). We consider the states corresponding to the n-th energy level (therefore R_n is the radius of the dominant cyclotron orbit). Top and bottom rows correspond to the different SO projections (in the absence of SO interaction we can identify the SO and spin indices σ).

for the sum over the quantum numbers and the completeness relation satisfied by the spinless vortex states (1.47). Eq. (3.5) also implies that the function $f_\sigma(\theta_n^\lambda)$ verifies the following sum rules

$$\sum_{\sigma=\pm} f_\sigma(\theta_n^{\lambda_1}) f_\sigma(\theta_n^{\lambda_2}) = \delta_{\lambda_1,\lambda_2}, \tag{3.10a}$$

$$\sum_{\lambda=\pm} f_{\sigma_1}(\theta_n^{\lambda}) f_{\sigma_2}(\theta_n^{\lambda}) = \delta_{\sigma_1,\sigma_2}, \tag{3.10b}$$

which can be understood as completeness relations that respectively hold in the λ and σ subspaces.

We close this section by discussing the geometrical properties of the SO vortex states. Due to the spinorial structure of the SO wave functions, the probability density $|\tilde{\Psi}_\nu(\mathbf{r})|^2$ of the state labeled by $\nu = \{n, \mathbf{R}, \lambda\}$ is composed, for each λ, of two quantum cyclotron rings with cyclotron radii R_n and $R_{n\mp1}$ (the latter associated to the components $\sigma = +$ and $-$, respectively) as it can be seen in column (b) of Fig. 3.3 or in the 3D plot in Fig. 3.4. The cyclotron rings collapse into a single one[5] in the limit of vanishing Rashba SO interaction as illustrated in column (a) of Fig. 3.3. For the SO vortex states, one of the cyclotron radii is dominant with respect to the other (so that the probability density is asymmetric in the radial direction). The spatial structure of the probability density already suggests a simple picture that can explain the disorder-driven spatial fluctuations in the presence of Rashba

[5]This is related to the fact that the structure of the spinor becomes trivial. Indeed, we have $\theta_n^\lambda \to (1+\lambda)\pi/4$ and $f_\pm(\theta_n^\pm) = 1$ so that the components of the spinor decouple and can be written as tensor products in the form $|n, \mathbf{R}, \pm\rangle = |n_\pm, \mathbf{R}\rangle|\pm\rangle$ before relabeling of the energy level index n.

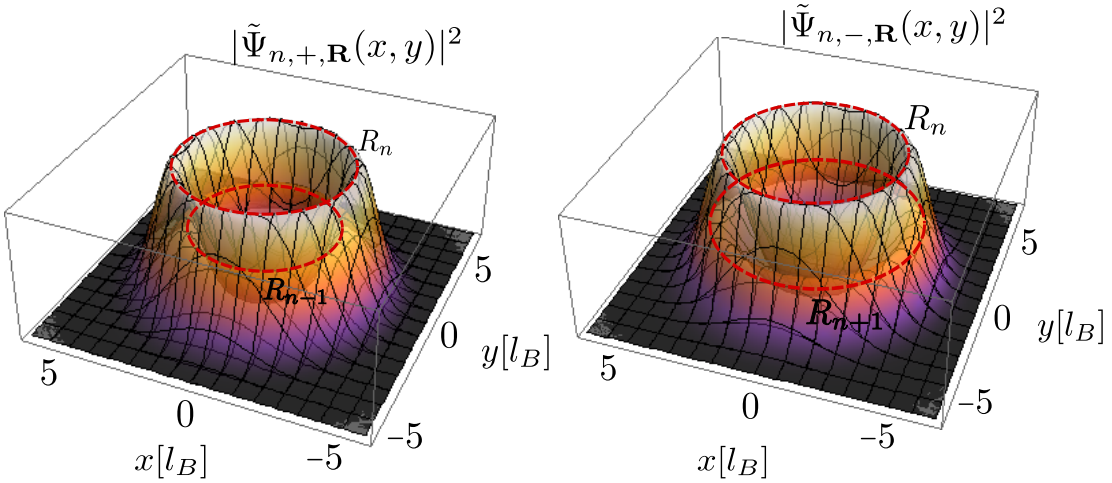

Figure 3.4 – Probability density $|\tilde{\Psi}_\nu(\mathbf{r})|^2$ of the SO vortex states (here shown for $n = 5$ and $\mathbf{R} = \mathbf{0}$). The electron position is measured in units of the magnetic length l_B, which also is the characteristic length scale related to the transverse spread of the wave function. As with the spinless counterparts, the probability density has a rotational symmetry around arbitrary vortex positions $\mathbf{R}$ shared by the two spinor components. This yields a great adaptability (or robustness) to local spatial variations of the potential energy landscape.

SO interaction: each of the components of the spinor (*i.e.* cyclotron rings) is sensitive to different disorder averages along the cyclotron trajectory and the interplay between the two components will give the signatures seen in the experiments.

3.3. Green's Function Formalism

3.3.1. Disorder and fluctuations of the spin-orbit interaction

Let us assume now that the electron is placed in the presence of a generalized (disorder) potential. Therefore, the single-particle Hamiltonian contains two different parts

$$\hat{\mathcal{H}} = \hat{\mathcal{H}}_0 + \hat{U}, \tag{3.11}$$

with $\hat{\mathcal{H}}_0$ the kinetic energy term given in Eq. (2.18) and $\hat{U}$ a potential energy term given by the operator

$$\hat{U} = \hat{V} + \delta\hat{\mathcal{H}}_{\mathrm{R}}. \tag{3.12}$$

The operator $\hat{U}$ itself also presents two distinct terms: the scalar potential [operator] $\hat{V} \equiv V(\hat{\mathbf{r}}) \otimes \mathbb{1}_{\mathrm{s}}$ diagonal in spin space and the fluctuating Rashba Hamiltonian [operator] $\delta\hat{\mathcal{H}}_{\mathrm{R}}$, already introduced in Eq. (2.8) in the absence of magnetic field, and written in the presence of magnetic field as

$$\delta\hat{\mathcal{H}}_{\mathrm{R}} = \frac{1}{2}\left[\delta\alpha(\hat{\mathbf{r}}), [\hat{\mathbf{\Pi}} \times \boldsymbol{\sigma}]_z\right]_+. \tag{3.13}$$

Here we remind that $[\,\cdot\,,\,\cdot\,]_+$ represents the anticommutator which guarantees that the fluctuating Rashba Hamiltonian is well hermitian.

In the local equilibrium regime, the scalar potential in Eq. (3.12) accounts for several contributions representing different physical mechanisms: first, an effective electrostatic term $V_{\text{eff}}(\mathbf{r})$ that includes the effect of random impurities, confinement and mean-field electron-electron interaction; and second, an external contribution proportional to a local electrochemical potential $\Phi(\mathbf{r})$ applied to the sample and related to nonequilibrium electromotive fields $\boldsymbol{\mathcal{E}}(\mathbf{r}) = -\boldsymbol{\nabla}_{\mathbf{r}}\Phi(\mathbf{r})$ that induce in the system a (nonequilibrium) response as a consequence of a voltage drop. We may note that this scalar potential can be very different from the bare one due to screening effects known for leading to the formation of an alternating pattern of compressible and incompressible stripes of different widths in the electron density at high magnetic fields [123, 124]. Therefore, in principle, it is necessary to include both Hartree and exchange components of the Coulomb interaction to self-consistently determine the total scalar potential seen by the electron [125, 126, 127] (we note here that this does not affect our results since all the observables are functionals of the potential energy). Moreover, it is known that exchange can enhance the Rashba SO parameter [128] and the Landé g-factor [129] in 2DEGs. The renormalization of Rashba SO coupling can be included in our approach through an additional fluctuation of $\alpha(\mathbf{r})$. In the case of the Landé g factor, this theory also accounts for a global enhancement through the replacement $g \to g_{\text{eff}}$ where the renormalized g_{eff} now can depend on the magnetic field, temperature, pressure or the electron density. Local enhancement of the g factor requires a minor modification to the theory where the spin-diagonal scalar potential is substituted by a scalar potential which depends on the spin projection, $\hat{V}_{\sigma}(\mathbf{r})$.

3.3.2. Dyson equation in the spin-orbit vortex representation

To investigate the combined effects of the smooth scalar potential and Rashba SO fluctuations on the electron dynamics, we have extended the coherent-state Green's function formalism described in chapter 1 for the standard 2DEG. To that purpose, we consider the Green's operator associated to the Hamiltonian (3.11) and satisfying Eq. (1.50). Projection onto the SO vortex representation $\{|\nu\rangle\}$ [which is allowed thanks to the completeness relation (3.8)] gives the equation of motion for the Green's function (the kernel of the Green's operator) in the energy space

$$(\omega - E_{n_1,\lambda_1} \pm i0^{+})G^{R,A}_{\nu_1;\nu_2}(\omega) = \langle \nu_1|\nu_2\rangle + \sum_{\nu_3} U_{\nu_1;\nu_3} G^{R,A}_{\nu_3;\nu_2}(\omega), \tag{3.14}$$

where ω is the variable conjugate (in the Fourier sense) to the time difference $\tau = t_1 - t_2$, $U_{\nu_1;\nu_2} = \langle \nu_1|\hat{U}|\nu_2\rangle$ are the matrix elements of the potential $\hat{U}$ and $G^{R,A}_{\nu_1;\nu_2}(\omega) = \langle \nu_1|\hat{G}^{R,A}(\omega)|\nu_2\rangle$ the matrix elements of the Green's operator. In this representation, the Green's function $G^{R,A}_{\nu_1;\nu_2}(\omega) = G^{R,A}(n_1,\lambda_1,\mathbf{R}_1;n_2,\lambda_2,\mathbf{R}_2;\omega)$ gives the probability amplitude for a vortex with circulation n_2 and SO quantum number λ_2 located at position $\mathbf{R}_2$ to be elastically scattered (since energy ω is conserved within the process) to a position $\mathbf{R}_1$ with the new circulation n_1 and SO quantum number λ_1. From Dyson equation (3.14) it is clear that whenever $\hat{U} \neq 0$, the Green's function will generally be no longer diagonal with respect to the discrete quantum numbers n and λ, the mixing between the latter depending on the particular form of the potential energy function $\hat{U}$. Clearly this is not the case in the clean limit ($\hat{U} = 0$) where the unperturbed Green's function is diagonal both in the Rashba-Landau and SO quantum numbers and presents the coherent states nonzero overlap for the dependence on the vortex position.

Generally, as we have seen in chapter 1 in the disordered spinless 2DEG case, finding an analytical solution to Dyson equation for an arbitrary potential $\hat{U}$ and all possible values of the magnetic field is unquestionably a *Herculean* task. However, we note that the coherent character of the degeneracy quantum number $\mathbf{R}$ is the same both for the spinless and the SO vortex states. Therefore, the matrix elements of the potential and the Green's function can be written in a similar way

$$U_{\nu_1;\nu_2} = \langle \mathbf{R}_1|\mathbf{R}_2\rangle T_{\mathbf{R}_{12}}\left[u_{n_1,\lambda_1;n_2,\lambda_2}(\mathbf{R}_{12})\right], \tag{3.15}$$

$$G^{R,A}_{\nu_1;\nu_2}(\omega) = \langle \mathbf{R}_1|\mathbf{R}_2\rangle T_{\mathbf{R}_{12}}\left[g^{R,A}_{n_1,\lambda_1;n_2,\lambda_2}(\mathbf{R}_{12};\omega)\right], \tag{3.16}$$

extracting the non-analytic dependence of the magnetic length to the overlap $\langle \mathbf{R}_1|\mathbf{R}_2\rangle$. Here, we remind that $T_{\mathbf{R}}$ is an infinite order differential operator given in Eq. (1.61) which delocalizes the vortex states along the equipotential lines of the generalized disorder potential and $\mathbf{R}_{12} = [\mathbf{R}_1 + \mathbf{R}_2 + i(\mathbf{R}_1 - \mathbf{R}_2)\times\hat{\mathbf{z}}]/2$. As in the spinless case, this functional dependence implies that the nonlocal Green's function is completely specified once the SO vortex Green's function $g_{n_1,\lambda_1;n_2,\lambda_2}(\mathbf{R}_{12};\omega)$ is known for coinciding vortex positions $\mathbf{R}_1 = \mathbf{R}_2 \equiv \mathbf{R}$. Following similar steps to those for the standard 2DEG and taking advantage of the coherent character of the SO vortex states, which present the same nature as that of the vortex states, shown in Sec. 1.5, the resulting local SO vortex Green's function $g(\mathbf{R},\omega)$ is found to obey the exact equation of motion

$$(\omega - E_{n_1,\lambda_1} \pm i0^+) g_{n_1,\lambda_1;n_2,\lambda_2}(\mathbf{R};\omega) = \delta_{n_1,n_2}\delta_{\lambda_1,\lambda_2} + \sum_{n_3,\lambda_3} u_{n_1,\lambda_1;n_3,\lambda_3}(\mathbf{R}) \star g_{n_3,\lambda_3;n_2,\lambda_2}(\mathbf{R};\omega), \tag{3.17}$$

where we have dropped the retarded and advanced superscripts (the corresponding local SO Green's function can be inferred from the sign of the infinitesimal imaginary part).

Due to the magnetic Groenewold-Moyal $\star$ product [defined in Eq. (1.63)], the previous equation is a complicated matrix partial differential equation of infinite order. However, as we show in the next section, solutions to this equation can be obtained for physically relevant cases under certain conditions. If a solution to Eq. (3.17) is found, we can then compute microscopic expressions for different observables writing the full Green's function, related to the local SO vortex Green's function through Eq. (3.16), in the electronic representation $\{|\mathbf{r}\rangle\}$, *i.e.* $G(\mathbf{r},\mathbf{r}',\omega) = \langle \mathbf{r}|\hat{G}(\omega)|\mathbf{r}'\rangle$. The change of representation from vortex to electronic can be performed via a change of basis

$$G(\mathbf{r},\mathbf{r}',\omega) = \sum_{\nu_1,\nu_2} G_{\nu_1;\nu_2}(\omega)\tilde{\Psi}^\dagger_{\nu_2}(\mathbf{r}')\tilde{\Psi}_{\nu_1}(\mathbf{r}), \tag{3.18}$$

where we remind that $\tilde{\Psi}_\nu(\mathbf{r}) = \langle \mathbf{r}|\nu\rangle$ are the SO vortex wave functions given in Eq. (3.6). Performing another change of coordinates $(\mathbf{R}_1,\mathbf{R}_2) \to (\mathbf{R}_{12},\mathbf{R}_{\rm rel})$ with relative coordinate $\mathbf{R}_{\rm rel} = (\mathbf{R}_2 - \mathbf{R}_1)/2$, together with a Taylor expansion of the integrand, it is possible to compute analytically the integral over the relative coordinate [130] so that the electronic Green's function may be evaluated at coinciding vortex positions $\mathbf{R}_{12} \equiv \mathbf{R}$. Furthermore, we can perform an additional integration by parts to obtain

$$G_{\sigma\sigma'}(\mathbf{r},\mathbf{r}',\omega) = \int \frac{d^2\mathbf{R}}{2\pi l_B^2} \sum_{n_1,\lambda_1}\sum_{n_2,\lambda_2} f_\sigma(\theta^{\lambda_1}_{n_1}) f_{\sigma'}(\theta^{\lambda_2}_{n_2}) \times F_{n_{1\sigma},n_{2\sigma'}}(\mathbf{r},\mathbf{r}',\mathbf{R})\, g_{n_1,\lambda_1;n_2,\lambda_2}(\mathbf{R};\omega), \tag{3.19}$$

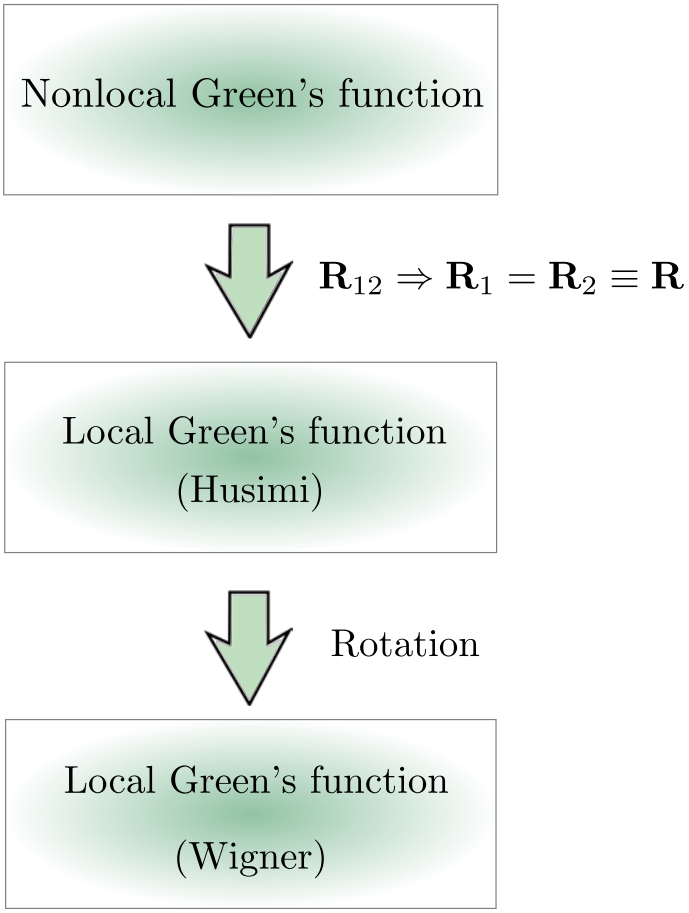

Figure 3.5 – Scheme of the procedure used to obtain Dyson equation (3.17) as done in Ref. [121] and described in detail both in Sec. 1.5 and the present section.

which is an exact expression for the matrix elements of the Green's function in spin space (where it is a 2×2 matrix with entries labeled by the spin indices $\sigma, \sigma' \in \{\pm\}$). The electronic kernel (also known as electronic structure factor [2]) is defined by

$$F_{n_1,n_2}(\mathbf{r}, \mathbf{r}', \mathbf{R}) \equiv T_{\mathbf{R}}^{-1} \left[\Psi_{n_2,\mathbf{R}}^{*}(\mathbf{r}') \Psi_{n_1,\mathbf{R}}(\mathbf{r}) \right], \tag{3.20}$$

with $\Psi_{n,\mathbf{R}}(\mathbf{r}) = \langle \mathbf{r} | n, \mathbf{R} \rangle$ the vortex wave functions given in Eq. (1.43) and $T_{\mathbf{R}}^{-1}$ the inverse of Eq. (1.61). This kernel function contains all the information about the electronic (vortex) wave functions[6] (and therefore, describes the quantum contribution to the cyclotron motion of the electrons subjected to the Lorentz force). Eq. (3.19) can then be understood as the quantum decomposition of the electronic motion into fast orbital and slow guiding center (vortex) degrees of freedom, with the latter given by the local SO vortex Green's function solution of Dyson equation (3.17).

3.3.3. Reduced matrix elements of the generalized disorder potential

The reduced matrix elements of the generalized potential $u_{n_1,\lambda_1;n_2,\lambda_2}(\mathbf{R})$ present in Dyson equation can be clearly written [see Eq. (3.12)] as a sum of the reduced matrix

[6] Note that the kernel is independent of the, otherwise, arbitrary potential energy.

elements of the scalar potential and the contribution to the Hamiltonian describing spatial fluctuations of the Rashba SO coupling

$$u_{n_1,\lambda_1;n_2,\lambda_2}(\mathbf{R}) = v_{n_1,\lambda_1;n_2,\lambda_2}(\mathbf{R}) + \delta\mathcal{H}_{n_1,\lambda_1;n_2,\lambda_2}(\mathbf{R}). \tag{3.21}$$

These reduced matrix elements find an exact expression in the SO vortex representation. First, for the scalar potential we get

$$v_{n_1,\lambda_1;n_2,\lambda_2}(\mathbf{R}) = \sum_{\sigma=\pm} f_\sigma(\theta_{n_1}^{\lambda_1}) f_\sigma(\theta_{n_2}^{\lambda_2}) v_{n_{1\sigma};n_{2\sigma}}(\mathbf{R}), \tag{3.22}$$

where

$$v_{n_{1\sigma};n_{2\sigma}}(\mathbf{R}) = T_{\mathbf{R}}^{-1}\langle n_{1\sigma}, \mathbf{R}|\hat{V}|n_{2\sigma}, \mathbf{R}\rangle, \tag{3.23}$$

$$= \int d^2\boldsymbol{\eta}\, F_{n_{1\sigma},n_{2\sigma}}(\boldsymbol{\eta}, \boldsymbol{\eta}, \mathbf{0}) V(\boldsymbol{\eta} + \mathbf{R}). \tag{3.24}$$

The former matrix elements, written as a convolution of the bare scalar potential $V(\mathbf{r})$ and the electronic structure factor, can be interpreted as an effective potential seen by the vortex located at position $\mathbf{R}$. This potential results after a partial average over the cyclotron motion that allows us to integrate out the fast angular degree of freedom[7].

Next, we compute in an analogous way the reduced matrix elements of the contribution to the generalized potential which describes the fluctuations in the Rashba SO parameter to obtain

$$\delta\mathcal{H}_{n_1,\lambda_1;n_2,\lambda_2}(\mathbf{R}) = -\frac{\hbar\sqrt{n_1}}{\sqrt{2}l_B} \sum_{\sigma=\pm} f_{-\sigma}(\theta_{n_1}^{\lambda_1}) f_\sigma(\theta_{n_2}^{\lambda_2}) \delta\alpha_{n_{1\sigma};n_{2\sigma}}(\mathbf{R}) + (1 \leftrightarrow 2), \tag{3.25}$$

where the notation $(1 \leftrightarrow 2)$ means exchanging indices 1 and 2 in the former expressions. Here, the matrix elements of the fluctuating Rashba parameter $\delta\alpha_{n_{1\sigma};n_{2\sigma}}(\mathbf{R})$ are defined using Eqs. (3.23) and (3.24) replacing the scalar potential $\hat{V}$ by the Rashba fluctuations $\widehat{\delta\alpha} \equiv \delta\alpha(\hat{\mathbf{r}})$. Similarly, the quantity $\delta\alpha_{n_{1\sigma};n_{2\sigma}}(\mathbf{R})$ can be regarded as an effective Rashba parameter resulting from the cyclotron averaging of the Rashba fluctuations.

Finally, we can make the following observation: both reduced matrix elements appearing in Eqs. (3.22) and (3.25) are linear combinations of the spinless matrix elements of the disorder potential / Rashba fluctuations, with the additional dependence on the SO quantum number λ (resulting from SO coupling) entering through the weights $f_\sigma(\theta_n^\lambda)$. However, Eq. (3.22) for the scalar potential shows that the matrix elements are necessarily diagonal in spin space while in Eq. (3.25), we clearly see that, as a consequence of the fluctuations in the Rashba parameter, spin is not a good quantum number. Therefore, we expect that each of these contributions to be always decoupled in the energy spectrum formula that can be derived from the poles of the Green's function.

[7] A consequence of this wave function averaging procedure is that the effective potential is always smoother than the bare one. For this reason, the condition of having smooth potentials at the scale of l_B, as presented in Sec. 1.5, can be relaxed and very rough bare potentials such as point-like δ-function disorder potentials can still be taken into account within the present theory [131].

3.4. Energy Spectrum in Locally Flat Generalized Potentials

3.4.1. Projection into a single Rashba-Landau energy level

The Dyson equation (3.17) is exact and can be considered, in principle, for any value of the external magnetic field. We now focus on the regime of high magnetic fields characterized by negligible mixing between the Rashba-Landau energy levels. Experimentally, this regime can be attained for reasonable values of the applied magnetic field $B \gtrsim 1$ T. Mathematically, we consider the regime $\omega_c \to +\infty$ with l_B finite (so that the vortex dynamics is still quantum-mechanical), equivalent to the formal limit $m^* \to 0$. Therefore, it is licit to project the dynamics into a single energy level n with reduced matrix elements of the potential $u_{n_1;\lambda_1;\lambda_2}(\mathbf{R}) \equiv u_{n_1,\lambda_1;n_2,\lambda_2}(\mathbf{R})\,\delta_{n_1,n_2}$ given by

$$u_{n;\lambda_1;\lambda_2}(\mathbf{R}) = v_{n;\lambda_1;\lambda_2}(\mathbf{R}) - \frac{\hbar\sqrt{2n}}{l_B}\sin(\theta_n^{\lambda_1}+\theta_n^{\lambda_2})\overline{\delta\alpha}_n(\mathbf{R}). \tag{3.26}$$

Here, the matrix elements of the scalar potential take the following form

$$v_{n;\lambda_1;\lambda_2}(\mathbf{R}) = \sum_{\sigma=\pm} f_\sigma(\theta_n^{\lambda_1}) f_\sigma(\theta_n^{\lambda_2}) v_{n_\sigma;n_\sigma}(\mathbf{R}), \tag{3.27}$$

where $v_{n_\sigma}(\mathbf{R}) \equiv v_{n_\sigma;n_\sigma}(\mathbf{R})$ can be deduced straightforwardly from Eq. (3.24). The term $\overline{\delta\alpha}_n(\mathbf{R})$ gives the average of the matrix elements of the Rashba fluctuations in the SO-split nth energy level

$$\overline{\delta\alpha}_n(\mathbf{R}) = \frac{1}{2}\left[\delta\alpha_{n-1}(\mathbf{R}) + \delta\alpha_n(\mathbf{R})\right], \tag{3.28}$$

with $\delta\alpha_n(\mathbf{R}) \equiv \delta\alpha_{n;n}(\mathbf{R})$. Note that the previous combination can be naturally expected due to the particular spinorial structure of the SO vortex wave functions.

Evidently, we find that the SO vortex Green's function is also diagonal in the Rashba-Landau level index

$$g_{n_1,\lambda_1;n_2,\lambda_2}(\mathbf{R};\omega) = g_{n_1;\lambda_1;\lambda_2}(\mathbf{R};\omega)\,\delta_{n_1,n_2}. \tag{3.29}$$

and Dyson equation (3.17) simplifies to

$$(\omega - E_{n,\lambda_1} \pm i0^+) g_{n;\lambda_1;\lambda_2}(\mathbf{R};\omega) = \delta_{\lambda_1,\lambda_2} + \sum_{\lambda_3} u_{n;\lambda_1;\lambda_3}(\mathbf{R}) \star g_{n;\lambda_3;\lambda_2}(\mathbf{R};\omega), \tag{3.30}$$

The diagonal SO vortex Green's function solution of the previous equation is clearly symmetrical in the SO $g_{n;\lambda_1;\lambda_2}(\mathbf{R};\omega) = g_{n;\lambda_2;\lambda_1}(\mathbf{R};\omega)$ as a consequence of symmetry properties of the high-field matrix elements of the generalized potential $u_{n;\lambda_1;\lambda_2}(\mathbf{R}) = u_{n;\lambda_2;\lambda_1}(\mathbf{R})$.

As discussed in chapter 1, the projection into a single energy level is a manifestation of the basic fact that the guiding center (vortex) motion and the cyclotron motion become decoupled at high magnetic fields. The ineffective energy exchange between the two degrees of freedom can only occur quantum-mechanically by a change of the (topological) Landau level index which *a priori* is forbidden due to the large band gap between the energy levels. In the presence of SO coupling, one has to be more careful with this approximation since the extra (spin) degree of freedom can induce transitions between the different energy levels. Moreover, as pointed out in Sec. 3.2, the energies $E_{n,\lambda}$ in the clean case are not equidistant in the presence of both SO and Zeeman interactions and are even characterized by level crossings for specific values of the magnetic field renormalized

Rashba parameter S. However, it is still easy to formulate a simple (smoothness) criterion that allows us to neglect the mixing between the energy levels in the presence of Rashba SO interaction: coupling between different Rashba-Landau energy levels can be neglected whenever it is energetically forbidden to elastically scatter [due to the generalized potential $u_{n_1,\lambda_1;n_2,\lambda_2}(\mathbf{R})$] from one state, with a given SO projection, to another, with opposite SO projection. It is possible to show [by writing Eq. (3.23) as a series of powers in the magnetic length, see chapter 4] that the first subdominant term in l_B induce a mixing between different Rashba-Landau levels n and SO quantum numbers λ and therefore the following inequality related to potential gradients has to be satisfied

$$l_B|\boldsymbol{\nabla}_{\mathbf{R}}U(\mathbf{R})| \ll |E_{n_2,\lambda} - E_{n_1,-\lambda}|. \tag{3.31}$$

Clearly, this condition is violated at the special (countable) degeneracy points where two different energy levels cross, but tells us that our high magnetic field approximation will hold as long as we are not working close to these points[8].

3.4.2. Quantum spin-orbit drift states

As in the spinless case, solving Eq. (3.30) is still a very hard problem due to the infinite-order pseudo-differential operator $\star$. This form of the magnetic Groenewold-Moyal product (which, we remind, is not unique) has been proved to be preferentially selected at high magnetic fields whenever the macroscopic degeneracy of the energy levels is lifted in the presence of a disorder potential [122, 132]. Moreover, it generates a hierarchy of local energy scales built from the subsequent spatial derivatives of the potential and which are related to intrinsic geometric invariants, *e. g.* local Gaussian curvature that involves second-order derivatives in orthogonal directions. The energy scales in this hierarchy decrease as the order of the derivatives involved increases, allowing us to develop a systematic and controlled calculation. This also expresses the robustness of the SO vortex representation at high magnetic fields, see Sec. 4.2.2. Remarkably, the solution to purely 1D problems can be obtained exactly within this form, since the $\star$ product operator reduces to a simple product between functions $\star \simeq \times$ (or, all subleading energy scales vanish). For arbitrary 2D potentials, we may expect that replacing the $\star$ product by a simple product is a very good quantitative approximation, *as long as* the curvature energy is smaller than the temperature energy scale. This is usually the case for a smooth potential where curvature plays an important role only close to the critical points of the potential landscape where the drift velocity vanishes. This is equivalent to considering that the equipotential lines of the potential are relatively straight and amounts to describing the generalized potential as a locally flat energy landscape. In this sense, we translate into the Green's function language, the quantum drift state approximation originally introduced by Trugman [104] for weakly curved disorder potentials in terms of wave functions but without the complicated parametrization of the equipotentials.

Therefore, at leading order in the drift approximation we can replace the $\star$-product operator by the usual product between functions. This leads to a considerable simplification since the system of linear coupled partial differential equations obeyed by the local SO vortex Green's function is reduced to a system of linear coupled algebraic equations with

[8] Actually, this is not a problem experimentally since we can move away from the degeneracy points using the tunable parameters α or $\mathbf{B}$.

exact solution

$$g_{n;\lambda_1;\lambda_2}(\mathbf{R};\omega) = \frac{[\omega - E_{n,\lambda_1} - u_{n;\lambda_1;\lambda_2}(\mathbf{R})]\delta_{\lambda_1,\lambda_2} + u_{n;-\lambda_1;-\lambda_2}\delta_{-\lambda_1,\lambda_2}}{[\omega - \xi_{n,+}(\mathbf{R}) \pm i0^+][\omega - \xi_{n,-}(\mathbf{R}) \pm i0^+]}. \tag{3.32}$$

The SO Green's function presents a double pole structure[9]. The poles of the local SO Green's function give the renormalized Rashba-Landau energy levels which contain the contribution of the generalized potential energy

$$\xi_{n,\epsilon}(\mathbf{R}) = \hbar\omega_c \left[n - \frac{\epsilon}{2}\Delta_n(\mathbf{R})\right] + \overline{v}_n(\mathbf{R}), \tag{3.33}$$

with $\epsilon \equiv \epsilon(n)$ a renormalized SO quantum number (due to the mixing between λ_1 and λ_2). This new quantum number also takes the values $\epsilon = \pm$ for $n \geq 1$ and $\epsilon = -$ for $n = 0$ as it happens for the SO quantum number λ. Note that expression (3.33) has clearly a structure similar to the clean spectrum (2.21) with

$$\Delta_n(\mathbf{R}) = \sqrt{[1 - Z_{n,\text{eff}}(\mathbf{R})]^2 + nS^2_{n,\text{eff}}(\mathbf{R})}, \tag{3.34}$$

$$\overline{v}_n(\mathbf{R}) = \frac{1}{2}\left[v_{n-1}(\mathbf{R}) + v_n(\mathbf{R})\right]. \tag{3.35}$$

and dressed Zeeman and Rashba SO parameters, which depend both on the level index n and the vortex position $\mathbf{R}$

$$Z_{n,\text{eff}}(\mathbf{R}) \equiv Z + \delta Z_n(\mathbf{R}) = Z + \frac{[v_{n-1}(\mathbf{R}) - v_n(\mathbf{R})]}{\hbar\omega_c}, \tag{3.36}$$

$$S_{n,\text{eff}}(\mathbf{R}) \equiv S + \delta S_n(\mathbf{R}) = \frac{2\sqrt{2}}{\omega_c l_B}\left[\alpha + \overline{\delta\alpha}_n(\mathbf{R})\right]. \tag{3.37}$$

As anticipated in Sec. 3.3.3, the smooth fluctuations of the Rashba and Zeeman parameters have distinct origins: the spatial fluctuations of the Rashba SO coupling leads to a spatial dependent SO parameter, $\delta S_n(\mathbf{R})$, while the fluctuations of the scalar disorder yield a spatially fluctuating part in the effective Zeeman coupling, $\delta Z_n(\mathbf{R})$. Both contributions drive different mechanisms for the spatial dispersion of the energy levels, together with the average effective potential $\overline{v}_n(\mathbf{R})$ involving different spinless Landau level indices (its structure can be traced back to the form of the SO vortex spinor). As a final remark, it is worth noting that the spectrum (3.33) still presents level crossings (accidental degeneracies). This is related to the fact that we have neglected Landau level mixing so that the projected Hamiltonian is (classically) integrable. It is expected that, whenever mixing between Rashba-Landau levels induced by the smooth disorder potential is included, anticrossings will appear due to level repulsion (see for example Refs. [91, 92]).

3.4.3. Interplay between disorder and spin-orbit fluctuations

In this section, we want to analyze the energy spectrum (3.33) obtained from Dyson equation and discuss several mechanisms which can participate in the spatial dispersion of the energy levels in arbitrary disorder potentials.

[9]For $n = 0$, the local SO Green's function has a single pole due to the fact that the energy level has half of the degeneracy in comparison to $n \geq 1$ energy levels. The obtained formula is still valid in this case since we have $v_{-1}(\mathbf{R}) \equiv 0$ and $\delta\alpha_{-1}(\mathbf{R}) \equiv 0$ as a consequence of the definition $\Psi_{-1,\mathbf{R}}(\mathbf{r}) \equiv 0$.

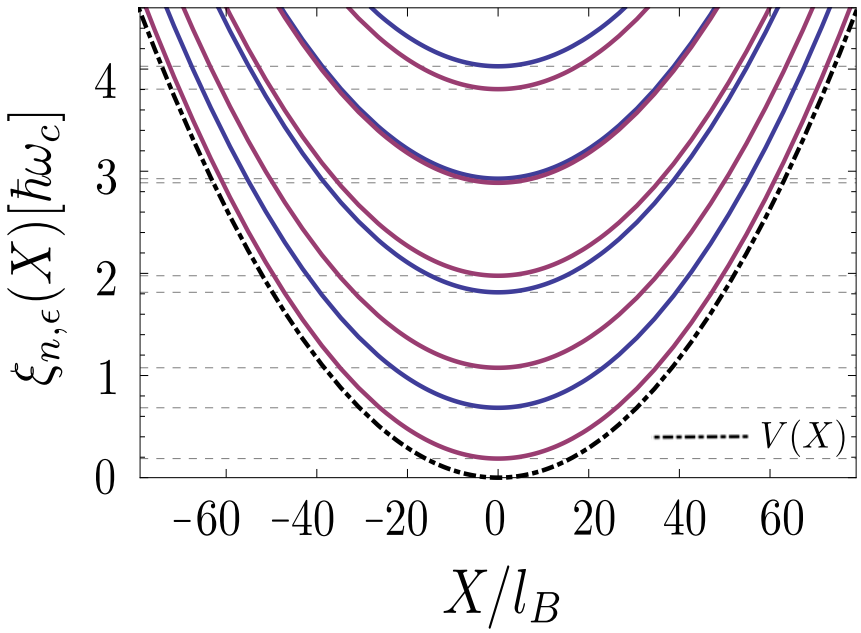

Figure 3.6 – Energy dispersion at high magnetic fields (measured in units of the cyclotron energy $\hbar\omega_c$) from Eq. (3.38), as a function of the normalized vortex position X/l_B. Each set of parabolas (blue/ red) presents opposite quantum number, $\epsilon_1 = -\epsilon_2$. The dashed-dotted parabola represents the quadratic 1D potential with a characteristic length scale chosen to be $l_0 = 4l_B$. The parameters are the same as in Fig. 2.3 which yields the SO strength $S_{\rm exp} = 0.88$. The dashed horizontal lines underline the energies at $X = 0$ which can be related to the energy levels in the absence of potential energy (vertical line in Fig. 2.3).

As a first simple situation, let us consider a (global) parabolic 1D potential $V(\mathbf{R})$ in the absence of Rashba fluctuations. This potential can be used as a toy model to describe the edge states within the Hall bar geometry, for which no analytical explicit solution is known in the presence of Rashba SO interaction. As discussed above, in this case the drift approximation is exact (since the Gaussian curvature is equal to zero) and the reduced matrix elements of the scalar potential, diagonal in the index $n \geq 0$, have the (exact) expression given in Eq. (1.65). For the potential profile $V(x) = (1/2)m^*\omega_0^2 x^2$ with characteristic length scale $l_0 = \sqrt{\hbar/(m^*\omega_0)}$ we then obtain from Eq. (3.33) the following analytical expression[10] for the eigenenergies

$$\begin{aligned}\xi_{n,\epsilon}(X) &= n\hbar\omega_c\left[1+\frac{1}{2}\left(\frac{\omega_0}{\omega_c}\right)^2\right]+\frac{\hbar\omega_0}{2}\left(\frac{X}{l_0}\right)^2 \\ &\quad -\frac{\epsilon}{2}\hbar\omega_c\sqrt{nS^2+\left[1-Z+\frac{1}{2}\left(\frac{\omega_0}{\omega_c}\right)^2\right]^2}. \end{aligned} \tag{3.38}$$

[10]This analytical solution is closely related to the implicit formula derived in Ref. [97] by using the mapping [96, 97, 98] between the quadratic model at high fields and the integrable Jaynes-Cummings model.

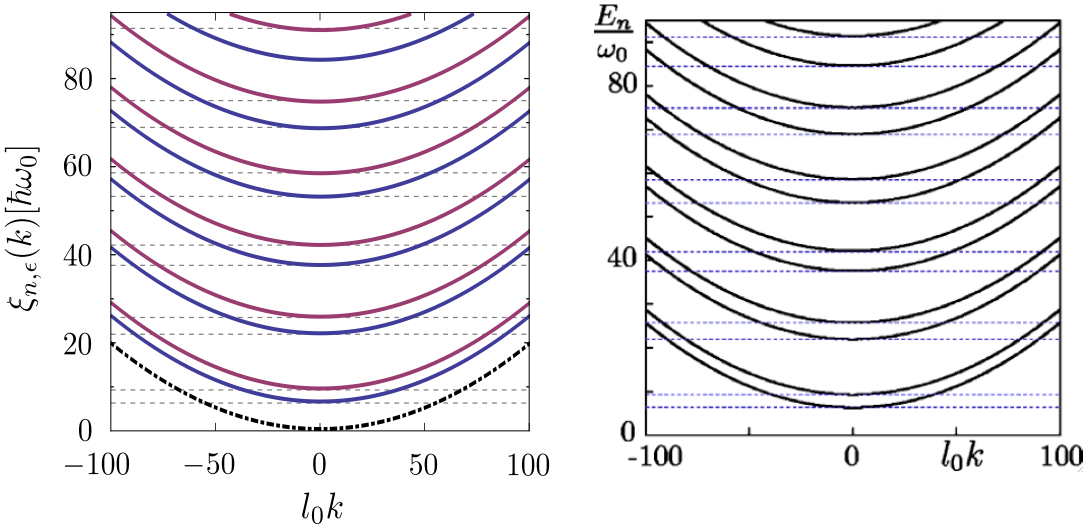

(a) (b)

Figure 3.7 – Energy spectra at high magnetic fields ($l_0 = 4l_B$), measured in units of the characteristic energy of the parabolic potential profile $\hbar\omega_0$, as a function of the adimensional quantity kl_0 (here k is a continuous quantum number defined as $k \equiv X/l_B^2$). Figure (a) has been obtained from Eq. (3.38) while (b) corresponds to a numerical calculation performed in Ref. [96]. In both cases, typical InAs parameters $m^* = 0.04m_0$, $\hbar\alpha = 1 \cdot 10^{-11}$ eV m, $g = -8$ are considered, while the characteristic length scale of the potential is fixed by the Rashba SO interaction imposing $l_0 = l_{\mathrm{SO}} \equiv \hbar/(2m^*\alpha)$. Note that the obtained energy spin-splitting between parabolas is quantitatively consistent between the analytical and numerical studies of the quantum wire model, further validating our analytical high-field theory. As before, the dashed-dotted parabola represents the confinement potential measured in units of $\hbar\omega_0$. The dashed horizontal lines are the signature of the eigenenergies of the Rashba system in the absence of confinement potential and can be mapped to the Jaynes-Cummings eigenenergies, well-known in quantum optics, which are the energies of a dissipationless two-level system interacting with a single quasi-resonant cavity mode in the rotating wave approximation [133]. Figure (b) reprinted with permission from [96]. Copyright 2005 by the American Physical Society.

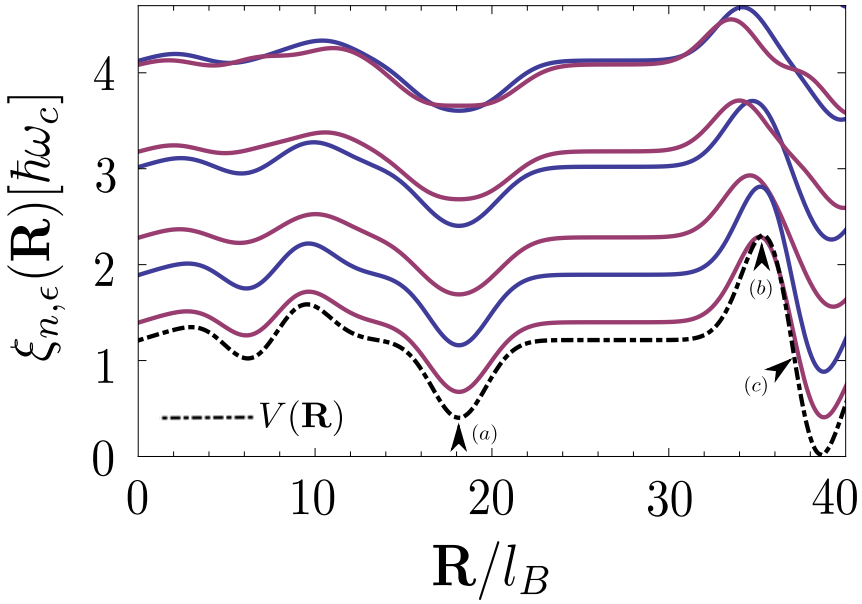

Figure 3.8 – Energy dispersion at high magnetic fields (in units of the cyclotron energy $\hbar\omega_c$) from Eq. (3.33), as a function of the normalized vortex position $\mathbf{R}/l_B$, for a random smooth quasi-1D potential (shown as a dashed-dotted line). We consider the same experimentally compatible parameters as in Fig. 2.3 with SO coupling strength $S_{\rm exp} = 0.88$. The labels (a), (b), (c) correspond respectively to the positions of a local minimum, local maximum, and strong gradient region, and represent the three typical STM tip positions to be considered in Fig. 3.9 when addressing the features of the local density of states.

We show the resulting energy levels in Figs. 3.6 and 3.7, the first figure made considering values for the parameters compatible with InSb while the latter figure is made for InAs typical parameters. In both figures, it is clear that the renormalized Rashba-Landau energy levels consist in a set of energy-shifted parabolas as a function of the spatial guiding center coordinate X (measured in the confinement direction). Moreover, one can see from the analytical expression that any two given parabolas will always follow the same parabolic dispersion and therefore will present a uniform energy splitting because the dressed Zeeman coupling (3.36) is independent of the vortex position for globally quadratic potentials. Indeed, according to Eq. (3.36), the second-order derivatives of the potential lead to a modification of the effective Zeeman parameter with respect to the free case by the (constant) quantity

$$\delta Z_n(\mathbf{R}) = -\frac{l_B^2 \Delta_{\mathbf{R}} V(\mathbf{R})}{2\hbar\omega_c} \tag{3.39}$$

for $n \geq 1$. As a consequence, the spatial dispersion of the energy spin-splitting can not occur for global quadratic potentials but dispersion is possible if the Laplacian of the potential varies spatially.

For an arbitrary smooth disorder potential, we have to consider therefore the expression (3.33) for the energy spectrum along with the general formulae (3.36) and (3.37) for the dressed Zeeman and Rashba SO parameters. We illustrate in Fig. 3.8 this energy dispersion for a random smooth quasi-1D potential $V(\mathbf{r})$ assuming again a uniform Rashba coupling constant. As expected, all the energy levels follow roughly the bare disorder potential, with

increasing flattening effects of the spatial dispersion when the Rashba-Landau level index n increases. This is a consequence of the stronger averaging effects in the effective potentials (3.24) over cyclotron orbits with larger radii. In addition, we notice that some energy levels cross for particular spatial positions. These crossings are expected to change into tiny anticrossings whenever the degeneracy is lifted by weak Rashba-Landau level mixing (neglected here). More importantly, it can be shown that the spin-splitting between pairs of energy levels with opposite SO quantum number depend on the vortex position. This effect is a consequence of the spatial variations of the term $\delta Z_n(\mathbf{R})$ appearing in the effective Zeeman coupling (3.36) and is weak for effective potentials $v_n(\mathbf{R})$ smooth at the scale of l_B. It is also reasonable to assume that, due to averaging over the cyclotron orbit, the spatial fluctuations of the effective SO coupling parameter $\delta S_n(\mathbf{R})$ are small [or $\delta\alpha_n(\mathbf{R})$ are smooth functions at the scale of l_B]. If the fluctuations have small amplitude, it is relevant to linearize the energy spectrum (3.33) with respect to $\delta Z_n(\mathbf{R})$ and $\delta S_n(\mathbf{R})$. We get

$$\xi_{n,\epsilon}(\mathbf{R}) \simeq E_{n,\epsilon} + \hbar\omega_c \frac{\epsilon}{2} \frac{(1-Z)\,\delta Z_n(\mathbf{R}) - nS\,\delta S_n(\mathbf{R})}{\sqrt{(1-Z)^2 + nS^2}} + \overline{v}_n(\mathbf{R}). \tag{3.40}$$

Application of Eq. (3.36) to express $\delta Z_n(\mathbf{R})$ in terms of the effective potential $v_n(\mathbf{R})$, we can use this result to obtain an approximate analytical expression for the energy spin-splitting within the first pair of Rashba-Landau energy levels $E_s(\mathbf{R}) = \xi_{0,-}(\mathbf{R}) - \xi_{1,+}(\mathbf{R})$,

$$\begin{aligned} E_s(\mathbf{R}) \simeq E_{0,-} - E_{1,+} + \frac{\hbar\omega_c}{2} \frac{S\,\delta S_1(\mathbf{R})}{\sqrt{(1-Z)^2 + S^2}} \\ + \frac{1}{2}\left[1 - \frac{1-Z}{\sqrt{(1-Z)^2+S^2}}\right] [v_0(\mathbf{R}) - v_1(\mathbf{R})]\,. \end{aligned} \tag{3.41}$$

The analysis of this expression reveals important information that can be useful to understand the experimental STS results presented in Sec. 3.1. First, both the Rashba SO fluctuations $\delta S_1(\mathbf{R})$ and the scalar potential fluctuations $[v_0(\mathbf{R}) - v_1(\mathbf{R})]$ can produce a spatial dispersion of the spin-splitting. Both mechanisms present different dependencies on the Rashba-Landau level index and the external magnetic field (so that, in principle, can be experimentally discriminated). Second, in the semiclassical limit $l_B \to 0$, only the contribution resulting from the fluctuations of the Rashba coupling coefficient does not vanish revealing that the dispersive term associated to the effective scalar potentials has a purely quantum-mechanical origin.

3.5. Local Density of States

3.5.1. General formula in locally flat disorder potentials

We aim in this section at obtaining an analytical formula for the LDoS at high magnetic fields in the quantum drift approximation. In addition to the energy spectrum, it is important to note that this observable also contains information about the wave functions. The spectral LDoS can be obtained from the retarded electronic Green's function (3.19) evaluated at coinciding electron positions, $\mathbf{r} = \mathbf{r}'$, using the general formula

$$\rho(\mathbf{r},\omega) = -\frac{1}{\pi}\mathrm{Im}\mathrm{Tr}\Big\{G^R(\mathbf{r},\mathbf{r},\omega)\Big\}, \tag{3.42}$$

and can be written as a sum of two spin-projected components (in the direction of the external magnetic field)

$$\rho(\mathbf{r},\omega) = \sum_{\sigma=\pm} \rho_\sigma(\mathbf{r},\omega), \tag{3.43}$$

with

$$\rho_\sigma(\mathbf{r},\omega) = -\frac{1}{\pi}\int \frac{d^2\mathbf{R}}{2\pi l_B^2} \sum_{n=0}^{+\infty} \sum_{\lambda_1,\lambda_2} f_\sigma(\theta_n^{\lambda_1}) f_\sigma(\theta_n^{\lambda_2}) F_{n_\sigma}(\mathbf{r}-\mathbf{R})\, \mathrm{Im}\, g^R_{n;\lambda_1;\lambda_2}(\mathbf{R};\omega). \tag{3.44}$$

Here, $F_{n,n}(\mathbf{r},\mathbf{r},\mathbf{R}) \equiv F_n(\mathbf{r}-\mathbf{R})$ are the diagonal elements of the electronic structure factors (3.20) (we recall that in the high magnetic field regime characterized by $\omega_c \to +\infty$ while l_B finite, the SO vortex Green's function is diagonal in the Rashba-Landau level and so are the kernel functions in the full Green's function). The diagonal structure (form) factors can be written as [132]

$$F_n(\mathbf{r}-\mathbf{R}) = \mathrm{e}^{-(l_B^2/4)\Delta_{\mathbf{R}}} |\Psi_{n,\mathbf{R}}(\mathbf{r})|^2, \tag{3.45a}$$

$$= \frac{(-1)^n}{\pi l_B^2} L_n\left[\frac{2(\mathbf{r}-\mathbf{R})^2}{l_B^2}\right] \mathrm{e}^{-(\mathbf{r}-\mathbf{R})^2/l_B^2}, \tag{3.45b}$$

$$= \frac{1}{\pi l_B^2 n!} \frac{\partial^n}{\partial s^n} \left.\frac{\mathrm{e}^{-A_s(\mathbf{r}-\mathbf{R})^2/l_B^2}}{1+s}\right|_{s=0}, \tag{3.45c}$$

with $L_n(z)$ the Laguerre polynomial of degree n and $A_s = (1-s)/(1+s)$. The function $F_n(\mathbf{r}-\mathbf{R})$ is a normalized oscillating function[11] which exhibits a sharp maximum of width l_B at $|\mathbf{r}-\mathbf{R}| = R_n$, with $R_n = l_B\sqrt{2n+1}$ being the (quantum) cyclotron radius introduced in Sec. 1.5. It is interesting to note that the in the expression for the LDoS per spin (3.44) the information about the wave functions is hidden in the kernel which, for $n \geq 1$, $F_n(\mathbf{r}-\mathbf{R})$ *is not* positive definite and therefore cannot be interpreted as a probability density but has to be understood as a Wigner-like distribution.

To interpret realistic LDoS data obtained in STS experiments, we must include the extrinsic thermal broadening of the LDoS. This can be taken into account by a convolution of the spectral LDoS with the derivative of the equilibrium electronic (Fermi-Dirac) distribution function. The spin-resolved LDoS probed at energy E and temperature T is thus

$$\rho_\sigma^{\mathrm{STS}}(\mathbf{r},E,T) = -\int d\omega \rho_\sigma(\mathbf{r},\omega) n'_{\mathrm{F}}(\omega), \tag{3.46}$$

with

$$n'_{\mathrm{F}}(\omega) = -\frac{1}{4k_BT}\frac{1}{\cosh^2[(\omega-E)/2k_BT]}. \tag{3.47}$$

Inserting the formula (3.32) for the SO vortex Green's function established within the quantum drift approximation into the previous formulae (3.44) and (3.46), we obtain after integration over the energies ω and summation over λ_1, λ_2 the following approximate

[11] We remind that the definition of the vortex wave function implies $F_{-1}(\mathbf{r}-\mathbf{R}) \equiv 0$ so that all the above formulas hold for $n = 0$.

analytical expression for the STS spin-resolved LDoS

$$\rho_\sigma^{\mathrm{STS}}(\mathbf{r},E,T)=-\frac{1}{2}\int\frac{d^2\mathbf{R}}{2\pi l_B^2}\sum_{n=0}^{+\infty}\sum_{\epsilon}n_{\mathrm{F}}'[\xi_{n,\epsilon}(\mathbf{R})] \times F_{n_\sigma}(\mathbf{r}-\mathbf{R})\left[1-\epsilon\sigma\sqrt{1-\frac{nS_{n,\mathrm{eff}}^2(\mathbf{R})}{\Delta_n^2(\mathbf{R})}}\right]. \quad (3.48)$$

This formula is the main result to be used in the interpretation of the STS experiments in Sec. 3.5.3. Clearly, even within the leading order quantum drift approximation, the electronic LDoS is a result of the intricate interplay (through the convolution integral) between the cyclotron and drift degrees of freedom, respectively described by the electronic structure factor representing the circular motion with the (thermal) vortex spectral density. In addition, the expression presents asymmetries between the spin-up and spin-down states produced by the presence of Rashba SO coupling (given by the factor in square brackets). The order of magnitude of this asymmetry between the spin components is typically small and difficult to estimate, mainly due to the many unknowns (effective temperature, particular shape of the potential landscape, precise experimental value of the Rashba parameter ...). A general trend can however be easily identified: the asymmetry is expected to decrease (and eventually disappear) for high values of the Rashba-Landau level index n.

Finally, let us note that, as stated in Sec. 3.4.2, inclusion of a finite temperature in the computation of observables fully justifies the non-perturbative gradient expansion theory used in this work. The obtained formulas in the SO vortex representation are controlled thanks to the temperature energy scale which acts as a cut-off in the hierarchy of local energy scales related to the smooth potential. Therefore it allows us to disregard smaller energy scales characterizing nonlocal quantum effects that can take place in a disorder potential at zero temperature. In this context, the quantum drift approximation encapsulates the most robust quantum features at finite temperature associated to the local gradients of the potential landscape.

3.5.2. Approximation for potentials smooth on the cyclotron radius

In order to get analytical insight in the energy scales involved in Eq. (3.48) the general formula can be studied in two particular limiting cases. The first simplification occurs in the high temperature (semiclassical) regime characterized by $k_BT \gg R_n\,|\boldsymbol{\nabla}_{\mathbf{R}}\xi_{n,\epsilon}(\mathbf{R})|$. Under this inequality we can make the replacement $\mathbf{R}\simeq\mathbf{r}$ inside the functionals with a smooth dependence on the vortex position, i.e., the derivative of the Fermi-Dirac distribution and the functionals $S_{n,\mathrm{eff}}(\mathbf{R})$ and $\Delta_n(\mathbf{R})$. The remaining dependence on the vortex position can then be integrated out taking into account the normalization condition of the electronic kernels $\int d^2\mathbf{R}\,F_n(\mathbf{R})=1$. As a result, we obtain the following simple semiclassical expression for the total LDoS

$$\rho_{\mathrm{sc}}^{\mathrm{STS}}(\mathbf{r},E,T)=-\frac{1}{2\pi l_B^2}\sum_{n=0}^{+\infty}\sum_{\epsilon}n_{\mathrm{F}}'[\xi_{n,\epsilon}(\mathbf{r})]. \quad (3.49)$$

In this limit, the LDoS is characterized by peaks of unitary height (in the appropriate units) and spatially constant width $2k_BT$ centered around the effective energies $\xi_{n,\epsilon}(\mathbf{r})$ given by Eq. (3.33).

In the opposite limit of low temperatures, the spatial dependence of the eigenenergies on the vortex position cannot be entirely disregarded. However, if the energy levels vary very smoothly on the scale of the cyclotron radius [R_n is the typical characteristic length scale set by the kernel function $F_n(\mathbf{R})$] we can expand the eigenenergies up to the gradient contribution by writing $\xi_{n,\epsilon}(\mathbf{R}) \simeq \xi_{n,\epsilon}(\mathbf{r}) + (\mathbf{R}-\mathbf{r})\cdot\boldsymbol{\nabla}_{\mathbf{r}}\xi_{n,\epsilon}(\mathbf{r})$ [the other functions $S_{n,\mathrm{eff}}(\mathbf{R})$ and $\Delta_n(\mathbf{R})$ are expanded similarly]. This linearization procedure certainly breaks down if the electron starts to feel random fluctuations of the disorder potential on the scale of R_n (thus, the approximation will not be valid for sufficiently large quantum numbers n). Next, using the Fourier representation of the derivative of the Fermi-Dirac distribution (3.47)

$$n'_{\mathrm{F}}[\xi_{n,\epsilon}(\mathbf{R})] = -\int_{-\infty}^{+\infty} \frac{dt}{2\pi} \frac{\pi T t}{\sinh(\pi T t)} \mathrm{e}^{it[\xi_{n,\epsilon}(\mathbf{R})-E]}, \tag{3.50}$$

and the expression (3.45c) for the electronic kernels[12] $F_n(\mathbf{R})$ we can perform the Gaussian integrals over the vortex position $\mathbf{R}$ in Eq. (3.48) as described in Ref. [122]. By taking the limit $T \to 0$, also the integral over the variable t in Eq. (3.50) can be analytically computed and we finally obtain the following low temperature expression for the spin-resolved LDoS

$$\begin{aligned}\rho_\sigma^{\mathrm{STS}}(\mathbf{r}, E, 0) \simeq{}& \frac{1}{2\pi l_B^2} \sum_{n=0}^{+\infty} \sum_{\epsilon=\pm} \frac{1}{\sqrt{\pi} l_B \left|\boldsymbol{\nabla}_{\mathbf{r}}\xi_{n,\epsilon}(\mathbf{r})\right|} \frac{1}{2^{n_\sigma+1}} \\ &\times \frac{1}{n_\sigma!} \left[1 - \epsilon\sigma\sqrt{1 - \frac{n S_{n,\mathrm{eff}}^2(\mathbf{r})}{\Delta_n^2(\mathbf{r})}}\right] H_{n_\sigma}^2 \left[\frac{\xi_{n,\epsilon}(\mathbf{r}) - E}{l_B \left|\boldsymbol{\nabla}_{\mathbf{r}}\xi_{n,\epsilon}(\mathbf{r})\right|}\right] \\ &\times \exp\left\{-\left[\frac{\xi_{n,\epsilon}(\mathbf{r}) - E}{l_B \left|\boldsymbol{\nabla}_{\mathbf{r}}\xi_{n,\epsilon}(\mathbf{r})\right|}\right]^2\right\},\end{aligned} \tag{3.51}$$

where $H_n(z)$ is the Hermite polynomial of degree n. In Eq. (3.51) we note the appearance of a local energy scale $l_B \left|\boldsymbol{\nabla}_{\mathbf{r}}\xi_{n,\epsilon}(\mathbf{r})\right|$ consequence of the quantum drift. This energy scale gives rise to an intrinsic (disorder-induced) energy broadening of the LDoS peaks which can be roughly estimated as $\sqrt{n} l_B \left|\boldsymbol{\nabla}_{\mathbf{r}}\xi_{n,\epsilon}(\mathbf{r})\right|$ when including the spread resulting from the Hermite polynomials in addition to the Gaussian exponential factors. This formula is also evidently invalid close to the critical points where the drift energy $l_B \left|\boldsymbol{\nabla}_{\mathbf{r}}\xi_{n,\epsilon}(\mathbf{r})\right| \simeq 0$. In the vicinity of these points the finite temperature becomes again the main mechanism of LDoS broadening[13] and thus has to be taken into account [as in the more general expression (3.48)].

3.5.3. Interpretation of STS experiments in InSb surface gases

Using the previous formulae, we are now in an excellent position to discuss in more detail the STS spectra (at fixed tip position) alluded to in Sec. 3.1. In Fig. 3.9 we show the results of the calculation for the LDoS at high magnetic fields (as in the experiments, we focus in the two lowest energy levels although the calculation can be performed for any Rashba-Landau level). Each of the curves (a), (b) and (c) correspond to the three different STM tip positions chosen in Fig. 3.8 for the case of a quasi-1D disorder potential and a

[12] This alternative form turns out to be specially convenient when considering the lower energy levels.

[13] Note that, at the critical points of the potential landscape, curvature effects also produce an intrinsic broadening of the LDoS peaks. This broadening is assumed to be overcome by temperature in the present quantum drift approximation.

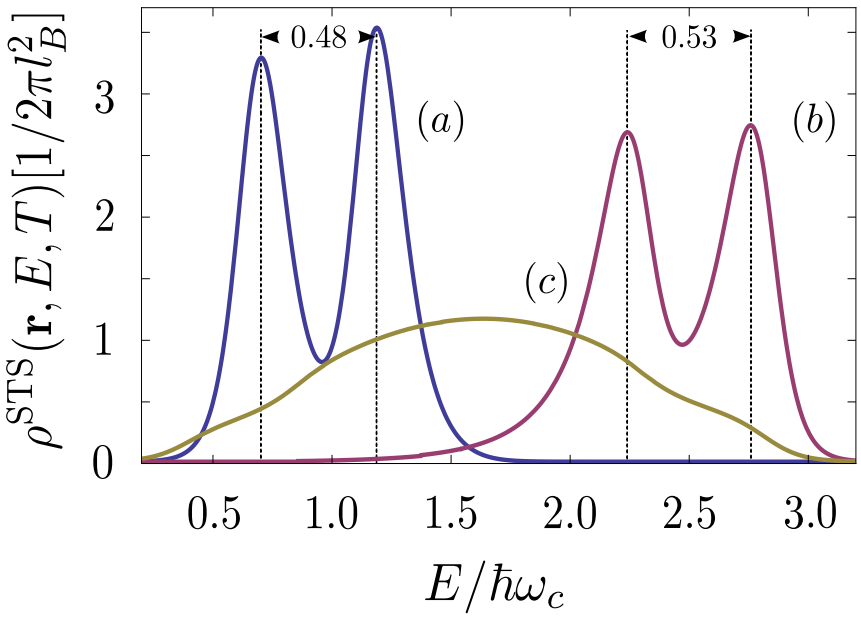

Figure 3.9 – Local density of states [in units of $1/(2\pi l_B^2)$] as a function of the normalized energy $E/\hbar\omega_c$, in the energy range where the first two energy levels characterized by the quantum numbers $(1,+)$ and $(0,-)$ are observed. The labels (a), (b), (c) of the curves correspond respectively to the calculated LDoS when the tip position is fixed close to a local minimum, maximum or region of strong gradient of the disorder potential (see Fig. 3.8). The spin-split energy levels are resolved only for the cases (a) and (b), with the energy spin-splitting expressed in units of the cyclotron energy given on the top. As in the experiment, reported in Refs. [11, 86] and shown in Fig. 3.2, the energy spin-splitting is bigger for maxima than minima of the potential energy landscape. An effective temperature of $T = 15$ K was considered here to simulate unknown broadening effects (temperature, experimental energy averaging, etc...).

magnetic field of 7 Teslas. We have also chosen the same material parameters as in Figs. 2.3 and 3.8, which are relevant for the experiments [11, 86] and considered that the spatial dispersion of the energy levels is only due to the scalar disorder potential.

The first observation is that in the case (c), when the STM tip is found in a region of strong potential gradients, the energy difference between the LDoS peaks cannot be resolved. In contrast, the energy spin-splitting in the LDoS spectrum can be clearly seen when the tip is located in valley (a) or hill (b) regions of the potential landscape. These markedly spatially dependent linewidths for the LDoS were also noticed in experiments and can be understood if the broadening of the LDoS is dominated by the energy scale related to drift motion $l_B\,|\boldsymbol{\nabla}_{\mathbf{r}}\xi_{n,\epsilon}(\mathbf{r})| \propto l_B\,|\boldsymbol{\nabla}_{\mathbf{r}}V(\mathbf{r})|$, as expected at low temperatures (see Sec. 3.5.2). Indeed, the drift energy gets strongly reduced in potential hills or valleys due to the small drift velocity, while it may exceed the energy spin-splitting in regions of strong potential gradients.

Another interesting feature that can be seen in Fig. 3.9 is the correlation between the energy spin-splitting and the disorder potential landscape. As reported in experiments [11, 86], an enhanced spin-splitting is found in hill regions in comparison to valley regions, with a variation of the order of 10 % for the parameters chosen here. These correlations are difficult

to understand if the spatial variations of the spin-splitting depend predominantly on the local fluctuations of the Rashba SO parameter. We believe therefore that the mechanism at play is a combination of a uniform Rashba SO interaction together with spatial fluctuations of the scalar disorder potential. Finally, note that the order of magnitude of the spin-splitting agrees qualitatively when comparing the experimental situation (where the value of the energy spin-splitting is roughly 14 meV when the tip position is fixed in a minima, see Fig. 3.2) and the theoretical one (where the energy spin-splitting for the same situation is of 12 meV, see Fig. 3.9). This clearly points to a certain degree of universality in the description of the effect as the specific details of the potential landscape are not known.

For weak spatial fluctuations, the analytical expression for the spin-splitting (3.41) can be further simplified. Noting $E_s(\mathbf{R}) = E_{0,-} - E_{1,+} + \delta E_s(\mathbf{R})$ and assuming a very smooth potential which can be approximated by Eq. (1.65), we can directly relate the spatial fluctuations $\delta E_s(\mathbf{R})$ of the energy spin-splitting $E_s(\mathbf{R})$ with the derivatives of the bare disorder potential $V(\mathbf{R})$

$$\delta E_s(\mathbf{R}) \simeq -\frac{l_B^2}{4}\left[1 - \frac{1-Z}{\sqrt{(1-Z)^2+S^2}}\right]\Delta_{\mathbf{R}} V(\mathbf{R}). \tag{3.52}$$

This formula makes explicit why a larger $E_s(\mathbf{R})$ is found at hills of the disorder potential: The quantity $\Delta_{\mathbf{R}} V(\mathbf{R})$ is typically negative at potential maxima, thus leading to $\delta E_s(\mathbf{R}) > 0$, *i.e.* to an enhancement of the spin-splitting. At potential minima, $\Delta_{\mathbf{R}} V(\mathbf{R})$ acquires the opposite sign, so that $E_s(\mathbf{R})$ is generally reduced in valley regions. Note that, according to the general spectrum (3.33), this spatial correlation of the spin-splitting with the potential landscape may be different when considering higher spin-split energy levels (*e.g.*, it may be reverse depending on the magnetic field).

Chapter 4

High-Field Local Equilibrium Properties

In this chapter, we discuss how using the coherent-state Green's function formalism detailed in previous chapter, we can shed some light onto the charge and spin transport properties of quantum Hall systems in a local equilibrium (hydrodynamic) regime, also accounting for the Rashba SO and Zeeman interactions. We prove how we can take advantage from a high-magnetic field expansion to get analytical insights into the peculiar features of the local particle, spin and current densities. Next, we show that neglecting inelastic scattering, the local nonequilibrium current density is characterized by a purely off-diagonal conductivity tensor from which we can extract an analytical formula for the (local) semiclassical Hall conductivity. This formula contains both the non-relativistic and relativistic-like quantization rules mentioned in Sec. 1.1. Then, we also point out how to define a local spin Hall conductivity in the presence of Rashba SO interaction that has a precise physical meaning and how it can be related to experimentally accessible macroscopic transport coefficients. We finally address the question of macroscopic transport and percolation properties at high fields in the presence of strong SO coupling. The results presented here have been published in Ref. [142].

Dans ce chapitre, nous discutons comment, en utilisant le formalisme de fonctions de Green basé sur des états de vortex cohérents détaillé dans le chapitre précédent, nous pouvons étudier en profondeur les propriétés de transport de charge et de spin dans un régime d'équilibre local (ou hydrodynamique) de l'effet Hall quantique entier avec des interactions SO Rashba et Zeeman. Nous démontrons comment pouvons-nous tirer parti d'une expansion en gradient à champs magnétiques forts pour en déduire, analytiquement, des propriétés de la densité de particules, de spin et de courant. Ensuite, nous montrons que, si on néglige la diffusion inélastique, la densité de courant locale à l'équilibre est caractérisée par un tenseur de conductivité non-diagonal à partir duquel nous pouvons obtenir une formule analytique de la conductivité de Hall (locale) valable dans le régime semi-classique. Cette formule contient simultanément les règles de quantification non-relativiste et relativiste signalées dans la Sec. 1.1. Par la suite, nous soulignons comment définir une densité de courant de spin locale en présence du SO Rashba qui possède une signification physique précise et, conséquemment peut être reliée aux coefficients de transport macroscopiques (mesurables expérimentalement). Finalement, nous considérons la problématique du transport macroscopique et les pro-

priétés de percolation à fort champ en présence de couplage SO. Les résultats présentés ici ont fait partie de la publication citée dans la Réf. [142].

4.1. Motivation

In the previous chapter, we derived an analytical nonperturbative expression for the disordered energy spectrum and the local density of states (LDoS) using a Green's function framework in the so-called quantum drift approximation. In this way, we were able to study local spectral properties in the quantum regime (for the guiding-center operators) and explain the particular features of the spin-split LDoS seen in the STS spectra at low temperatures. We turn now to the more complicated task of studying transport in 2DEGs with strong Rashba SO interaction and Zeeman coupling in the quantum Hall regime (therefore, in the presence of arbitrary smooth disorder). One of the main interests for studying quantum transport properties in these systems is that, at high magnetic fields, the effect of disorder can be understood semiclassically [34, 104, 105] with the charge transport being the result of the combination of a fast cyclotron rotation with a slow guiding center drift in an arbitrary smooth potential landscape (see also discussion in chapter 1) .

From a purely theoretical perspective, some works [93, 95, 96, 112, 113, 134, 136] have considered the problem of transport properties of 2DEGs under strong magnetic fields in the presence of Rashba SO coupling, either in bulk clean systems [112, 113, 134, 136] or 2DEGs with simple confinement potential profiles [93, 95, 96] (hard-wall or quadratic potentials). However, none of these papers take into account the peculiarities of the quantum Hall regime and the effect of Rashba SO and Zeeman interactions in the electronic drift states. One of the reasons, as we saw in chapter 1, is that the problem of lifting the macroscopic level degeneracy of the Landau levels by long-range disorder has a nonperturbative nature and, as a consequence, the standard perturbation theory techniques fail. Another important difficulty to address, which we discuss in the next section, is that the computation of the current necessarily needs to include Landau level mixing in a controlled way (this is a general problem that arises both in the presence and absence of SO coupling). Moreover, we know that in the presence of disorder potentials the microscopic observables can be very different from the macroscopic experimentally measurable quantities due to the fractal nature of the percolation network of drift states. In this sense, it has been suggested that under certain circumstances disordered quantum Hall systems with Rashba SO coupling may belong to a different universality class (characterized by different percolation exponents) than the spinless 2DEGs under perpendicular magnetic field [137, 138, 139]. We prove in the last part of this chapter that this is not true at high temperatures in the integer quantum Hall regime.

In addition, another significant feature to consider is the spin (angular momentum) transport in the quantum Hall regime. As discussed extensively in Sec. 2.3.2 previous theoretical works for clean systems have suggested that the macroscopic spin Hall conductance (related to the transverse spin current which appears in the presence of SO coupling as a response to an external in-plane electric field) can diverge at the accidental double degeneracy points between two SO-split energy levels with opposite SO quantum number [112, 113, 114, 140]. The performed calculations exclusively rely on perturbative theoretical tools which are not well-suited for the quantum Hall regime. Moreover, this resonant

behavior has not been measured in experiments until now due to the lack of experimental probes that couple to the spin current and the difficulties on discriminating the intrinsic versus extrinsic origin of the SO interaction (see the important Ref. [141] where spin accumulation - which should be a consequence of the spin current - is measured in the absence of external magnetic fields). In addition, at high magnetic fields one has to consider the problem of the definition of the spin current discussed in Sec. 2.3 and which is still controversial. We stress again that the spin current definition used in all of these papers *does not* satisfy a continuity equation, crucial to relate the local microscopic spin current density to the macroscopic observable spin current.

4.2. Spin-Orbit Vortex Green's Functions at High Magnetic Fields

4.2.1. The high magnetic field expansion

In Sec. 3.3, we saw that the SO vortex Green's function satisfies an exact equation of motion (3.17) in the presence of spatial fluctuations of the Rashba SO coupling parameter and the Zeeman interaction. Now, for the sake of simplicity, we assume that the spatial fluctuations of the SO interaction are negligible compared to the typical amplitude of the disorder potential and we will further disregard the random fluctuations of the Rashba field [therefore the reduced matrix elements $u_{n_1,\lambda_1;n_2,\lambda_2}(\mathbf{R}) \equiv v_{n_1,\lambda_1;n_2,\lambda_2}(\mathbf{R})$ in the rest of the chapter]. A solution to the equation of motion (3.32) was also found in the regime of negligible mixing between Rashba-Landau energy levels by projection (and solution) of Dyson equation within a single level n (this regime corresponds to the formal limit $m^* \to 0$). In principle, this procedure seems to be inadequate to obtain the Green's function which describes drift transport properties at high magnetic fields because the matrix elements of the current density operator couple adjacent energy levels [55, 130]. Another mathematical reason of why the limit $m^* \to 0$ is insufficient is the fact that the current density is proportional to the energy scale $\hbar\omega_c$, as a difference to the particle density or the LDoS, and we need the corrective term coming from the level mixing in the SO vortex Green's function to generate the compensating prefactor $1/(\hbar\omega_c)$. For these reasons, one has to be able to obtain, at least, the first contribution introducing Rashba-Landau level mixing to describe quantum drift transport[1].

A possible approach to this problem, valid at sufficiently high magnetic fields when the arbitrary scalar potential is smooth at the scale of the cyclotron radius, is to obtain a solution to Dyson equation performing an expansion of the (reduced) matrix elements of the potential (3.22) [more precisely, the spin-resolved matrix elements given in Eq. (3.24)] in a power series of the magnetic length l_B [130],

$$v_{n_{1\sigma};n_{2\sigma}}(\mathbf{R}) = \sum_{j=0}^{+\infty} \left(\frac{l_B}{\sqrt{2}}\right)^j v^{(j)}_{n_{1\sigma};n_{2\sigma}}(\mathbf{R}), \tag{4.1}$$

where $v^{(j)}_{n_{1\sigma};n_{2\sigma}}(\mathbf{R})$ are expansion coefficients independent of l_B, and to write the SO vortex

[1] Actually, we have found that it is possible to relate the diagonal part of the SO vortex Green's function to the off-diagonal contributions and use Eq. (3.32) to compute the current density at high magnetic fields (unpublished result).

Green's function in a similar way

$$g_{n_1,\lambda_1;n_2,\lambda_2}(\mathbf{R};\omega) = \sum_{j=0}^{+\infty} \left(\frac{l_B}{\sqrt{2}}\right)^j g^{(j)}_{n_1,\lambda_1;n_2,\lambda_2}(\mathbf{R};\omega). \tag{4.2}$$

Each of the contributions $g^{(j)}_{n_1,\lambda_1;n_2,\lambda_2}(\mathbf{R},\omega)$ to the power series defining the SO vortex Green's function can be obtained solving Eq. (3.17) recursively order by order in powers of the magnetic length. Note that this procedure is the gradient expansion discussed in Sec. 1.5.2 in which l_B was the smallest length scale with respect to the correlation length scale of the smooth disorder potential. This expansion allows us to obtain quantum microscopic expressions at finite l_B for any observable in the local equilibrium regime under the form of functionals of the potential energy $V(\mathbf{r})$.

We want to give at this point an explicit expression for the matrix elements in Eq. (4.1) and discuss the properties of the two main contributions relevant for the present work. First, it has been recently shown [121] that the full power series may be written as

$$v_{n_{1\sigma};n_{2\sigma}}(\mathbf{R}) = \sum_{j=0}^{+\infty}\sum_{k=0}^{+\infty} \frac{(-\Delta_{\mathbf{R}})^j}{j!} \left(\frac{l_B}{2}\right)^{2j+k} v^{(k)}_{n_{1\sigma};n_{2\sigma}}(\mathbf{R}), \tag{4.3}$$

with coefficients

$$v^{(k)}_{n_{1\sigma};n_{2\sigma}}(\mathbf{R}) = 2^{k/2} \sum_{l=0}^{k} \frac{(n_{1\sigma}+l)!}{\sqrt{n_{1\sigma}!\, n_{2\sigma}!}} \frac{\delta_{n_{1\sigma}+l,n_{2\sigma}+k-l}}{l!(k-l)!} \partial_+^l \partial_-^{k-l} V(\mathbf{R}). \tag{4.4}$$

where we remind that $\partial_\pm \equiv \partial_X \pm i\partial_Y$. Using Eqs. (3.22), (4.3) and (4.4) it is straightforward to deduce that the leading order (non-zero contribution in the semiclassical limit $l_B \to 0$) is, as expected, diagonal in the Rashba-Landau level index n and the SO quantum number[2] λ

$$v^{(0)}_{n_1,\lambda_1;n_2,\lambda_2}(\mathbf{R}) = \delta_{n_1,n_2}\delta_{\lambda_1,\lambda_2} V(\mathbf{R}). \tag{4.6}$$

The first order contribution (subdominant) in l_B can be obtained from the previous formulas without much difficulty and reads

$$v^{(1)}_{n_1,\lambda_1;n_2,\lambda_2}(\mathbf{R}) = \sum_{\sigma=\pm} f_\sigma(\theta^{\lambda_1}_{n_1}) f_\sigma(\theta^{\lambda_2}_{n_2}) \Big[\sqrt{n_{1\sigma}+1}\,\delta_{n_{1\sigma}+1,n_{2\sigma}} \partial_+ V(\mathbf{R}) + \text{c.c.}\,(1 \leftrightarrow 2)\Big], \tag{4.7}$$

where the notation c.c. $(1 \leftrightarrow 2)$ means exchanging indices and taking the complex conjugation in the former expression. It is therefore clear that, as difference to the dominant contribution, the subdominant term linear in the magnetic length induces a mixing between adjacent Rashba-Landau levels n and different values of the SO quantum number λ in the presence of a non-zero gradient of the smooth arbitrary potential. Moreover, we may note that, as we saw in the previous chapter, even when processes mixing Rashba-Landau levels are negligible, interesting effects related to the combination of the two projections of λ exist [for instance, at quadratic order in l_B, processes involving second-order derivatives of

[2] If a similar expansion is done for Eq. (3.25) the leading order contribution at high magnetic fields reads

$$\delta\mathcal{H}^{(0)}_{n_1,\lambda_1;n_2,\lambda_2}(\mathbf{R}) = -\frac{\hbar\sqrt{n_1}}{\sqrt{2}l_B} \sin(\theta^{\lambda_1}_{n_1} + \theta^{\lambda_2}_{n_2}) \delta_{n_1,n_2}\, \delta\alpha(\mathbf{R}), \tag{4.5}$$

which is still diagonal in the level index n, but now still induces a mixing in the SO quantum number λ.

the potential $V(\mathbf{R})$ yield a mechanism for the spatial dispersion of the energy spin-splitting in the LDoS [121]].

Now, we come back to the derivation of the SO vortex Green's functions at high magnetic fields. The leading order component of the SO vortex Green's function satisfies an equation of motion that can be easily found setting $j = k = 0$ in Eq. (4.3) and $j = 0$ in Eq. (4.2). Eq. (3.17) has then a closed form with the solution

$$g^{(0)}_{n_1,\lambda_1;n_2,\lambda_2}(\mathbf{R};\omega) = \frac{\delta_{n_1,n_2}\delta_{\lambda_1,\lambda_2}}{\omega - \xi_{n_1,\lambda_1}(\mathbf{R}) \pm i0^+}. \tag{4.8}$$

The dominant SO Green's functions presents therefore a well-known simple pole structure with eigenenergies $\xi_{n,\lambda}(\mathbf{R}) = E_{n,\lambda} + V(\mathbf{R})$. We see that the primary effect of the potential energy is to locally lift the macroscopic degeneracy of the Rashba-Landau energy levels with respect to the guiding center position $\mathbf{R}$, while keeping n and λ as good quantum numbers.

As anticipated above, the leading order SO vortex Green's function cannot be responsible for drift transport since the latter is related to local electric fields (gradients of the potential energy) that produce Rashba-Landau level mixing. Therefore, we carry on our analysis to include the first subdominant corrections at high magnetic fields (linear in l_B) in the SO vortex Green's function (4.2). This subleading term is obtained from the algebraic equation

$$\left[\omega - \xi_{n_1,\lambda_1}(\mathbf{R}) \pm i0^+\right] g^{(1)}_{n_1,\lambda_1;n_2,\lambda_2}(\mathbf{R};\omega) = \sum_{n_3,\lambda_3} v^{(1)}_{n_1,\lambda_1;n_3,\lambda_3}(\mathbf{R}) g^{(0)}_{n_3,\lambda_3;n_2,\lambda_2}(\mathbf{R};\omega), \tag{4.9}$$

whose solution reads

$$g^{(1)}_{n_1,\lambda_1;n_2,\lambda_2}(\mathbf{R};\omega) = \frac{v^{(1)}_{n_1,\lambda_1;n_2,\lambda_2}(\mathbf{R})}{[\omega - \xi_{n_1,\lambda_1}(\mathbf{R}) \pm i0^+][\omega - \xi_{n_2,\lambda_2}(\mathbf{R}) \pm i0^+]}. \tag{4.10}$$

We point out that this iterative algorithm can be used to obtain further (smaller) contributions to the SO vortex Green's function up to any order in the high magnetic field expansion. However, due to the already complicated expressions (as a result of Rashba SO interaction) we disregard here higher order contributions in l_B which only lead to weak quantitative corrections for potentials smooth at the scale of the cyclotron radius.

4.2.2. Discussion of the high-field expansion

To end this section, we make some observations related to the high-field expansion used here. It is important to remark that the l_B expansion discussed in this thesis affects only the slow (guiding center) drift contribution to the electronic Green's function (3.19). For this reason, our expressions for the observables in the quantum (low temperature) regime preserves through the electronic structure factors (3.20) some quantum-mechanical features such as wave function spreading or interference effects related to the nodal pattern of the quantized cyclotron motion. Purely semiclassical (high temperature) expressions can be recovered if the diagonal elements of the electronic kernels are replaced by 2D Dirac delta functions $F_n(\mathbf{r} - \mathbf{R}) \simeq \delta^{(2)}(\mathbf{r} - \mathbf{R})$, with only the kinetic energy quantization kept intact while the full internal spatial structure resulting from quantum interferences being neglected (this is equivalent to identify the electronic and vortex densities).

In some way, we can understand that the dependence on l_B of the full Green's function has two different origins, each linked to the two intertwined (through a convolution) electronic motions. This distinction is, nevertheless, very subtle, because the representation of the $\star$-product is not unique [60, 64, 143] and we can modify the Groenewold-Moyal $\star$-product by performing a rotation in phase space. For example, an integration by parts in Eq. (3.19) has as a consequence that the operator $T_{\mathbf{R}}^{-1}$ in the electronic kernels now acts onto the SO vortex Green's function, which satisfies a new Dyson equation with renormalized potential matrix elements and a different infinite order pseudo-differential product. This phase space rotation corresponds to an infinite order resummation of a whole class of l_B terms which yields a localized structure factor given by the product $\Psi^*_{n_2,\mathbf{R}}(\mathbf{r}')\Psi_{n_1,\mathbf{R}}(\mathbf{r})$ of two vortex wave functions. Importantly, the choice of the Groenewold-Moyal $\star$ product has been proved to be preferentially selected [122, 132] whenever the Landau level degeneracy is lifted, since it systematically generates a hierarchy of local energy scales from the spatial derivatives of the potential energy. This hierarchy is controlled by temperature which acts as an energy cut-off and justifies the use of a gradient expansion theory of asymptotic nature. The existence of a hierarchy of energy scales can be understood from the physical point of view as the expression of the stability property of the chosen representation of quantum states.

4.3. Electron Density and Spin Polarization

4.3.1. Quantum expression

To check the validity of the high-field approach, we shall study in this section the local equilibrium properties of the electron density and the spin polarization. The local spectral density can be evaluated using the lesser component of the Green's function, $G^<$ written in the electronic representation and evaluated at coinciding electron positions $\mathbf{r} = \mathbf{r}'$

$$n(\mathbf{r},\omega) = \mathrm{Tr}\left\{-iG^<(\mathbf{r},\mathbf{r},\omega)\right\}, \tag{4.11}$$

and can be written as the sum of two spin-resolved components (in the $\hat{\mathbf{z}}$ direction perpendicular to the 2D plane)

$$n(\mathbf{r},\omega) = \sum_{\sigma=\pm} n_\sigma(\mathbf{r},\omega). \tag{4.12}$$

Taking the difference between the spin-up and spin-down electronic populations instead of the sum we get the spin polarization / density in the direction parallel to the applied magnetic field

$$\Pi^z(\mathbf{r}) = \frac{\hbar}{2}\left[n_+(\mathbf{r}) - n_-(\mathbf{r})\right]. \tag{4.13}$$

The lesser component of the Green's function, which plays the role of a distribution function, can be obtained from the relation

$$-iG^<(\mathbf{r},\mathbf{r},\omega) = in_{\mathrm{F}}(\omega)[G^R(\mathbf{r},\mathbf{r},\omega) - G^A(\mathbf{r},\mathbf{r},\omega)], \tag{4.14}$$

that relates the equilibrium retarded and advanced Green's functions to the Fermi-Dirac distribution function

$$n_{\mathrm{F}}(\omega) = \frac{1}{1+\exp[(\omega-\mu)/k_BT]} \tag{4.15}$$

at temperature T and constant electrochemical potential $\mu = e\Phi$ (we also designate by k_B the Boltzmann constant). Although this relation is, in principle, only valid in the equilibrium regime it also holds at high magnetic fields in a nonequilibrium stationary regime [55, 130]. This is due to the installation of a local hydrodynamic equilibrium in the 2DEG which is physically expected as at the relevant length scales (typically larger than the smallest length scale, l_B) all the degrees of freedom are in thermodynamic equilibrium. We can therefore divide the system into several subsystems where thermodynamic variables can be introduced.

Inserting Eq. (3.19) into (4.14) and using afterwards Eq. (4.11), we obtain the following general formula for the local electronic density per spin after an integration over the energies

$$n_\sigma(\mathbf{r}) = -i \int \frac{d\omega}{2\pi} \int \frac{d^2\mathbf{R}}{2\pi l_B^2} \sum_{n_1,\lambda_1} \sum_{n_2,\lambda_2} f_\sigma(\theta_{n_1}^{\lambda_1}) f_\sigma(\theta_{n_2}^{\lambda_2}) \times F_{n_{1\sigma};n_{2\sigma}}(\mathbf{r},\mathbf{r},\mathbf{R})\, g^{<}_{n_1,\lambda_1;n_2,\lambda_2}(\mathbf{R};\omega). \tag{4.16}$$

Here, the SO vortex lesser Green's function $g^{<}(\mathbf{R};\omega)$ is defined in terms of the retarded and advanced SO vortex components in the same way as the full electronic lesser Green's function $G^{<}(\mathbf{r},\mathbf{r},\omega)$. Note that, as in Eq. (4.14), the Fermi-Dirac distribution function is included by definition inside the lesser component of the Green's function.

Using the leading order (in the series expansion) lesser component of the SO vortex Green's function resulting from Eqs. (4.8) and (4.14)

$$g^{<\,(0)}_{n_1,\lambda_1;n_2,\lambda_2}(\mathbf{R};\omega) = 2\pi i n_{\mathrm{F}}(\omega)\delta_{n_1,n_2}\delta_{\lambda_1,\lambda_2}\delta[\omega - \xi_{n_1,\lambda_1}(\mathbf{R})], \tag{4.17}$$

we can straightforwardly compute the dominant contribution to the spin-polarized electron density which reads

$$n_\sigma^{(0)}(\mathbf{r}) = \frac{1}{2}\int \frac{d^2\mathbf{R}}{2\pi l_B^2} \sum_{n=0}^{+\infty} \sum_{\lambda} n_{\mathrm{F}}[\xi_{n,\lambda}(\mathbf{R})] F_{n_\sigma}(\mathbf{r}-\mathbf{R}) \left[1 + \sigma\lambda\sqrt{1 - \frac{nS^2}{\Delta_n^2}}\right]. \tag{4.18}$$

Here, the diagonal elements of the electronic structure factors, $F_n(\mathbf{r}-\mathbf{R})$, are given[3] in Eqs. (3.45).

An important take-home message from formula (4.18) is that its range of validity is larger than any semiclassical (high temperature) expression that can be derived taking the strict limit $l_B \to 0$ [both in the cyclotron and vortex parts of the Green's function] since it still accounts for spatial (quantum) broadening and electron delocalization features encapsulated in the electronic kernels. More precisely, this expression is expected to be accurate in a wide range of temperatures (see comparison between the quantum functionals and numerical results in Ref. [130]) as long as the thermal energy scale is larger than the local curvature energy scale. In addition, one can easily see that, as it happened in Sec. 3.5, as a consequence of the spin not being a good quantum number each of the spin-projected components contributes to the spatial dependence of the full electron density (4.12) with unequal weights. However, it is possible to be convinced that both λ projections present equal unitary weights which is the signature of λ being a good quantum number at high magnetic fields. In this sense, we can understand the high magnetic field result

[3] We remind that, as in the preceding chapter, we take $F_{-1}(\mathbf{r}-\mathbf{R}) \equiv 0$ so that all formulas are also valid for $n = 0$.

(4.18) as being robust with respect to the Rashba SO interaction, with the only trace of SO coupling appearing in the energy functionals inside the argument of the distribution function controlling the width of the spatial density plateaus.

To conclude this subsection, I would like to compare the quantum results derived in the framework of the l_B expansion with the quantum results which can be obtained using the local SO vortex Green's function for the quantum drift approximation (3.32). The latter allows us, for observables at equilibrium, to include all the nonperturbative l_B contributions to the vortex spectral density. This means that the fine structure effects related to the disorder-renormalized energy levels (together with the renormalization of the SO quantum number and the angular parameters) can be taken into account to improve the accuracy of the functionals at low temperatures. In the case of the local spin-resolved electronic density, we find

$$n_\sigma(\mathbf{r}) = \frac{1}{2}\int \frac{d^2\mathbf{R}}{2\pi l_B^2} \sum_{n=0}^{+\infty} \sum_{\epsilon} n_{\mathrm{F}}[\xi_{n,\epsilon}(\mathbf{R})] F_{n_\sigma}(\mathbf{r}-\mathbf{R}) \left[1 - \epsilon\sigma \sqrt{1 - \frac{nS_{n,\mathrm{eff}}^2(\mathbf{R})}{\Delta_n(\mathbf{R})}}\right], \tag{4.19}$$

which clearly satisfies

$$\rho_\sigma^{\mathrm{STS}}(\mathbf{r}, E, T) = \left[\frac{\partial n_\sigma(\mathbf{r})}{\partial \mu}\right]_{\mu=E} \tag{4.20}$$

when the chemical potential lies at energy E. Compared to Eq. (4.18), we see that the local density in the quantum drift approximation has the same functional form but presents the renormalized Rashba-Landau energy levels (3.33) in the arguments of the Fermi-Dirac distribution function together with the substitution of the bare dimensionless gap between energy levels, Δ_n, and SO parameter, S, by the corresponding renormalized quantities (3.34) and (3.37).

It is worth emphasizing that the quantum functionals (4.18) and (4.19) can be very useful to discuss electron-electron interaction effects at the mean-field level in the integer quantum Hall regime and in the presence of strong Rashba SO interaction. As mentioned in Sec. 3.3.1 (nonlinear) screening effects yield an electrostatic potential usually very different from the bare one related to confinement or random impurities. Original works [123, 144] that investigated screening properties at high magnetic fields used semiclassical expressions such as Eq. (4.21) (to be discussed in the next subsection) as a starting point for the calculations. However, further work [145] has shown that even simple 1D confinement toy models considered in the Hartree approximation lead to important quantitative deviations in the pattern of compressible and incompressible regions. This justifies the necessity of working preferentially with quantum functionals such as (4.18) or (4.19) for realistic calculations.

4.3.2. Semiclassical expression

The high temperature (semiclassical) regime, which can be inferred from Eqs. (4.12) and (4.18), is a very simple but interesting limiting case. This regime is characterized by the chain of inequalities $k_B T \gg R_n|\boldsymbol{\nabla}_{\mathbf{R}}\xi_{n,\lambda}(\mathbf{R})| \simeq R_n|\boldsymbol{\nabla}_{\mathbf{R}}V(\mathbf{R})| \gtrsim l_B|\boldsymbol{\nabla}_{\mathbf{R}}V(\mathbf{R})|$ under which it is allowed to make the substitution $\mathbf{R} \simeq \mathbf{r}$ inside the (smooth) functionals of the potential energy and trace out the orbital degrees of freedom, $\boldsymbol{\eta} = \mathbf{r} - \mathbf{R}$, taking into account the normalization of the electronic structure factors. As discussed above, this is equivalent to considering a semiclassical regime where the vortex and electronic degrees of

freedom can be identified, *i.e.* pure $l_B \to 0$ limit, and the quantum nonlocal functionals transform into purely local functionals. As a result, we get the well-known semiclassical expression for the local particle density

$$n_{\rm sc}(\mathbf{r}) = \frac{1}{2\pi l_B^2} \sum_{n=0}^{+\infty} \sum_{\lambda} n_{\rm F}[\xi_{n,\lambda}(\mathbf{r})], \tag{4.21}$$

in which, as anticipated above, the SO quantum number λ can be interpreted as a dressed spin quantum number which is a good quantum number at high magnetic fields.

A notable result can also be obtained when considering the spin polarization (4.13) in this limit. The semiclassical expression valid at high magnetic fields reads

$$\Pi_{\rm sc}^{z}(\mathbf{r}) = \frac{\hbar}{4\pi l_B^2} \sum_{n=0}^{+\infty} \sum_{\lambda} \lambda n_{\rm F}[\xi_{n,\lambda}(\mathbf{r})] \sqrt{1 - \frac{nS^2}{\Delta_n^2}}. \tag{4.22}$$

This quantity shows an explicit dependence on the (magnetic field) dressed Rashba SO parameter S and the SO quantum number λ as a consequence of the spin not being a good quantum number in the presence of SO interaction. It is noteworthy to mention that this formula is in agreement with the expectation value of the $\hat{\mathbf{z}}$ component of the spin operator calculated in Refs. [112, 113], up to a global minus sign which can be attributed to the opposite orientation of the external magnetic field.

4.3.3. Analysis of the functionals for a one-dimensional parabolic confinement model

To discuss the relevance of the obtained functionals, let us consider the case of the typical toy model for the quantum Hall edge channels given by a 1D parabolic potential $V(x) = (1/2)m^*\omega_0^2 x^2$ with chosen characteristic confinement energy $\omega_0 = \omega_c/8$ (this assures that the potential is smooth enough on the scale of the magnetic length). The spatial dispersion of the eigenenergies, $\xi_{n,\lambda}(x) = E_{n,\lambda} + V(x)$, consists of a set of parabolas shifted in energy (see, for instance, Fig. 3.6 where we also considered fine structure disorder effects). We show in Fig. 4.1 the spatial dispersion of the electron density [expressed in units of $1/(2\pi l_B^2)$] using the quantum nonlocal formula (4.18) and the semiclassical local expression (4.21) (note that the "correct" behavior is actually provided by the quantum expression at the temperatures considered in this figure). In the semiclassical regime, the particle density is quantized in integral steps which differ strongly when comparing the situation of finite and vanishing SO interaction (*e.g.* different spatial widths and positions of the density plateaus). This is especially obvious far from the edges when higher energy levels are involved and for which their energy spectra are markedly different. The difference between the two situations can be understood from the fact that, whenever $S \neq 0$, the number of Rashba-Landau levels below the chemical potential is altered (or, equivalently, the bulk density changes). The disparity is not seen for the quantum expression (the curve for $S = 0$ is not shown for the sake of readability) which present a strongly smoothed spatial dependence.

We illustrate in Fig. 4.2 the spatial distribution of the spin polarization [in units of $\hbar/(4\pi l_B^2)$] for the same parabolic confinement potential and temperatures which have been used in Fig. 4.1. Again, we consider the quantum formula obtained through the combination of Eqs. (4.13) and (4.18) and the semiclassical expression (4.22), the latter

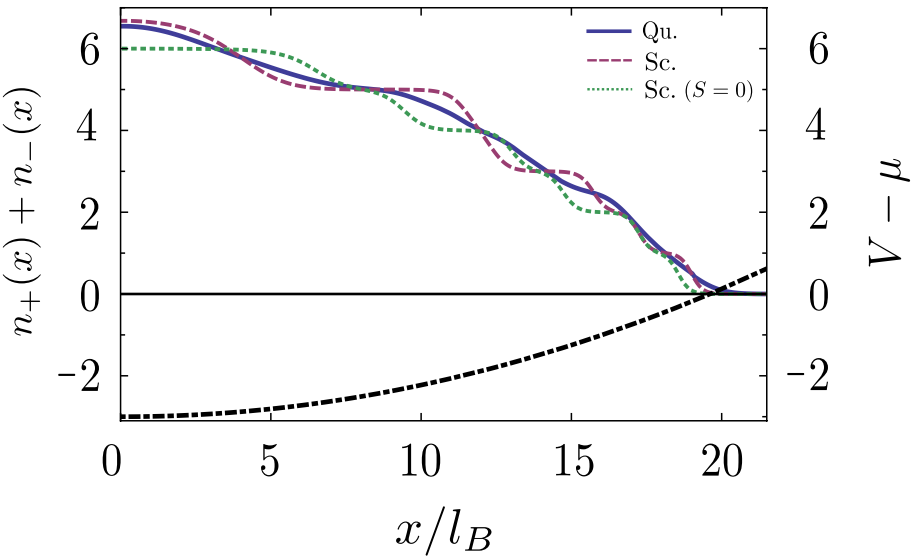

Figure 4.1 – Quantum (solid blue curve) and semiclassical (dashed purple and green dotted curves) local electronic density $n(x)$ as a function of the normalized electron position x/l_B. We consider a quadratic 1D potential confinement (shown in units of $\hbar\omega_c$ as a shifted dashed-dotted black half-parabola) with $\omega_0 = \omega_c/8$ and equilibrium chemical potential $\mu = 3\hbar\omega_c$. In the three curves, relatively high temperature is chosen as $k_BT/(\hbar\omega_c) = 0.06$. Pertinent numerical values for the dressed SO and Zeeman parameters are taken from Ref. [121], $S = 0.88$ and $Z = -0.37$, and correspond to typical values experimentally found in InSb semiconductors, characterized by strong SO interaction. In the semiclassical approximation, comparison is made between Eq. (4.21) in the presence (dashed purple line) and the absence (green dotted line) of Rashba SO interaction.

both in the presence and absence of Rashba SO interaction. In the case of vanishing Rashba coupling (green dotted curve), the semiclassical result for the spin polarization presents the expected oscillations (between 0 and almost 1 due to temperature effects) caused by the filling of the spin-split energy levels. Whenever the SO coupling is switched on, one of the primary effects is to reduce the amplitude of the spatial oscillations, preserving characteristic beatings (both within the quantum and semiclassical results) related to the different spatial dispersion of each of the spin-projected components of the particle density. As it was the case for the particle density, the oscillations are also considerably smoothed when considering the leading quantum expression compared to the semiclassical formula.

More interestingly, in the presence of strong Rashba SO coupling the spin polarization can become negative for certain spatial regions, as can be seen for the semiclassical result (dashed purple curve). This behavior can be understood if we consider the successive filling of the Rashba-Landau energy levels starting from the edges of the confinement: the first contribution of the state $(1,+)$ has a positive amplitude $\sqrt{1-S^2/\Delta_1^2}$ which is compensated by the filling of the state $(0,-)$ that presents opposite SO projection and unit amplitude. As a result, the spin polarization becomes negative in the spatial region where only these two energy levels are filled. Remarkably, it can be shown that this behavior is actually generic: neither limited to the boundaries of the confinement nor the semiclassical expression. Therefore, clear spatial signatures of Rashba SO interaction in the quantum Hall regime could be experimentally studied by local probes capable of detecting the spatial

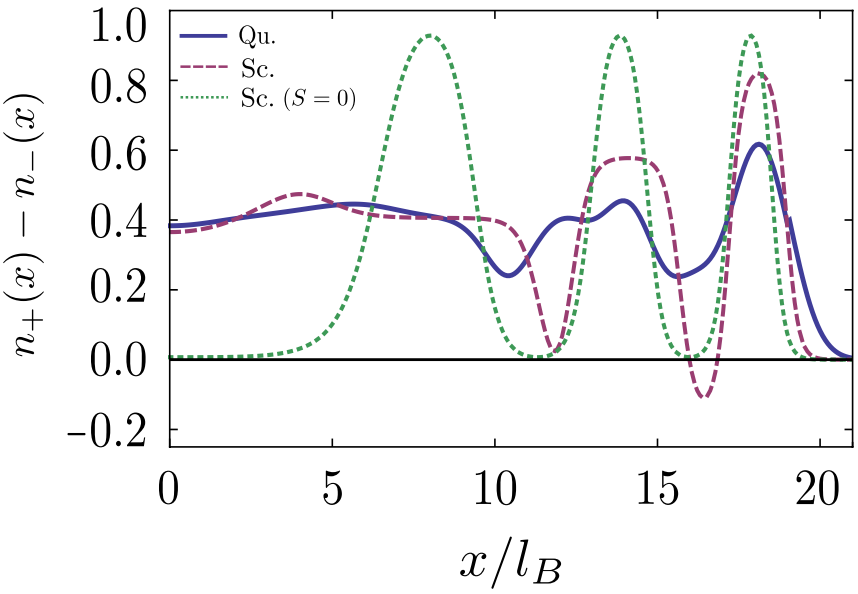

Figure 4.2 – Quantum (solid blue curve) and semiclassical (the dashed purple curve correspond to the situation $S \neq 0$ and green dotted curve to $S = 0$) local spin polarization $\Pi^z(x)$ as a function of the electron position x/l_B. We consider a quadratic 1D potential confinement (not shown here) with $\omega_0 = \omega_c/8$, equilibrium chemical potential $\mu = 3\hbar\omega_c$ and relatively high temperature $k_B T/(\hbar\omega_c) = 0.06$. We use the same numerical values for the magnetic field dressed SO and Zeeman parameters as in Fig. 4.1.

dispersion in the spin imbalance.

4.4. Electron Current Density

4.4.1. General expression

We come now for good to the electron current density. The electron current operator is defined by the standard relation

$$\hat{\mathbf{j}} = e\hat{\mathbf{v}}, \tag{4.23}$$

with the velocity operator given by the Heisenberg equation of motion

$$\hat{\mathbf{v}} = \frac{d}{dt}\hat{\mathbf{r}} = \frac{i}{\hbar}[\hat{\mathcal{H}}, \hat{\mathbf{r}}]. \tag{4.24}$$

Evaluation of the commutator for the Hamiltonian (1.48) (with $\delta\hat{\mathcal{H}}_{\mathrm{R}} \equiv 0$) gives an expression for the local electron current operator which can be written as the sum of two components $\hat{\mathbf{j}} = \hat{\mathbf{j}}_1 + \hat{\mathbf{j}}_2$ with different symmetries[4]. The first term is the usual U(1) electron current operator diagonal in spin space whose origin is the Lorentz force acting on the electric charge

$$\hat{\mathbf{j}}_1 = \frac{e}{m^*}\left[\hat{\mathbf{p}} - \frac{e}{c}\mathbf{A}(\hat{\mathbf{r}})\right] \otimes \mathbb{1}_s, \tag{4.25}$$

[4]This is logical since the Hamiltonian has two parts, one which is diagonal in spin space - the quadratic and Zeeman terms - and the other which is off-diagonal - the Rashba term. The decomposition simply pinpoints the underlying local U(1) × SU(2) symmetry of the Hamiltonian.

while the second is a spatially constant term

$$\hat{\mathbf{j}}_2 = \frac{e^2}{m^* c}\tilde{\mathbf{A}}, \tag{4.26}$$

proportional to a fictitious SO dependent vector potential

$$\tilde{\mathbf{A}} = -\frac{\alpha m^* c}{e}\hat{\mathbf{z}} \times \boldsymbol{\sigma}. \tag{4.27}$$

The vector potential $\tilde{\mathbf{A}}$ is a non-Abelian SU(2) gauge field with the Rashba SO parameter playing the role of a SU(2) coupling constant [analogous to the electric charge in electrodynamics where the gauge group is instead U(1)]. This gauge interpretation of the SO coupling is certainly not new [146] but has been received considerable attention in the literature in recent years to study SO interaction terms linear in the momentum [147, 148] since, in principle, it ensures proper definition of spin-related quantities which automatically satisfy covariant conservation laws from the corresponding Yang-Mills equation of the motion.

The spectral electron current density can now be obtained following the usual steps using the electronic local equilibrium distribution function (4.14). First, we compute the trace of this function with the projected, and properly symmetrized, electron current density operator $\mathbf{j}(\mathbf{r},\mathbf{r}') = [\langle\mathbf{r}|\hat{\mathbf{j}}|\mathbf{r}\rangle + \langle\mathbf{r}'|\hat{\mathbf{j}}|\mathbf{r}'\rangle^*]/2$ written in real space representation

$$\mathbf{j}(\mathbf{r},\omega) = \mathrm{Tr}\left\{\mathbf{j}(\mathbf{r},\mathbf{r}')[-iG^<(\mathbf{r},\mathbf{r}',\omega)]\right\}\Big|_{\mathbf{r}=\mathbf{r}'}. \tag{4.28}$$

As for the local particle density and the LDoS, it seems convenient to express the spectral electron current density as a sum over two spin-resolved components

$$\mathbf{j}(\mathbf{r},\omega) = \sum_{\sigma=\pm}\mathbf{j}_\sigma(\mathbf{r},\omega), \tag{4.29}$$

and split-up the terms which present different gauge symmetries [U(1) and SU(2) components]. The explicit expression of the spin-resolved U(1) contribution in terms of the electronic structure factors and the vortex spectral density yields

$$\begin{aligned}\mathbf{j}_{1\sigma}(\mathbf{r},\omega) = \frac{e\hbar}{2m^*}\int\frac{d^2\mathbf{R}}{2\pi l_B^2}\sum_{n_1,\lambda_1}\sum_{n_2,\lambda_2} f_\sigma(\theta_{n_1}^{\lambda_1})f_\sigma(\theta_{n_2}^{\lambda_2}) \\ \times\left[(\boldsymbol{\nabla}_{\mathbf{r}'}-\boldsymbol{\nabla}_{\mathbf{r}}) + \frac{2ie}{\hbar c}\mathbf{A}(\mathbf{r})\right]F_{n_{1\sigma};n_{2\sigma}}(\mathbf{r},\mathbf{r}',\mathbf{R})\, g^<_{n_1,\lambda_1;n_2,\lambda_2}(\mathbf{R};\omega)\Big|_{\mathbf{r}=\mathbf{r}'}.\end{aligned} \tag{4.30}$$

This formula can be manipulated to get rid of all the gradients acting on the non-diagonal elements of the electronic kernels following the steps detailed in Ref. [130] for the spin-resolved 2DEG. We get

$$\begin{aligned}\mathbf{j}_{1\sigma}(\mathbf{r},\omega) = -\frac{ie\hbar}{2m^*}\int\frac{d^2\mathbf{R}}{2\pi l_B^2}\sum_{n_1,\lambda_1}\sum_{n_2,\lambda_2} f_\sigma(\theta_{n_1}^{\lambda_1})f_\sigma(\theta_{n_2}^{\lambda_2}) \\ \times\mathbf{J}_{n_{1\sigma};n_{2\sigma}}(\mathbf{r},\mathbf{R})\, g^<_{n_1,\lambda_1;n_2,\lambda_2}(\mathbf{R};\omega),\end{aligned} \tag{4.31}$$

with $\mathbf{J}_{n_{1\sigma},n_{2\sigma}}(\mathbf{r},\mathbf{R})$ an electronic current kernel that contains the contribution of the orbital motion (wave functions) defined as

$$\mathbf{J}_{n_{1\sigma};n_{2\sigma}}(\mathbf{r},\mathbf{R}) = \hat{\mathbf{z}} \times \boldsymbol{\nabla}_{\mathbf{r}} F_{n_{1\sigma};n_{2\sigma}}(\mathbf{r},\mathbf{r},\mathbf{R}) - \frac{i\sqrt{2}}{l_B} \times \Bigg[\sqrt{n_{2\sigma}+1} F_{n_{1\sigma};n_{2\sigma}+1}(\mathbf{r},\mathbf{r},\mathbf{R}) \begin{pmatrix} 1 \\ i \end{pmatrix} + \sqrt{n_{1\sigma}+1} F_{n_{1\sigma}+1;n_{2\sigma}}(\mathbf{r},\mathbf{r},\mathbf{R}) \begin{pmatrix} -1 \\ i \end{pmatrix} \Bigg]. \tag{4.32}$$

We therefore recover in Eq. (4.31) the same decomposition into orbital and guiding center motion, convoluted through the integral over the vortex coordinates, that holds for the electronic Green's function (3.19).

The spin-resolved SU(2) component of the electron current density is obtained analogously and reads

$$\mathbf{j}_{2\sigma}(\mathbf{r},\omega) = \alpha e \int \frac{d^2\mathbf{R}}{2\pi l_B^2} \sum_{n_1,\lambda_1} \sum_{n_2,\lambda_2} f_\sigma(\theta_{n_1}^{\lambda_1}) f_{-\sigma}(\theta_{n_2}^{\lambda_2}) F_{n_{1\sigma};n_{2-\sigma}}(\mathbf{r},\mathbf{r},\mathbf{R}) \times g^{<}_{n_1,\lambda_1;n_2,\lambda_2}(\mathbf{R};\omega) \begin{pmatrix} \sigma \\ i \end{pmatrix}. \tag{4.33}$$

Up to this point, everything has been exact and no approximation has been made. Therefore, if we would know the full SO vortex Green's function (with its off-diagonal elements in the Rashba-Landau quantum number n), we could compute the electron current density taking into account all the l_B contributions related to the vortex degree of freedom. This is certainly a complicated task which we will not pursue here, since we are mostly interested in the most significant contribution to the electron current density at high magnetic fields. As mentioned in Sec. 4.2.1, the dominant contribution to the electron current density comes both from the leading order and first subleading contributions[5] to the SO vortex Green's function power series (4.2) because we have to compensate for the prefactor $1/m^*$ in Eq. (4.31) [note that in Eq. (4.33) level mixing appears naturally since the operator $\hat{\mathbf{j}}_2$ naturally selects the off-diagonal components of the Green's function]. In the following we will distinguish these two terms in the electron current density which originate from $g^{(0)}(\mathbf{R};\omega)$ and $g^{(1)}(\mathbf{R};\omega)$ and correspond to the so-called density-gradient and drift current densities, respectively.

4.4.2. Density-gradient current

Following our program, we consider the leading order term of the lesser component of the SO vortex Green's function (4.17) and inject its expression into Eq. (4.31) to compute the U(1) current density. The current kernel (4.32) presents then combinations of structure factors of the form $\sqrt{n+1}F_{n;n+1}(\mathbf{r},\mathbf{r},\mathbf{R}) \pm \text{c.c.}$ (where c.c stands for complex conjugate). Using that the non-diagonal elements of the structure factor which differ in

[5] In contrast, to obtain the dominant contribution to the particle density at high magnetic fields it is enough to know the leading order contribution to the SO vortex Green's function.

only one Rashba-Landau level index satisfy the identity [130]

$$\sqrt{n+1}F_{n;n+1}(\mathbf{r},\mathbf{r},\mathbf{R}) = \frac{l_B}{\sqrt{2}}\sum_{q=0}^{n}\partial_- F_q(\mathbf{r}-\mathbf{R}), \tag{4.34}$$

and the relation $\boldsymbol{\nabla}_{\mathbf{R}}F_n(\mathbf{r}-\mathbf{R}) = -\boldsymbol{\nabla}_{\mathbf{r}}F_n(\mathbf{r}-\mathbf{R})$, the current kernel adopts the simpler expression

$$\mathbf{J}_{n_\sigma;n_\sigma}(\mathbf{r},\mathbf{R}) = \hat{\mathbf{z}}\times\boldsymbol{\nabla}_{\mathbf{r}}\Big[F_n(\mathbf{r}-\mathbf{R}) - 2\sum_{q=0}^{n_\sigma}F_q(\mathbf{r}-\mathbf{R})\Big]. \tag{4.35}$$

Performing an integration over the frequencies [*i.e.*, we define the local current $\mathbf{j}(\mathbf{r}) = (2\pi)^{-1}\int d\omega\,\mathbf{j}(\mathbf{r},\omega)$] we obtain the following quantum formula for the U(1) current density

$$\mathbf{j}^{\mathrm{dg}}_{1\sigma}(\mathbf{r}) = -\frac{e}{h}(\hbar\omega_c)\,\hat{\mathbf{z}}\times\boldsymbol{\nabla}_{\mathbf{r}}\int d^2\mathbf{R}\sum_{n=0}^{+\infty}\sum_{\lambda}f_\sigma^2(\theta_n^\lambda)n_{\mathrm{F}}[\xi_{n,\lambda}(\mathbf{R})] \times\left[\sum_{q=0}^{n_\sigma}F_q(\mathbf{r}-\mathbf{R}) - \frac{1}{2}F_{n_\sigma}(\mathbf{r}-\mathbf{R})\right]. \tag{4.36}$$

Now, for the SU(2) part of the electron current density, we follow the same steps: first, insert the leading order term of the lesser SO vortex Green's function into Eq. (4.33), then perform an integration over the frequencies to get

$$\mathbf{j}^{\mathrm{dg}}_{2\sigma}(\mathbf{r}) = i\alpha e\int\frac{d^2\mathbf{R}}{2\pi l_B^2}\sum_{n=1}^{+\infty}\sum_{\lambda}f_\sigma(\theta_n^\lambda)f_{-\sigma}(\theta_n^\lambda)n_{\mathrm{F}}[\xi_{n,\lambda}(\mathbf{R})]F_{n_\sigma;n_{-\sigma}}(\mathbf{r},\mathbf{r},\mathbf{R})\begin{pmatrix}\sigma\\ i\end{pmatrix}. \tag{4.37}$$

Next, we observe that the spin-resolved SU(2) electron current density is not real. This is simply a consequence of the fact that in the presence of Rashba SO interaction the spin σ is not a good quantum number and there is *a priori* no reason why the electron current density can be expressed in terms of two independent spin-resolved components (but it can, nevertheless, be decomposed into two SO-resolved components, see Sec. 4.5). Technically, the sum of the two spin-projected components allows us to combine the terms coming from the off-diagonal elements of the electronic kernels $F_{n;n+1}(\mathbf{r},\mathbf{r},\mathbf{R})$ with their complex conjugates to obtain the following (real) expression for the total current density

$$\mathbf{j}^{\mathrm{dg}}_{2}(\mathbf{r}) = \frac{e}{h}(\hbar\omega_c)\frac{S}{2}\hat{\mathbf{z}}\times\boldsymbol{\nabla}_{\mathbf{r}}\int d^2\mathbf{R}\sum_{n=1}^{+\infty}\sum_{\lambda}f_+(\theta_n^\lambda)f_-(\theta_n^\lambda)n_{\mathrm{F}}[\xi_{n,\lambda}(\mathbf{R})] \times\frac{1}{\sqrt{n}}\sum_{q=0}^{n-1}F_q(\mathbf{r}-\mathbf{R}). \tag{4.38}$$

Note the vector product in Eqs. (4.36) and (4.38) that ensures that, at this order, the contributions to the current density present zero bulk average.

In the high temperature limit, the integral over the vortex positions can be performed as in Sec. 4.3.2 and we get the semiclassical expression for the electron current density

from the quantum functionals (4.36) and (4.38)

$$\mathbf{j}_{\mathrm{sc}}^{\mathrm{dg}}(\mathbf{r}) = \frac{e}{2h}(\hbar\omega_c)\sum_{n=0}^{+\infty}\sum_{\lambda}\sum_{\sigma=\pm}\left\{\left(n_\sigma+\frac{1}{2}\right)\left[1-\sigma\lambda\sqrt{1-\frac{nS^2}{\Delta_n^2}}\right]\right.$$
$$\left.-\frac{\lambda}{4}\frac{nS^2}{\Delta_n^2}\right\}\boldsymbol{\nabla}_{\mathbf{r}}n_{\mathrm{F}}[\xi_{n,\lambda}(\mathbf{r})]\times\hat{\mathbf{z}}. \quad (4.39)$$

This functional (and the quantum counterpart) correspond to the so-called density-gradient [130] (or edge [149]) contribution to the electron current density. It represents the electron flow, in the presence of Rashba SO interaction and Zeeman coupling, which appears as a response to a change in the particle density. As such, it vanishes in the incompressible parts of the sample where the gradient of the density is quasiconstant while presenting sharp peaks (broadened by temperature and quantum smearing effects) in the compressible regions where the density is inhomogeneous. It is also interesting to note that in this formula both the U(1) and SU(2) yield a dependence on the parameter S whose clear signatures could, in principle, be experimentally studied at high temperatures by performing a careful analysis of the spatial structure of the edge states in the 2DEG.

4.4.3. Drift current

As discussed previously, the drift [130] (or bulk [149]) contribution to the electronic current density can be obtained when considering the subleading term in the SO vortex Green's function expansion characterized by Rashba-Landau level mixing in the presence of gradients of the potential energy. From a practical perspective, we compute this term by inserting the subdominant (off-diagonal) component of the lesser SO vortex Green's function [obtained by using Eq. (4.10) and definition (4.14)] into Eqs. (4.31) and (4.33). After some algebra, we get the following expression for the spin-resolved U(1) term

$$\mathbf{j}_{1\sigma}^{\mathrm{dr}}(\mathbf{r}) = \frac{e}{h}\int d^2\mathbf{R}\sum_{n=0}^{+\infty}\sum_{\lambda_1,\lambda_2}\sum_{\sigma'=\pm}\sqrt{\frac{n_{\sigma'}+1}{n_\sigma+1}}f_\sigma(\theta_n^{\lambda_1})f_{\sigma'}(\theta_n^{\lambda_1})$$
$$\times f_\sigma(\theta_{n+1}^{\lambda_2})f_{\sigma'}(\theta_{n+1}^{\lambda_2})\,\hat{\mathbf{z}}\times\left[\boldsymbol{\nabla}_{\mathbf{R}}V(\mathbf{R})\sum_{q=0}^{n_\sigma}F_q(\mathbf{r}-\mathbf{R})\right.$$
$$\left.+\,l_B^2\left[\boldsymbol{\nabla}_{\mathbf{R}}V(\mathbf{R})\cdot\boldsymbol{\nabla}_{\mathbf{r}}\right]\boldsymbol{\nabla}_{\mathbf{r}}\sum_{q=0}^{n_\sigma}\left(n_\sigma+\frac{1}{2}-q\right)F_q(\mathbf{r}-\mathbf{R})\right]$$
$$\times\,\hbar\omega_c\frac{n_{\mathrm{F}}[\xi_{n+1,\lambda_2}(\mathbf{R})]-n_{\mathrm{F}}[\xi_{n,\lambda_1}(\mathbf{R})]}{\xi_{n+1,\lambda_2}(\mathbf{R})-\xi_{n,\lambda_1}(\mathbf{R})}, \quad (4.40)$$

and for the full SU(2) term (after the sum over $\sigma = \pm$ has been performed)

$$\begin{aligned}\mathbf{j}_2^{\rm dr}(\mathbf{r}) = -\frac{e}{h}\frac{S}{2}\int d^2\mathbf{R}\sum_{n=0}^{+\infty}\sum_{\lambda_1,\lambda_2}\sum_{\sigma'=\pm}\sqrt{n_{\sigma'}+1}f_{\sigma'}(\theta_n^{\lambda_1})f_{\sigma'}(\theta_{n+1}^{\lambda_2})\\ \times f_-(\theta_n^{\lambda_1})f_+(\theta_{n+1}^{\lambda_2})\,\hat{\mathbf{z}}\times\Bigg(\boldsymbol{\nabla}_{\mathbf{R}}V(\mathbf{R})\Bigg\{F_n(\mathbf{r}-\mathbf{R})\\ +\frac{1}{\sqrt{n+1}\sqrt{n+2}}\left[\sum_{q=0}^{n}F_q(\mathbf{r}-\mathbf{R})-(n+1)F_{n+1}(\mathbf{r}-\mathbf{R})\right]\Bigg\}\\ +\frac{l_B^2\left[\boldsymbol{\nabla}_{\mathbf{R}}V(\mathbf{R})\cdot\boldsymbol{\nabla}_{\mathbf{r}}\right]\boldsymbol{\nabla}_{\mathbf{r}}}{\sqrt{n+1}\sqrt{n+2}}\sum_{q=0}^{n}(n+1-q)F_q(\mathbf{r}-\mathbf{R})\Bigg)\\ \times\hbar\omega_c\frac{n_{\rm F}[\xi_{n+1,\lambda_2}(\mathbf{R})]-n_{\rm F}[\xi_{n,\lambda_1}(\mathbf{R})]}{\xi_{n+1,\lambda_2}(\mathbf{R})-\xi_{n,\lambda_1}(\mathbf{R})}.\end{aligned}\tag{4.41}$$

A detailed derivation of the quantum functionals (4.40) and (4.41) is provided in Appendix C.

The obtained formula for the drift current density, given by the sum of Eqs. (4.40) and (4.41), is very complicated. To get some analytical insight, and for reasons of clarity, we shall consider in the rest of the chapter the high temperature limit (*i.e.* the semiclassical limit $l_B \to 0$) only. This regime is obtained straightforwardly after the integration over the orbital degree of freedom $\boldsymbol{\eta}$ and yields the following expression for the total semiclassical drift current density in the presence of Rashba and Zeeman interactions

$$\begin{aligned}\mathbf{j}_{\rm sc}^{\rm dr}(\mathbf{r}) = \frac{e}{h}\sum_{n=0}^{+\infty}\sum_{\lambda_1,\lambda_2}\left[\sum_{\sigma'=\pm}\sqrt{n_{\sigma'}+1}f_{\sigma'}(\theta_n^{\lambda_1})f_{\sigma'}(\theta_{n+1}^{\lambda_2})\right]\\ \times\left[\sum_{\sigma=\pm}\sqrt{n_\sigma+1}f_\sigma(\theta_n^{\lambda})f_\sigma(\theta_{n+1}^{\lambda_2})-\frac{S}{2}f_-(\theta_n^{\lambda_1})f_+(\theta_{n+1}^{\lambda_2})\right]\\ \times\hbar\omega_c\frac{n_{\rm F}[\xi_{n+1,\lambda_2}(\mathbf{r})]-n_{\rm F}[\xi_{n,\lambda_1}(\mathbf{r})]}{\xi_{n+1,\lambda_2}(\mathbf{r})-\xi_{n,\lambda_1}(\mathbf{r})}\,\hat{\mathbf{z}}\times\boldsymbol{\nabla}_{\mathbf{r}}V(\mathbf{r}),\end{aligned}\tag{4.42}$$

which will be the basis for the analysis of transport properties in the next section. It is also a good and not difficult exercice to check that the well-known expression for the semiclassical drift current density [130, 149] can be smoothly recovered in the limit of vanishing SO coupling ($|S| \to 0$). In this limit the angular parameters $\theta_n^{\lambda} \to (1+\lambda)\pi/4$, *i.e.* $f_\pm(\theta_n^{\pm}) = 1$ independently of the Rashba-Landau level index. The SU(2) contribution to the semiclassical drift current density vanishes trivially and we obtain from the U(1) part

$$\mathbf{j}_{\rm sc}^{\rm dr}(\mathbf{r})_{\alpha\to 0} = \frac{e}{h}\sum_{n=0}^{+\infty}\sum_{\sigma=\pm}n_{\rm F}[\xi_{n,\sigma}(\mathbf{r})]\boldsymbol{\nabla}_{\mathbf{r}}V(\mathbf{r})\times\hat{\mathbf{z}},\tag{4.43}$$

where the Zeeman-split effective energies in the presence of an electrostatic potential[6] are given by the expression $\xi_{n,\sigma}(\mathbf{r}) = \hbar\omega_c(n+1/2+\sigma Z/2)+V(\mathbf{r})$.

[6] We remind the reader that in this limit we must relabel the Rashba-Landau energy levels according to $n_{-\sigma}+1 \to n$ and $\lambda \to \sigma$ to recover the image of the Zeeman spin-split Landau levels.

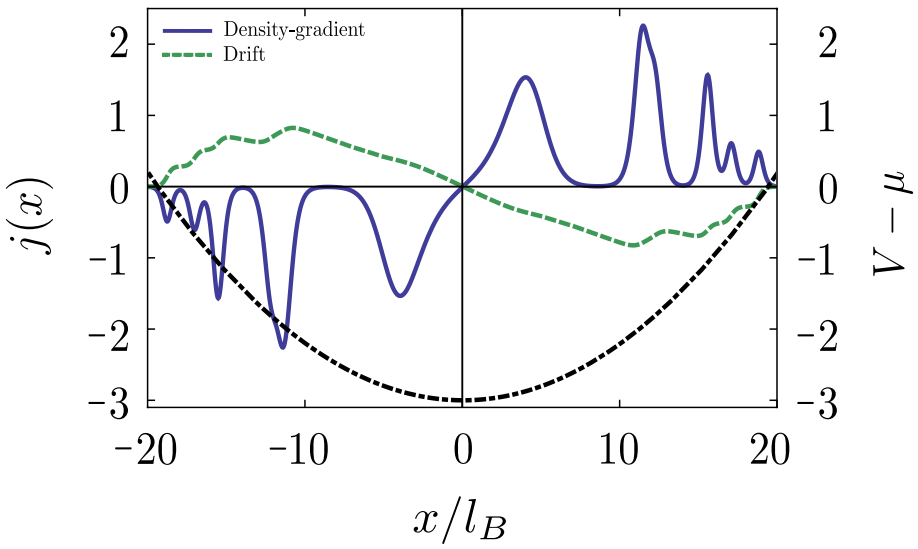

Figure 4.3 – Spatial distribution of the semiclassical density-gradient (solid blue curve) and drift (green dashed curve) current density contributions for a quadratic 1D potential confinement model (represented in units of $\hbar\omega_c$ by the shifted dashed-dotted parabola) with $\omega_0 = \omega_c/8$, $\mu = 3\hbar\omega_c$ and $k_BT/(\hbar\omega_c) = 0.06$. The SO and Zeeman parameters S and Z are chosen to be the same as in Fig. 4.1. Note the alternating sign of each of the contributions that combine to give important spatial oscillations of the total electron current density.

To wrap up this section, we show in Fig. 4.3 the spatial distribution of the semiclassical density-gradient (4.39) and drift (4.42) current density contributions at equilibrium [in units of $e\omega_c/(2\pi l_B)$] as a function of the normalized electron position x/l_B. Here, we also choose for confinement a smooth parabolic 1D potential toy model $V(x) = (1/2)m^*\omega_0^2x^2$ where $\omega_0 = \omega_c/8$. The density-gradient contribution, as expected, displays temperature-broadened peaks representing the (symmetric in this simple confinement potential) spatial dispersion of the edge states. These peaks can be perfectly matched with the spatial compressible regions where the particle density is inhomogeneous in Fig. 4.1. Simultaneously, the density-gradient current flow gets strongly reduced[7] in the incompressible regions (of constant particle density) in the disordered 2DEG. In contrast to the relatively complex density-gradient current, the drift current does not vanish, except at the bottom of the potential well, and is almost structureless showing no special features. Remarkably, the combination of both terms (with different signs) produces spatial oscillations in the total current density which can be attributed to the fact that the compressible stripes and the regions of strong potential gradients yield opposite currents at finite temperature [149].

4.5. Transport Properties

4.5.1. Local Hall conductivity

As we have seen in the preceding sections, the high field expansion technique allows us to derive quantum and semiclassical expressions for local observables in the form of

[7]Density-gradient current even vanishes at $T = 0$.

functionals of the potential energy $V(\mathbf{r})$. This general character allows us to treat on equal footing equilibrium and nonequilibrium local electric fields in the nonperturbative high magnetic field regime and, in particular, deal with nonequilibrium potentials as occurring in a transport experiment. In the linear response regime, we can assume that the nonequilibrium electrostatic potential has the form $V_{\rm neq}(\mathbf{r}) = e\Phi(\mathbf{r})$ giving rise to an electromotive field $\boldsymbol{\mathcal{E}}(\mathbf{r}) = -\boldsymbol{\nabla}_{\mathbf{r}}\Phi(\mathbf{r})$. This field induces in the system a nonequilibrium drift current density which, at high temperatures, can be deduced directly from Eq. (4.42). As expected, this observable in the local equilibrium regime satisfies a local Ohm's law $\mathbf{j}_{\rm neq}(\mathbf{r}) = \bar{\sigma}(\mathbf{r})\boldsymbol{\mathcal{E}}(\mathbf{r}) = \sigma_{\rm H}(\mathbf{r})\hat{\mathbf{z}} \times \boldsymbol{\mathcal{E}}(\mathbf{r})$, where the conductivity tensor $\bar{\sigma}(\mathbf{r})$ is purely off-diagonal with Hall component

$$\begin{aligned}\sigma_{\rm H}(\mathbf{r}) = -\frac{e^2}{h}\sum_{n=0}^{+\infty}\sum_{\lambda_1,\lambda_2}\left[\sum_{\sigma'=\pm}\sqrt{n_{\sigma'}+1}f_{\sigma'}(\theta_n^{\lambda_1})f_{\sigma'}(\theta_{n+1}^{\lambda_2})\right] \\ \times\left[\sum_{\sigma=\pm}\sqrt{n_\sigma+1}f_\sigma(\theta_n^{\lambda})f_\sigma(\theta_{n+1}^{\lambda_2}) - \frac{S}{2}f_-(\theta_n^{\lambda_1})f_+(\theta_{n+1}^{\lambda_2})\right] \\ \times\hbar\omega_c\frac{n_{\rm F}[\xi_{n+1,\lambda_2}(\mathbf{r})] - n_{\rm F}[\xi_{n,\lambda_1}(\mathbf{r})]}{\xi_{n+1,\lambda_2}(\mathbf{r}) - \xi_{n,\lambda_1}(\mathbf{r})}.\end{aligned} \tag{4.44}$$

Eq. (4.44) describes the (local) semiclassical Hall conductivity in the presence of uniform Rashba SO interaction, Zeeman coupling and smooth disorder potentials. This is an important result since it gives information on the characteristic values of the Hall plateaus depending on the strength of the Rashba SO interaction. It also constitutes a highly nontrivial formula due to the simultaneous dependence on two SO quantum numbers λ_1 and λ_2 together with the mixing between adjacent Rashba-Landau energy levels.

At first sight, one may think from Eq. (4.44) that the quantization of the Hall conductivity in units of the conductance quantum, e^2/h, can be affected by Rashba SO interaction at low temperatures. Nevertheless, it can be proved by symbolic calculation[8] that the Hall conductivity adopts the form

$$\sigma_{\rm H}(\mathbf{r}) = \frac{e^2}{h}\sum_{n=0}^{+\infty}\sum_{\lambda} n_{\rm F}[\xi_{n,\lambda}(\mathbf{r})], \tag{4.45}$$

for any *finite* value of the SO coupling parameter S. Actually, this result was already suggested by the semiclassical expression for the electron density: Eq. (4.45) can be recovered using Eq. (4.21) and the classical Hall formula that relates the local electron density and the Hall conductivity $\sigma_{\rm H}(\mathbf{r}) = (ec/B)n(\mathbf{r})$ (this is, of course, not true from the moment that we use the full quantum expression for the electron current density that includes the electronic structure factors). We therefore conclude that the local semiclassical Hall conductivity is robust with respect to any finite Rashba SO coupling and is quantized at fairly low temperatures in units of e^2/h.

4.5.2. Hall conductivity in a disordered topological insulator surface

Remarkably, the general formula (4.44) can also be used to compute the local Hall conductivity on a topological insulator (single) surface. At low energies, the latter can be

[8] Analytical calculations can be performed up to order $\mathcal{O}(S^3)$.

described by a simple model consisting in a single Dirac cone obtained from the effective Hamiltonian for a finite film within the slab geometry neglecting any possible coupling between the two (top and bottom) surfaces and all the contributions from the bulk nonlinear in the momentum. This situation corresponds to the disordered 2DEG with Rashba SO interaction and Zeeman coupling in the limit $|S| \to +\infty$ (more precisely to the simultaneous formal limits $m^* \to +\infty$ and $g \to 0$) for which the kinetic part of the Hamiltonian is equal to Eq. (1.29) up to a unitary transformation.

First, we recall (see Sec. 3.2) that for the Rashba-Landau energy levels (2.21) this limit yields a gapless and purely relativistic-like energy spectrum

$$\xi_{n,\lambda}(\mathbf{r}) = -\lambda\sqrt{n}\hbar\Omega + V(\mathbf{r}), \tag{4.46}$$

where $\Omega = \alpha\sqrt{2}/l_B$ is the SO dependent characteristic frequency. We recover thus the well-known result for effective Dirac Hamiltonians describing relativistic-like electrons in a perpendicular magnetic field which present a characteristic energy scale no longer proportional to the magnetic field, $\hbar\omega_c \propto B$, but $\hbar\Omega \propto \sqrt{B}$. More importantly, the energy spectrum (4.46) is no more bounded from below as it happens with the Rashba-Landau energy levels for finite SO interaction. As a result, there is an infinite number of filled relativistic Landau levels below a given value of the chemical potential μ. Usually, this imposes to soundly alter the definition of the current, defined now in terms of the imbalance between the electron and hole current[9].

Let us now show how we can perform a regularization procedure within our scheme[10] to obtain the correct result for the local Hall conductivity without the need to introduce the relativistic definition for the current density. To that purpose, we simply consider the limit $|S| \to +\infty$ in Eq. (4.44) taking into account that the angular parameters appearing in the weighting functions $f_\sigma(\theta_n^\lambda)$ approach the finite values $\theta_n^\lambda = \lambda\pi/4$ independently of the level index n. In addition, it can be seen by inspection of Eq. (4.44) that the U(1) part of the expression tends to zero while the SU(2) term tends towards a finite value. Further straightforward simplifications give the well-known result for the local Hall conductivity in low-energy graphene [151]

$$\sigma_{\mathrm{H}}(\mathbf{r}) = \frac{e^2}{h}\sum_{n=0}^{+\infty}\sum_{\lambda}\left(n+\frac{1}{2}\right)\left\{n_{\mathrm{F}}[\tilde{\xi}_{n,\lambda}(\mathbf{r})] - n_{\mathrm{F}}[\tilde{\xi}_{n+1,\lambda}(\mathbf{r})]\right\}, \tag{4.47}$$

up to a global prefactor (Hall conductivity here appears to be four times smaller due to the lack of spin and valley degeneracies). Consequently, we expect a sequence of Hall plateaux pinned at values $\pm 1/2$, $\pm 3/2$, $\pm 5/2$,... of the conductance quantum[11]. Formula (4.47) can be (formally) rewritten as

$$\sigma_{\mathrm{H}}(\mathbf{r}) = \frac{e^2}{h}\left\{\frac{1}{2}n_{\mathrm{F}}[\tilde{\xi}_{0,-}(\mathbf{r})] + \sum_{n=1}^{+\infty}\sum_{\lambda=\pm} n_{\mathrm{F}}[\tilde{\xi}_{n,\lambda}(\mathbf{r})]\right\}, \tag{4.48}$$

[9] This is, of course, an artifact of the low energy approximation for the band spectrum in the Dirac cone. For the complete band structure, there are natural cut-offs due to the finite band width and the number of Landau levels below the chemical potential is finite.

[10] Other regularization procedures such as the point-splitting regularization technique, where ultraviolet divergencies appearing as a consequence of the unbounded spectrum are removed "by hand" thanks to the formal rule $\lim_{\mathbf{r}\to\mathbf{r}'}\delta(\mathbf{r}-\mathbf{r}') = 0$ can be used to get the same result [150].

[11] Note that, in principle, half-integer quantization cannot be observed in a transport experiment within the slab geometry because both top and bottom surfaces are measured in parallel [152].

where we clearly see that the $n = 0$ relativistic Landau level presents half of the degeneracy compared to higher $n \geq 1$ Landau levels (we stress that this way of writing is purely formal since the second half of the previous expression diverges). This is, to our knowledge, the first time that this interesting result has been obtained from a microscopic nonperturbative theory in the presence of disorder[12]. For clean systems, half-integer quantization of the $n = 0$ Landau level was predicted thirty years ago [40] and is related to the fact that Dirac massless Hamiltonians have always a bound state at zero energy due to their supersymmetric structure.

In the light of Eqs. (4.44), (4.45) and (4.47) we also want to discuss here a recently obtained theoretical result [136]. This paper studies the quantization of the Hall conductivity in a topological insulator surface, taking also into account a so-called "Schrödinger" term quadratic in the momentum. Although we consider the same Hamiltonian in this thesis[13] and agree with the authors on the quantized values of the Hall conductivity in the two limiting cases ($|S| \to 0$ which corresponds to a pure quadratic dispersion relation and $|S| \to +\infty$ which corresponds to a pure linear one in the momentum), our conclusions for the case $0 < |S| < +\infty$ are strikingly different: Ref [136] gets deviations to both the integer and half-integer quantization depending on the value of the SO parameter S, while we find in our work that the Hall conductivity remains *exactly* quantized in units of R_{K}^{-1}. In other terms, we get that the quantization of the Hall conductivity is purely dictated by the topology of the Fermi surface. Both results seem to differ due to the different formulations of transport theory used: Ref. [136] used a perturbatively based transport theory (Kubo) whose validity is questionable at high magnetic fields while we derived Eq. (4.44) from a nonperturbative semiclassical transport theory with a smooth electrostatic potential. Indeed, one can clearly doubt of the results derived from Kubo formula in the quantum Hall regime as the general Kubo formulation is obtained for the diffusive regime after disorder averaging in an ergodic system [159] while the present transport regime is strongly inhomogeneous with characteristic percolating features.

4.5.3. Spin Hall conductivity in the quantum Hall regime

We have previously seen in Sec. 4.3 that, at high magnetic fields, the SO quantum number λ can be seen as a good quantum number in the presence of a smooth disorder potential. The fact that λ is a good quantum number also manifests in the quantum functionals (4.40) and (4.41) for the drift current density which can be decomposed as a sum over two independent SO components

$$\mathbf{j}(\mathbf{r}) = \sum_{\lambda} \mathbf{j}_{\lambda}(\mathbf{r}). \tag{4.49}$$

This property can also be understood as being a consequence of the local equilibrium regime at high magnetic fields. This produces the angle θ_n^{λ}, which is related to the Rashba precession axis in spin space, to be spatially constant and unaffected by the electrostatic potential. When taking into account quantum effects related to the guiding center (which were neglected in this chapter) it can also be seen that a similar decomposition also holds [*e.g.* Eqs. (3.44) and (4.19)], where the observables are still expressed as a sum over

[12] Standard calculations in a perturbative regime (Kubo formula) for clean systems (not in the quantum Hall regime) in the presence of surface hybridization can be found in the literature [153].

[13] It is, unfortunately, unnoticed by the authors that the helical fermions are described by the Rashba Hamiltonian (2.18).

two SO-resolved components with respect to a renormalized SO quantum number. The precession angle in this case can be seen to be renormalized and slowly depends on the vortex position as a result of the smooth local variations of the disorder potential landscape.

Now, in the semiclassical limit ($l_B \to 0$) we have seen (4.45) that the SO-polarized electron current density reads

$$\mathbf{j}_\lambda(\mathbf{r}) = \frac{e^2}{h} \sum_n n_{\rm F}[\xi_{n,\lambda}(\mathbf{r})]\, \hat{\mathbf{z}} \times \boldsymbol{\mathcal{E}}(\mathbf{r}). \tag{4.50}$$

This expression (similar reasoning can be made using the quantum formula too) allows us to define a nonequilibrium local spin current density $\mathbf{j}^s_{\rm neq}(\mathbf{r})$ from which we can extract a local spin Hall conductivity $\sigma^s_{\rm H}(\mathbf{r})$ for electrons with their spin polarized along the SO-dependent axis for which λ is a good quantum number. The nonequilibrium current is interpreted as the combination of two independent SO-polarized currents in which electrons with different SO quantum number flow in opposite directions without net charge transport. Therefore, we write

$$\mathbf{j}^s_{\rm neq}(\mathbf{r}) = \frac{\hbar}{2e}\Big[\mathbf{j}_+(\mathbf{r}) - \mathbf{j}_-(\mathbf{r})\Big], \tag{4.51}$$

which automatically gives the local spin Hall conductivity

$$\sigma^s_{\rm H}(\mathbf{r}) = \frac{e}{4\pi} \sum_n \Big\{ n_{\rm F}[\xi_{n,+}(\mathbf{r})] - n_{\rm F}[\xi_{n,-}(\mathbf{r})] \Big\}. \tag{4.52}$$

The defined spin Hall current density evidently reduces to the difference between the spin-up and spin-down polarized current densities in the limit of vanishing SO coupling. The associated spin Hall conductivity is also free of divergencies, even at $T = 0$, contrary to the formula for the spin Hall conductivity discussed in Refs. [112, 113, 140] [we note that Eq. (4.42) and consequently Eq. (4.51) appear to be mathematically very different to the expressions given in the those references]. In addition, it is also clear that a spin current defined in this way can only be transverse [only the Hall components of the spin conductivity tensor $\bar{\sigma}^s(\mathbf{r})$ are non-zero] and satisfies by construction a continuity equation

$$\boldsymbol{\nabla}_{\mathbf{r}} \cdot \mathbf{j}^s_{\rm neq}(\mathbf{r}) = 0. \tag{4.53}$$

As a result, we avoid all the problems encountered with the "traditional" definitions of the spin current in 2DEGs where the non-conservation of the spin current in the $\hat{\mathbf{z}}$ direction has to be cured by a source term in the continuity equation[14] (see discussion in Ref. [109] for example). Moreover, the present formulation also removes the ambiguity in the definition of the spin flow with SO interaction which creates persistent equilibrium currents, both in the absence [157] and presence of magnetic field, since our angular momentum current density appears only as a response to nonequilibrium electric fields.

We end this section with a comparison of the semiclassical charge and spin Hall conductivities in the quantum Hall regime. Both quantities are shown in Fig. 4.4, where they are plotted (in appropriate units) for a fixed position $\mathbf{r}_0$ as a function of the quantity $\mu/\hbar\omega_c$. As in the rest of the chapter, we consider the parameters used for Fig. 4.1 which correspond to common experimental values to be found in semiconductors with strong SO interaction. The Hall conductivity, as expected in this regime, shows quantized plateaus of different

[14] This term has to be present in any case to satisfy covariant conservation laws [147]. See also our discussion in Sec. 2.3.1.

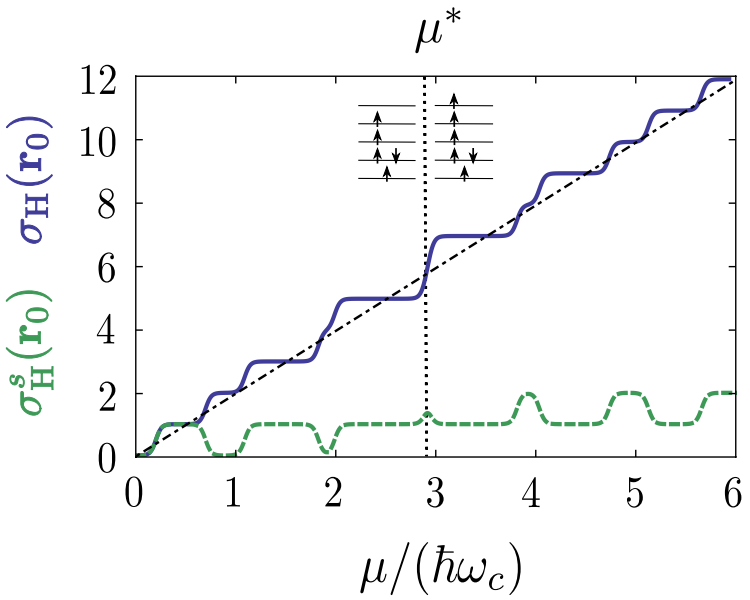

Figure 4.4 – Semiclassical Hall (4.44) and spin Hall conductivity (4.52) (represented respectively by the blue solid and green dashed lines) expressed in units of e^2/h and $e/4\pi$ as a function of the quantity $\mu/\hbar\omega_c$. Here, SO and Zeeman parameters S and Z are the same as in Fig. 4.1 and the temperature is chosen as $k_BT/(\hbar\omega_c) = 0.03$. The dashed-dotted black line represents the classical result where the Hall conductivity grows linearly with the inverse of the magnetic field. The perpendicular dotted line marks the jump in the Hall conductivity that can be related to the crossing of an accidental degeneracy, from where the energy levels are populated differently compared too the usual Zeeman pattern (as represented by the picture on top of the figure in which the perpendicular lines represent the Rashba-Landau levels and the arrows each of the possible SO projections: up arrow for $\lambda = -$ and down arrow for $\lambda = +$).

widths related to the fact that the Rashba-Landau energy levels are not equidistant in the energy space. In addition, the spin Hall conductivity also exhibits quantized plateaux smeared by temperature whose value oscillates between 0 and 1 for $\mu \lesssim \mu^*$. This oscillation is a consequence of the imbalance between the two populations of SO resolved states. At the special value $\mu = \mu^*$ a jump in the Hall conductivity occurs and, for $\mu \gtrsim \mu^*$, the spin Hall conductivity oscillates between 1 and 2. The finite jump is related to an accidental degeneracy in the energy spectrum at the chemical potential μ^* where the levels $(n, +)$ and $(n-1, -)$ swap their positions [with $(n, +)$ now energetically lower than $(n-1, -)$]. As a consequence, the energy levels are populated differently compared to the usual Zeeman pattern (see small schema on top of the figure). More jumps like the latter appear every time the chemical potential crosses new accidental degeneracies in the (disordered) energy spectrum with an eventual saturation of the SO imbalance for large values of the chemical potential. Finally, one can be easily convinced by looking at Fig. 2.3 that in the presence of level repulsion at each of the degeneracy points, the previous results hold except for the fact that the spin Hall conductivity will not show the jumps at the expected level crossings but, instead, will always oscillate between 0 and 1 for all possible values of μ (equivalently, we can think of this case as the limit $\mu^* \to +\infty$).

4.5.4. Macroscopic transport

Until now, we have only considered local transport quantities in the quantum Hall regime and not yet discussed macroscopic transport coefficients. As emphasized in chapter 1, the conductances in quantum Hall systems can be very different from the local conductivities because the system is very inhomogeneous and does not self-average (it is not "enough" chaotic and presents large spatial fluctuations). Instead, transport is described by percolation mechanisms: electron and spin current densities are spread through an extended complex (percolation) network, as confirmed by scanning tunneling experiments in non-relativistic bulk 2DEGs [42]. From a theoretical perspective, the formulation of a consistent transport theory at high magnetic fields thus requires to combine the concept of percolation (and fractality) for electrons subjected to the Lorentz force and random local electric fields in addition to dissipative processes, such as quantum tunneling through the saddle-points of the disordered potential landscape, or interactions with phonons.

This is an old puzzle [154] which was revisited recently for the high temperature regime in Refs. [155, 156], where a semiclassical transport theory is developed neglecting quantum coherence effects. In this case, the problem of computing the macroscopic current is purely classical [except for the determination of $\bar{\sigma}(\mathbf{r})$ for which quantum mechanics is still necessary, see above]: starting from a local conductivity approach, *i.e.* a local form of Ohm's law $\mathbf{j}(\mathbf{r}) = \bar{\sigma}(\mathbf{r})\boldsymbol{\mathcal{E}}(\mathbf{r})$, where the local conductivity tensor

$$\bar{\sigma}(\mathbf{r}) = \begin{pmatrix} \sigma_0 & -\sigma_{\mathrm{H}}(\mathbf{r}) \\ \sigma_{\mathrm{H}}(\mathbf{r}) & \sigma_0 \end{pmatrix}, \tag{4.54}$$

is assumed, one has to solve the continuity equation $\boldsymbol{\nabla}_{\mathbf{r}} \cdot \mathbf{j}(\mathbf{r}) = 0$ in order to calculate an effective conductivity tensor satisfying $\langle \mathbf{j} \rangle = \bar{\sigma} \langle \boldsymbol{\mathcal{E}} \rangle$ (here we denote by $\langle \cdots \rangle$ the spatial average) in agreement with the discussion in Sec. 1.2. In Eq. (4.54) the spatially homogeneous longitudinal component σ_0 is a phenomenological term describing (classical) dissipative processes such as electron-phonon interaction and the Hall component $\sigma_{\mathrm{H}}(\mathbf{r})$ is given by Eq. (4.45). The quantum Hall regime is characterized by small dissipation $\sigma_0 \to 0$ together with large random spatial fluctuations of the Hall conductivity [typically $\langle \delta\sigma_{\mathrm{H}}^2(\mathbf{r}) \rangle \gg \sigma_0^2$ where $\delta\sigma_{\mathrm{H}}(\mathbf{r}) = \sigma_{\mathrm{H}}(\mathbf{r}) - \langle \sigma_{\mathrm{H}}(\mathbf{r}) \rangle$]. The macroscopic transport coefficients can then be studied by an extrapolation of the nonperturbative series expansion [in powers of $\langle \delta\sigma_{\mathrm{H}}^2(\mathbf{r}) \rangle / \sigma_0^2$] using Padé techniques. In this case, the only assumption is that the Hall conductivity (and the disorder potential) follows a random Gaussian distribution with Gaussian correlator[15].

Now, we come back to the transport problem in the presence of Rashba SO interaction. We have seen that the semiclassical Hall conductivity is unaffected by Rashba SO coupling (4.45), so that the theory established in the absence of SO interaction described in the previous paragraph can be applied immediately to the case under study. As a consequence, we obtain the Hall conductance

$$G_{\mathrm{H}} = \frac{e^2}{h} \sum_{n=0}^{+\infty} \sum_{\lambda} n_{\mathrm{F}} \left[E_{n,\lambda} \right], \tag{4.55}$$

where $E_{n,\lambda}$ is the clean spectrum defined in Eq. (2.21). Moreover, we get that the longitudinal conductance has the same classical percolation exponent $\kappa \approx 0.77$ than in the

[15] This happens at temperatures $k_B T \gg \sqrt{\langle |V(\mathbf{r})|^2 \rangle}$ such that the fluctuations $\delta\sigma_{\mathrm{H}}(\mathbf{r})$ are proportional to the disorder potential fluctuations $\sqrt{\langle |V(\mathbf{r})|^2 \rangle}$.

absence of Rashba SO interaction

$$G_L = C\sigma_0^{1-\kappa} \left| \frac{e^2}{h} \sqrt{\langle |V(\mathbf{r})|^2 \rangle} \sum_{n=0}^{+\infty} \sum_{\lambda} n'_{\mathrm{F}} \left[E_{n,\lambda} \right] \right|^{\kappa}, \tag{4.56}$$

with C a nonuniversal constant and $n'_{\mathrm{F}}(\omega)$ given in Eq. (3.47). This result is consistent with previous studies focused on the critical behavior in the quantum Hall regime [137, 138, 139]. Changes in the universality class [139] can be expected only for the quantum percolation problem (at zero temperature) when SO scattering with short-range correlation severely affects the tunneling at saddle points. In contrast, smooth forms of disorder [137, 138] are not expected to lead to drastic modifications in the percolation transition when considering the presence of SO interaction.

Part II

Bicomplex Representation for the Fractional Quantum Hall Effect

Chapter 5

Fractional Quantum Hall Effect in a Nutshell

In this chapter we succinctly present the main features characterizing the fractional quantum Hall effect, as a warm-up for the final chapter of this thesis. First, we describe the phenomenology of this regime compared to the integer quantum Hall regime which was the framework of the first part of this manuscript. We also briefly, but critically, review the usual theoretical approaches used to deal with the problem of computation of the spectral gaps, response functions and correlators for the most stable and important odd-denominator fractions at high magnetic fields: exact numerical diagonalization, trial wave functions (à la Laughlin, à la Jain), X. G. Wen's edge state theory, a reformulated version of the Chern-Simons field theory and the Hamiltonian theory pioneered by R. Shankar and G. Murthy.

Dans ce chapitre, nous présentons de manière concise les principales caractéristiques qui décrivent l'effet Hall quantique fractionnaire, comme un échauffement pour le chapitre final de cette thèse. D'abord, nous introduisons la phénoménologie de ce régime en comparant avec le régime de l'effet Hall quantique entier qui était le cadre de la première partie de ce manuscrit. Ensuite, nous réexaminons d'un œil critique les approches théoriques standards qui sont typiquement utilisés dans l'étude et le calcul des gaps énergétiques, les fonctions de réponse et les corrélateurs dans les fractions avec dénominateur impair les plus stables à fort champ magnétique. À cet effet, nous exposons brièvement les techniques de diagonalisation exacte (numérique), les fonctions d'onde d'essai (à la Laughlin, à la Jain), la théorie des états de bord de X. G. Wen, une version reformulée de la théorie de champs de Chern-Simons et la théorie Hamiltonienne promue par R. Shankar et G. Murthy.

5.1. Phenomenology of Many-Body Effects

Two years after the discovery of the integer quantum Hall effect by K. von Klitzing, G. Dorda and M. Pepper [12, 13], experimentalists D. C. Tsui, H. L. Stormer and A. C.

Gossard in Bell Laboratories found new plateaus in the Hall resistance measured in high-mobility GaAs-$Al_xGa_{1-x}As$ heterostructures at $T = 1.2$ K, which could be described by the "simple" formula $R_H = R_K/\nu_f$ with $\nu_f \in \mathbb{Q}_{>0}$ a simple rational fraction [23]. In their original measurements, the fractional filling factors $\nu_f = 1/3$ and $\nu_f = 2/3$ were identified while the number of observed fractions which can now be observed has drastically increased, as shown in Fig. 5.1 (even new fractions are being discovered nowadays as progress in the synthesis of cleaner semiconductor heterostructures is made [10]). The phenomenology related to the Hall steps was, nevertheless, similar to the integer counterpart described in Sec. 1.1: electrical resistance measurements show that the transverse resistance in the sample, $R_{xy} = -R_H$, is quantized to relatively large and accurate steps of finite width as a function of the external magnetic field. At the same time, there is an exponential drop in the longitudinal magnetoresistance, R_{xx}, to values near zero across the plateau only increasing again exponentially when the transition to the next (fractional) step is attained. The vanishing longitudinal magnetoresistance hints to dissipationless currents and incompressible states in the bulk 2DEG. The temperature dependence of the magnetoresistance in the plateau region also follows a thermal activation law $R_{xx} \sim R_0(B)\exp[-\Delta/(k_BT)]$ which points out to the presence of gaps Δ in the energy spectrum [51]. Finally, the system is also robust to smooth forms of disorder but not as robust as the integer quantum Hall effect, since relatively clean samples (compared to the latter) are needed to properly observe the fractional quantum Hall plateaus [160, 161].

In spite of the striking similarity of the fractional steps in the Hall resistance to the integer Hall plateaus, the new fractional plateaus were almost immediately related to strong Coulomb interaction between the electrons [23, 161]. Indeed, for very strong magnetic fields ($B \simeq 15$ T in the original experiment [23]) electrons populate the lowest Landau level (LLL) for which the filling factor $0 < \nu_f < 1$. In the single-particle picture, the 2DEG is gapless within the LLL (even in the presence of smooth disorder which partially lifts the macroscopic degeneracy of the Landau levels) and, therefore, correlations between the electrons are necessary to create spectral gaps in the excitation spectrum and incompressible states [41]. The lift of the degeneracy has then to be related to other energy scales rather than the disorder potential[1]. Actually, for the Coulomb interaction, characterized by the energy scale $V_C \simeq e^2/(\epsilon l_B)$ per particle, we have the following hierarchy of energies [20]

$$\hbar\omega_c \gtrsim \frac{e^2}{\epsilon l_B} \gg V(\mathbf{r}), \tag{5.1}$$

where ϵ is the dielectric constant and $V(\mathbf{r})$ represents the one-body (bulk) disorder and / or confinement potential. Since V_C scales as $V_C \sim \sqrt{B}$ and $\hbar\omega_c \sim B$, it is reasonable to assume that, at high magnetic fields, the degeneracy of the energy will be lifted within a Landau level due to a "small" Coulomb interaction compared to the single-particle energy gap.

From a theoretical point of view, the appearance of a quantum liquid phase in the strongly interacting or fractional quantum Hall regime was also surprising. This is because electrons occupying partially filled Landau levels were believed to condense into a solid crystalline phase at low temperatures and low densities [20]. This phase, called Wigner crystal and proposed in 1934 by Wigner [163], appears for small filling factors $\nu_f \lesssim (1/7)$ when the Coulomb energy is minimized through the formation of a highly symmetric trian-

[1] This does not mean that the disorder potential can be disregarded since it is crucial to explain the formation of the Hall plateaus seen in transport experiments by the classical localization mechanism.

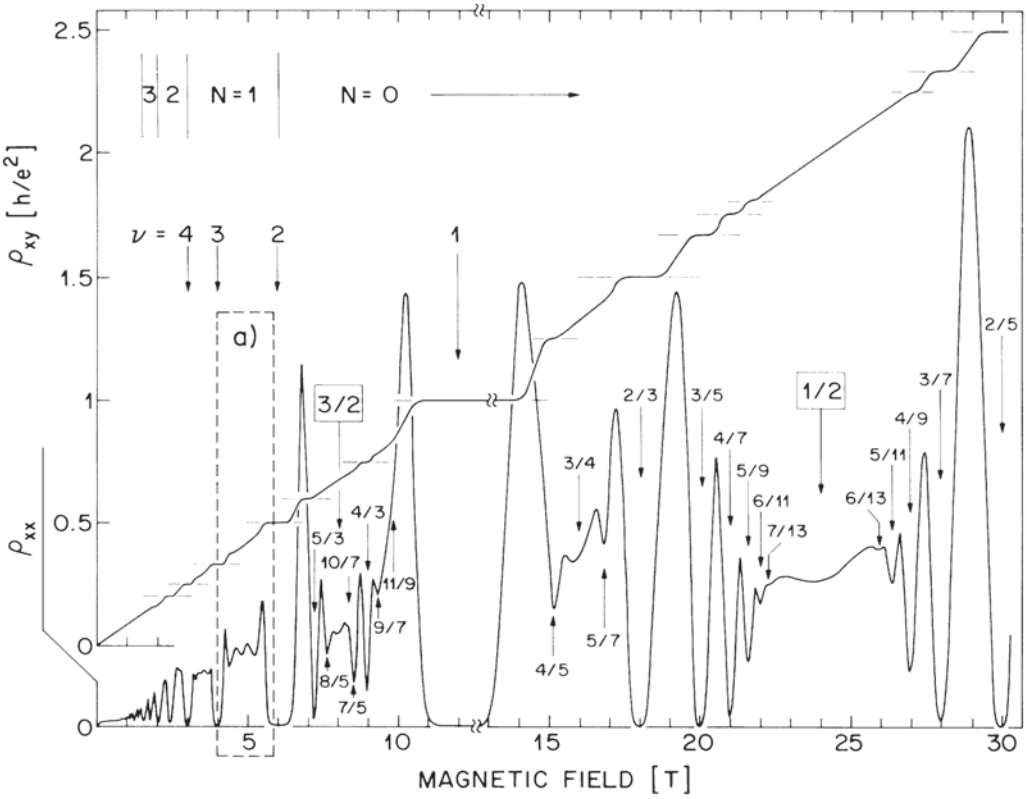

Figure 5.1 – Shape of the transverse resistance R_{xy} and the longitudinal magnetoresistance R_{xx}, both measured in units of the von Klitzing's constant $R_{\rm K} = h/e^2$, as a function of the external magnetic field, B, measured in teslas. Transport measurements are performed in a GaAs/Al_xGa_{1-x}As heterostructure at very low temperatures $T = 85 - 150$ mK (note that this temperature is three orders of magnitude smaller than the temperature appearing in Fig. 1.2). Note the dips in R_{xx} for $\nu_f = p/q$ with q mainly odd, apart from $\nu_f = 1/2$, $\nu_f = 3/2$ and $\nu_f = 5/2$ [labeled as (a) but hardly visible in this data set] which present even denominators. The filling factor $\nu_f = 1/3$ that triggered all this research field is on the right-hand side, out of this plot. Reprinted figure with permission from [162]. Copyright 1987 by the American Physical Society.

gular lattice [160, 165]. As for the fractional quantum Hall effect, electrons lie exclusively in the LLL all with the same seemingly frozen kinetic energy which, *a priori* drops out from the problem. We could then expect the formation of a Wigner crystal at low temperatures. However, this Wigner solid does not account for the observed transport features shown in Fig. 5.1. First, the electronic crystal should be pinned by the defects in the underlying ion lattice and, therefore, the Hall conductivity vanishes. Next, breaking of the translation and rotation invariance through the formation of a crystal gives energy gapless bosonic quasiparticles (according to Goldstone's theorem) that, in this case, correspond to collective acoustic waves. As a consequence, the excitations are described by compressible states, *i.e.*, not separated from the ground state by an energy gap, a situation which confronts the experimental findings for the fractional quantum Hall effect.

5.2. Review of Standard Theoretical Approaches

We come now for good to the theoretical description of the the many-body problem and consider a 2DEG containing N electrons of charge $e = -|e|$ and effective mass m^* located at positions $\mathbf{r}_j = (x_j, y_j)$, with $j \in \{1 \ldots, N\}$, in the presence of a perpendicular magnetic field $\mathbf{B} = B\hat{\mathbf{z}}$. Each electron is in principle influenced by a one-body (arbitrary) potential energy $V_j \equiv V(\mathbf{r}_j)$ while different electrons interact pairwise through the Coulomb long-range potential. As a first approximation, we also consider that the electrons are spinless particles that feel the applied magnetic field exclusively via the Lorentz force[2]. The Hamiltonian of the many-body quantum fluid is written as

$$\hat{\mathcal{H}} = \sum_{j=1}^{N} \hat{\mathcal{H}}_j + \hat{\mathcal{H}}_{ee}, \tag{5.2}$$

where the first term is the sum of N single-particle Hamiltonians, each of them given by Eq. (1.48) evaluated for the N different electronic positions and momenta, and the second term represents the electron-electron interaction described by the two-body operator

$$\hat{\mathcal{H}}_{ee} = \frac{1}{2} \sum_{j \neq k} v(\hat{\mathbf{r}}_j - \hat{\mathbf{r}}_k). \tag{5.3}$$

For the moment, we also assume that the long-range Coulomb interaction is isotropic (and set the scalar dielectric constant to unity), so that the two-body potential has the usual expression

$$v(\mathbf{r}_j - \mathbf{r}_k) = v(|\mathbf{r}_j - \mathbf{r}_k|) = \frac{e^2}{|\mathbf{r}_j - \mathbf{r}_k|}. \tag{5.4}$$

One of the goals of a theory of the fractional quantum Hall effect is to solve the eigenvalue equation for the Hamiltonian (5.2), *i.e.* $\hat{\mathcal{H}}\Psi = E\Psi$, in the Hilbert space of the Landau states, in order to understand the appearance of incompressible states (associated to spectral gaps) in 2DEGs under high magnetic fields. Although very far from more

[2]This is not completely exact since the electrons are always fermions with an intrinsic half-integer spin degree of freedom. As a consequence, the Pauli principle imposes the global many-body wave function to be antisymmetric. More precisely, we are assuming here that the Zeeman gap is much larger than the cyclotron and Coulomb characteristic energies so that the coupling between the spin and the external magnetic field can be safely neglected. This is, of course, a model assumption to fix the basic ideas since in a realistic system we usually have a Zeeman gap much smaller than the characteristic Coulomb energy.

complicated problems related to transport, finding the eigenvalues and eigenfunctions of this Hamiltonian is already extremely hard for several reasons [10, 164]: First, the problem is intrinsically non-perturbative when a projection into a single Landau level has been made. Indeed, we already encountered a similar situation in the one-body integer quantum Hall effect described in chapter 1, since, once the projection to a Landau level has been performed, there is a single relevant energy scale. As a consequence, there are no small parameters and standard perturbative approaches (*i.e.* Hartree-Fock) fail. Second, we need to deal with the problem of lifting the macroscopic degeneracy of the single (clean) Landau level, which forbids the use of stationary perturbation theory already in the absence of Coulomb interactions. Finally, there are no clear symmetries in the problem that could be considered to simplify it, apart from the trivial permutation symmetry of the many-body fermionic wave function or the conservation of total angular momentum in the symmetrical gauge, if the presence of a disorder potential energy landscape is ignored.

Evidently, another major goal of a microscopic theory of the fractional quantum Hall effect is to explain the magic fractions in the Hall resistance. A complete theory must also explain why, within the ensemble of fractions, certain values for ν_f are preferred with respect to others. For example, the most important fractions appear to be described by [10, 224]

$$\nu_f = \frac{\nu_f^*}{2m\nu_f^* + 1}, \tag{5.5}$$

with $\nu_f^* \in \mathbb{N}_{>0}$ and $m \in \mathbb{N}$. These fractions correspond to the so-called Jain's sequence and seem to be more robust than others such as the even denominator fractions mentioned in Fig. 5.1. Therefore, it is necessary to understand the origin (and order) of the hierarchy of fractions, *i.e.* what is the reason why 1/3, 2/5, 3/7 or 4/9 appear to be more stable to disorder and high temperatures than 5/2. The theory has to be able to account for the absence of certain "simple" fractions like 1/2.

Finally, we are also interested in the precise nature of the correlations in the fractional quantum Hall regime. It is known from the work of X. G. Wen in this field that the correlations in the quantum liquid have a *topological nature* and that the fractional quantum Hall states possess an intrinsic topological (long-range) order which cannot be described by the presence / absence of any symmetry [167]. As a consequence, fractional quantum Hall liquids present an internal structure which appears as a result of the correlated motion of the electrons, whose movement is the combination of quantized cyclotron orbits that avoid each other due to the Coulomb interaction. When considering also Fermi-Dirac statistics, this yields topological winding numbers that can be related to the fractional filling factors seen in the experiment. The topological order is a property of the ground state wave function unrelated to the symmetries of the Hamiltonian and the topological defects are the charge excitations or quasiparticles. Therefore, it is clear that a full understanding of the fractional quantum Hall regime goes through the consideration of the robust (topological) properties of the eigenstates of the Hamiltonian (5.2), which takes into account Coulomb interactions. The described approach is close to the ideas advanced in the first part of this thesis to describe the integer quantum Hall effect and I give my contribution to the understanding of this fragment of the puzzle in the strongly correlated regime along the next chapter.

5.2.1. Exact numerical diagonalization

One of the possibilities to solve the Schrödinger equation for the many-body Hamiltonian (5.2) is to consider the exact diagonalization of this quantum operator by numerical techniques. Numerical diagonalization is a computationally hard problem since the accessible Hilbert space grows exponentially with the number of particles (therefore, the problem is clearly intractable in the thermodynamic limit and numerical calculations become extremely difficult for more than $N \gtrsim 15 - 20$ particles [164]). However, within this "low level" method, the only approximation to be made to the original model is to put the electrons on a surface of finite size instead of an infinite plane. To study bulk effects, a locally flat surface without boundary, such as the sphere [169, 170] or the torus (*i.e.* a finite rectangular manifold with periodic boundary conditions [171]) is typically chosen. We assume then that we are able to distinguish the finite size effects (from the interaction effects) and extrapolate the behavior to the thermodynamic limit where the number of particles is macroscopically large[3] . Edge effects, on the other hand, can be incorporated by using the disk geometry which was used in Laughlin's original work and is also the preferred geometry for interacting quantum dots [172]. Note that exact diagonalization techniques present the advantage of being able to take into account, in principle, Landau level mixing while this is a challenge for the rest of the theoretical approaches that are discussed afterwards. Nevertheless, only the Coulomb interaction are considered and including disorder is out of question[4].

The approach to numerical diagonalization can be described as follows [172]: first, we fix the number of particles N and the number of flux quanta piercing the sample (the magnetic field) M. This also fixes the number of allowed states per Landau level and therefore the single-particle filling factor, which is written as $\nu_f = N/M$, see Sec. 1.3 [we note here that for the sphere one also has to take into account the "shift problem", see Eq. (5.12)]. The M possible single-particle wave functions in the LLL are characterized by the chosen boundary conditions (torus / sphere / disk). This indirectly means that the system is divided into "elementary cells" by the choice of a basis. Then, we simply compute the N-body states formed by the Slater determinant of the single-particle orbitals, the matrix elements of the Hamiltonian and try to diagonalize a huge matrix in order to obtain the eigenenergies and its associated eigenvectors. The size of the matrix can be reduced either using symmetries or, in the case of a simulation in which periodic boundary conditions are chosen, applying density matrix renormalization group techniques[5].

To finish this section, we may note that this seemingly naïve technique can be used to extract a considerable amount of useful information from fractional quantum Hall systems; notably the energy gaps [174], the overlaps with trial wave functions to be described in the next section [52] or, more recently the topological properties of the state manifold through the computation of the entanglement entropy and spectra [175, 176]. The latter

[3]Extrapolation to the thermodynamic limit can even fail [168] so that sometimes this limit is also inaccessible in this way.

[4]Exact diagonalization is mostly done in the lowest Landau level approximation (kinetic energy being quenched) with other Landau levels being neglected to relatively avoid an explosion of the size of the Hilbert space.

[5]This is a variational iterative technique useful to consider the low-energy properties of strongly correlated quantum systems as it produces an efficient truncation of the size of the allowed Hilbert space. Originally devised for one-dimensional systems, it was used for 2DEGs in the fractional quantum Hall regime when it was realized that certain boundary conditions effectively reduce the dimension of the system by one [173].

quantity measures entanglement between different parts of a system and it is computed partitioning the Hilbert space into two sectors, rewriting the many-body states using the Schmidt decomposition and tracing out one of the parts. The resulting "Hamiltonian" with associated "energy levels" contain information about the topological properties of the many-body wave function (in particular, bulk gapped systems with topological order seem to contain nontrivial gapless edge modes). Also, the energy level counting appear to be "universal" and reveals the model state that can be associated to a selected filling factor ν_f. Finally, fractional charge (and fractional statistics) can also be inferred from the numerical study of finite size effects [177].

5.2.2. Trial wave functions

Laughlin's wave function

In 1983, R. B. Laughlin suggested a clever variational many-body wave function [160, 166] capable of explaining the $\nu_f = 1/3$ and $\nu_f = 2/3$ steps in the Hall resistance found the previous year[6]. This wave function, as a difference to the naïvely expected Wigner crystal, did not describe a solid but a strongly correlated quantum liquid invariant under translations and rotations. The proposed ground state and excited state wave functions were also found to be consistent with the family of odd-denominator fractional filling factors

$$\nu_f = \frac{1}{2m+1}, \tag{5.6}$$

where we remind that $m \in \mathbb{N}$ [these fractional fillings correspond to the case $\nu_f^* = 1$ in Jain's sequence (5.5), the case $m = 0$ being special since it corresponds to a fully occupied single-particle Landau level]. The states form a sequence that crystalizes into a Wigner solid at specific temperatures for $m \gg 1$, as shown experimentally in Ref. [165] (note that, conversely, we can see the fractional quantum Hall state as a melted Wigner crystal when quantum fluctuations are strong). Therefore, Laughlin's wave function works as a remarkable lucky *ansatz* which describes the physics of a certain class of fractional quantum Hall states (5.6).

We sketch here the main steps that led to its proposal. First, let us consider the the single-particle clean Hamiltonian given in Eq. (1.11) and express it in the natural representation for the symmetrical gauge

$$\hat{\mathcal{H}}_0 = \frac{\hbar\omega_c}{2}\Big[- l_B^2 \Delta_{\mathbf{r}} + \frac{\mathbf{r}^2}{4l_B^2} + i(y\partial_x - x\partial_y)\Big]. \tag{5.7}$$

Here, we have introduced the natural units of energy (the cyclotron energy, $\hbar\omega_c$) and length (the magnetic length, l_B) of our problem and noted by $\Delta_{\mathbf{r}} \equiv \partial_x^2 + \partial_y^2$ the Laplacian operator taken with respect to the electronic position. Diagonalization in this gauge shows that the single-particle wave function describing an electron in the LLL can be written as [178]

$$\Psi(\zeta) = f(\zeta) \exp\left(-\frac{1}{2}|\zeta|^2\right), \tag{5.8}$$

[6] It is still a highly debated issue whether $\nu_f = 2/3$ is a Laughlin state in a realistic system in which the Zeeman gap is smaller than the Coulomb gap.

where $\zeta = (x - iy)/(\sqrt{2}l_B)$ are reduced variables[7] and $f(\zeta)$ is an analytic function of the electron variables (this function can be written as a Taylor series in ζ and does not contain any ζ^*). A convenient choice for a basis is therefore $f(\zeta) = \zeta^q/(\sqrt{\pi q!})$ where q labels the allowed states in a disk of radius R in the symmetrical gauge (for this choice of analytic function, the wave function $\Psi_q(\zeta)$ is an eigenstate of the total angular momentum operator and q has as upper bound the total angular momentum M in the thermodynamic limit). Now, we can guess that the many-body wave function describing the ground state of the N-electron system in the LLL and the presence of Coulomb interactions (5.3) is written as [160, 166]

$$\Psi(\{\zeta_j\}) = P(\{\zeta_j\}) \exp\left(-\frac{1}{2}\sum_{j=1}^{N}|\zeta_j|^2\right) \tag{5.9}$$

where $P(\{\zeta_j\})$ is an antisymmetric polynomial in the electron variables (due to the Fermi-Dirac statistics). We want to obtain these polynomials with the constraint of having M as maximal degree of any of the electron variables[8]. In addition, in the absence of disorder potential, we have to describe a quantum liquid without broken continuous symmetries. As a consequence, we limit ourselves to polynomials $P(\{\zeta_j\})$ which depend on the electronic variables through the combination $\Pi_{j<k} f(\zeta_j - \zeta_k)$ with $f(\zeta)$ odd (these functions are called Jastrow factors and ensure that, for each given pair of electrons, the wave function only depends on their mutual distance, with the electrons avoiding each other since the Jastrow factor decreases fast to zero whenever $\zeta_j \to \zeta_k$). Invariance under rotations implies conservation of the total angular momentum M and that $\Pi_{j<k} f(\zeta_j - \zeta_k)$ is a homogeneous polynomial of degree M (this fact is also compatible with the discussion of the maximal power of any variable, see above). We have therefore obtained the non-normalized wave function

$$\Psi_m(\{\zeta_j\}) = \prod_{j<k}(\zeta_j - \zeta_k)^{2m+1} \exp\left(-\frac{1}{2}\sum_{j=1}^{N}|\zeta_j|^2\right), \tag{5.11}$$

and we need now to determine the value of m that minimizes the energy of the system, m being the only variational parameter left.

At this point, several comments are in order to explain the achievements of $\Psi_m(\{\zeta_j\})$. First, we note that in Eq. (5.11) the dependence on the center-of-mass is absent. Indeed, if this dependence was present, the center-of-mass would carry angular momentum and the state would describe an electron liquid with a continuous broken spatial symmetry. The fact that the wave function depends on the relative distance between arbitrary particles also implies that Laughlin's states describe a homogeneous quantum liquid. Second, it is

[7] Note that we chose to define in this chapter the dimensionless electronic coordinates ζ with the opposite sign in their imaginary part compared to the variables z (or Z) appearing in Eq. (1.43) and to the dimensionless electronic variable used in Appendix A. The main reason is that, with this definition, the functions $f(\zeta)$ appearing in the single-particle wave function for an electron in the LLL are analytic and not anti-analytic [41]. This choice can also be understood as a change in the direction of the external magnetic field which points now towards $-\hat{\mathbf{z}}$ instead of $\hat{\mathbf{z}}$.

[8] This is due to the fact that we can formally expand Eq. (5.9) as

$$\Psi(\{\zeta_j\}) = \sum_{\{k_r\}} \mathcal{C}_{k_1,\ldots,k_N} \zeta_1^{k_1}\zeta_2^{k_2}\ldots\zeta_N^{k_N} \exp\left(-\frac{1}{2}\sum_{j=1}^{N}|\zeta_j|^2\right), \tag{5.10}$$

with complex amplitudes $\mathcal{C}_{k_1,\ldots,k_r}$ and interpret the polynomial as a polynomial in a single variable ζ_j (the others being constants) so that $k_j \leq M$.

astonishing that the form of Laughlin's wave function does not depend on the explicit form of the Coulomb interaction but only on the symmetries. We would also like to point out that $\Psi_m(\{\zeta_j\})$ is not exactly a variational wave function since the values of m are fixed by the filling factor ν_f. To understand this, recall that for a given electron ζ_k the maximal value of the power was fixed by the total angular momentum, M. Also, looking at Eq. (5.11) it is clear that for ζ_k we will have $N-1$ factors of the form $(\zeta_k-\zeta_j)^{2m+1}$ for some j. Therefore, the highest power of ζ^k is also $(2m+1)(N-1)$ and we obtain the relation

$$(2m+1)N-\delta=M, \tag{5.12}$$

where δ is a shift of order unity negligible in the thermodynamic limit $N,M\to+\infty$. As a result we get the family of odd-denominator filling factors (5.6). Laughlin's original argument [20, 160] made use of the classical one-component 2D plasma mapping [the probability density $|\Psi_m(\{\zeta_j\})|^2$ was mapped to the partition function of this system in the presence of a neutralizing background density; neutrality imposing $\nu_f=1/(2m+1)$] to obtain the same result, with the advantage that Monte-Carlo techniques can be used in this case to numerically evaluate the energy or density-density correlation functions to high precision [172]. Finally, we should note that Laughlin's wave function is not an eigenstate of the long-range Coulomb interaction [51, 164] (although it can be shown that it is an eigenstate of the hard-core [20] and the harmonic interactions [178]). It is nevertheless noteworthy to mention that exact diagonalization shows an extremely good overlap of this wave function with the numerically obtained ground states for a wide class of repulsive potentials, including the Coulomb potential [164, 170]. It is in this sense that we believe that $\Psi_m(\{\zeta_j\})$ is probably close to the exact ground state in the thermodynamic limit in a [fractional quantum Hall] regime described by the family of filling factors (5.6) although any kind of analytical conclusive proof is still lacking.

As a closing point of this section, let us briefly talk about the excited states of the Laughlin's fractional quantum liquid [166], focusing only on the so-called elementary excitations (we refer the interested reader to the literature [105] for the collective charge density wave modes at fixed charge). A remarkable property of the elementary excitations, which are obtained from a fluctuation of the system charge, is that they present fractional charge. As an example, consider the positive excitation created by adding a zero to the ground state wave function

$$\Psi^+_{\zeta_0}(\{\zeta_j\})=\prod_{j=1}^{N}(\zeta_j-\zeta_0)\Psi_m(\{\zeta_j\}). \tag{5.13}$$

This procedure injects adiabatically a quantum flux into the system and slightly perturbs the filling factor[9]. Indeed, expanding Laughlin's wave function as in Eq. (5.10), Eq. (5.13) yields for $\zeta_0=0$,

$$\Psi^+_{\zeta_0}(\{\zeta_j\})=\sum_{\{k_r\}}\mathcal{C}_{k_1,\ldots,k_r}\zeta_1^{k_1+1}\ldots\zeta_N^{k_N+1}\exp\left(-\frac{1}{2}\sum_{j=1}^{N}|\zeta_j|^2\right). \tag{5.14}$$

This means that each electron has changed from the state of angular momentum k to the state $k+1$ increasing the size of the disk and that a positively charged hole (a deficit of

[9]Note that ν_f may also be changed by acting on the particle density via the chemical potential.

electrons) has appeared at the position ζ_0. To determine the precise charge of the hole, we recall that the quantum liquid is incompressible (there is a spectral gap between the ground and excited states) so that the addition of a quantum flux necessarily has to be compensated by the creation of a quasiparticle due to the relation $(2m+1)\delta N = \delta M$. Therefore, this procedure generates an excitation with fractional charge $e^* = |e|/(2m+1) > 0$.

The negative excitations are created by removing a quantum flux from the system. This is done through a prefactor of the form $\prod_{j=1}^{N}(\zeta_j^* - \zeta_0^*)$ but since the resulting wave function is no longer analytical it is necessary to formally project again onto the LLL

$$\Psi^-_{\zeta_0}(\{\zeta_j\}) = \hat{\mathcal{P}}_{\mathrm{LLL}} \prod_{j=1}^{N}(\zeta_j^* - \zeta_0^*)\Psi_m(\{\zeta_j\}). \tag{5.15}$$

A popular way of dealing with this projection operator is to replace the non-analytic variables ζ_j^* by derivatives $\sqrt{2}l_B\partial/\partial_{\zeta_j}$ only in the polynomial part of the wave function [178]. The resulting polynomial in the wave function is then analytic and the derivatives generate the desired terms in ζ_j^* when applied to the ubiquitous Gaussian factor. Again, a similar analysis as for the positively charged excitation shows that the wave function (5.15) represents a state of fractional charge $e^* = e/(2m+1) < 0$.

Finally, one of the most remarkable properties of the many-body fractionalization of the charge in 2DEGs is fractional statistics of the elementary excitations [179, 180]. This basically means that in 2D, topology implies that pair permutation between two particles generates a non-trivial phase factor. Since the phase factor can take any value between 0 and 2π, the particles are called *anyons*. This phenomenon, which has a universal character and appears in any many-body wave function, is exclusively related to dimensionality and deeply discussed in Refs. [181, 182].

Extensions to Laughlin's wave function

In spite of the enormous success of Laughlin's wave function, new plateaus in the Hall resistance associated to fractional filling factors which did not belong to the Laughlin's family (5.6) were discovered in subsequent experiments (*e.g.* $\nu_f = 2/5, 3/7, 4/9\ldots$). One of the first approaches to explain these new states was proposed by F. M. D. Haldane [169] and B. Halperin [179] and amounts to considering that the new plateaus are generated from the stable Laughlin ones by the condensation of a "small quantity" of excitations from a stable ground state. This yields a hierarchical scheme in which descendant states condense thanks to the residual Coulomb interaction between the excitations and the new fractional filling factors are computed either by a continued fraction expansion or by a set of iterative equations. As an example, in this scheme the states $\nu_f = 2/5$ and $\nu_f = 2/7$ appear by condensation of the excitations of the $1/3$ incompressible parent state. However, it was soon clear that this procedure, although systematic, is not satisfactory as it predicted sequences of fractions whose stability was not compatible with the experimental data [10, 51]. Indeed, a considerable amount of excitations (and steps down in the hierarchy) are necessary to generate some stable fractions, such as $\nu_f = 6/13$ which belong to Jain's sequence and are found experimentally to be well defined.

An alternative to this proposal is the phenomenological composite fermion approach pioneered by J. Jain [183] within the framework of trial wave functions. Jain rewrites Eq.

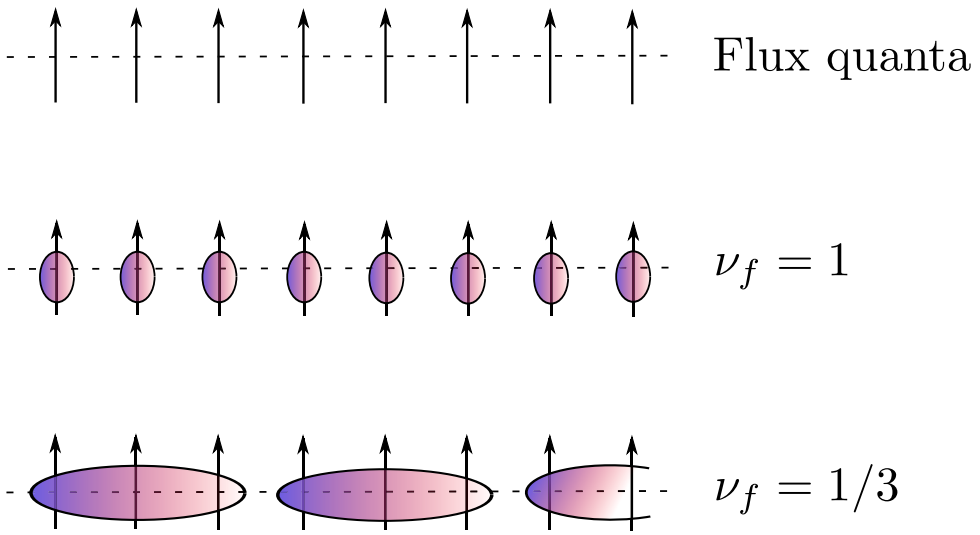

Figure 5.2 – Schematic illustration of the phenomenological flux attachment in the formation of composite fermions. In the first line, we represent by arrows the quanta of magnetic flux piercing the sample (here one-dimensional for simplicity). When the lowest Landau level is completely filled, $\nu_f = 1$, one quantum of flux is assigned to each of the electrons as by definition $N = M$. This case is depicted in the second line. In the third line, we sketch the situation at $\nu_f = 1/3$, the most robust of the Laughlin's states. According to the composite fermion interpretation of the fractional quantum Hall effect, the electron has picked up and neutralized $\theta = 2m = 2$ [thus $m = 1$, see Eq. (5.6)] flux quanta and can be regarded as being a "fat electron". Effectively, this renormalizes the external magnetic field which gets reduced to $B^* = B - 2n\Phi_0$ and gives a new integer quantum Hall effect of weakly interacting composite fermions (in this case, at filling factor $\nu_f^* = 1$), as reported by Eq. (5.5). Note that the functional form of the two-body interaction has not played any role during this mechanism of flux attachment.

(5.11) as

$$\Psi_m(\{\zeta_j\}) = \prod_{j<k}(\zeta_j - \zeta_k)^{2m}\Psi_1(\{\zeta_j\}), \tag{5.16}$$

where

$$\Psi_1(\{\zeta_j\}) = \prod_{j<k}(\zeta_j - \zeta_k)\exp\left(-\frac{1}{2}\sum_{j=1}^{N}|\zeta_j|^2\right), \tag{5.17}$$

is the wave function of N electrons completely filling the LLL (this is nothing but a Slater product state up to a global normalization factor $1/\sqrt{N!}$ written in the compact Vandermonde determinant form). Since Laughlin's wave function and Eq. (5.17) are both antisymmetric, we are tempted to interpret these $2m$ zeroes as flux quanta attached to each of the electrons. The dressed electron composed by a bare electron and an even number of flux quanta is called *composite fermion* (see Fig. 5.2). Note that as the number of flux quanta attached to each particle is even, the bare electrons and the composite fermions both present the same Fermi-Dirac statistics.

An alternative interpretation goes as follows: consider Eq. (5.11) describing N electrons homogeneously distributed in a disk and let us focus on the coordinate of a particle ζ^k, the

others being fixed. We know from previous arguments that the highest power associated to this electronic coordinate is N/ν_f for $N \to +\infty$. The function $f(\zeta_k) = \Psi_m(\zeta_k; \{\zeta_j\}_{j\neq k})$ is therefore a polynomial of the same degree (apart from the ubiquitous exponential factor) and we conclude that any particle performing a loop around the disk feels N/ν_f flux quanta bound by the wave function ($1/\nu_f$ flux quanta or zeroes per electron). However, of the $1/\nu_f$ zeroes per particle, only one is required to satisfy the Pauli exclusion principle and therefore we have $1/\nu_f - 1 = 2m$ zeroes left which present unobservable Aharonov-Bohm phases of 2π. The $2m$ zeroes are understood as vortices attached to the electron by some unknown mechanism [10] which somehow keeps electrons away from each other in a very effective way (in this context, it has been said that this wave function has *no wasted zeroes* [215]) The vortices attached to the electron explains the absence of gapless excitations since the new composite object belongs to the filled lowest Landau level of composite fermions (and promoting a composite fermion to the first excited composite fermion Landau level has an energy cost of $\hbar\omega_c^*$).

The generalization proposed by Jain is to replace $\Psi_1(\{\zeta_j\})$ by the wave function which describes $\nu_f^* \in \mathbb{N}_{>0}$ filled composite fermion Landau levels as

$$\Psi_{\nu_f}(\{\zeta_j\}) = \hat{\mathcal{P}}_{\mathrm{LLL}} \prod_{j<k} (\zeta_j - \zeta_k)^{2m} \Psi_{\nu_f^*}(\{\zeta_j\}). \tag{5.18}$$

Let us analyze the effect of this substitution. It is clear, from the previous discussion of the zeroes in the Laughlin's wave function that the number of flux quanta bound by this new wave function is renormalized as $M^* = M - 2mN$. This amounts to a screening of the magnetic field by $B^* = B - 2mn\Phi_0$ and the filling factor $\nu_f^{*\,-1} = \nu_f^{-1} - 2m$. As a consequence, Eq. (5.18) is *a priori* a good guess for the family of fractional fillings given in Eq. (5.5). On the basis of Eq. (5.18), we now introduce the composite fermion picture of the fractional quantum Hall effect: at low energies, the fractional quantum Hall effect where electrons interact strongly is mapped to the integer quantum Hall effect of weakly interacting composite fermions. The ground state of the incompressible quantum liquid is described by Jain's generalization of Laughlin's wave function and gapped elementary excitations consist of a composite fermion *living* in Landau level ν_f^* being promoted to the level $\nu_f^* + 1$ with the characteristic energy of the excitations given, in principle, by a renormalized cyclotron frequency $\omega_c^* = |e|B^*/(m^*c)$. However, we note now that this energy scale does not have the same order of magnitude than the energy gap between the ground and excited states obtained computing the quantum average of Eq. (5.3) within the electronic states (5.18) (see Refs. [10, 215]). It also presents an incorrect scaling with the magnetic field since the energy gap grows linearly in B^* and not as $\sqrt{B^*}$. This is an unsolved problem related to the definition of the renormalized composite fermion mass $m^*(\nu_f)$ that appears to depend on the observable being calculated [10]. The composite fermion phenomenological wave function-based picture also seems to explain the existence of a gapless Fermi liquid of composite fermions when $\nu_f^* \to +\infty$. Indeed, as shown in Fig. 5.3 exponentially-damped Shubnikov-de Haas oscillations in the longitudinal magnetoresistance have been experimentally reported around the effective magnetic field $B^* = 0$, at which it is speculated that composite fermions behave as a weakly interacting Fermi liquid. The oscillations at a given temperature are well-fitted using the Lifshitz-Kosevich formula using as parameters the effective magnetic field B^*, the composite fermion filling factor ν_f^*, a composite fermion cyclotron mass m_{cyc}^* and the quasiparticle lifetime τ^* (assumed to be temperature independent). This partially confirms the theoretical studies

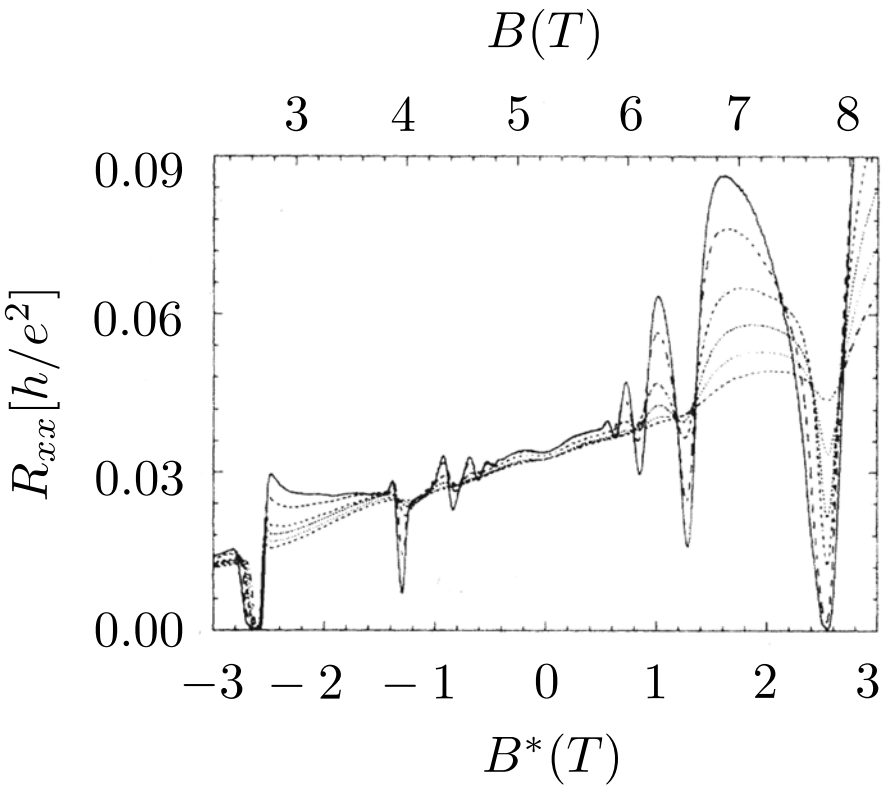

Figure 5.3 – Experimental values for the longitudinal magnetoresistance R_{xx} (expressed in units of the von Klitzing's constant) as a function of the external magnetic field B (bottom axis) and the reduced effective magnetic field B^* (top axis). Both magnetic fields are measured in teslas (T). Each of the curves (solid, dashed, dotted, *etc.*) corresponds to different temperatures of 320, 409, 570, 740, 870, and 1100 mK. At $B^* = 0$ the resistance is temperature independent pointing out to the existence of a metallic Fermi liquid state. Reprinted figure with permission from [186]. Copyright 1994 by the American Physical Society.

[196] predicting a metallic Fermi liquid for $\nu_f^* \to +\infty$.

Although it is not hard to understand why this view of the fractional quantum Hall effect has become quite popular in the community - it gives a simple one-body image of a complicated many-body problem and provides a specific trial wave function to be compared with exact diagonalization studies - we are left with the impression that Eq. (5.18) provides the only source for the nevertheless interesting composite fermion picture. Moreover, in spite of the great number of successes, such as the explanation of the compressibility at $\nu_f = 1/2$ or the very good overlap ($\geq 99\%$ for certain filling factors) between Jain's wave function and the ground state obtained by exact diagonalization [10, 184], some other points still remain unclear. A very important one is the nature of the projector $\hat{\mathcal{P}}_{\mathrm{LLL}}$ in Eq. (5.18): this construction is, from the physical point of view rather bizarre, since it is not clear why for the LLL higher Landau levels of some dressed electrons ν_f^* need to be involved in the wave function and, after that, project back onto the LLL. It is also not at all evident how the electron binds the flux quanta to form the composite fermion, since the flux quanta are not independent physical entities pre-existing in the 2D plane. Another point concerns the choice of the trial wave function to be compared with the exact ground

states for small N: other families of trial wave functions similarly show a very good overlap [164] as it does Eq. (5.18), so that we may wonder what is the relation between them or what is the reason behind the great success of seemingly different variational states[10].

5.2.3. Edge state theory

Before considering in depth the effective theories which are used to put Jain's ideas on more firm ground, we make a detour to briefly discuss the edge state theory of the fractional quantum Hall effect. Together with the exact numerical diagonalization, the edge state theory of fractional quantum Hall liquids stays a bit aside from the mainstream trial wave function or composite fermion approaches. This one-dimensional microscopic phenomenological framework, to be sketched here in its hydrodynamical form, was pioneered in the nineties by X. G. Wen [167, 187, 188]. As a powerful generalization of M. Büttiker theoretical methods 1.4.1, the theory is essentially a single-mode approach to the edge excitations for Laughlin's states, in which we remind that $\nu_f = 1/(2m+1)$. It can be generalized afterwards to a hierarchical scheme to deal with more complex fractional filling factors (as in Haldane and Halperin's construction described above [187]), where multiple electron channels are considered, or to be related to trial wave functions and low energy effective field theories in the bulk (*e.g.* Chern-Simons theory considered in Sec. 5.2.4). The latter connection is topological since the structure of the edge states is determined by the topological order in the bulk thanks to the bulk-boundary correspondence [50]. Another interesting aspect of this theory is that it allows us to consider simultaneously the effect of disorder and long-range interactions in the transport properties of the electron liquid but at the price of reducing the dimensionality of the system (one cannot consider, for instance, the complex phenomena related to the percolation network).

Let us first discuss a classical theory in which we consider a finite droplet of volume Ω in the fractional quantum Hall regime, the details of its geometry being of no relevance in what follows. The droplet is confined at the boundary $\partial\Omega$ by some confining potential whose electric field generates a persistent current density $\mathbf{j} = \sigma_{\mathrm{H}}\hat{\mathbf{z}} \times \boldsymbol{\mathcal{E}}$ where σ_{H} is the global (spatially averaged) Hall conductivity. We further assume that the bulk of this system is "rigid" or incompressible so that low energy bulk excitations below the bulk energy gap can not exist (this is true whenever the chemical potential lies in a plateau so that we also have $\sigma_{\mathrm{H}} = R_{\mathrm{H}}^{-1} = R_{\mathrm{K}}^{-1}\nu_f$). As a consequence, the only possible low energy excitations come from deformations or distortions of the boundaries which are considered one-dimensional strongly interacting quantum fluids where backscattering is suppressed due to chirality. The deformations of the droplet profile are characterized by a density profile $n_s(x)$ where x parametrizes $\partial\Omega$. Considering now the continuity equation, we can describe the propagation of the distortion wave at the edge by the "wave equation"

$$\left[\frac{\partial}{\partial t} + v_d \frac{\partial}{\partial x}\right] n_s(x) = 0 \tag{5.19}$$

where v_d is the modulus of the drift velocity (1.38) assumed spatially independent at this point (that is, we neglect disorder). Thus, the continuity equation is interpreted as a chiral "wave equation" for the surface sound waves. Note that the density profile is proportional

[10] More open questions not mentioned here are the influence of temperature, which destroys the composite fermion or the role of disorder [185].

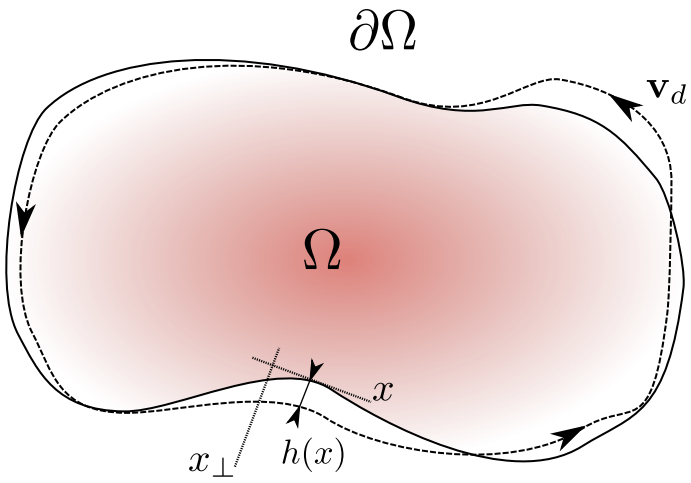

Figure 5.4 – Creation of a surface wave excitation in a fractional quantum Hall droplet. The bulk Ω is assumed to be incompressible, with finite energy gaps, while the edges at the boundary $\partial\Omega$ accept gapless modes that propagate along the parallel direction x (orthogonal to $x_\perp$ in a local coordinate system). The average velocity of the surface (sound) wave is the electronic drift velocity $\mathbf{v}_d$ given in Eq. (1.38). The height profile $h(x)$ caused by the surface wave is related to a density profile $n_s(x)$ of the droplet, since the bulk has constant particle density.

to the deformation profile[11] $h(x)$ with $n_s(x) = n_s h(x)$ and $n_s = \nu_f/(2\pi l_B^2)$. The previous situation is depicted in Fig. 5.4. We now compute the classical energy (the Hamiltonian function) which reads

$$\mathcal{H} = \int_0^L dx \frac{1}{2}|e| n_s(x) h(x) \mathcal{E} = \frac{\pi \hbar v_d}{\nu_f} \int_0^L dx n_s^2(x), \tag{5.21}$$

where L is the length of the edge. This result is simply the energy of moving a charge of density $n_e(x) = e n_s(x)$ a distance $h(x)$ in an electric field $\boldsymbol{\mathcal{E}}$. Going to the momentum space by using the Fourier transform

$$n_s(x) = \frac{1}{\sqrt{L}} \sum_q n_s(q) \mathrm{e}^{-iqx}, \tag{5.22}$$

with $q = 2\pi p/L$ and $p \in \mathbb{Z}$, together with the identity

$$\delta_{q,0} = \frac{1}{L} \int_0^L dx \mathrm{e}^{-iqx}, \tag{5.23}$$

we see that Eq. (5.19) becomes a first order ordinary differential equation, $(\partial_t - iqv_s) n_s(q) = 0$, and that the energy is rewritten as

$$\mathcal{H} = \frac{2\pi}{\nu_f} \hbar v_d \sum_{q=0}^{+\infty} n_s(q) n_s(-q), \tag{5.24}$$

[11] Indeed, we have

$$n_s(x)dx = \frac{\nu_f}{2\pi l_B^2} \int_0^{h(x)} dx_\perp dx = \frac{\nu_f}{2\pi l_B^2} h(x) dx. \tag{5.20}$$

with $n_s(-q) = n_s^*(q)$. From this expression, it is straightforward to verify, applying Hamilton equations, that it is possible to identify the reciprocal density $n_s(q)$ with a generalized coordinate $Q_q \equiv n_s(q)$, for $q > 0$, and obtain a conjugate (canonical) momentum $P_q = 2\pi\hbar n_s(-q)/(iq\nu_f)$ for $q < 0$. Note that both canonical coordinates are generated from a unique displacement field $h(x)$, a fact that is related to the chiral nature of the edge states. Using Dirac's canonical quantization rule as in Sec. 1.3, we have $[\hat{Q}_q, \hat{P}_{q'}] = i\hbar\delta_{q,q'}\mathbb{1}$, which implies

$$[\hat{n}_s(q), \hat{n}_s(q')] = \frac{\nu_f q}{2\pi}\delta_{q+q',0}\mathbb{1}, \tag{5.25}$$

$$[\hat{\mathcal{H}}, \hat{n}_s(q)] = \hbar q v_d \hat{n}_s(q), \tag{5.26}$$

where now $q, q' > 0$. These commutator relations are similar to those appearing in the Tomonga-Luttinger one-dimensional quantum liquids where the commutator between density operators satisfies the U(1) Kac-Moody algebra $[\hat{n}_s(q), \hat{n}_s(q')] \propto q\delta_{q,-q'}$ [189, 190]. The quantized Hamiltonian (5.24) describes a collection of independent quantum harmonic oscillators (a free plasmon bath) with charge neutral excitations and is equivalent to the Hamiltonian obtained after bosonization of a liquid of chiral interacting fermions. In other words, the edge is a chiral Tomonaga-Luttinger liquid. Charged excitations can then be studied using standard bosonization techniques. For example, the field

$$\hat{\Psi}(x) = \exp\left[i2\pi\hbar\nu_f^{-1}\int^x dx'\hat{n}_s(x')\right] = \exp\left[i\nu_f^{-1}\hat{\phi}(x)\right], \tag{5.27}$$

where we used the relation between the edge density and the field $\phi(x)$, $\partial_x\phi(x) = 2\pi\hbar n_s(x)$, creates a Laughlin excitation in the edge at a given position in space-time (x, t). Using the Kac-Moody algebra (5.25), which for the field operator $\hat{\phi}(x)$ yields $[\hat{\phi}(x), \hat{\phi}(x')] = i\pi\,\mathrm{sgn}(x - x')/\nu_f$, we can show that this excitation possesses fractional statistics

$$\hat{\Psi}(x)\hat{\Psi}(x') = \mathrm{e}^{i\pi\nu_f\,\mathrm{sgn}(x-x')}\hat{\Psi}(x')\hat{\Psi}(x), \tag{5.28}$$

and fractional charge $e^* = \nu_f e$. The single-particle propagator of the excitations can be computed from the fermionic fields [188]

$$G^{R,A}(x; 0; \tau) = \mp i\Theta(\pm\tau)\langle[\hat{\Psi}(x), \hat{\Psi}^\dagger(0)]_+\rangle \sim \frac{1}{(x - v_d\tau)^{\nu_f}}, \tag{5.29}$$

with τ being the relative time difference. Note that for $m = 0$ ($\nu_f = 1$) the Green's function (5.29) corresponds to the propagator of a chiral Fermi liquid. The power law dependence of the Green's function (and therefore, the density of states), together with the presence of a universal Luttinger parameter ν_f^{-1}, are hallmarks of a Tomonaga-Luttinger liquid-like behavior that should be observed in experiments (*e.g.* by performing edge tunneling conductance measurements). Experimental results seem to confirm the presence of a chiral Tomonaga-Luttinger liquid at the edges (for instance, in shot-noise measurements) although non-universal features have also been found suggesting that this picture may need a careful reconsideration [190].

5.2.4. Composite fermion flavors

We come back to the main line of discussion, where we consider now two of the approaches which go beyond the inspired *ansatz* technique. In particular we discuss the

Chern-Simons field theory, first put forward in the fermion language by A. López and E. Fradkin [191] on the basis of a mapping to an interacting bosonic problem with a statistical gauge field [192, 193], and the Hamiltonian formulation proposed by G. Murthy and R. Shankar [198, 215]. Both theories present the important advantage, with respect to the trial wave function approaches, of allowing the analytic calculation of relevant observables such as the particle or the current density.

Chern-Simons field theory

The objective of this section is to introduce the basic Chern-Simons transformation without entering too much into technical details of this topological field theory. We shall take a quite pedestrian look at the field theory, originally developed in the language of second-quantized path integrals [191] and which can be reformulated into a much simple form [194].

The basic idea of the Chern-Simons theory is to embed the flux attachment to the electrons directly into the Hamiltonian instead of working with the wave function as in Jain's version. Then, a very complicated problem for interacting electrons is transformed into another (very complicated) problem for charge-flux composites that interact with each other through a statistical gauge field, $\mathbf{A}_{\rm CS}(\mathbf{r})$, and the Coulomb two-body potential. Finally, we make a mean-field (Hartree) approximation to hopefully obtain a simple one-body problem, where we have gauged away the huge degeneracy of the initial many-body problem. Corrections due to interactions or quantum fluctuations of the gauge field are then computed using standard perturbation techniques (random phase approximation, Feynman diagrams ...).

To this purpose, we perform the following one-parameter unitary gauge transformation on the electronic wave function $\Psi_\theta(\{\zeta_j\}) = U_\theta \Psi_{\rm CS}(\{\zeta_j\})$ with

$$U_\theta = \prod_{j<k} \frac{(\zeta_j - \zeta_k)^\theta}{|\zeta_j - \zeta_k|^\theta} = \exp\left(i\theta \sum_{j<k} \alpha_{jk} \right). \tag{5.30}$$

Here θ is a *a priori* arbitrary parameter, which corresponds to the coupling constant when writing the Chern-Simons action, and $\alpha_{jk} = \alpha(\zeta_j - \zeta_k) \equiv \arg(\zeta_j - \zeta_k)$ is the angle between the vector $\mathbf{r}_j - \mathbf{r}_k \in \mathbb{R}^2$ and a reference axis such as $\hat{\mathbf{x}}$ [*i.e.* $\arg(\zeta) = \arctan(y/x)$]. The local unitary gauge transformation is singular since α_{jk} is not defined when $\mathbf{r}_j \to \mathbf{r}_k$ and presents branch cuts when performing loops around the origin [the angle $\alpha(\zeta)$ is defined modulo 2π] but it does not change the particle density as we clearly have $|\Psi_\theta(\{\zeta_j\})|^2 = |\Psi_{\rm CS}(\{\zeta_j\})|^2$. The transformation also does not introduce any new energy scale since the observables described by a topological field theory are exclusively determined by the topological properties of the manifold under consideration.

Using Eq. (5.30), the Hamiltonian (5.2) which satisfies the usual eigenvalue equation $\hat{\mathcal{H}}\Psi(\{\zeta_j\}) = E\Psi(\{\zeta_j\})$ is transformed as $\hat{\mathcal{H}}_{\rm CS} = U_\theta^\dagger \hat{\mathcal{H}} U_\theta$ and allows us to map the initial problem into the eigenvalue problem $\hat{\mathcal{H}}_{\rm CS}\Psi_{\rm CS}(\{\zeta_j\}) = E\Psi_{\rm CS}(\{\zeta_j\})$ for the new Hamiltonian $\hat{\mathcal{H}}_{\rm CS}$ defined correspondingly but with its kinetic terms (1.11) replaced by

$$\mathcal{H}_{j,{\rm CS}} = \frac{1}{2m^*}\left[\mathbf{p}_j - \frac{e}{c}\mathbf{A}(\mathbf{r}_j) - \frac{e}{c}\mathbf{A}_{\rm CS}(\mathbf{r}_j) \right]^2. \tag{5.31}$$

The novelty of this transformation is the appearance of a new gauge field $\mathbf{A}_{\rm CS}(\mathbf{r})$, the

so-called Chern-Simons vector potential, given by

$$\mathbf{A}_{\mathrm{CS}}(\mathbf{r}) = -\frac{\Phi_0}{2\pi}\theta \sum_{k=1}^{N} \boldsymbol{\nabla}_{\mathbf{r}}\, \alpha(\mathbf{r}-\mathbf{r}_k), \tag{5.32}$$

where Φ_0 is the flux quantum defined in chapter 1. This gauge field is chosen such that we obtain a flux in the opposite direction to the external magnetic field through the value of the parameter θ. The gauge field satisfies the Coulomb gauge $\boldsymbol{\nabla}_{\mathbf{r}} \cdot \mathbf{A}_{\mathrm{CS}} = 0$, as it can be shown by using the Cauchy-Riemann differential equations, and yields a Chern-Simons magnetic field equal to

$$\begin{aligned} \mathbf{B}_{\mathrm{CS}}(\mathbf{r}) &= \boldsymbol{\nabla}_{\mathbf{r}} \times \mathbf{A}_{\mathrm{CS}}(\mathbf{r}), \\ &= -\Phi_0\, \theta\, n(\mathbf{r})\hat{\mathbf{z}}. \end{aligned} \tag{5.33}$$

The non-zero value of the Chern-Simons "magnetic field" is related to the fact that the gauge transformation is singular and satisfies the Poisson equation in a two-dimensional potential

$$[\boldsymbol{\nabla}_{\mathbf{r}} \times \boldsymbol{\nabla}_{\mathbf{r}}\, \alpha(\mathbf{r})] \cdot \hat{\mathbf{z}} = 2\pi n(\mathbf{r}) = 2\pi \sum_{k=1}^{N} \delta^{(2)}(\mathbf{r}-\mathbf{r}_k), \tag{5.34}$$

instead of $\boldsymbol{\nabla}_{\mathbf{r}} \times \boldsymbol{\nabla}_{\mathbf{r}}\, \alpha(\mathbf{r}) = \mathbf{0}\ \forall \mathbf{r} \in \mathbb{R}^2$.

It is also easy to see that the Chern-Simons transformation acts as a statistical gauge transmutation since it can transform fermions to bosons in two-dimensions. Indeed, we have from the definition of the angle $\alpha_{jk} = \alpha_{kj} + \pi$ that the exchange between two different particles generates a global phase factor of $\exp(i\pi\theta)$. If $\theta = 2m+1$ with $m \in \mathbb{N}$, the gauge field changes fermions into bosons (or vice versa) [193]. On the other hand, if both $\Psi_\theta(\{\zeta_j\})$ and $\Psi_{\mathrm{CS}}(\{\zeta_j\})$ describe a N-body state of fermionic nature, the parameter θ has necessarily to be even, $\theta = 2m$. Therefore, the statistics of the ground-state wave function of the electronic state and the analogue function of the composite fermions fix the value of the Chern-Simons coupling.

We are now in position to apply the average field approximation (which is equivalent to a mean field treatment). Thus, we consider that the quantum fluctuations of the statistical gauge field, $\mathbf{A}_{\mathrm{CS}}(\mathbf{r}) = \mathbf{A}_{\mathrm{CS}} + \delta\mathbf{A}_{\mathrm{CS}}(\mathbf{r})$, vanish on average, *i.e.* $\langle \delta\mathbf{A}_{\mathrm{CS}}(\mathbf{r}) \rangle = \mathbf{0}$. This amounts to considering that the particle density is homogeneous, $n(\mathbf{r}) = n$ and that the interaction between the electrons is the average interaction of each particle with a uniformly charged background. The flux quanta are then uniformly distributed generating a magnetic field

$$\mathbf{B}^* = \mathbf{B} + \mathbf{B}_{\mathrm{CS}} = B(1 - \Phi_0\theta n)\hat{\mathbf{z}}. \tag{5.35}$$

As a result, we obtain Jain's sequence if we choose the value $\theta = 2m$, $m \in \mathbb{N}$, for the coupling constant. The wave function statistics resulting from the gauge transformation is then compatible with that of a fermion liquid in the presence of an external reduced magnetic field.

A strength of the Chern-Simons theory sketched above is to be able to obtain Jain's sequence without the need of reprojecting onto the LLL after the introduction of the composite fermion Landau levels ν_f^*. Note also that, compared to Eq. (5.18), the gauge transformation does not bind zeroes to the electronic wave function but only the phases of those zeroes (the vortex part [172]). The Chern-Simons theory appears to be very successful

for the calculation of the low energy sector of the spectrum and yields, in the Haldane compact geometry, the correct results for the correlation functions which do not involve the energy gap [168, 195] at all (*e.g.* density-density correlation function). The Chern-Simons approach has also proved to be very useful in the description of the compressible states like $\nu_f = 1/2$ obtained when $\nu_f^* \to +\infty$ and which present phenomena accounting for Fermi liquid-like behavior (overdamped modes, coupling to surface acoustic waves ...) [196].

On the other hand, the Chern-Simons theory gives an incorrect scaling for the excitation spectrum at the mean-field level [164]. Indeed, as in Sec. 5.2.2, we obtain that the excitation gap in the LLL has a characteristic energy of $\hbar\omega_c^* \propto B^*$ instead of $e^2/(\epsilon l_B) \propto \sqrt{B^*}$. The first energy scale also involves the bare electronic effective mass, m^*, while this physical quantity clearly does not play any role in the Coulomb interaction [the electronic mass is expected to be renormalized to the composite fermion mass $m^*(\nu_f)$ when considering quantum fluctuations of the gauge field beyond the random phase approximation [194]]. In this sense, as the gauge transformation only affects the kinetic energy, it is also not clear why the gaps in the LLL disappear when the Coulomb interaction goes to zero with the mass of the particles kept constant. We may also wonder what physical meaning assign to the newly appeared Chern-Simons "magnetic field" completely independent of the measurable magnetic field $\mathbf{B}$.

More worryingly, there are other important pathologies regarding the mean field treatment. First, it is usually admitted that, at this level, the fluctuations of the gauge Chern-Simons field and the Coulomb interaction cancel each other. However, as we have mentioned in the previous paragraph, both quantities present very different energy scales so that cancellation is extremely difficult. Moreover, it is possible to show that the Chern-Simons mean field theory gives an incorrect result for the Hall conductance / resistance [194]. To prove this statement, let us, at this point, consider the clean limit for which the disorder potential felt by each particle can be neglected and for which we know from chapter 1 that we can identify resistivity and resistance (up to geometrical sample dependent factors) . Since we have mapped our problem of interacting electrons to a problem of nearly-free composite fermions with filling factor ν_f^*, Galilean invariance [197] gives $R_{\rm H}^{\rm MF} = R_{\rm K}/\nu_f^*$ instead of $R_{\rm H}^{\rm MF} = R_{\rm K}/\nu_f$. To obtain the correct result for the Hall resistance one has to go beyond mean field and consider the Chern-Simons random phase approximation. In this case, it is argued that the composite fermions can be thought as nearly-free fermions which responds to the external electric field $\boldsymbol{\mathcal{E}}$ and a self-induced electric field $\boldsymbol{\mathcal{E}}_{\rm CS}$. The latter is a consequence of the fluctuations in the gauge field $\delta B_{\rm CS}(\mathbf{r}) = 2\pi\theta\,\delta n(\mathbf{r})$ and satisfies the local Ohm's law

$$\boldsymbol{\mathcal{E}}_{\rm CS} = \bar{R}_{\rm CS}\,\mathbf{j}, \tag{5.36}$$

where $\bar{R}_{\rm CS}$ is a purely off-diagonal tensor with Hall component $R_{\rm H}^{\rm CS} = R_{\rm K}\theta$. Note that the effect of these fluctuations is <u>not</u> pertubative since $R_{\rm H}^{\rm CS}$ is indeed larger than $R_{\rm H}^{\rm MF}$ (or, θ which is the only possible small parameter is actually larger than the unity). Amazingly, adding both the mean-field and Chern-Simons resistance tensors as $\boldsymbol{\mathcal{E}}_{\rm T} \equiv \boldsymbol{\mathcal{E}} + \boldsymbol{\mathcal{E}}_{\rm CS} = (\bar{R}^{\rm MF} + \bar{R}^{\rm CS})\mathbf{j} \equiv \bar{R}_{\rm T}\mathbf{j}$ we get a purely off-diagonal resistance tensor with components

$$R_{\rm H}^{\rm T} = \left(\frac{1}{\nu_f^*} + \theta\right) R_{\rm K}, \tag{5.37}$$

where the term in parenthesis is just the inverse filling factor, $1/\nu_f$, given in Eq. (5.5). To sum up, we recover the reduced magnetic field seen by the composite fermions at the

mean-field level but one has to go beyond that approximation, using fluctuations that present the same order of magnitude than the mean-field result at high magnetic fields, to obtain the corresponding filling factor ν_f in the transport coefficients.

Finally, we may mention that the Chern-Simons approach also shares with Jain's trial wave functions the bizarre fact that it somehow involves higher composite fermion Landau levels for the construction of the charge-flux composites which, in principle, can be thought to be irrelevant in the high magnetic field limit [164]. Opposite to the trial wave functions, however, this approach is unable to give the correct fractional charge for the excitations which present, instead of fractional charge, a charge equal to e, since only flux tubes (and not zeroes) are attached to the particles [215].

Hamiltonian theory

A possible solution to some of the previous problems (in particular, the gap energy scaling) was proposed by G. Murthy and R. Shankar [198, 215] who developed what is now called the (extended) Hamiltonian theory. This is a microscopic theory which allows to perform more controlled approximations than the original Chern-Simons field theory and cures what appears to be some amazing chances in the random phase approximation discussed above. The theory is also, apart from the direct numerical methods for reduced particle numbers, one of the most developed approaches to a full theory of the fractional quantum Hall effect and allows us to compute, between other quantities, energy and transport gaps at the mean-field level [200], correlation (Green's) functions [199] or relaxation rates and polarization of gapped and gapless states at finite temperature in the thermodynamic limit [201].

The basic idea of Murthy and Shankar's theory, which is said to be complementary to trial wave functions and / or exact diagonalization of the Hamiltonian, is to obtain a projected Hamiltonian operator for the LLL that properly scales with the Coulomb energy $e^2/(\epsilon l_B)$. Then, we try to systematically build a Hilbert space for the composite charged-flux particles without attaching zeroes to the wave functions, but working exclusively with operators, with the goal of getting a unique ground state at the level of Hartree-Fock (mean-field) theory. In that sense, the problem of lifting the huge degeneracy of the LLL by the Coulomb interaction is circumvented, while keeping track of the relevant energy scales (*i.e.* without involving the mass m^* of the bare electron as in the Chern-Simons approach). Moreover, the composite fermions created in this way should have the expected attributes missing in the Chern-Simons field theory such as the reduced fractional charge e^* or the mass $m^*(\nu_f)$.

To that purpose, a projection into the LLL, in which one gets rid of the kinetic energy (the latter is, *a priori* at this level, a simple shift in the energy) is considered[12] and we use

$$\hat{\mathcal{P}}_{\mathrm{LLL}} \exp\left(i\mathbf{q}\cdot\mathbf{r}\right) = \hat{\mathcal{P}}_{\mathrm{LLL}} \exp\left[i\mathbf{q}\cdot(\boldsymbol{\eta}+\mathbf{R})\right] = \exp\left(-\frac{q^2 l_B^2}{4}\right)\exp(i\mathbf{q}\cdot\mathbf{R}), \tag{5.38}$$

where $\mathbf{q}$ is the wave vector conjugate to the electronic variable $\mathbf{r}$, $\mathbf{R} = (X, Y)$ is the non-commuting guiding center coordinate of each electron (1.19) and $\boldsymbol{\eta} = \mathbf{r} - \mathbf{R}$. This

[12]This projection can be done, in principle, for any Landau level and we recover the full electronic structure factor introduced in Eq. (3.45).

projection transforms the Hamiltonian (5.2) into

$$\begin{aligned}\hat{\mathcal{H}}_{\mathrm{LLL}} &= \frac{1}{2}\sum_{i,j=1}^{N}\int \frac{d^2\mathbf{q}}{(2\pi)^2} v(q)\exp\left(-\frac{q^2 l_B^2}{2}\right)\exp\left[\mathbf{q}\cdot(\hat{\mathbf{R}}_i-\hat{\mathbf{R}}_j)\right], \\ &= \frac{1}{2}\int \frac{d^2\mathbf{q}}{(2\pi)^2}\hat{\rho}(\mathbf{q})v(q)\exp\left(-\frac{q^2 l_B^2}{2}\right)\hat{\rho}(-\mathbf{q}),\end{aligned} \tag{5.39}$$

with $v(q) = 2\pi e^2/(\epsilon q)$ the Fourier transform of the Coulomb potential (5.4) and $\hat{\rho}(\mathbf{q})$ the projected density operator

$$\hat{\rho}(\mathbf{q}) = \sum_{j=1}^{N}\exp\left(-i\mathbf{q}\cdot\hat{\mathbf{R}}_j\right). \tag{5.40}$$

We note that the projected density operator can be recognized as a magnetic translation operator (since its algebra is isomorphic to the latter [202])

$$[\hat{\rho}(\mathbf{q}),\hat{\rho}(\mathbf{q}')] = 2i\sin\left[\frac{l_B^2(\mathbf{q}\times\mathbf{q}')\cdot\hat{\mathbf{z}}}{2}\right]\hat{\rho}(\mathbf{q}+\mathbf{q}'). \tag{5.41}$$

Here the last term can be understood as a twist in the phase as a consequence of a translation in the plane. The density operator algebra is embedded in the more general W_∞ algebra, that connects the Landau problem with the deformation of the algebra of two-dimensional area preserving maps [203]. These are the canonical transformations in two-dimensions and, therefore, it is not surprising that the structure factor of this algebra has a functional form related to the Groenewold-Moyal bracket introduced in chapter 1 and which can be traced back to the non-commutativity of the guiding center coordinates $\mathbf{R}$ in real space.

Since we have dropped out the kinetic energy, our problem has only one dynamical degrees of freedom (the coordinates of the electronic guiding center) and the Hilbert space is enlarged to introduce a new object, called pseudo-vortex, whose guiding center coordinates $\mathbf{R}_v = (X_v, Y_v)$ satisfy the commutator

$$[\hat{R}_{vj},\hat{R}_{vk}] = -\epsilon_{jk}\frac{il_B^2}{\vartheta}\mathbb{1}, \tag{5.42}$$

with ϑ being the parameter

$$\vartheta = 2m\nu_f = \frac{2m\nu_f^*}{2m\nu_f^*+1} \leq 1. \tag{5.43}$$

The pseudo-vortex describes an objet of charge $-\vartheta^2 e$ loosely bound to the electron (it is not, as we have said before, associated to any zeroes of the wave function like in Jain's approach). This is an auxiliary degree of freedom meant to model to some extent the correlation hole bound to the single electron in the interacting 2DEG. As such, this object has no dynamics since its density can be defined as

$$\hat{\chi}_v(\mathbf{q}) = \sum_{j=1}^{N}\exp\left(-i\mathbf{q}\cdot\hat{\mathbf{R}}_{v,j}\right), \tag{5.44}$$

with algebra

$$[\hat{\chi}(\mathbf{q}),\hat{\chi}(\mathbf{q}')] = -2i\sin\left[\frac{l_B^2(\mathbf{q}\times\mathbf{q}')\cdot\hat{\mathbf{z}}}{2}\right]\hat{\chi}(\mathbf{q}+\mathbf{q}'), \tag{5.45}$$

and commutes with the Hamiltonian $[\hat{\mathcal{H}}_{\mathrm{LLL}}, \hat{\chi}(\mathbf{q})] = 0$ thanks to the constraint $[\hat{\mathbf{R}}, \hat{\mathbf{R}}_v] = 0$ for all $j = 1, \ldots, N$. It is also interesting to mention that the pseudo-vortex is defined so that it ensures that, when the electron performs a closed loop around this object, it acquires a phase of $2\pi\theta$ as if it was feeling $\theta = 2m$ flux tubes (see Sec. 5.2.2).

As a next step, the guiding center coordinates of the electron and the pseudo-vortex are combined to build the composite fermion. The composite fermion coordinates are defined

$$\mathbf{R}_{\mathrm{CF}} = \frac{\mathbf{R} - \vartheta^2 \mathbf{R}_v}{1 - \vartheta^2}, \tag{5.46}$$

$$\boldsymbol{\eta}_{\mathrm{CF}} = \frac{\vartheta}{1 - \vartheta^2}(\mathbf{R}_v - \mathbf{R}), \tag{5.47}$$

where the first equality means that the center-of-mass of the composite fermion is the weighted sum of the center-of-mass of the electron and the pseudo-vortex. The second equality is found demanding $\boldsymbol{\eta}_{\mathrm{CF}}$ to be linear in $\mathbf{R}$ and $\mathbf{R}_v$ and taking into account that we have the commutators $[\hat{\eta}_{\mathrm{CF},j}, \hat{\eta}_{\mathrm{CF},k}] = i\epsilon_{jk} l_B^{*2} \mathbb{1}$ and $[\hat{R}_{\mathrm{CF},j}, \hat{R}_{\mathrm{CF},k}] = -i\epsilon_{jk} l_B^{*2} \mathbb{1}$. Here, we have introduced the relevant energy scale related to the composite fermion states, the effective magnetic length l_B^*, defined by

$$l_B^* = \frac{l_B}{\sqrt{1 - \vartheta^2}}. \tag{5.48}$$

Note that, since the pseudo-vortex has a charge of $-\vartheta^2 e$, the composite fermion has a charge equal to $e^* = e(1 - \vartheta^2) = e/(2m\nu_f^* + 1)$ as predicted from Jain's wave function [10].

Rewriting Eq. (5.39) in the composite fermion coordinates, we get a Hamiltonian in the LLL which presents a non-degenerate Hartree-Fock ground state. However, the price to pay for working in the new Hilbert space is that it contains "non-physical" states which have to be gauged away through a projection to the vector space that contains only the "physical" states. This is done by imposing the condition

$$\hat{\chi}_v(\mathbf{q})|\Psi_{\nu_f}\rangle = 0, \tag{5.49}$$

or, $\hat{\chi}_v(\mathbf{q}) \simeq 0$, that is, the pseudo-vortex density vanishes weakly within the correlation functions [198]. Condition (5.49) can be interpreted in the following way: the pseudo-vortex are excitations of the incompressible electronic fluid and the number of excitations in the ground-state wave function is therefore equal to zero.

Let us close the section with a critical view of the sketched Hamiltonian theory. This theory is able to solve some of the problems of the Chern-Simons approach and can address many issues both qualitatively and quantitatively (gaps, polarization, relaxation rates ...) within a seemingly good range of accuracy compared to the experimental results. However, in the aftermath of the previous theoretical discussion, one is left with the impression that the pseudo-vortex (5.42) as well as the parameter ϑ (5.43) are introduced in some arbitrary way, with the only purpose of reproducing the expected properties of the composite fermion [that is, the parameters do not result from a microscopic derivation that starts with the full Hamiltonian (5.2)]. It is also a crucial open problem for this theory to microscopically compute the transport coefficients in the presence of disorder, essential to the formation of the Hall plateaus. This amounts to a rigorous and careful description of the edges and bulk in a dirty 2DEG at high magnetic fields, which is one of the main goals of our work. A step towards this objective is presented in chapter 6.

Chapter 6

Bicomplex Vortex Representation for the Generalized Two-Body Problem

In the last chapter, we reconsider the problem of the fractional quantum Hall effect in a new light. To that purpose, as a preliminary stage, we focus on the two-body problem in the presence of one-body and two-body potentials, and, motivated by the topological ideas underlying the theory of the integer quantum Hall effect described in the first chapter of this thesis introduce a new representation of the two-body quantum states. This representation naturally encodes long-range correlations between the cyclotron motion of the two electrons. In this sense, we first devote a non-negligible part of the chapter to describe the mathematical framework necessary to introduce the Hilbert space where these states are defined. Next, we show that our preferred representation of states, called bicomplex vortex states, are eigenstates of the free two-body Hamiltonian and define an overcomplete semiorthogonal basis in an enlarged (bicomplex) Hilbert space. We then compute the matrix elements of the potential and obtain the equation of motion for the Green's function in this representation. Finally, we close this chapter with a discussion on the consistency of our Green's function approach, the necessity of going beyond the semiclassical approximation to obtain the spectral gaps and fractional values in the Hall conductance and a mathematical proof of the closure relation of the bicomplex vortex states.

Dans ce dernier chapitre, nous reconsidérons le problème de l'effet Hall quantique fractionnaire sous une nouvelle lumière. Pour cela, et comme échauffement préliminaire, nous nous focalisons dans un problème à deux corps en présence des potentiels à une et à deux particules et, motivés par les idées topologiques sous-jacentes dans la théorie de l'effet Hall quantique entier décrites dans le premier chapitre de cette thèse, nous introduisons une nouvelle représentation d'états quantiques à deux électrons. Cette représentation encode d'une façon naturelle des corrélations à longue portée entre le mouvement cyclotron des deux électrons. À cause de cette particularité, nous consacrons une partie non négligeable de ce chapitre à la description du cadre mathématique dont nous avons besoin pour introduire l'espace de Hilbert où ces états sont définis. Ensuite, nous montrons que cette représentation robuste d'états propres de la partie cinétique de l'Hamiltonien à deux corps, appelés états de vortex bicomplexes, détermine une base semi-orthogonale surcomplète dans un espace de Hilbert bicomplexe élargi.

Puis, nous calculons les éléments de matrice du potentiel généralisé et obtenons l'équation du mouvement de la fonction de Green dans cette réprésentation. Finalement, nous clôturons ce chapitre avec une discussion sur la consistance de l'approche avec des fonctions de Green, la nécessité d'aller au-delà de l'approximation semi-classique pour obtenir les gaps spectrales et les valeurs fractionnaires de la conductance de Hall et nous donnons une démonstration mathématique de la relation de fermeture associée aux états de vortex bicomplexes.

6.1. Motivation

An important observation can be made at the level of Eq. (5.2). Indeed, we note that the N-body Hamiltonian can be written as

$$\hat{\mathcal{H}} = \frac{1}{2}\sum_{j\neq k}^{N}\Big[\hat{\mathcal{H}}_j + \hat{\mathcal{H}}_k + v(\hat{\mathbf{r}}_j - \hat{\mathbf{r}}_k)\Big], \tag{6.1}$$

where the first two contributions correspond to *single-particle* Hamiltonians while the last term is the two-body interaction. Since the interaction involves a pair of particles, one can intuitively think of considering as the basic object to microscopically describe the fractional quantum Hall effect regime not the single electron but the *pair* of electrons. As a consequence, we would like to rewrite the kinetic part in Eq. (6.1) and express it as a sum of Hamiltonians for all the possible pairs taken from the N indistinguishable electrons[1]. The coupling between the different pairs will then appear whenever the one-body potential is switched on (each electron of the pair will feel different local potential energy).

Therefore, it seems judicious to start analyzing the kinetic part of Hamiltonian (5.2) for $N = 2$ particles

$$\hat{\mathcal{H}}_0^{(N=2)} = \frac{1}{2m^*}\left[\mathbf{p}_1 - \frac{e}{c}\mathbf{A}(\mathbf{r}_1)\right]^2 + \frac{1}{2m^*}\left[\mathbf{p}_2 - \frac{e}{c}\mathbf{A}(\mathbf{r}_2)\right]^2. \tag{6.2}$$

Here, as in previous chapters, the term in brackets represents the kinetic momentum of each particle with $\mathbf{p}_j$ the canonical momentum and $\mathbf{A}(\mathbf{r}_j) = \mathbf{B}\times\mathbf{r}_j/2$ is the vector potential chosen in the symmetrical gauge and evaluated at position $\mathbf{r}_j = (x_y, y_j)$. To obtain the eigenenergies and eigenstates of the Hamiltonian (6.2), a natural idea would be to consider the product state of two single-particle vortex wave functions (1.43), so that $\Psi(\mathbf{r}_1, \mathbf{r}_2) = \Psi_{n_1,\mathbf{R}_1}(\mathbf{r}_1)\Psi_{n_2,\mathbf{R}_2}(\mathbf{r}_2)$. The eigenenergies associated to this state can be easily calculated and amount to consider the energies of two independent harmonic oscillators labeled by the vortex circulations n_1 and n_2, *i.e.* $E_{n_1,n_2} = \hbar\omega_c(n_1 + n_2 + 1)$. One then proceeds to project to the lowest Landau level (LLL), $n_1 = n_2 = 0$, and argue that the properly antisymmetrized two-body wave function written in terms of the 2×2 Slater determinants gives a unique analytic wave function which can be expressed as a product of the center-of-mass and relative eigenfunctions [41, 210]. Each product state is respectively characterized by a total angular momentum $M_{\mathrm{L}} \geq 0$ and a relative angular momentum $m_{\mathrm{L}} \geq 0$ of the electron pair. Next, it is usually inferred that, since the interaction Hamiltonian (5.3) is

[1] From this point of view, the kinetic energy and the Coulomb interaction are considered on equal footing.

invariant under rotations, the relative angular momentum of the pair of electrons m_{L} has to be a good quantum number. As a consequence, the spectral decomposition of Eq. (5.3) in the two-body basis is given by

$$\hat{\mathcal{H}}_{ee} = \frac{1}{2} \sum_{j \neq k} \sum_{m_{\mathrm{L}} \geq 0} v_{m_{\mathrm{L}}} \hat{\mathcal{P}}_{jk}^{m_{\mathrm{L}}} \tag{6.3}$$

where $\hat{\mathcal{P}}_{jk}^{m_{\mathrm{L}}}$ is an operator which projects particles j and k onto a state of relative angular momentum m_{L} and the set of discrete coefficients $v_{m_{\mathrm{L}}} \in \mathbb{R}$ independent of M_{L} are denominated Haldane pseudopotentials. Physically, these eigenvalues of the interaction Hamiltonian[2] projected onto the LLL give the energy necessary for having the electronic pair (j, k) with relative angular momentum m_{L} and lift partially the huge degeneracy of the LLL. The Haldane pseudopotentials also fully characterize the energy spectrum of the full Hamiltonian in the absence of one-body potential energy (5.4) because each particle in the pair must have the same kinetic energy [20].

In the presence of smooth disorder, which is usually disregarded as we saw in chapter 5, the spectral gaps between the discrete energy levels are expected to remain open, with the one-body potential being responsible for the lift of the degeneracy with respect to the center-of-mass of the electronic pair[3]. As such, the non-vanishing excitation gap is usually considered to be the main cause of the stability of the fractional plateaus, as well as the existence of dissipationless edge modes. However, a crucial point has been swept under the carpet. Indeed, we know that the fractional filling factors which characterize the Hall resistance in the fractional quantum Hall regime present *two* robust integers, while the two-body problem in the LLL only yields a single quantum number after projection, m_{L}. In addition, another point which has been overlooked is that a realistic Hamiltonian describing the fractional quantum Hall liquid cannot have exactly the form (5.4) but instead must present broken continuous symmetries due to the anisotropy of the interactions and the disorder potential. As a consequence, we conclude that building from a microscopic principle a two-body and a many-body wave function in a truly existing quantum Hall system probably relies on the adoption of a distinct strategy[4].

The approach to be taken here as a preliminary step towards the solution of the full many-body problem will be radically different and inspired by the vortex theory of the integer quantum Hall effect. To this purpose, we are going to take advantage of the fact that the Landau levels of the pair of electrons are macroscopically degenerate to identify the adequate basis, labeled by quantum numbers of topological origin, of the free Hamiltonian (6.2). This set of states, dubbed two-body vortex states and describing the composite object, has to be characterized by robust (topological) quantum numbers present in the phase of the wave function (*i.e.* we have a topological defect robust to interactions and disorder). The most natural quantum number to be considered is the Landau level of the pair of electrons n which, when considering the product state, appears as a sum of two independent circulations n_1 and n_2. Following the analogy with the

[2]Note that this Hamiltonian does not present broken continuous symmetries since it is translationally and rotationally invariant.

[3]Nevertheless, disorder is crucial to explain the macroscopic transport properties which is the main experimental feature of quantum Hall effects as we have seen in chapter 1.

[4]The doubt is confirmed by the fact that the Laughlin's wave function introduced in Sec. 5.2.2, which is nothing but a generalization of the two-body wave function discussed above, is the ground state of the Hamiltonian if, and only if, the set $\{v_{m_{\mathrm{L}}}\}$ is chosen in the framework of an artificial purely hard-core or harmonic interaction.

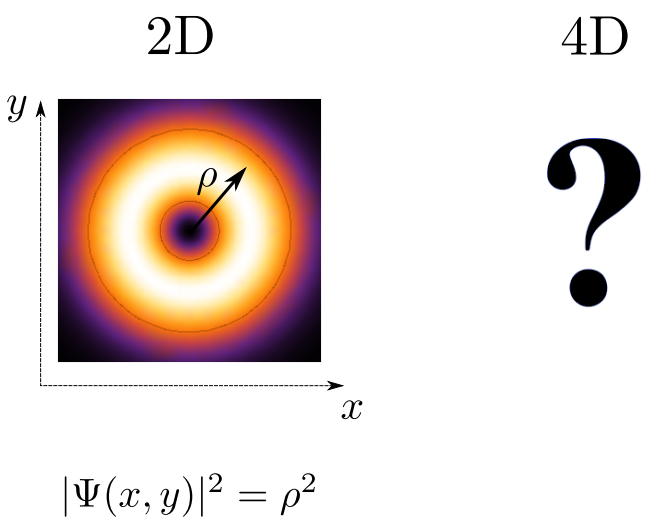

Figure 6.1 – A 2D vortex can be characterized by the zeroes of a complex scalar field $\Psi(x,y) = \rho\exp(i\theta)$ for which the modulus vanishes, $\rho = \rho(x,y) \equiv 0$, and the phase, $\theta = \theta(x,y)$, stays undefined or singular. We represent such a vortex in the contour plot of the left-hand side of this figure. Any closed loop around the singularity is characterized by an integer, the winding number, whose values are necessarily dictated by the topology of the manifold where the curve is embedded. The winding number is topological in the sense that it is still a good quantum number even in the presence of strong perturbations. A question comes now: how to define a vortex in a 4D phase space and which are the corresponding winding number(s)?

one-body problem, the Landau level of the pair can be conjectured to be related to the flux quantization in a four-dimensional space for a vortex representation (the non-trivial phases can be therefore understood as associated to a four-dimensional Aharonov-Bohm flux characterized by peculiar winding numbers). Note that the topological defect is fully four-dimensional (it cannot be reduced to some composition of 2D objects) and does not present a classical analog. As such, it is not guaranteed in any case that the higher-dimensional vortex exists as, before finding it, we first need to mathematically specify the phase space that accommodates this object and the winding numbers characterizing the four-dimensional phase singularity, see Fig. 6.1.

Besides, we shall treat the disorder potential and the Coulomb interaction on the same footing and without specifying its functional form, in correspondence to the situation described in chapters 1 and 3. The disorder potential will again be expected to lift the quantum degeneracy with respect to the center-of-mass position of the electron pair. Not making explicit the form of the interaction to be purely long-range in the form $v(q) \propto e^2/q$ seems reasonable since the exact form of the interaction Hamiltonian in a realistic 2DEGs is not given by Eq. (5.3) but instead shows the effects of the confinement in the perpendicular direction[5], anisotropy due to a spatially varying dielectric constant $\epsilon(\mathbf{r})$

[5]The transverse extent of the electronic wave function in the $\hat{\mathbf{z}}$ direction has a quantitative repercussion in the electron-electron coupling [10] since it produces an effective interaction which differs from the long-range Coulomb potential at short distances. To account for this effect, which can be physically understood as the electrons acquiring a finite size, a self-consistent solution of the Schrödinger and Poisson equations has to be found [216].

from the 3D insulating medium, etc. Finally, note that the strategy followed here mimics in some sense the treatment of the integer quantum Hall effect as we are splitting the fast (cyclotron motion and Coulomb interaction) and slow (disorder potential) degrees of freedom but now at the level of the electron pair. The pairs must present topological robust quantum numbers which yield spectral gaps protected from local perturbations. As for the one-body case, the gaps in the energy spectrum must then be used to explain the existence of dissipationless edge states and Hall resistance plateaus in the fractional [quantum Hall] regime.

To wrap up this section, I would like to pause here to mention the different (unsuccessful) approaches that were considered in our quest to obtain two-body vortex states of the free Hamiltonian describing a single topological defect in four dimensions. This paragraph will also motivate why it is necessary to "think outside the box" and move forward the usual theoretical attempts to describe strong correlations in the quantum Hall regime. Our first idea to solve this problem was to use a generalization of polar coordinates to d dimensions, the so-called hyperspherical coordinates [235]. This coordinate system proved to be problematic because, for $d > 2$, it does not define a privileged direction in space (whereas 2DEGs present a preferred direction perpendicular to the plane and parallel to the external magnetic field). As a second option, we considered the so-called Hopf coordinates which describe the Hopf fibration or Hopf bundle [211, 212]. This transformation, which is exclusive of the 3-sphere[6] maps this four-dimensional manifold to $\mathbb{C}^2\backslash\{\mathbf{0}\}$ (that is, a pair of complex numbers). The stereographic projection into $\mathbb{R}^3$ gives a very nice physical picture since it describes a completely filled Euclidean space with tori made of two linked (Villarceau) circles. Each fiber in the bundle can then be physically interpreted as the representation of two correlated particles under the influence of the Lorentz force. Unfortunately, even if the bundle is globally non-trivial (as it happens with the Möbius band), it is locally a Cartesian product space (trivial). As such, we can show that the two-body wave functions are necessarily written as a product state with two phase singularities living in the same complex plane. As a consequence, we arrive to the conclusion that it is necessary to use other algebras beyond complex numbers in order to obtain a single phase singularity associated to closed trajectories describing the pair motion in four dimensions. Thus, we arrive at the third fruitless direction which was taken, the use of quaternionic coordinates. The quaternionic algebra is one of the four normed division algebras over the real numbers and it had already been proposed to describe a generalization of quantum mechanics [213]. The main argument to adopt quaternions in order to extend axiomatically quantum mechanics is that they form an algebraic field. However, they do not form a commutative algebra and, as a consequence, quaternionic functions cannot satisfy the Cauchy-Riemann equations (therefore, the construction of an analytic function theory is not possible because left and right derivatives do not commute). This is highly inconvenient since even the eigenvalue problem for the Laplacian operator, appearing in the position representation of the wave function equation of motion, is not well-posed. A solution is, nevertheless, possible: we can consider instead of the standard quaternions their commutative version, so-called *commutative quaternions* or *bicomplex numbers*. The commutative quaternions form a non-trivial set of numbers not much studied in the mathematical literature and we shall have a closer look at them in the next section.

[6] A d-sphere of radius R, noted S^d, is the generalization of the sphere in $\mathbb{R}^{d+1}$.

1	i	j	k
i	-1	k	$-j$
j	k	1	i
k	$-j$	i	-1

Table 6.1 – Multiplication table defining the bicomplex algebra. This table consists of a 4×4 matrix which includes the multiplicative identity noted by 1 (and, which also represents the unit versor). The matrix is symmetric with respect to the main diagonal pointing out to the fact that bicomplex numbers form a commutative algebra.

6.2. Bicomplex Numbers

6.2.1. Generalities

Bicomplex numbers[7] are a type of hypercomplex numbers[8] defined by the following set

$$\mathbb{B} \equiv \Big\{ q = x_1 + iy_1 + jx_2 + ky_2 \,|\, x_1, x_2, y_1, y_2 \in \mathbb{R};\; i, j, k \notin \mathbb{R}; \\ i^2 = k^2 = -j^2 = -1 \Big\}, \quad (6.4)$$

together with the commutative product rule $ij = ji \equiv k$. From the definition given in Eq. (6.4) we clearly see that both versors i and k behave as the standard imaginary unit while j, albeit being similar, satisfies the particular rule $j^2 = 1$. For reasons to be clarified later, this versor is dubbed a hyperbolic unit. In addition, we note that due to the constraint imposed by the commutativity product rule only two versors, i and j, are actually independent.

The precedent rules define an algebra over the real numbers, $\mathbb{R}$, where the bilinear operation is characterized by the table of products shown in Table 6.1. Apart from the associativity, the table sums up the main properties of the bicomplex algebra, namely commutativity and existence of unity.

Alternatively, the bicomplex algebra can also be seen as an algebra over the complex numbers $\mathbb{C}$ since we can write any element $q \in \mathbb{B}$ as a pair of complex numbers $z_1, z_2 \in \mathbb{C}$ linked by a hyperbolic unit (or, a hyperbolic tuple with complex coefficients)

$$q = \underbrace{x_1 + iy_1}_{z_1} + j \underbrace{(x_2 + iy_2)}_{z_2} = z_1 + jz_2. \quad (6.5)$$

As a consequence, we can understand the bicomplex numbers (6.5) as a peculiar union of two complex numbers, each of them defined in a "characteristic" [complex] plane. This interpretation is close to the original procedure of "complexification of complex numbers" proposed by Corrado Segré in 1892 for the introduction of the bicomplex numbers. In fact, we can consider the following operation: let $z = x + iy \in \mathbb{C}$ and substitute each of the variables x and y by complex ones $z_i = x_i + ky_i$ for $i = \{1, 2\}$ where k is an imaginary unit different from i (we can imagine that i and k belong to two independent axis in the

[7] Also known by the name of tessarines, Segré commutative quaternions or canonical elliptic quaternions [205].

[8] See Sec. D.2 in Appendix D for the precise meaning of this term. We also refer to this Appendix for the definitions of abstract algebra appearing in this chapter.

module). Then, we define the map $z \to q = x_1 + ky_1 + ix_2 + (ik)y_2$ in which we impose the commutativity condition $ik = j = ki$. The result is a four dimensional (bi)complex number with a table of products isomorphic to Table 6.1 (the latter can be obtained by defining the isomorphism that replace k by i and x_2 by y_2).

Two important subalgebras can be straightforwardly identified in the set $\mathbb{B}$ equipped with the algebra detailed in Table 6.1. First, we recognize the well-known set of complex numbers defined by

$$\mathbb{C} \equiv \Big\{ z = x + iy \,|\, x, y \in \mathbb{R}; i \notin \mathbb{R}; \, i^2 = -1 \Big\}, \tag{6.6}$$

which appears when the second complex component in Eq. (6.5) vanishes (so that the hyperbolic character of the bicomplex numbers disappears). Second, we have the so-called hyperbolic numbers[9] represented by the set

$$\mathbb{D} \equiv \Big\{ q = x_1 + jx_2 \,|\, x_1, x_2 \in \mathbb{R}; \, j \notin \mathbb{R}; \, j^2 = 1 \Big\}. \tag{6.7}$$

Both sets can be somewhat seen as a "duplication" of $\mathbb{R}$. However, the algebra which is built in each of them is radically different due to the seemingly innocent change of the imaginary unit i by the hyperbolic unit j, which soundly alters the intrinsic geometry of the modules. Indeed, complex numbers encode the standard Euclidean geometry in two dimensions, with metric signature $(+,+)$ according to the definition of the squared modulus $|z|^2 \equiv zz^{*^i} = x^2 + y^2$. On the other hand, hyperbolic numbers algebraically contain the structure of two-dimensional Minkowski space-time characterized by a pseudo-Euclidean geometry [with metric signature $(+,-)$ as it can be seen in the bilinear form $|q|^2 \equiv qq^{*^j} = x_1^2 - x_2^2$, see Fig. 6.2]. Additionally, fingerprints of this intrinsic geometry can be seen when working in polar coordinates[10]: in the first case, terms of the form $\exp(i\theta)$ where $\theta \in [0, 2\pi)$ is an angular parameter are representations of the elements of the one-dimensional special unitary (Lie) group U(1) describing rotations[11] in $\mathbb{R}^2$; in the second case, the elements $\exp(j\varphi)$ with $\varphi \in (-\infty, +\infty)$ are parametrizations of hyperbolic rotations or boosts which are determined by the connected component containing the identity of the restricted Lorentz group $\mathrm{SO}^+(1,1)$. Bicomplex numbers will then present a peculiar mixture of the two previous algebras in which the simultaneous presence of a compact support for the polar / circular angles and a non-compact one for the hyperbolic angle plays a crucial role in the correlations between the electrons.

Note that, as a consequence of having three non-trivial versors $i, j, k = ij$, bicomplex numbers present three different types of conjugation depending on the versors affected by the conjugation operation. These are defined as

$$q^{*^i} \equiv x_1 - iy_1 + jx_2 - ijy_2 = z_1^* + jz_2^*, \tag{6.8a}$$

$$q^{*^j} \equiv x_1 + iy_1 - jx_2 - ijy_2 = z_1 - jz_2, \tag{6.8b}$$

$$q^{*^{ij}} \equiv x_1 - iy_1 - jx_2 + ijy_2 = z_1^* - jz_2^*. \tag{6.8c}$$

As it happens with the usual complex numbers, elements from the subsets $\mathbb{R}$, $\mathbb{C}$ and $\mathbb{D}$ contained in $\mathbb{B}$ can be obtained through the combination of the different bicomplex

[9] Also known by the name of real tessarines, split-complex or perplex numbers.

[10] We define the polar coordinates in $\mathbb{C}$ as $z = \rho\exp(i\theta)$ with $\exp(i\theta)$ given by Euler's formula. In the case of $\mathbb{D}$, we have $q = \rho\exp(j\varphi)$ and we use its hyperbolic version $\exp(j\varphi) = \cosh\varphi + j\sinh\varphi$.

[11] It is well known that the following Lie groups are isomorphic $\mathrm{U}(1) \cong \mathrm{SO}(2) \cong \mathbb{T}$ with $\mathbb{T}$ the circle group.

conjugations: for example, one straightforwardly gets $qq^{*^i} \in \mathbb{D}$, $qq^{*^j} \in \mathbb{C}$ or $qq^{*^i}q^{*^j}q^{*^{ij}} \in \mathbb{R}$. Note that the way the modulus is defined in the different subalgebras, $\mathbb{C}$ and $\mathbb{D}$, also points towards the fact that within the bicomplex number algebra the invariant form is of fourth order and built from the combination of Eqs. (6.8a)-(6.8c).

Finally, let us discuss the simple algebraic structure of the bicomplex numbers. From the point of view of abstract algebra, bicomplex numbers form a commutative ring. Importantly, as a difference to the quaternions they are not an algebraic field (or integral domain) because not all of the elements of the bicomplex ring are units. As a consequence, bicomplex numbers present zero divisors[12]. As such, the product of two particular non-zero bicomplex numbers can be zero (or, in the same manner, $\exists q \in \mathbb{B}$ for which q^{-1} is not defined, in a similar way as 0^{-1} does not exist). Zero divisors will be called singular bicomplex numbers as opposed to regular bicomplex numbers for which $\exists q^{-1}$. The existence of zero divisors in the bicomplex ring is a consequence of the hyperbolic character[13] induced by the presence of the versor j. Indeed, one can easily show that $q = z(1+j)$ and $q' = z'(1-j)$ with $z, z' \in \mathbb{C}$ but otherwise arbitrary are a pair of zero divisors since

$$qq' = zz'(1+j)(1-j) = zz'(1-j^2) = 0, \tag{6.9}$$

but $q, q' \neq 0$. The zero divisors are forbidden zones similar to the light-cone that appears in special relativity [204]. Indeed, the standard light-cone in $1+1$ space-time reappears in this algebraic way for the hyperbolic numbers $\mathbb{D}$, in which $z, z' \in \mathbb{R}$, as shown in Fig. 6.2.

6.2.2. Representations

Matrix representation

As generically explained in Sec. D.2.2 of Appendix D, it is possible to map the algebra of the bicomplex numbers to the algebra of commutative 2×2 matrices with complex coefficients (a subalgebra of the algebra of 2×2 matrices which contains itself the algebra of complex numbers). The isomorphism is defined by

$$q = z_1 + jz_2 \rightarrow M_q = \begin{bmatrix} z_1 & z_2 \\ z_2 & z_1 \end{bmatrix}, \tag{6.10}$$

where the versors are represented by $1 \rightarrow \mathbb{1}$ and $j \rightarrow \sigma_x$ (we note by $\mathbb{1}$ the identity matrix and by σ_γ the $\gamma \in \{x, y, z\}$ component of the Pauli matrices). It is a straightforward calculation to show that the product of two arbitrary matrices M_q and $M_{q'}$ is commutative, $M_q M_{q'} = M_{q'} M_q$, and that the result of this product is consistent with the multiplication of two bicomplex numbers q and q' using the rules presented in Table 6.1.

Clearly, we can also map the algebra of the bicomplex numbers to the algebra of commutative 4×4 real matrices (a subalgebra of the algebra of complex 4×4 matrices). The isomorphism connecting both representations is given by

$$q = x_1 + iy_1 + jx_2 + ijy_2 \rightarrow \tilde{M}_q = x_1 M_1 + y_1 M_i + x_2 M_j + y_2 M_{ij}, \tag{6.11}$$

where the versors now have the matrix representation $M_1 \equiv \mathbb{1} \otimes \mathbb{1}$, $M_i \equiv \mathbb{1} \otimes (-i\sigma_y)$, $M_j \equiv \sigma_x \otimes \mathbb{1}$ and $M_{ij} \equiv M_i M_j$ (for the latter, we use the fact that for two matrices,

[12] Since the ring is commutative, obviously left and right zero divisors are equal and we shall simply refer to these elements of the ring as zero divisors.

[13] More precisely, the existence of singular bicomplex numbers is a consequence having non-trivial idempotent elements in the ring.

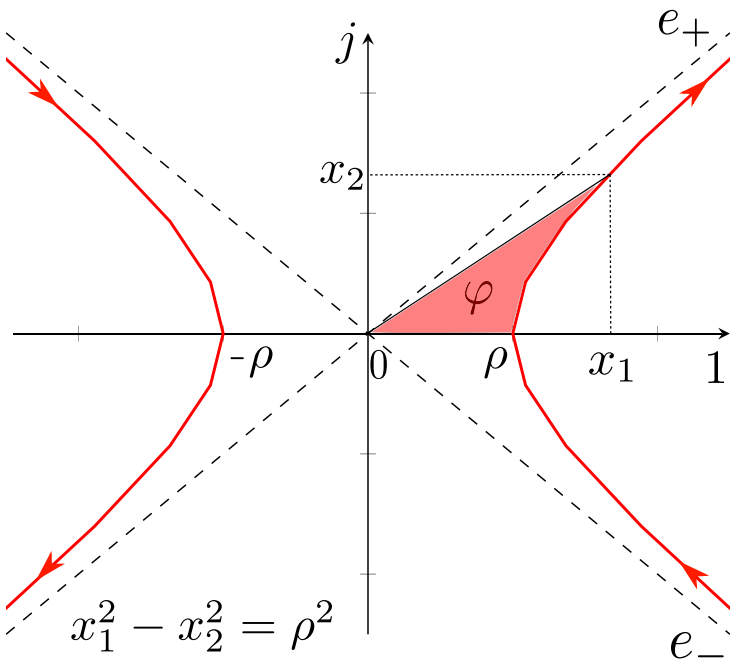

Figure 6.2 – Representation of the hyperbolic space using the basis $\{1, j\}$. This space is isomorphic to the pseudo-Euclidean Minkowski spacetime in $1+1$ dimensions with metric signature $(+,-)$. This is exemplified by the norm $\eta(q,q) \equiv \sqrt{|q|^2} = \sqrt{x_1^2 - x_2^2}$ where $\eta(\cdot,\cdot)$ is the Minkowski bilinear form or inner product. Note that the hyperbolas defined by the equation $\eta(q,q) = \rho$ with $-\infty < \varphi < +\infty$ are located in the space-like region of the Minkowski spacetime, the transition to the time-like region being forbidden because we have to approach and cross the light-cone (represented here by dashed straight lines).

$V = A_1 \otimes B_1$ and $W = A_2 \otimes B_2$, their tensor product is given by $V \otimes W = A_1 A_2 \otimes B_1 B_2$). The matrix representation of q, which in this context is called *characteristic matrix* [205], yields

$$\tilde{M}_q = \left[\begin{array}{c|c} A & B \\ \hline B & A \end{array}\right] = \begin{bmatrix} x_1 & -y_1 & x_2 & -y_2 \\ y_1 & x_1 & y_2 & x_2 \\ x_2 & -y_2 & x_1 & -y_1 \\ y_2 & x_2 & y_1 & x_1 \end{bmatrix} \tag{6.12}$$

This matrix has a block structure with 2×2 size blocks suggesting that this representation of the bicomplex ring is reducible. Indeed, as we will see in Sec. 6.2.2, this is actually the case since $\mathbb{B}$ can be seen as two independent copies of the complex plane embedded in a peculiar non-Euclidean space, *i.e.* $\mathbb{B} = \mathbb{C} \oplus \mathbb{C}$.

The matrix representations of the bicomplex numbers, (6.10) and (6.12), also show some nice advantages with respect to the standard or the complex tuple representations (6.4) and (6.5). First, they allow us to identify the subring of zero divisors since singular bicomplex numbers cannot be inverted and therefore their characteristic matrices (6.10) and (6.12) must have a vanishing determinant. Thus, singular bicomplex numbers are defined by the solutions of the equation

$$\det M_q = z_1^2 - z_2^2 = (z_1 + z_2)(z_1 - z_2) \stackrel{!}{=} 0 \tag{6.13}$$

which yields the condition $z_1 = \pm z_2$. This means that zero divisors have the complex

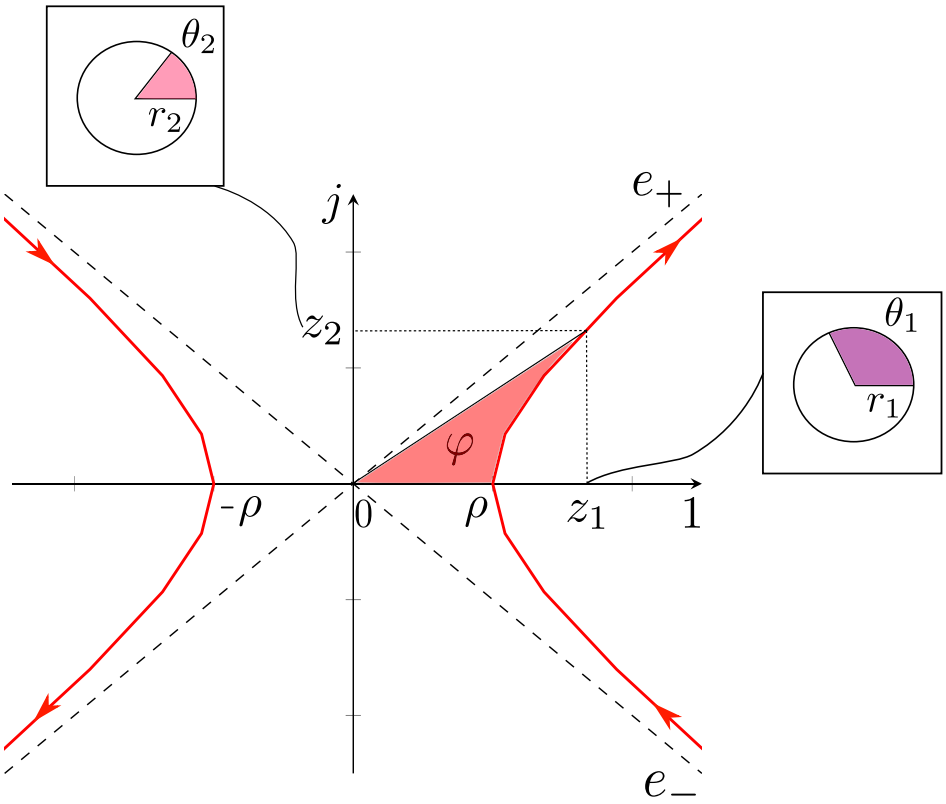

Figure 6.3 – Similarly to Fig. 6.2, the bicomplex numbers can be seen as an algebraic structure embedded in a hyperbolic space but now to each point of the space we associate a tuple of complex numbers (instead of real numbers). As such, we can understand the bicomplex module as a fibre (vector) bundle over the base manifold $\mathbb{D}$ in which the fibres are complex numbers, *i.e.* $\mathbb{B}$ is homeomorphic to $\mathbb{D} \times \mathbb{C}$. Note that figure is schematic in the sense that we do not know the position of z_1 and z_2 on each axis as complex numbers are not an ordered field.

matrix representation

$$M_q = \begin{bmatrix} z & \pm z \\ \pm z & z \end{bmatrix}, \tag{6.14}$$

or, considering the inverse map, $q = z(1 \pm j)$. This is the same result that we stated in Sec. 6.2.1: the pair of bicomplex numbers $q = z(1+j)$ and $q' = z'(1-j)$ with (complex) matrix representation M_q and $M_{q'}$ are zero divisors (note that we can check that $M_q M_{q'} = 0$). The complex planes defined by the equation $z_1 = \pm z_2$ form the subset of zero divisors within the bicomplex ring which we shall note by $\Xi \subset \mathbb{B}$. The set Ξ is sometimes called in the literature the *null-cone* [206, 207] due the similarities to the light-cone appearing in special relativity. A representation of Ξ in the hyperbolic space (in which z_1 and z_2 are purely real and Ξ is actually the light-cone) has been seen in Fig. 6.2 where it corresponds the dashed straight lines.

Second, and equally important, the matrix representation of a bicomplex number can be used to understand some intrinsic geometrical properties of the module (a full understanding can be gained only within the polar representation). In particular, the determinant of the characteristic matrix (or characteristic determinant) gives access to quantities

invariant under the allowed symmetry transformations (since it is itself an invariant). Using the representation of the algebra in terms of real matrices (6.12) and taking into account that, for a matrix with block structure, the determinant can be computed as $\det\tilde{M}_q = \det(A^2 - B^2) = \det[(A+B)(A-B)] = \det(A+B)\det(A-B)$ we get

$$\det\tilde{M}_q = [(x_1+x_2)^2 + (y_1+y_2)^2][(x_1-x_2)^2 + (y_1-y_2)^2], \tag{6.15}$$

which can be trivially connected to the complex representation as $\det\tilde{M}_q = |\det M_q|^2$. As anticipated, this is a form of degree four invariant under the isometries which will reappear along the next paragraphs.

Idempotent representation

As we said in Sec. 6.2.1, the bicomplex algebra presents singular elements and we have used in the previous paragraph the matrix representation to easily identify them. Amazingly, the singular elements in the bicomplex ring can be used to considerably simplify the bicomplex algebra when used as versors in a $\mathbb{C}\oplus\mathbb{C}$ decomposition. Inspired by Eq. (6.9) we define the following hyperbolic numbers

$$e_\pm \equiv \frac{1}{2}(1 \pm j), \tag{6.16}$$

which can be geometrically seen as the rotated counterparts (in the Euclidean sense) of the versors $\{1, j\}$ by an angle of $\pi/4$. It is straightforward to check that the sum of these hyperbolic numbers is equal to the multiplicative identity, *i.e.* $e_+ + e_- = 1$, and that their difference yields the hyperbolic unit, $j = e_+ - e_-$. As a consequence, we may write any bicomplex number (6.5) as

$$q = \sum_{\sigma=\pm} z_\sigma e_\sigma = z_+ e_+ + z_- e_-, \tag{6.17}$$

with $z_\pm = z_1 \pm z_2$. As before, each of the complex numbers $z_\pm$ with polar form $z_\pm = \rho_\pm \exp(i\theta_\pm)$, are independent variables defined in two apparently disconnected complex planes. The representation (6.17) is dubbed idempotent or orthogonal decomposition of the bicomplex number q and $\{e_+, e_-\}$ is the so-called idempotent basis. One can easily verify that the elements of this basis satisfy the relation $e_\sigma e_{\sigma'} = e_\sigma \delta_{\sigma,\sigma'}$ and are therefore idempotents (see Appendix D) and mutually annihilating. The last property also allows us to assign to this representation projective properties as

$$e_\sigma q = z_\sigma e_\sigma, \tag{6.18}$$

can be understood as the orthogonal projection onto one of the characteristic complex planes. Therefore, multiplication by one of the idempotent elements of the ring immediately gauges away half of the degrees of freedom of the bicomplex number[14]. We show the consequences of this projection in Fig. 6.4.

The representation (6.17) presents computational advantages with respect to the canonical representation used in Eq. (6.4), in particular with respect to the multiplication. This is so because the isomorphic table of products is diagonal so that the product of $q, q' \in \mathbb{B}$

[14]Note that if we multiply exclusively by the hyperbolic unit j the final result is a swap of the complex coordinates, as $jq = j(z_1 + jz_2) = z_2 + jz_1$.

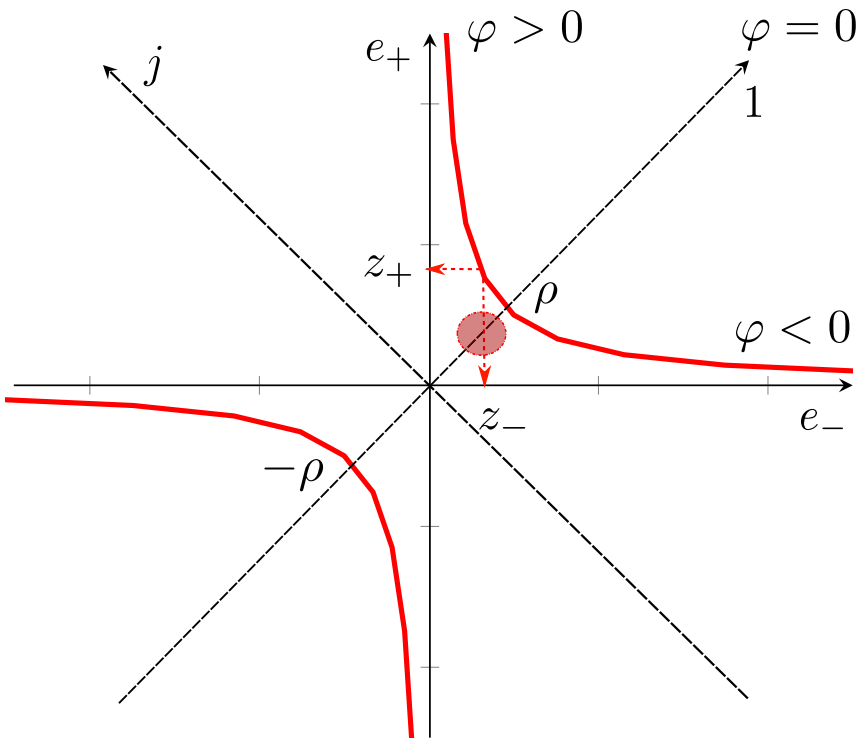

Figure 6.4 – Orthogonal projection of a bicomplex number $q = z_+e_+ + z_-e_-$ by performing the multiplication with the corresponding idempotent units. Note that the projection goes into the forbidden region Ξ and does not respect the intrinsic geometry of $\mathbb{B}$, since it modifies the modulus of the bicomplex number (in general q has a non-zero modulus while the projected components have a vanishing modulus, see next subsection). In the hyperbola defined in the first quadrant, we label the value of the hyperbolic angle φ, with the origin of coordinates being the single point in which it is not defined.

simply reads $qq' = z_+z'_+e_+ + z_-z'_-e_-$. As a consequence, the powers of any bicomplex number can be calculated effortlessly in this form as

$$q^n = z_+^n e_+ + z_-^n e_-, \tag{6.19}$$

which holds $\forall n \in \mathbb{Q}$ (and in particular, for $n = -1$ if the inverse of q exists). Moreover, it is also trivial to get the singular bicomplex numbers in this decomposition as they must have one of the components equal to zero, *i.e.* $q \in \Xi \Leftrightarrow z_+ = 0$ or $z_- = 0$. Consequently, the zero divisors of the bicomplex ring are given by the zeros of the characteristic complex planes. The point $q = 0$ is special since it corresponds to a singular term which belongs to the two complex planes as it satisfies simultaneously the equations $x_1 \pm x_2 = 0$ and $y_1 \pm y_2 = 0$.

Let us finish this section with the observation that the orthogonal representation also arises naturally in the matrix form of the bicomplex algebra. Indeed, one can see that the matrix representation in the idempotent basis corresponds to the spectral decomposition of Eq. (6.10), $\det(M_q - \lambda \mathbb{1}) = 0 \Rightarrow \lambda_\pm = z_1 \pm z_2$ with the normalized eigenvectors in the basis $\{1, j\}$ given by

$$\mathbf{v}_\pm = \frac{1}{\sqrt{2}} \begin{pmatrix} 1 \\ \pm 1 \end{pmatrix}. \tag{6.20}$$

The matrix representation of the idempotents is then obtained from the tensor product of each eigenvector with itself

$$e_\pm \to M_{e_\pm} = \mathbf{v}_\pm \otimes \mathbf{v}_\pm = \frac{1}{2}\begin{pmatrix} 1 & \pm 1 \\ \pm 1 & 1 \end{pmatrix}. \tag{6.21}$$

Polar representation

The polar decomposition is the third possible representation of a bicomplex number. We can define it by following the analogy to the polar form in $\mathbb{C}$ as

$$q = \rho \exp(i\theta_i) \exp(j\varphi) \exp(ij\,\theta_{ij}), \tag{6.22}$$

where $\rho \in [0, +\infty)$ is the modulus and the three associated arguments are given by the phases $\theta_i, \theta_{ij} \in [0, 2\pi)$ and $\varphi \in (-\infty, +\infty)$. Note that the first two arguments are circular angles and have to be defined in a compact interval [see Sec. 6.2.4] while the latter is defined in a non-compact space due its hyperbolic character. The relation between bicomplex polar and cartesian coordinates (both in the canonical and idempotent basis) can be obtained straightforwardly using Euler's formula

$$\rho = \sqrt[4]{q q^{*^i} q^{*^j} q^{*^{ij}}} = \sqrt[4]{|\mathrm{det} M_q|^2} = \sqrt{|z_+||z_-|} = \sqrt{\rho_+ \rho_-}, \tag{6.23a}$$

$$\theta_i = \frac{1}{2}\arctan\left[\frac{\mathrm{Im}\,(z_+ z_-)}{\mathrm{Re}\,(z_+ z_-)}\right] = \frac{1}{4i}\log\left(\frac{z_+ z_-}{z_+^* z_-^*}\right) = \frac{1}{2}(\theta_+ + \theta_-), \tag{6.23b}$$

$$\varphi = \frac{1}{2}\mathrm{arctanh}\left(\frac{|z_+|^2 - |z_-|^2}{|z_+|^2 + |z_-|^2}\right) = \frac{1}{4}\log\left(\left|\frac{z_+}{z_-}\right|^2\right) = \frac{1}{2}\log\left(\frac{\rho_+}{\rho_-}\right), \tag{6.23c}$$

$$\theta_{ij} = \frac{1}{2}\arctan\left[\frac{\mathrm{Im}\,(z_+ z_-^*)}{\mathrm{Re}\,(z_+ z_-^*)}\right] = \frac{1}{4i}\log\left(\frac{z_+ z_-^*}{z_+^* z_-}\right) = \frac{1}{2}(\theta_+ - \theta_-). \tag{6.23d}$$

Here in Eq. (6.23b) and (6.23d) we used the relation

$$\arctan x = \frac{1}{2i}\log\left(\frac{1+ix}{1-ix}\right), \tag{6.24}$$

while Eq. (6.23c) is obtained from the well-known identity $\tanh(ix) = i\tan x$. We note that the polar decomposition clearly shows that zero divisors, which have either $z_\sigma = 0$, present a vanishing modulus, $\rho = 0$, with hyperbolic phase $\varphi = \pm\infty$. A unique phase singularity in the four dimensional space is located at the origin, $q = 0$, where $\rho = 0$ and neither of the circular or the hyperbolic angles are defined.

The polar form is certainly preferred to the two previous ones (matrix and idempotent representations) to fully understand the intrinsic geometry of the bicomplex module [205]. This geometry, which is naturally present in any hypercomplex algebra, is characterized by the invariants (under the allowed transformations of the modular group[15], Γ) of the characteristic matrix, *i.e.* the trace and the determinant. Modular / unimodular geometrical transformations can therefore be understood in the present context as the generalization

[15]The modular group Γ of order n [209], also denoted $\mathrm{GL}_n(\mathbb{Z})$, can be represented by all the matrices of dimension n with integer entries and determinant equal to ± 1. When working over an arbitrary ring $\mathcal{R}$ instead of $\mathbb{Z}$, unimodular usually refers to matrices whose determinant is equal to the unity in the ring, $\pm 1_\mathcal{R}$.

of orthogonal transformations, which preserve the distance function in a Euclidean vector space, to any given algebra. Likewise, we can think of these matrices as elements of a generalized rotation group in an hypercomplex non-Euclidean algebra[16]. In general, any element of the modular group U_Γ presents $n-1$ free parameters, the reduction of -1 coming from the condition of unimodularity: $|\det U_\Gamma| = 1$. If, in addition, we consider the translations in the n-dimensional module, we arrive to the conclusion that the group of isometries, describing distance-preserving maps in the hypercomplex algebra, has $2n-1$ degrees of freedom. Distance-preserving maps also fix the topology of the metric space and this metric can be obtained from the corresponding invariant form of degree n [205].

For the bicomplex algebra over $\mathbb{B}$, we therefore have $n = 4$, which yields three free parameters related to generalized rotations (as $\rho = 1$ by the unimodularity condition). The metric can be related to the determinant of the matrix $\tilde{M}_q$ which defines a quartic form invariant under geometrical transformations of the four-dimensional unimodular multiplicative group. The three remaining parameters will then appear as phases describing generalized rotations in the polar representation (6.22). In the bicomplex algebra, two of the rotations are circular rotations describing the motion of a point along a circle of constant radius while another is a hyperbolic rotation or boost where the translation is performed along an hyperbola of constant focal radius (as a difference to the circle, the path here is an open curve). We may represent this transformation simply by $q' = U_\Gamma\, q$ where

$$U_\Gamma = \exp\left[i\theta_i + j\varphi + ij\theta_{ij}\right]. \tag{6.25}$$

Distance preserving maps are therefore given by $q \to q' = U_\Gamma\, q + Q$ with $Q \in \mathbb{B}$ non-singular describing the four dimensional translations (there are, then, seven degrees of freedom). For $Q = 0$, we may also check that the combinations of the form $q_0 q_1^{*^i} q_2^{*^j} q_3^{*^{ij}}$ with arbitrary $q_\alpha \in \mathbb{B}$ for $\alpha \in \{0,1,2,3\}$ are preserved under isometries and can be related to the invariant quartic form $\det\tilde{M}_q$ whenever $q_0 = q_1 = q_2 = q_3$. As a consequence, they must represent a scalar in the algebra to which we can associate a quartic "scalar product". This observation will prove crucial in Sec. 6.2.4 in order to define a (functional) scalar product in the bicomplex Hilbert space which affects the wave function probability distribution.

6.2.3. Bicomplex rings and modules

Let us now analyze the structure of the bicomplex ring and the bicomplex module from the abstract algebra point of view. From the considerations depicted previously in Sec. 6.2.2, we know that the zero divisors represent an important subset of the bicomplex ring and that they are not randomly scattered, but are always well-localized at the null-cone. Moreover, according to Sec. 6.2.2, any zero divisor will also have one of the two complex coordinates equal to zero, univocally identifying which of the idempotents is used to perform the projection to the null-cone. These two observations suggest to define the following subrings

$$\mathcal{I}^\pm = \{q \in \mathbb{B} \,|\, z_\pm = 0\}, \tag{6.26}$$

which exclusively contain zero divisors with z_+ (resp. z_-) coordinate equal to zero. The subrings $\mathcal{I}^\pm$ are ideals of the bicomplex ring. As commented previously, both ideals intersect at a single point, $\mathcal{I}^+ \bigcap \mathcal{I}^- = \{q = 0\}$, the zero element of the full ring. The null-cone

[16] If the algebra is commutative and its dimension is higher than 2, it must be unavoidably non-Euclidean [205].

is obtained as the union of the two ideals, $\Xi = \mathcal{I}^+ \bigcup \mathcal{I}^-$. The whole subset Ξ can therefore be seen as the natural extension of the zero element $0 \in \mathbb{C}$ to the bicomplex space [206] and contains all singular bicomplex numbers. The set $\tilde{\mathbb{B}} = \mathbb{B} \setminus \Xi$ presents only elements of the bicomplex ring with a multiplicative inverse, being the natural domain for the study of analytic functions of bicomplex variable (see next section).

The subrings $\mathcal{I}^{\pm}$ also satisfy the following properties:

- The two subrings are proper ideals of the ring $\mathbb{B}$ since $\forall q \in \mathbb{B}$ and $i \in \mathcal{I}^{\pm}$, we have $iq = qi \in \mathcal{I}^{\pm}$.
- The two ideals are principal since they are generated by a unique element in the hyperbolic space (each of the idempotents $e_{\pm}$). These versors project any bicomplex number onto the correspondent ideal ring as shown by Eq. (6.18).
- Both ideals are also prime. Indeed, if for two arbitrary elements of the ring q, q' we have $qq' \in \mathcal{I}^{\pm}$ then either q or q' (or both) are elements of a single subring $\mathcal{I}^{\pm}$.
- The proper ideals in the bicomplex ring are maximal according to Def. 9 in Appendix D. Moreover, since $\mathcal{I}^+ \oplus \mathcal{I}^- = \mathbb{B}$ they are also comaximal.
- Finally, Theorem 4 in Appendix D is also satisfied because the full ring is commutative and the ideals are fields (the coefficient of the generator in each ideal is a complex number).

The module structure in the ring $\mathbb{B}$ can be very easily accomplished if we consider the multiplication by a scalar in the following way: for $q \in \mathbb{B}$ and $\lambda \in \mathbb{R}$, $\lambda q = \lambda x_1 + i(\lambda y_1) + j(\lambda x_2) + ij(\lambda y_2)$ while if $\lambda \in \mathbb{C}$ we simply have that $\lambda q = \lambda z_1 + j(\lambda z_2)$. This module clearly presents a non-empty basis with basis vectors $\{1, i, j, ij\}$ and $\{1, j\}$ for each representation respectively, when thought as a generalized vector space over $\mathbb{R}$ or $\mathbb{C}$. Note that in either case the module can be seen as a free module over the real or complex numbers but with a particular intrinsic non-Euclidean geometry explained in Sec. 6.2.2 (note that this is equivalent to say that the module will never be isomorphic to an Euclidean space over $\mathbb{R}$ or $\mathbb{C}$).

6.2.4. Bicomplex functional analysis

Gathering all our understanding of the bicomplex algebra we are now in position to extend these results to functions and Hilbert spaces that are built using the bicomplex module. Therefore, in this section, we analyze in detail the most important points related to the notions of bicomplex function, derivative, integral and scalar product, correcting previous misconceptions which can be found in the literature. Note that the choice of an appropriate scalar product, verifying both the constraints imposed by the geometry of the bicomplex space and quantum mechanics, is crucial in order to understand how the well-known probabilistic nature of the wave function in quantum theory is preserved in our formalism.

Bicomplex analytic functions

A bicomplex function f, defined in a domain $\Omega \subset \mathbb{B}$ is a mapping from the subset Ω in the bicomplex module to another subset of $\mathbb{B}$, $f : \Omega \to \Omega' \subset \mathbb{B}$. Let us take,

without any loss of generality, $\Omega = \Omega' = \tilde{\mathbb{B}}$. By analogy to complex-valued functions, any bicomplex function may be written as a bicomplex combination of four real-valued functions, $f_\alpha : \Omega \to \mathbb{R}$ for $\alpha \in \{1, i, j, ij\}$,

$$f(q) = f_1(q) + if_i(q) + jf_j(q) + ijf_{ij}(q). \tag{6.27}$$

As such, we can generalize results of 2D complex analysis to a four-dimensional function space. For example, a bicomplex function is said to be analytic in the open set Ω if $\forall q_0 \in \Omega$ it admits a locally convergent Taylor series representation

$$f(q) = \sum_{n=0}^{+\infty} f_n (q - q_0)^n \quad \text{with} \quad f_n \in \tilde{\mathbb{B}}. \tag{6.28}$$

Using the idempotent decomposition [in which we know that versors are (hyperbolic) orthogonal and idempotent, $e_\sigma e_{\sigma'} = e_\sigma \delta_{\sigma,\sigma'}$] and assuming $q_0 = 0$ for simplicity we also have

$$f(q) = \sum_{\sigma=\pm} f_\sigma(z_\sigma) e_\sigma, \tag{6.29}$$

where the functions $f_\sigma(z_\sigma)$ are analytic functions of a complex variable in the complex plane. Notably, the functions $f_+(z_+)$ and $f_-(z_-)$ are not independent from each other: for the function f to be analytic in the bicomplex function space, the projected components $f_\sigma(z_\sigma)$ cannot be zero simultaneously for any q. These properties, which can be interpreted as a trace of the correlations between the two quasi-independent complex coordinates induced by the non-Euclidean metric, allow us to write spatial singularities characterized by vortices in the four-dimensional space. Physical quantities defined by these objects will then be expected to be robust to strong perturbations which do not affect the manifold topology.

We note that additional constraints in the form of the functions can appear when the codomain is restricted to a subfield of the bicomplex numbers such as $\mathbb{C}$ or $\mathbb{R}$. For instance, if $f(q) \in \mathbb{C}$ then $f(q) = f^{*^j}(q) \Rightarrow f_\sigma(z_\sigma) = f_{-\sigma}(z_{-\sigma})$ and therefore, after using the relation $e_+ + e_- = 1$, we find $f(q) = f_+(z_+) = f_-(z_-)$. This means that the function exclusively lives in one of the characteristic complex planes or that f is a projection into one of the characteristic planes (note that this is not a projection onto Ξ as the hyperbolic nature has disappeared thanks to the completeness of the idempotent basis). Furthermore, if $f(q) \in \mathbb{R}$, we additionally have to fulfill the condition $f(q) = f^{*^i}(q)$ and therefore $f_\sigma(z_\sigma) = f^*_\sigma(z_\sigma)$. The latter is just the analogous restriction found in complex functions when their codomain is the real line.

Differential and integral calculus

We shall devote this subsection to correctly take care of the derivative and integral operations in the space of functions of bicomplex variable. To begin with, let us briefly discuss the differentiation operation. From the properties of the bicomplex module, which is built as a distinctive union of two copies of the complex plane, it is natural to expect that local operations (in which the role of the forbidden null-set is not important) such as the derivative, defined by a limit that approaches some value, work similarly to those in the complex plane [205, 206]. As a consequence, it is possible to derive a set of Cauchy-Riemann equations to be used to characterize any holomorphic function (that can be expanded in a Taylor series) in the bicomplex functional space.

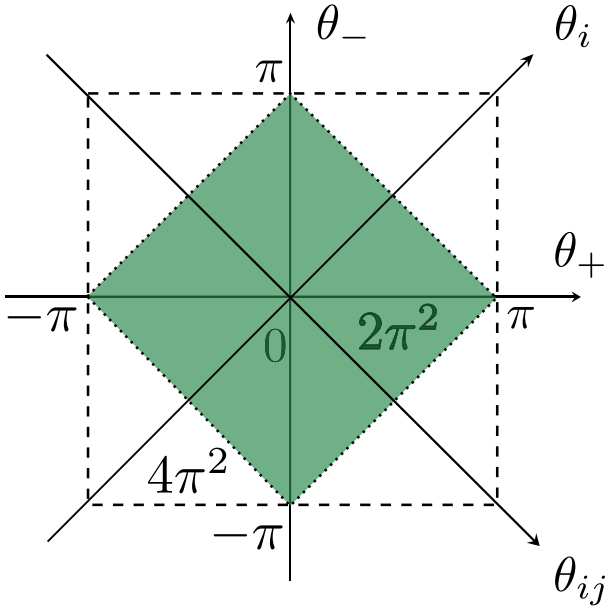

Figure 6.5 – Integration domain for the circular angles. The angles $\theta_\pm$ related to the complex coefficients $z_\pm$ appearing in the idempotent representation vary between $-\pi$ and π, defining the dashed square of area $4\pi^2$. On the other hand, θ_i and θ_{ij} are defined in the rotated green squared region which presents half of the surface, $2\pi^2$.

Now, although the properties of the derivative are well-known (we suggest the reader to check, for instance, Ref. [205]) this is not the case with the integral which is not even defined in the literature. In order to introduce the integration procedure in the non-Euclidean bicomplex functional space, we first discuss the geometrical properties of the integral operation correctly taking into account the space topology (and the associated metric). The integrals are then calculated from a practical "physicist's approach" using the method described in Appendix F. To begin with, we recall that the proper way to describe the space topology is to consider polar coordinates which have been defined in Sec. 6.2.2. The polar coordinates also allow us to easily get rid of the zero divisors, as they present vanishing modulus, and preserve the non-Euclidean correlations of analytic functions. Any four-dimensional integration of a bicomplex-valued function can therefore be calculated using one of the following set of variables

$$\begin{aligned}\int d^4\mathbf{r} &= \int d^2\mathbf{r}_1 \int d^2\mathbf{r}_2 = \frac{1}{4}\int d^2\mathbf{r}_+ \int d^2\mathbf{r}_- \\ &= \int_0^{+\infty} d\rho\, \rho^3 \int_{-\infty}^{+\infty} d\varphi \int d\theta_i \int d\theta_{ij},\end{aligned} \tag{6.30}$$

where the last line is obtained using the change of coordinates described the Appendix E.1.

Let us first discuss the consequences of the integration over the circular degrees of freedom. According to the transformation defined in Eqs. (6.23b) and (6.23d), we can relate the angular parameters θ_i and θ_{ij} (which present intricated integration limits) to $\theta_\pm \in [-\pi, \pi)$ [here, we remind that the complex numbers $z_\pm$ are written in polar coordinates as $z_\pm = \rho_\pm \exp(i\theta_\pm)$]. This transformation takes place only in the characteristic complex planes and, therefore, it does not introduce any zeros into the Jacobian, $J(\rho, \theta_i, \varphi, \theta_{ij}) = \rho^3$.

An alternative way of looking at this is to notice that the circular angles are related only to $\theta_\pm$ [remember that $\theta_\pm = 2(\theta_i \pm \theta_{ij})$] while the pair (ρ, φ) defined in Eqs. (6.23a) and (6.23c) can be written in terms of the modulus $\rho_\pm$ [by using the relations $\rho = \sqrt{\rho_+\rho_-}$ and $\exp\varphi = \sqrt{\rho_+/\rho_-}$]. The coordinate transformation $\{\theta_i, \theta_{ij}\} \to \{\theta_+, \theta_-\}$ yields

$$\int d\theta_i \int d\theta_{ij} = \frac{1}{2}\int_{-\pi}^{\pi} d\theta_+ \int_{-\pi}^{\pi} d\theta_-, \tag{6.31}$$

or $J(\rho, \theta_+, \varphi, \theta_-) = \rho^3/2$, so that change of variables in the circular angles will simply multiply the "old" Jacobian by a constant factor of $1/2$.

We tackle now the integration problem in the hyperbolic space $\mathbb{D}$. Our goal here is to define a mathematically consistent and coherent integration rule in a non-Euclidean hyperbolic space for functions with $\varphi \neq 0$ (as if $\varphi = 0$ no hyperbolic correlations are present and the integrals can be calculated using the variables $\mathbf{r}_1, \mathbf{r}_2$ or $\mathbf{r}_+, \mathbf{r}_-$). This integration is strongly constrained by the presence of the set of zero divisors in the bicomplex module, Ξ, which are forbidden zones of the module as it happens in special relativity with the light-cones. The main reason is that this set is not a null set[17]. In addition, the set can be understood as a kind of generalization of the branch cut singularities in the complex plane where analytic functions are not defined. The null-cone Ξ divides then the hyperbolic plane into four simple connected domains where the natural curves are oriented hyperbolas of radius ρ. These subspaces exclusively contain regular elements of $\mathbb{B}$ and, in each domain, the integration has to be performed independently taking into account the orientation of the open paths. The orientation of the hyperbolas can be easily found using the hyperbolic polar coordinates, $x_\pm^\lambda = \lambda\rho\exp(\pm\lambda\varphi)$ with $\lambda = \pm$ a branch index which takes the value $-$ for the left branch and $+$ for the right branch. The resulting orientated integration paths are shown in Fig. 6.6.

For practical purposes, we now perform a rotation in this space and focus on the idempotent representation [despite this, observe that we do not introduce $\rho_\pm$ to keep the long-range (topological) correlations in the non-Euclidean space]. This is done to define a parametrization of the open contours in order to simplify integration over the curve. In addition, it is easy to be convinced by looking at Fig. 6.7 that the easiest integration path is a deformed hyperbola which almost coincides with the idempotent axis. However, we already explained that these axis correspond to the null-cone which contains the zero divisors and the region has therefore to be avoided [it is a subspace of the bicomplex space where the Jacobian (E.3) vanishes and transformation to polar coordinates is not allowed]. To overcome the difficulty of projection onto the idempotent axis, we follow a procedure sketched in Fig. 6.7: we deform conformally the integration paths. A conformal mapping will preserve the hyperbolic angles locally and, as a consequence, the volume element (so that the value of the integral remains unchanged). We also show this map in Fig. 6.7

[17] We say that a set A is a null set or a set of measure zero if it is in some sense "negligible". This kind of sets can be ignored when performing certain mathematical operations such as Lebesgue integrals. For example, consider a 2D plane and remove from it an infinite straight line. This infinite set of points is of measure zero since the 2D plane remains invariant. Another example comes from the Lebesgue integration theory (ubiquitous in the mathematical framework of quantum mechanics when dealing with distribution functions). Given a space where a positive measure function μ exists [239] the Lebesgue integral of a function f over a subset such that $\mu(A) = 0$ satisfies

$$\int_A f d\mu = 0.$$

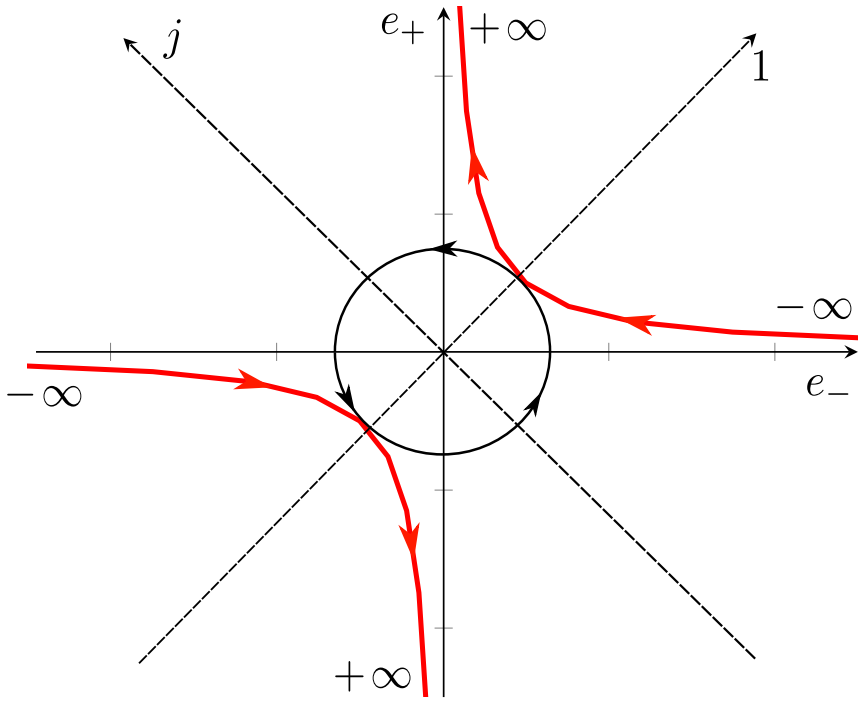

Figure 6.6 – Orientated integration paths (red solid curves) in the hyperbolic module $\mathbb{D}$ represented in the idempotent basis (the basis $\{1, j\}$ is also given for comparison). Each hyperbola is described by a fixed radius ρ and an angular parameter defined in the interval $\varphi \in (-\infty, +\infty)$. We also give as a benchmark the oriented integration contour of a closed circular path in $\mathbb{C}$. Comparison of the orientation suggests that the orientation of the allowed paths in the spaces $\mathbb{C}$ and $\mathbb{D}$ have to be compatible in order to define a well-behaved globally oriented integration path in the bicomplex module.

where the two red-shaded hyperbolic sectors have the same area and can be mapped by a conformal map (which in this context is called squeeze map). To properly define the projection, we consider an infinitesimal φ and two deformed hyperbolas in the plane. We then define a closed integration contour with two straight lines which connect the two hyperbolas. The orientation of the paths shows that the contribution from the straight segments vanishes while the two hyperbolas get connected only changing the circulation along the integration path (this is equivalent to use a Cauchy integral formula for analytic functions in the hyperbolic space as in Ref. [227]). If, at this moment, we completely deform the hyperbola to be infinitesimally close to the idempotent axis the result is the following integration rule

$$\int_{-\infty}^{+\infty} d\varphi f(\rho, \varphi) = \sum_{\sigma=\pm} e_\sigma \int_{-\infty}^{+\infty} d\varphi \, \Theta(\sigma\varphi) f(\rho, \sigma\varphi), \tag{6.32}$$

where $\Theta(\varphi)$ is the Heaviside step function [$\Theta(\varphi) = 0$ if $\varphi < 0$ and $\Theta(\varphi) = 1$ if $\varphi \geq 0$], the notation $f(\rho, \sigma\varphi)$ means that the function has been projected to the idempotent axis (so that we got rid of the hyperbolic unit transferred to the idempotents) and we defined the function

$$f(\rho, \varphi) \equiv \int d\theta_i \int d\theta_{ij} f(q). \tag{6.33}$$

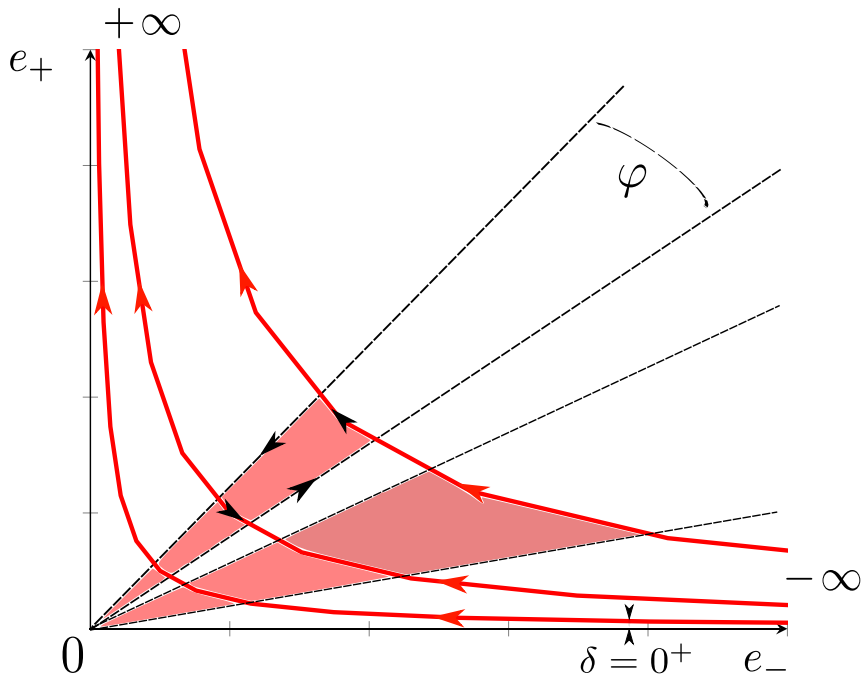

Figure 6.7 – Conformal mapping in the bicomplex space: the hyperbolas approach the idempotent axis conformally as the radius ρ is varied but without touching them (they remain at a distance $\delta = 0^+$). The red-shaded hyperbolic sectors both have the same area and can be mapped through a squeeze map [226]. For an infinitesimal sector of angle φ, we can move from one hyperbola to another by only changing the orientation of the path. The combination of the two observations allows us to define the integration rule in the hyperbolic space given in Eq. (6.32).

Note that Eq. (6.32) points out to a delicate fact of the idempotent representation and bicomplex integration. First, the projection onto the idempotent basis and the integration are global operations which do not commute and have to be performed in a very specific order. This fact was misconceived in Refs. [225, 207] where the authors consider that the projection onto the idempotent axis as if no hyperbolic correlations existed in the bicomplex space.

Inner product

At this point, we are also in position to discuss the metric structure of the bicomplex space and introduce the notion of functional scalar / inner product. This concept is crucial to correctly define a Hilbert space[18], which is the underlying mathematical playground of quantum mechanics. When built over the bicomplex ring, this mathematical object has been incorrectly treated in the literature, mainly because the non-Euclidean geometry was not properly defined as the hyperbolic correlations were missing (see Refs. [206, 207] and [225]).

The first observation to be made when looking for the correct expression of the bi-

[18] A Hilbert space is a complete vector space (a Banach space where any function can be expanded in a series such as any Cauchy sequence converges [239]), usually of infinite dimension, which possesses a scalar product law, that yields an induced metric and a norm.

complex functional scalar product is that the invariant form in the bicomplex algebra is a quartic form[19]. As a consequence, the natural distance function which gives to the space of functions the structure of a metric space is not quadratic. This distance function defines a natural or metric topology in the functional space which also has to be compatible with the intrinsic geometry of the bicomplex module. At the same time, we would still like to preserve all the basic properties of a distance function induced by any (linear) scalar product (that is, symmetry, positive definiteness and, in particular, the triangle inequality). Nevertheless, it can be seen that to preserve the triangle inequality, the inner product and the induced metric have to be bilinear forms [239]. Fortunately, we have found that there is a (unique) way of reconciling both situations: this is the following scalar product law

$$\langle f|g\rangle = \int d^4\mathbf{r}\, f^{*^i}(\mathbf{r})g(\mathbf{r}), \tag{6.34}$$

where we have used standard bra-ket notation. This is an inner product which possesses the same form as the inner product in the standard space of squared integrable functions used in quantum mechanics but defined in $\mathbb{B}$ with target space being also $\mathbb{B}$. Note that we can recover an expression invariant under isometries if we constrain the form of the functions f and g to be bilinear forms in the bicomplex variable q [then, as as a consequence, the functional inner product generates the desired quartic form in the bicomplex variable (see also Sec. 6.3.2)]. Finally, we would like to stress that, given Eq. (6.34) it is not obvious how we can get a positive real norm $\langle f|f\rangle \geq 0$, as desired to satisfy the properties of the scalar product. Nonetheless, we will show in Sec. 6.3.2 that for the set of wave functions that diagonalize the free Hamiltonian this is always the case and the norm is always real. The problem of coming back to $\mathbb{R}$ or $\mathbb{C}$ from $\mathbb{B}$ can nevertheless appear in more complex observables as a consequence of the choice of the scalar product (for example, see the discussion about the matrix elements of the potential in Sec. 6.4.1).

6.3. Two-Body Vortex States

6.3.1. Hamiltonian operator in the bicomplex vortex representation

As already mentioned in Sec. 6.1, a potential solution, exclusive to four dimensions, to develop a vortex theory for the two-body problem is to consider the bicomplex algebra described in detail in Sec. 6.2. To that purpose, we consider the bicomplex coordinate $q = (x_1 + iy_1) + j(x_2 + iy_2) = z_1 + jz_2$ built up from the complex coordinates of each of the members of the pair, *i.e.* $z_j = x_j + iy_j$ with $j \in \{1, 2\}$. Within this approach, the position of the two electrons in the electronic pair is topologically correlated via the non-Euclidean metric from the choice of variables that describe the pair. Note that, for this combination, the idempotent representation naturally encodes the center-of-mass and relative coordinates of the electronic pair. The Hamiltonian (6.2) can then be written in terms of the variables q (and its conjugated counterparts $q^{*^i}, q^{*^j}, q^{*^{ij}}$) using the linear transformation detailed in Appendix E.2

$$\hat{\mathcal{H}}_0^{(N=2)} = \frac{\hbar\omega_c}{2}\Big[-8l_B^2\Delta + \frac{1}{8l_B^2}\left(qq^{*^i} + q^{*^j}q^{*^{ij}}\right) + \left(q\partial_q - q^{*^i}\partial_{q^{*^i}}\right) + \left(q^{*^j}\partial_q^{*^j} - q^{*^{ij}}\partial_{q^{*^{ij}}}\right)\Big]. \tag{6.35}$$

[19] Sometimes the term "Finslerian" as related to Finsler geometry is used [208].

Here, the bicomplex Laplacian operator takes the form

$$\Delta = 8\left(\partial_q \partial_{q^{*i}} + \partial_{q^{*j}} \partial_{q^{*ij}}\right), \tag{6.36}$$

and we have used that

$$\mathbf{r}_1^2 + \mathbf{r}_2^2 = \frac{1}{2}\left(\mathbf{r}_+^2 + \mathbf{r}_-^2\right) = \frac{1}{2}\left(qq^{*^i} + q^{*^j} q^{*^{ij}}\right), \tag{6.37}$$

for $\mathbf{r}_\pm = \mathbf{r}_1 \pm \mathbf{r}_2$ (each coordinate is the vector representation in $\mathbb{R}^2$ of the complex numbers $z_\pm$).

It is clear that Eq. (6.35) is composed of two separable parts which are mutually hyperbolic conjugate

$$\hat{\mathcal{H}}_0^{(N=2)} = \hat{\mathcal{H}}(q, q^{*^i}) + [\hat{\mathcal{H}}(q, q^{*^i})]^{*^j}. \tag{6.38}$$

This points out to an additional degeneracy in the eigenvalues of the problem $\hat{\mathcal{H}}_0^{(N=2)}\Psi = E\Psi$ as the eigenenergies of the Hamiltonian are real numbers, $E = E^{*^j}$. The degeneracy comes from the fact we map the original (complex) Hilbert space to a new (bicomplex) Hilbert space where the Hamiltonian is written in the bicomplex variables. The map, however, is not one-to-one but we have instead extended the space of solutions of Schrödinger equation to allow new types of quantum states to be eigenstates of the Hamiltonian operator. We can also be tempted to think that this seemingly innocent change of coordinates is analogous to the mathematical trick, well-known in solid-state physics, in which we look for a complex solution to the equation of motion for the wave function even if the Hamiltonian is purely real. However, in the present case, the extension of the Hilbert space has also modified the topology of the state space, which is no longer Euclidean, and introduced the zero divisors mentioned in Sec. 6.2. As a consequence, we may expect new physics to appear which otherwise would never be obtained by exact numerical diagonalization of the original Hamiltonian.

We also want to remark here that the procedure of extending the Hilbert space by increasing the dimension is not something unknown in standard quantum mechanics. For example, this is a very useful technique in the toolkit of quantum information physicists where it forms part of a method called purification of mixed states [214]. Purification refers to the fact that to any mixed state in a finite-dimensional Hilbert space, a pure state defined in a higher dimensional Hilbert space can be associated, the statistical mixture appearing by the reduction of the latter by means of a partial trace operation. From a different perspective, the enlargement of the Hilbert space is also needed in the Hamiltonian theory of the fractional quantum Hall effect (see Ref. [215] or Sec. 5.2.4). In this case, we have to include new degrees of freedom (the pseudovortices attaching $2m$ flux quanta to the electron in the lowest Landau level) which combine with the single electrons to build the composite fermion. Furthermore, transformations in the topology of the Hilbert space (and its related metric) are also known to be possible at least in the context of high-energy physics (in particular, in quantum gravity [217] and topological quantum field theories [218, 219]). In this case, it has been shown under very general conditions that the topology of the Hilbert space can be altered smoothly by an appropriate choice of additional degrees of freedom which control the boundary conditions for the operators in the phase space. As such, changes in these boundary conditions, which are preserved under unitary transformations, allow the interpolation between Hilbert spaces built over topologically distinct manifolds (this is not at all surprising since the transformation of the

base space manifold naturally has to affect the corresponding Hilbert space). The relation between the vector space (the wave function) and the topology of the phase space (global geometrical properties of the manifold) is deep and indeed it has been suggested [220] that the connection between the elements of any quantum theory built on the former and the topology of the differential manifold is a topological quantum field theory which acts as a homomorphism between the two mathematical structures[20].

Finally, we note that the ideas of using a new metric different, from the Euclidean one, have also started to percolate into the community devoted to the theoretical study of the fractional quantum Hall effect. For instance, recent works have suggested that the wave functions which describe the quantum liquid in this regime may not be rotationally invariant (see also the discussion above) but can present a geometrical degree of freedom related to the guiding center coordinates. This freedom can be interpreted as the signature of an intrinsic non-Euclidean metric [222, 223]. As such, the well-known trial wave functions (Laughlin or Read-Rezayi, for instance) can be generalized to a family of states that define a topological family characterized by some unimodular metric tensor.

6.3.2. Bicomplex vortex eigenstates

Once we are equipped with all the machinery of bicomplex numbers, diagonalization of the free two-body Hamiltonian is an easy task. Indeed, it can be shown by solving the Schrödinger equation that the (non-normalized) two-body bicomplex vortex states

$$\begin{aligned}\Psi_{n,m}(\mathbf{r}) &\propto q^n (q^{*^{ij}})^m \exp\left[-\frac{1}{8l_B^2}\left(qq^{*^i} + q^{*^j} q^{*^{ij}}\right)\right] \\ &= \rho^{n+m} \exp\left[i(n-m)\theta_i\right] \exp\left[j(n-m)\varphi\right] \exp\left[ij(n+m)\theta_{ij}\right] \qquad (6.39) \\ &\times \exp\left[-\frac{|z_+|^2 + |z_-|^2}{4l_B^2}\right], \qquad (6.40)\end{aligned}$$

are eigenstates of Hamiltonian (6.35) with eigenenergies $E_n = \hbar\omega_c(n+1)$. The composite pair position $q = \sum_{\sigma=\pm} z_\sigma e_\sigma$ is represented here as a 4D vector $\mathbf{r} = (\mathbf{r}_+, \mathbf{r}_-)$. The bicomplex vortex states present a polynomial part characterized by two integers $(n, m) \in \mathbb{N}^2$, the first integer n being associated to a vortex in the variable q and the second integer m appearing in an *anti*vortex in the hyperbolic conjugate counterpart[21]. Both integers evidently and necessarily characterize the phase singularity (topological defect) in the four-dimensional bicomplex module which appears whenever $\rho = 0$ together with the undefined arguments θ_i, φ and θ_{ij}. In addition, the wave function presents the common Gaussian factor that multiplies the polynomials in q and $q^{*^{ij}}$, and can be decomposed in a product of Gaussians affecting exclusively either qq^{*^i} and the hyperbolic conjugate counterpart. Note that this decomposition of Eq. (6.39) into a product state in which hyperbolic conjugate variables are separated (as well as the integer n and m, by the way) follows immediately from Eq. (6.38) and it is a consequence of the fact that the original Hamiltonian is complex.

As for the one-body vortex states, the complete family of coherent bicomplex vortex states is generated upon translation of coordinates in the bicomplex Hilbert module. Note that, due to the direct sum structure of the bicomplex algebra (associated to the ideals $\mathcal{I}^{\pm}$

[20] Until a recent proof was found this map was known as the cobordism hypothesis [221].

[21] Note that, as discussed in the subsection where the inner product was defined this wave function respects the non-Euclidean metric of the Hilbert space when computing scalar products using Eq. (6.34), as two wave functions generate the quartic form $q_0 q_1^{*^i} q_2^{*^j} q_3^{*^{ij}}$ up to a real factor.

of the bicomplex ring), or equivalently, because of the structure of the Gaussians in Eq. (6.39), we can perform this translation independently in each of the characteristic complex planes. As such, the Gaussian part is formally equivalent to that of the one-body vortex states (1.43) and, using the following identity,

$$16 \int \frac{d^4\mathbf{r}}{(2\pi)^2}\, q^n (q^{*^i})^n (q^{*^j})^m (q^{*^{ij}})^m \exp\left[-\left(q q^{*^i} + q^{*^j} q^{*^{ij}}\right)\right] = n!m!, \tag{6.41}$$

which is proven in Appendix F, we can immediately write the normalized two-body vortex wave function

$$\Psi_{n,m,\mathbf{R}}(\mathbf{r}) = \frac{1}{(2\pi l_B^2)^2} \frac{1}{\sqrt{n!m!}} \left(\frac{q-Q}{2l_B}\right)^n \left(\frac{q^{*^{ij}} - Q^{*^{ij}}}{2l_B}\right)^m \times \exp\left[-\frac{q q^{*^i} + q^{*^j} q^{*^{ij}} + Q Q^{*^i} + Q^{*^j} Q^{*^{ij}} - 2q^{*^i} Q - 2q^{*^{ij}} Q^{*^j}}{8 l_B^2}\right]. \tag{6.42}$$

The bicomplex vortex states, written as $\Psi_\nu(\mathbf{r}) = \langle \mathbf{r}|\nu\rangle$ using the Dirac notation are labeled by the collection of quantum numbers $\nu = \{n, m, \mathbf{R}\}$ where $n \geq 0$ is the Landau level of the pair and the degeneracy is given both by the integer $m \geq 0$ and the bicomplex number $\mathbf{R} = (\mathbf{R}_+, \mathbf{R}_-) \in \tilde{\mathbb{B}}$ with $\mathbf{R}_\pm = \mathbf{R}_1 \pm \mathbf{R}_2 \in \mathbb{R}^2$. The latter vector characterizes the position of the zeroes of the wave function that lie in the regular part of the four-dimensional bicomplex space (*i.e.* it characterizes the topological defect or vortex in the presence of a light-cone). Note that this quantum number can be equally written as a bicomplex number $Q = \sum_{\sigma=\pm} Z_\sigma e_\sigma$ with $Z_\pm = Z_1 \pm Z_2 \in \mathbb{C}$. As it happens with the one-body vortex states, this degeneracy quantum number does not result from any boundary conditions or symmetries imposed to the wave function. Therefore, we expect the two-body bicomplex vortex states to be the preferentially selected to describe realistic fractional quantum Hall systems in the presence of strong two-body correlations by the extension of the gradient expansion theory described in chapter 1.

6.3.3. Properties of the bicomplex vortex eigenstates

The bicomplex vortex wave function (6.42) possesses important properties that merit a more detailed discussion. First, it describes a topologically correlated state of the two particles by means of the non-Euclidean metric, since the polynomial part of each wave function cannot be written as a simple product state of two uncorrelated factors affecting exclusively one of the two electrons.

Moreover, as it happened with the one-body vortex counterparts, it can be shown that the bicomplex vortex states are semiorthogonal. However, the overlap between two different bicomplex vortex states is slightly different from the standard coherent states overlap (1.45) because the states are also non-orthogonal with respect to the discrete degeneracy quantum number m, *i.e.* $\langle \nu|\nu'\rangle = \delta_{n,n'}\langle m, \mathbf{R}|m', \mathbf{R}'\rangle$. We provide a demonstration of this statement in Sec. 6.4.2.

Finally, as mentioned above, the set of bicomplex vortex states forms an overcomplete basis in the extended Hilbert space associated to the Hamiltonian (6.2). As such they obey a closure relation, which allows us to project the dynamics (and any arbitrary operator)

into the bicomplex vortex state representation, given by

$$\int \frac{d^4\mathbf{R}}{(2\pi l_B^2)^2} \sum_{n=0}^{+\infty} \sum_{m=0}^{+\infty} |n, m, \mathbf{R}\rangle\langle n, m, \mathbf{R}| = \mathbb{1}. \tag{6.43}$$

From this identity, we conclude that the set of bicomplex two-body vortex states is complete if we associate the volume $\Omega = (2\pi l_B^2)^2$ to each quantum state. It is interesting to notice that, even in the presence of the intrinsic topological order coupling the two particles and induced by the non-Euclidean metric, the degeneracy of the energy levels (deduced from the measure of the closure integral) is equal to the naïve guess $(B/\Phi_0)^2 = (2\pi l_B^2)^{-2}$. Eq. (6.43) is proved essentially in two ways: first, by computing

$$\sum_{\nu} \langle \mathbf{r}|\nu\rangle\langle\nu|\mathbf{r}'\rangle = \sum_{\nu} \Psi_\nu(\mathbf{r})\Psi_\nu^{*^i}(\mathbf{r}'), \tag{6.44}$$

and showing that it is proportional to a Dirac delta distribution in four dimensions; second, by considering the Dyson equation expressed in the bicomplex vortex representation and assuming $\hat{G}(\omega) = \mathbb{1}$ [and, therefore, $\hat{G}^{-1}(\omega) = \mathbb{1}$ so that the Hamiltonian is trivial, $\hat{\mathcal{H}} = \mathbb{1}$]. The former way of proving the completeness of the bicomplex vortex states thoroughly uses the bicomplex integral calculus developed in Sec. 6.2.4. This method, however, is quite cumbersome and obscure and will not be described here. We instead take for the moment Eq. (6.43) for granted and prove it *a posteriori* in Sec. 6.5 using the Green's function technique.

6.4. Matrix Elements of the Generalized Potential

6.4.1. General expression

In this section, we aim to give a general expression for the matrix elements of the potential written in the bicomplex vortex representation. The potential $V(\mathbf{r}_1, \mathbf{r}_2)$ can be considered to be any arbitrary real (smooth) function depending on the coordinates of the two electrons forming the pair, and which contains both one-body and two-body (interaction) terms [we shall write this function formally as a bicomplex-valued function $V(\mathbf{r})$ with $\mathbf{r} \in \tilde{\mathbb{B}}$]. The Hamiltonian of the system under consideration is, therefore,

$$\hat{\mathcal{H}} = \hat{\mathcal{H}}_0^{(N=2)} + \hat{V}, \tag{6.45}$$

with $\hat{\mathcal{H}}_0^{(N=2)}$ defined in Eq. (6.35) and $\hat{V} \equiv V(\hat{\mathbf{r}}_1, \hat{\mathbf{r}}_2)$. The matrix elements of the potential defined as $V_{\nu;\nu'} \equiv V_{n,m;n',m'}(\mathbf{R}, \mathbf{R}') = \langle n, m, \mathbf{R}|\hat{V}|n', m', \mathbf{R}'\rangle$ then read

$$\begin{aligned} V_{n,m;n',m'}(\mathbf{R};\mathbf{R}') = {} & \frac{1}{(2\pi l_B^2)^2} \frac{1}{\sqrt{n!n'!m!m'!}} \int d^4\mathbf{r}\, V(\mathbf{r}) \\ & \times \left(\frac{q^{*^i} - Q^{*^i}}{2l_B}\right)^n \left(\frac{q - Q'}{2l_B}\right)^{n'} \left(\frac{q^{*^j} - Q^{*^j}}{2l_B}\right)^m \left(\frac{q^{*^{ij}} - Q'^{*^{ij}}}{2l_B}\right)^{m'} \\ & \times \exp\left[-\frac{|z_1|^2 + |Z_1'|^2 - 2Z_1'z_1^*}{4l_B^2}\right] \exp\left[-\frac{|z_1|^2 + |Z_1|^2 - 2Z_1^*z_1}{4l_B^2}\right] \\ & \times \exp\left[-\frac{|z_2|^2 + |Z_2'|^2 - 2Z_2'z_2^*}{4l_B^2}\right] \exp\left[-\frac{|z_2|^2 + |Z_2|^2 - 2Z_2^*z_2}{4l_B^2}\right]. \end{aligned} \tag{6.46}$$

We have to arrange the previous expression of the matrix elements by performing some manipulations. First, we combine the complex exponential factors to extract a kind of overlap function but which affects exclusively the continuous quantum number $\mathbf{R}$ [this quantity is somehow analogue to Eq. (1.45)]. To that purpose, we perform the change of variables

$$\begin{aligned} 2l_B\tilde{\mathbf{r}}_\alpha &\equiv \mathbf{r}_\alpha - \tilde{\mathbf{R}}_\alpha, \\ &= \mathbf{r}_\alpha - \frac{\mathbf{R}_\alpha + \mathbf{R}'_\alpha}{2} + i\frac{\mathbf{R}_\alpha - \mathbf{R}'_\alpha}{2} \times \hat{\mathbf{z}}, \end{aligned} \tag{6.47}$$

where $\alpha \in \{1,2\}$ and $\mathbf{r}_\alpha, \mathbf{r}'_\alpha, \mathbf{R}_\alpha, \mathbf{R}'_\alpha$ are 2D vectors. We also choose to define the bicomplex number $\tilde{\mathbf{R}} = (\tilde{\mathbf{R}}_1, \tilde{\mathbf{R}}_2)$. As a consequence, it can be shown that each of the exponential factors can be centered in their respective characteristic complex planes to get

$$\begin{aligned} V_{n,m;n',m'}(\mathbf{R};\mathbf{R}') = \frac{4}{\pi^2}\frac{\langle \mathbf{R}|\mathbf{R}'\rangle}{\sqrt{n!n'!m!m'!}} \int d^4\tilde{\mathbf{r}}\, V(2l_B\tilde{\mathbf{r}} + \tilde{\mathbf{R}}) \\ \times \exp\left[-2(\tilde{x}_1^2 + \tilde{y}_1^2)\right] \exp\left[-2(\tilde{x}_2^2 + \tilde{y}_2^2)\right] (\tilde{q}^{*^i})^n\, \tilde{q}^{n'} \\ \times \left[\tilde{q}^{*^j} - \frac{(Q-Q')^{*^j}}{2l_B}\right]^m \left[\tilde{q}^{*^{ij}} - \frac{(Q'-Q)^{*^{ij}}}{2l_B}\right]^{m'}. \end{aligned} \tag{6.48}$$

Here, we have used the short-hand notation

$$\begin{aligned} \langle \mathbf{R}|\mathbf{R}'\rangle &\equiv \langle \mathbf{R}_1|\mathbf{R}'_1\rangle\langle \mathbf{R}_2|\mathbf{R}'_2\rangle, \\ &= \exp\left[-\frac{QQ^{*^i} + Q^{*^j}Q^{*^{ij}}}{8l_B^2}\right] \exp\left[-\frac{Q'Q'^{*^i} + Q'^{*^j}Q'^{*^{ij}}}{8l_B^2}\right] \\ &\times \exp\left[\frac{Q'Q^{*^i} + Q'^{*^j}Q^{*^{ij}}}{4l_B^2}\right]. \end{aligned} \tag{6.49}$$

Note that, as a difference to the one-body case [55], this change of variables to the dimensionless electronic positions, $\tilde{\mathbf{r}}$, does not allow to simultaneously center around the bicomplex origin the vortex part of the matrix elements, with positive circulations n and n' and related to the Landau levels of the states $|\nu\rangle$ and $|\nu'\rangle$, and the antivortex part with negative circulations m and m'. The polynomials in the variables $(Q'-Q)^{*^j}$ and $(Q-Q')^{*^{ij}}$, appearing in Eq. (6.48), are now expanded using Newton's binomial formula. This step introduces a pair of auxiliary integers, p and p', respectively related to the degeneracy quantum numbers m and m' . Furthermore, taking into account the analyticity property of the potential energy function, we can deform the contours in each characteristic complex plane to the real axis[22] to obtain

$$\begin{aligned} V_{n,m;n',m'}(\mathbf{R};\mathbf{R}') = \langle \mathbf{R}|\mathbf{R}'\rangle \sum_{p=0}^{+\infty}\sum_{p'=0}^{+\infty} \sqrt{\frac{p!p'!}{m!m'!}} \binom{m}{p}\binom{m'}{p'} \\ \times \left[\frac{(Q'-Q)^{*^j}}{2l_B}\right]^{m-p} \left[\frac{(Q-Q')^{*^{ij}}}{2l_B}\right]^{m'-p'} v_{n,p;n'p'}(\tilde{\mathbf{R}}), \end{aligned} \tag{6.50}$$

[22]Note that doing this procedure the bicomplex numbers are still regular since the change of variables has not affected the hyperbolic part of the module.

where the reduced matrix elements $v_{n,p;n',p'}(\tilde{\mathbf{R}})$ have been defined as

$$v_{n,p;n'p'}(\tilde{\mathbf{R}}) \equiv \frac{4}{\pi^2}\frac{1}{\sqrt{n!n'!p!p'!}}\int d^4\mathbf{r}\, V(2l_B\mathbf{r}+\tilde{\mathbf{R}})(q^{*^i})^n\, q^{n'}\left(q^{*^j}\right)^p\left(q^{*^{ij}}\right)^{p'} \times \exp\left[-\left(qq^{*^i}+q^{*^j}q^{*^{ij}}\right)\right], \quad (6.51)$$

with the notation $\mathbf{r}\equiv\tilde{\mathbf{r}}$. This choice in the representation of the matrix elements, which also suggests a functional form of the *ansatz* for the Green's function (to be used in the equation of motion in Sec. 6.5.1), allows the following useful identification between the full and the reduced matrix elements of the potential energy function when the latter are evaluated at coinciding vortex positions $\mathbf{R}=\mathbf{R}'=\tilde{\mathbf{R}}$, $V_{n,m;n',m'}(\mathbf{R}) \equiv V_{n,m;n',m'}(\mathbf{R},\mathbf{R}) = v_{n,m;n',m'}(\mathbf{R})$. Note that the matrix elements of the potential are actually bicomplex numbers [this is because Eq. (6.38) does not hold for $V(\mathbf{r}_1,\mathbf{r}_2)$ real as the symmetry with respect to the pairs $qq^{*^{ij}}$ and $q^{*^i}q^{*^j}$ is broken]. Nevertheless, this fact can be cured if we construct, using the bicomplex vortex basis, spinor states which are still vortices (and form a basis in an extended Hilbert space). A new quantum number $\lambda=\pm$, similar to the SO quantum number introduced in Sec. 2.2.3, appears in the problem and the potential becomes a matrix in this new space. To get rid of the hyperbolic character, one needs to perform an additional diagonalization in this space. As this procedure is still under active research we will not pursue it here and the results will be published elsewhere.

6.4.2. Overlap

We prove in this subsection that the bicomplex vortex states, as it happened with the single-particle vortex states (1.44) and anticipated above, are semiorthogonal. To that purpose, we simply consider the expression for the matrix elements of the potential (6.50) that trivially yields the scalar product of two bicomplex vortex states, $\langle\nu|\nu'\rangle$, if we consider the situation $\hat{V}=\mathbb{1}$. In this case, we get from Eq. (6.51) that $v_{n,p;n'p'}(\mathbf{R})=\delta_{n,n'}\delta_{p,p'}$ after using the mathematical results from Appendix F. Therefore, Eq. (6.50) becomes

$$\langle\nu|\nu'\rangle = \delta_{n,n'}\langle m,\mathbf{R}|m',\mathbf{R}'\rangle \quad (6.52)$$

$$= \delta_{n,n'}\langle\mathbf{R}|\mathbf{R}'\rangle\sum_{p=0}^{+\infty}\sum_{p'=0}^{+\infty}\sqrt{\frac{p!p'!}{m!m'!}}\binom{m}{p}\binom{m'}{p'} \times\left[\frac{(Q'-Q)^{*^j}}{2l_B}\right]^{m-p}\left[\frac{(Q-Q')^{*^{ij}}}{2l_B}\right]^{m'-p'}\delta_{p,p'}. \quad (6.53)$$

Not surprisingly, the scalar product between two bicomplex vortex states is diagonal with respect to the quantum number n that characterizes the energy levels. The overlap part, for different continuous bicomplex coordinates $\mathbf{R}$ and $\mathbf{R}'$ and integers m and m', depends nonlocally on the quantum numbers defining the degeneracy of the Landau levels. It also gets exponentially reduced whenever the two bicomplex vortex states are spatially separated by more than a few magnetic lengths. Note also again the presence of the auxiliary integers p and p'. These numbers, defined for $p\in[0,m]$ and $p'\in[0,m']$, correspond to a partition of the discrete degeneracy quantum number and can be interpreted as being similar to the notion of Jain's quasi-Landau levels [10]. This interpretation gets reinforced by the fact that our overlap is also diagonal with respect to this emergent degree of freedom.

Finally, as an easy check (which allows us to cross-verify the normalization of the wave function), let us show that we recover, for coinciding bicomplex vortex positions, the result $\langle\nu|\nu\rangle = 1$. Indeed,

$$\langle\nu|\nu\rangle = \delta_{n,n'} \sum_{p=0}^{+\infty} \sum_{p'=0}^{+\infty} \sqrt{\frac{p!p'!}{m!m'!}} \binom{m}{p} \binom{m'}{p'} \delta_{m,p}\delta_{m',p'}\delta_{p,p'}, = 1 \tag{6.54}$$

where we have also used that $\langle\mathbf{R}|\mathbf{R}\rangle = 1$.

6.5. Green's Function Formalism

6.5.1. Dyson equation in the bicomplex vortex representation

In this section, we derive the Dyson equation which describes the dynamics of the electron pair in the presence of a generalized one-body / two-body potential that accounts for the combined effects of a smooth scalar disorder, nonequilibrium potential and/ or electron-electron interactions. We therefore consider the Green's operator associated to the time-independent Hamiltonian (6.45), which is written as in Eq. (1.50), and use the completeness relation of the two-body vortex states to project the equation of motion onto this representation

$$\sum_{\nu''} \left[(\omega - E_n \pm i0^+)\langle\nu|\nu''\rangle - V_{\nu;\nu''}\right] G^{R,A}_{\nu'';\nu'}(\omega) = \langle\nu|\nu'\rangle. \tag{6.55}$$

Here, as usual, ω is the variable conjugated to the time difference in the Fourier sense and we have noted by $G^{R,A}_{\nu;\nu'} = \langle\nu|\hat{G}^{R,A}(\omega)|\nu'\rangle$ the matrix elements of the Green's operator. Inspired by Eq. (6.50), we propose the following *ansatz* for the Green's function

$$\begin{aligned} G^{R,A}_{n,m;n',m'}(\mathbf{R};\mathbf{R}';\omega) = \langle\mathbf{R}|\mathbf{R}'\rangle \sum_{p=0}^{+\infty} \sum_{p'=0}^{+\infty} \sqrt{\frac{p!p'!}{m!m'!}} \binom{m}{p} \binom{m'}{p'} \\ \times \left[\frac{(Q'-Q)^{*^j}}{2l_B}\right]^{m-p} \left[\frac{(Q-Q')^{*^{ij}}}{2l_B}\right]^{m'-p'} g^{(m,m')}_{n,p;n',p'}(\tilde{\mathbf{R}};\omega), \end{aligned} \tag{6.56}$$

where we dropped the retarded and advanced superscripts in the reduced vortex Green's function $g(\mathbf{R};\omega)$, since each Green's function is identified from the sign of its infinitesimal imaginary part. It can be proved that this simple form for the Green's function gives a self-consistent Dyson equation when injected again into Eq. (6.55). Note that, as a difference to the matrix elements of the potential, we cannot exclude a non-local dependence of the reduced vortex Green's function on the quantum numbers m and m'. This dependence on the discrete degeneracy quantum number may even be expected as m and $\mathbf{R}$ are both coupled through the polynomials in the variables $(Q'-Q)^{*^j}$ and $(Q-Q')^{*^{ij}}$ appearing as prefactors in the full Green's function (6.56). Moreover, it is also clear, as for the one-body vortex theory presented in chapter 1, that as a consequence of the coherent character of the quantum number $\mathbf{R}$, the diagonal representation of the Green's function obtained for coinciding vortex positions, $\mathbf{R} = \mathbf{R}'$, fully determines the functional form of the non-local Green's function. However, there is a subtlety in the present case (6.56) compared to the single-particle Green's function (1.55) from the one-body vortex

theory due to the more complicated prefactors (involving a sum over p and p'). Let us consider here coinciding vortex positions, $\mathbf{R} = \mathbf{R}' = \tilde{\mathbf{R}}$ so that the Green's function is diagonal in the coherent-state degree of freedom. As a consequence, Eq. (6.56) reads $G^{R,A}_{n,p;n',p'}(\mathbf{R};\mathbf{R};\omega) = g^{(m,m')}_{n,p;n',p}(\mathbf{R},\omega)\delta_{m,p}\delta_{m',p'}$ and the auxiliary integers p and p' disappear. Therefore, locality on the continuous degeneracy quantum number does not imply locality on the discrete degeneracy quantum number. To have locality in m we further consider the projection to a single pair Landau level. In this case, an additional constraint appears in the Green's function in the form of locality with respect to the n and the quasi-Landau level p. The latter implies, by a product of Kronecker delta functions $\delta_{m,m'} = \delta_{p,p'}\delta_{m,p}\delta_{m',p'}$ and therefore the Green's function is diagonal in the discrete degeneracy quantum number m. This observation is has to be taken into account at the level of Dyson equation.

Substitution of Eqs. (6.50) and (6.52), together with Eq. (6.56) into Dyson equation (6.55) yields the following form of the Dyson equation

$$\begin{aligned}
&\int \frac{d^4\mathbf{R}''}{(2\pi l_B^2)^2} \sum_{n''=0}^{+\infty}\sum_{m''=0}^{+\infty}\sum_{p=0}^{+\infty}\sum_{p'=0}^{+\infty}\sum_{p''=0}^{+\infty}\sum_{p'''=0}^{+\infty} \Bigg\{ \binom{m}{p}\binom{m'}{p'}\binom{m''}{p''}\binom{m''}{p'''} \\
&\times \frac{\sqrt{p!p'!p''!p'''!}}{m''!} \frac{\langle\mathbf{R}|\mathbf{R}''\rangle\langle\mathbf{R}''|\mathbf{R}'\rangle}{\langle\mathbf{R}|\mathbf{R}'\rangle} \left[\frac{(Q''-Q)^{*^j}}{2l_B}\right]^{m-p} \\
&\times \left[\frac{(Q-Q'')^{*^{ij}}}{2l_B}\right]^{m''-p''} \left[\frac{(Q'-Q'')^{*^j}}{2l_B}\right]^{m''-p'''} \left[\frac{(Q''-Q')^{*^{ij}}}{2l_B}\right]^{m'-p'} \\
&\times \Big[(\omega - E_n \pm i0^+)\delta_{n,n''}\delta_{p,p''} - v_{n,p;n'',p''}(\mathbf{R};\mathbf{R}'')\Big] g^{(m'',m')}_{n'',p''';n',p'}(\mathbf{R}'';\mathbf{R}';\omega) \Bigg\} \\
&= \delta_{n,n'} \sum_{p=0}^{+\infty}\sum_{p'=0}^{+\infty} \sqrt{p!p'!}\binom{m}{p}\binom{m'}{p'} \left[\frac{(Q'-Q)^{*^j}}{2l_B}\right]^{m-p} \left[\frac{(Q-Q')^{*^{ij}}}{2l_B}\right]^{m'-p'} \delta_{p,p'},
\end{aligned} \tag{6.57}$$

where the combination

$$\begin{aligned}
\frac{\langle\mathbf{R}|\mathbf{R}''\rangle\langle\mathbf{R}''|\mathbf{R}'\rangle}{\langle\mathbf{R}|\mathbf{R}'\rangle} &= \exp\left\{-\frac{1}{2l_B^2}\left[\mathbf{R}_1'' - \left(\frac{\mathbf{R}_1'+\mathbf{R}_1}{2} + i\frac{\mathbf{R}_1'-\mathbf{R}_1}{2}\times\hat{\mathbf{z}}\right)\right]^2\right\} \\
&\times \exp\left\{-\frac{1}{2l_B^2}\left[\mathbf{R}_2'' - \left(\frac{\mathbf{R}_2'+\mathbf{R}_2}{2} + i\frac{\mathbf{R}_2'-\mathbf{R}_2}{2}\times\hat{\mathbf{z}}\right)\right]^2\right\},
\end{aligned} \tag{6.58}$$

is, by construction, twice Eq. (1.57), one term for each of the particles in the electron pair. We also remind that in Eq. (6.57), the reduced matrix elements of the potential and the Green's function formally depend on the vortex variables through the combination $\tilde{\mathbf{R}}$ defined above, but with $\mathbf{R}, \mathbf{R}'$ substituted by the corresponding values indicated in the arguments of each of the functions.

We now proceed similarly to Sec. 1.5.2 with the goal of analytically computing the integral over the bicomplex vortex coordinates $\mathbf{R}''$, then obtain a new bidifferential infinite order operator which governs the dynamics of the Green's function in the diagonal representation for the guiding center coordinates and derive a closed equation for the vortex Green's function. Therefore, we consider the change of variables similar to Eq. (6.47) but for the variable $\mathbf{R}''_\alpha$ with $\alpha \in \{1,2\}$ instead of $\mathbf{r}_\alpha$ (we also keep the dimensionality of

the continuous variable $\mathbf{R}''$). The change of variables allows us to center the exponentials around the origin in each of the characteristic complex planes by deforming the contour of the integration in the variables $\mathbf{R}''_\alpha$ to the real axis after taking advantage of the analyticity of the exponential function. Relabeling $\tilde{\mathbf{R}}_\alpha \to \mathbf{R}_\alpha$ for the sake of simplicity and noting $\delta Q \equiv Q' - Q$ we obtain

$$\begin{aligned}
&\int \frac{d^4\mathbf{R}''}{(2\pi l_B^2)^2} \sum_{n''=0}^{+\infty}\sum_{m''=0}^{+\infty}\sum_{p=0}^{+\infty}\sum_{p'=0}^{+\infty}\sum_{p''=0}^{+\infty}\sum_{p'''=0}^{+\infty} \left\{ \binom{m}{p}\binom{m'}{p'}\binom{m''}{p''}\binom{m''}{p'''} \right. \\
&\times \exp\left[-\frac{\mathbf{R}_1''^2 + \mathbf{R}_2''^2}{2l_B^2}\right](-1)^{p''+p'''}\frac{\sqrt{p!p'!p''!p'''!}}{m''!} \\
&\times \left(\frac{Q''^{*j}}{2l_B} + \frac{\delta Q^{*j}}{2l_B}\right)^{m-p}\left(\frac{Q''^{*ij}}{2l_B}\right)^{m''-p''}\left(\frac{Q''^{*j}}{2l_B}\right)^{m''-p'''}\left(\frac{Q''^{*ij}}{2l_B} - \frac{\delta Q^{*ij}}{2l_B}\right)^{m'-p'} \\
&\left.\times \Big[(\omega - E_n \pm i0^+)\delta_{n,n''}\delta_{p,p''} - v_{n,p;n'',p''}(\mathbf{R};\mathbf{R}'')\Big] g^{(m'',m')}_{n'',p''';n',p'}(\mathbf{R}'';\mathbf{R}';\omega)\right\} \\
&= \delta_{n,n'}\sum_{p=0}^{+\infty}(-1)^{m'-p}p!\binom{m}{p}\binom{m'}{p}\left(\frac{\delta Q^{*j}}{2l_B}\right)^{m-p}\left(\frac{\delta Q^{*ij}}{2l_B}\right)^{m'-p}. \qquad (6.59)
\end{aligned}$$

At this point, we clearly see that at large magnetic fields (small values of the magnetic length l_B), the main contribution in the integral over the bicomplex vortex position $\mathbf{R}''$ when $\delta Q \to 0$ has to come from the contributions of $\mathbf{R}''$ close to $\mathbf{R}$ and $\mathbf{R}'$. This means that it is enough to consider the reduced Green's function, and the matrix elements of the potential, for $\delta Q = 0$ (that is, at coinciding vortex positions $Q = Q'$ or $\mathbf{R} = \mathbf{R}'$). We then expand the functions $v(\tilde{\mathbf{R}})$ and $g(\tilde{\mathbf{R}};\omega)$ evaluated in this way in a Taylor series for $\mathbf{R}''$ close to $\mathbf{R}$. The latter can be performed thanks to the fact that analytic functions exist in the bicomplex module whenever we move away from the localized set of zero divisors Ξ. Collecting the terms in the Taylor expansion in a closed form as in Ref. [132], expanding the polynomials in δQ by using again Newton's binomial theorem and further considering the limit $\delta Q = 0$ in the polynomials as discussed above we arrive at the following form for the Dyson equation

$$\begin{aligned}
&4\int \frac{d^4\mathbf{u}''}{\pi^2} \sum_{n''=0}^{+\infty}\sum_{m''=0}^{+\infty}\sum_{p=0}^{+\infty}\sum_{p'=0}^{+\infty}\sum_{p''=0}^{+\infty}\sum_{p'''=0}^{+\infty}\sum_{k_1=0}^{+\infty}\sum_{k_2=0}^{+\infty} \left\{ \binom{m}{p}\binom{m'}{p'}\binom{m''}{p''}\binom{m''}{p'''} \right. \\
&\times \binom{m-p}{k_1}\binom{m'-p'}{k_2}(-1)^{p''+p'''}\frac{\sqrt{p!p'!p''!p'''!}}{m''!}\delta_{k_1,m-p}\delta_{k_2,m'-p'} \\
&\times \left(Q''^{*j}_u\right)^{k_1}\left(Q''^{*ij}_u\right)^{m''-p''}\left(Q''^{*j}_u\right)^{m''-p'''}\left(Q''^{*ij}_u\right)^{k_2}\exp\left(-Q_uQ^{*i}_u - Q^{*j}_uQ^{*ij}_u\right) \\
&\times \Big[(\omega - E_n \pm i0^+)\delta_{n,n''}\delta_{p,p''} - v_{n,p;n'',p''}(\mathbf{R})\,\mathrm{e}^{2l_B\left(u_1\overleftarrow{\partial}_{Z_1}+u_2\overleftarrow{\partial}_{Z_2}\right)}\Big] \\
&\left.\times \mathrm{e}^{2l_B\left(u_1^*\overrightarrow{\partial}^*_{Z_1}+u_2^*\overrightarrow{\partial}^*_{Z_2}\right)} g^{(m'',m')}_{n'',p''';n',p'}(\mathbf{R};\omega)\right\} = \delta_{n,n'}\sum_{p=0}^{+\infty}(-1)^{m'-p}p! \\
&\times \binom{m}{p}\binom{m'}{p}\delta_{m,m'}\delta_{m,p}. \qquad (6.60)
\end{aligned}$$

In the previous expression, we have shifted the primed vortex positions by $\mathbf{R}'' - \mathbf{R} \to \mathbf{R}''$, afterwards introduced the dimensionless variables $Q'' = 2l_B Q_u$ [or $\mathbf{R}'' = 2l_B \mathbf{u} = 2l_B(\mathbf{u}_1, \mathbf{u}_2)$] and we have used, for $\alpha \in \{1, 2\}$, the dimensionless complex numbers $u_\alpha = u_{\alpha x} + i u_{\alpha y} \in \mathbb{C}$ and the partial derivatives $\partial_{Z_\alpha} = (\partial_{X_\alpha} - i\partial_{Y_\alpha})/2$, with the arrow above the partial derivative pointing towards which side the derivative has to be applied.

Projection into a single pair Landau level

Up to this moment everything was exact but we consider, as for the one-body problem, a high magnetic field limit in which Landau level mixing can be neglected since the energy gap between pairs Landau levels is large enough that scattering of states from one Landau level to another is energetically forbidden. In that case, we can project the dynamics onto a single pair energy level n and assume that the matrix elements of the potential and the local bicomplex vortex Green's function are diagonal in the quasi-Landau level p, a property suggested by Eq. (6.52). As a consequence, the matrix elements of the potential read $v_{n,p;n',p'}(\mathbf{R}) = v_{n,p;n',p'}(\mathbf{R})\delta_{n,n'}\delta_{p,p'} \equiv v_{n;p}(\mathbf{R})\delta_{n,n'}\delta_{p,p'}$ and the local Green's function is equal to $g^{(m,m')}_{n,p;n',p'}(\mathbf{R};\omega) = g^{(m,m')}_{n,p;n',p'}(\mathbf{R};\omega)\delta_{n,n'}\delta_{p,p'}\delta_{m,m'} \equiv g^{m}_{n,p}(\mathbf{R};\omega)\delta_{n,n'}\delta_{p,p'}\delta_{m,m'}$ (here, as anticipated above, the diagonal representation of the Green's function forces a condition on the discrete degeneracy quantum number m). Therefore, we get

$$\begin{aligned} 4\int \frac{d^4\mathbf{u}''}{\pi^2} \sum_{p=0}^{+\infty}\sum_{p'=0}^{+\infty} \Bigg\{ & \binom{m}{p}\binom{m'}{p'}\binom{m'}{p}\binom{m'}{p'}(-1)^{p+p'}\frac{p!p'!}{m!m'!} \\ & \times \left(Q_u^{*^j}\right)^{m+m'-p-p'} \left(Q_u^{*^{ij}}\right)^{m+m'-p-p'} \exp\left(-Q_u Q_u^{*^i} - Q_u^{*^j} Q_u^{*^{ij}}\right) \\ & \times \Big[\omega - E_n \pm i0^+ - v_{n,p}(\mathbf{R})\Big]\, \mathrm{e}^{2l_B\left(u_1 \overleftarrow{\partial}_{Z_1} + u_2 \overleftarrow{\partial}_{Z_2}\right)} \\ & \times \mathrm{e}^{2l_B\left(u_1^* \overrightarrow{\partial}^*_{Z_1} + u_2^* \overrightarrow{\partial}^*_{Z_2}\right)} g^{m'}_{n,p'}(\mathbf{R};\omega) \Bigg\} = 1. \end{aligned} \tag{6.61}$$

This equation can be written in compact form

$$\begin{aligned} \sum_{p=0}^{+\infty}\sum_{p'=0}^{+\infty} \Bigg\{ & \binom{m}{p}\binom{m'}{p'}\binom{m'}{p}\binom{m'}{p'}(-1)^{p+p'}\frac{p!p'!}{m!m'!} \\ & \times \Big[\omega - E_n \pm i0^+ - v_{n,p}(\mathbf{R})\Big] \bowtie^{m,m'}_{p,p'} g^{m'}_{n,p'}(\mathbf{R};\omega) \Bigg\} = 1, \end{aligned} \tag{6.62}$$

if we define

$$\begin{aligned} \bowtie^{m,m'}_{p,p'} \equiv 4\int \frac{d^4\mathbf{u}''}{\pi^2} & \left(Q_u^{*^j}\right)^{m+m'-p-p'} \left(Q_u^{*^{ij}}\right)^{m+m'-p-p'} \exp\left(-Q_u Q_u^{*^i} - Q_u^{*^j} Q_u^{*^{ij}}\right) \\ & \times \mathrm{e}^{2l_B\left(u_1 \overleftarrow{\partial}_{Z_1} + u_2 \overleftarrow{\partial}_{Z_2}\right)} \mathrm{e}^{2l_B\left(u_1^* \overrightarrow{\partial}^*_{Z_1} + u_2^* \overrightarrow{\partial}^*_{Z_2}\right)} \end{aligned} \tag{6.63}$$

Several comments are now in order. First, at a glance, we can see that the equation of motion obtained after projection in the [topologically] correlated two-body problem is radically different from the one-body Dyson equation (1.62). The first difference [and which is also the main obstacle for solving Eq. (6.62)] lies in the complex and unusual

form of the local infinite order differential operator (6.63), acting on the vortex Green's function $g(\mathbf{R};\omega)$ and the matrix elements of the potential $v(\mathbf{R})$. This is a two-body version of the product between functions in the deformation quantization sense, that has still to be integrated over the continuous degree of freedom $\mathbf{u}$ in order to obtain an operator analogous to the Voros bidifferential $\bowtie$ product given in Eq. (1.59). Interestingly, we have recently proved (not shown here) that the integral can be computed by using the methods presented in the Appendix F. We effectively recover a modified version of Eq. (1.59) (which reduces to $\bowtie$ in the single-particle limit) with additional partial derivatives that result from the correlations between the two particles. Another crucial point concerns the coupling between the matrix elements of the potential and the reduced vortex Green's function through the discrete integers p and p'. This coupling is not direct, but affects both functions indirectly, also by means of the degeneracy quantum numbers m and m' and, therefore, the bidifferential operator $\bowtie_{p,p'}^{m,m'}$.

From Eq. (6.62), we can also discuss the type of controlled approximations which can be considered in order to look for an analytic solution to the equation of motion. Naïvely, we might think that for high magnetic fields, a semiclassical $l_B \to 0$ expansion scheme as used in chapter 4 could work in order to obtain the most robust spectral gaps within each of the Landau levels. Let us prove that, at leading order, it is not possible to generate energy gaps (due to the intra-pair Coulomb interaction) in the energy spectrum to be deduced from the poles of the Green's function. To that purpose, we take the strict limit $l_B = 0$ both in $v(\mathbf{R})$ and $g(\mathbf{R};\omega)$, *i.e.* the lowest order terms in the gradient expansion in powers of the magnetic length. At the same time, the exponential bidifferential operators in Eq. (6.63) are reduced to the identity and the integral over the bicomplex variable $\mathbf{u}$ is purely Gaussian (again, we compute the integral using the general formulas of Appendix F). As a result, we derive from Eq. (6.62) the following equation of motion for the semiclassical Green's function $\mathfrak{g}(\mathbf{R};\omega)$

$$\sum_{p=0}^{+\infty}\sum_{p'=0}^{+\infty} \beta_{p,p'}^{m,m'} \left[\omega - E_n - V(\mathbf{R}) \pm i0^+\right] \mathfrak{g}_{n,p'}^{m'}(\mathbf{R};\omega) = 1, \tag{6.64}$$

where we defined the coefficient $\beta_{p,p'}^{m,m'}$ as

$$\beta_{p,p'}^{m,m'} \equiv \binom{m}{p}\binom{m}{p'}\binom{m'}{p}\binom{m'}{p'}(-1)^{p+p'}\frac{p!p'!}{m!m'!}(m+m'-p-p')!. \tag{6.65}$$

Note that this coefficient is symmetric under the interchange $(m,p) \leftrightarrow (m',p')$. Moreover, Eq. (6.64) can be inverted formally since for $l_B = 0$ the potential and the vortex Green's function are no longer coupled. Unfortunately, it is also obvious that for infinite magnetic fields, and contrary to the one-body case, the degeneracy is only partially lifted by the potential energy $V(\mathbf{R})$ and the energy spectrum deduced from the poles of the Green's function is continuous (without spectral gaps). The underlying cause for this behavior is that in the gradient expansion we have not yet separated the fast degree of freedom hidden in $V(\mathbf{R})$, and related to the Coulomb interaction, from the slower degrees of freedom. Indeed, for the gradient expansion theory it is strictly necessary to perform this splitting because the Coulomb interaction has an unbounded gradient for short distances and does not generate any length scale. Another aspect overlooked by the strict $l_B = 0$ limit is that a possible transformation related to a resummation of l_B terms in the Green's function probably awaits to be realized (and discovered). This transformation should be similar

to Eqs. (1.60a)-(1.60b) which dresses the $\bowtie$ product into the $\star$ product and gives the preferred form for the Green's function when the degeneracy of the Landau levels is fully lifted.

Finally, let us mention the differences regarding the projection procedure to a single Landau level between the traditional picture of two electrons interacting by the Coulomb force discussed in chapter 5 and our Green's function approach. First, it is clear that the present theory is more general because the electron is not immediately assumed to be in the lowest Landau level from the beginning, all the Landau levels of the pair being treated on equal footing. Focusing on the LLL only, the projection performed in standard approaches necessarily freezes two degrees of freedom out of four possible, since we must have $n_1 = n_2 = 0$, the two harmonic oscillators related to each particle being considered independently in the absence of disorder and interactions. However, in our Green's function framework, this projection only affects a single integer in the two-body state, as only take $n = 0$, due to the correlations between the two particles already incorporated into the wave function by the non-Euclidean metric (these correlations disappear if we project independently the two single-particle Landau levels). The one-body and two-body potential energy will then lift the degeneracy of the LLL with respect to the other quantum numbers, $m \geq 0$ and $\mathbf{R} = (\mathbf{R}_+, \mathbf{R}_-) \in \tilde{\mathbb{B}}$. As it was the case with the Haldane pseudopotentials (6.3), if the potential is weakly anisotropic the assumption of invariance under rotations due to the two-body interaction will yield a discrete quantum number associated to $\mathbf{R}_-$. The disorder is then expected to lift the degeneracy with respect to the center-of-mass of the composite pair object $\mathbf{R}_+$, similarly to the one-body case discussed in the first part of this thesis. The result of this procedure is that the dynamics of the electron pair in the bicomplex representation is then characterized by at least two robust discrete quantum numbers while the standard approaches give only one[23] (the relative angular momentum m_{L}).

6.5.2. Consistency of the Green's function formalism: proof of the closure relation of the bicomplex vortex states

As a final result to this chapter, let us examine the consistency of our Green's function theory by proving the closure relation introduced in Eq. (6.43). As we anticipated in Sec. 6.3.2, it is clear that we can reproduce the completeness relation from Dyson equation (6.55) if we consider that the Green's operator is proportional to the identity operator. This means that, for arbitrary Landau level index n and degeneracy quantum number m, the function $\beta_{p,p'}^{m,m'}$ has to satisfy the identity

$$\sum_{p=0}^{+\infty} \sum_{p'=0}^{+\infty} \beta_{p,p'}^{m,m'} = 1, \tag{6.66}$$

or

$$\sum_{p=0}^{+\infty} \binom{m'}{p} (-1)^p \sum_{p'=0}^{+\infty} \binom{m}{p'} (-1)^{p'} \binom{m-p+m'-p'}{m'-p'} = 1. \tag{6.67}$$

We focus on the left-hand side of this identity and prove that it is equal to one. In order to perform the sums over p and p', we first note that we can interpret the binomial coefficient

[23] A good idea in this case, which is left for a future work, would be to calculate the equivalent of the Haldane pseudopotentials using our approach.

as a polynomial with rational coefficients [228]. Indeed, a binomial coefficient

$$p(z) = \binom{z}{k} = \frac{(z)_k}{k!}, \tag{6.68}$$

where $(z)_k = z(z-1)\dots(z-k+1) = \Gamma(z+1)/\Gamma(z-n+1)$ is the Pochhammer symbol for the falling factorial [here z is an indeterminate either real or complex and $\Gamma(z)$ is the Gamma function], can be understood as a polynomial in z. These polynomials are called Newton polynomials because they appear in the generalized Newton's binomial theorem or binomial series [*i.e.* the Taylor expansion around $z = 0$ of the function $(1+z)^\alpha$ with $\alpha \in \mathbb{C}$]. In addition, the finite summation can be interpreted as an operator

$$D^k \equiv \sum_{j=0}^{+\infty} \binom{k}{j} (-1)^j, \tag{6.69}$$

acting on the polynomial $p(z)$. This operator is known as the forward difference operator of order k and it is formally understood as a discrete version of the k-derivative representing the quasilocality [229]. The action of the forward difference operator D on the Pochhammer symbol $(z)_k$ can be studied using the calculus of finite differences and it is analog to the action of the derivative on the power z^k. In this sense, we can identify $D\,(z)_k$ with $\partial_z z^k$ and get the rules[24]

$$D\,(z)_k = k\,(z)_{k-1}, \tag{6.70a}$$

$$D^j (z)_k = j!\,\delta_{j,k} \quad \text{for} \quad j \geq k, \tag{6.70b}$$

$$D^n (z)_{n+1} = (n+1)!\,z. \tag{6.70c}$$

The forward difference operator is therefore a linear operator on the space of polynomials that reduces the degree of any polynomial function $p(z)$ by one. Note that Eq. (6.70) is actually a formal rule which allows a nice approach to the summations, even if it may seem to have no meaning since we are considering the indices in the Pochhammer symbol as exponents. However, this procedure can be made mathematically rigorous using linear functionals on the space of polynomials as in Ref. [230].

By construction (6.68), the last binomial coefficient which appears in Eq. (6.67) can be written as

$$\binom{m-p+m'-p'}{m'-p'} = \frac{(m'-p'+m-p)_{m-p}}{(m-p)!} = \frac{(m-p+m'-p')_{m'-p'}}{(m'-p')!}, \tag{6.71}$$

and interpreted as a polynomial of degree $m-p$ in the variable $m'-p'$ or a polynomial of degree $m'-p'$ in the variable $m-p$. The action of the forward difference operator of order m

[24] This type of relations between the calculus of finite differences for polynomial sequences and the differential calculus of real or complex variable are studied in a branch of combinatorics called umbral calculus. For example, the umbral calculus version of the Taylor expansion is the Newton's forward difference expansion or Newton series of a function $f(z)$

$$f(z) = \sum_{k=0}^{+\infty} \frac{[D^k f](0)}{k!} (z)_k.$$

This expansion holds for almost all analytic functions [228] [in particular, polynomials $p(z)$] and allows to represent any function by means of differences [230].

(or m') yields $D^{m}(m'-p'+m-p)_{m-p} = m!\,\delta_{m,m-p} = m!\,\delta_{0,p}$ [or $D^{m'}(m-p+m'-p')_{m'-p'} = m''!\,\delta_{m',m'-p'} = m'!\,\delta_{0,p'}$]. As a result, the left-hand side in Eq. (6.67) is equal to the unity and we have simultaneously proved the completeness relation of the bicomplex vortex states

$$\sum_{\nu} |\nu\rangle\langle\nu| = \mathbb{1} \Leftrightarrow \int \frac{d^4\mathbf{R}}{(2\pi l_B^2)^2} \sum_{n=0}^{+\infty} \sum_{m=0}^{+\infty} |n, m, \mathbf{R}\rangle\langle n, m, \mathbf{R}| = \mathbb{1}, \tag{6.72}$$

and checked the consistency of the full Green's function approach.

Conclusions and Outlook

Rashba Spin-Orbit Interaction in the Integer Quantum Hall Regime

In the first part of this thesis, we have studied spectral and transport properties of disordered (integer) quantum Hall systems which combine the presence of Rashba SO and Zeeman interaction. To this purpose, we have extended a coherent-state Green's function formalism, well-suited to describe the effects of smooth electrostatic disorder in 2DEGs, to incorporate the non-trivial coupling between the orbital and spin degrees of freedom at high magnetic fields. This formalism allows us to obtain analytical and controlled microscopic expressions of local spectrum-related and transport-related observables [such as the local density of states (LDoS), the particle and spin densities or the particle and spin currents] for different temperature regimes.

The main ingredients to understand the microscopic mechanisms at play in Rashba-coupled 2DEGs under perpendicular magnetic fields have been presented in the first two chapters of this manuscript. In the first chapter, we introduced the (integer) quantum Hall regime by a careful description of the observed outstanding experimental features, both in the non-relativistic "standard" case, that is found in semiconductor heterostructures, and the relativistic-like or anomalous situation, proper to graphene and topological insulators. We have then discussed the effect of disorder onto the electronic drift states and sketched a sophisticated theory which provides a fully analytical and quantum-mechanical framework where we can quantitatively address this peculiar transport regime. In the second chapter, we have presented our second constituent, namely Rashba SO interaction. We have described its physical origin, the generation of SO coupling in low-dimensional semiconductors and deeply discussed the particularities of the energy levels in a clean two-dimensional electron gas with Rashba and Zeeman couplings. As a final warm-up, we have critically reviewed the spin dynamics in 2DEGs in the form of spin currents pointing out to the inconsistencies in the commonly used definition of the spin current operator at high magnetic fields. These inconsistencies manifest themselves by the presence of unphysical resonances in the spin Hall conductance for disorder-free 2D systems.

As mentioned earlier, one of the main achievements of the thesis is the extension of the vortex theory of the integer quantum Hall effect to include additional parameters such as the spin of the electron (and its interaction with the orbital motion of the electrons induced by the Lorentz force). The general theoretical framework has been described in the third chapter of the present manuscript where we have introduced a new set of spinors,

dubbed SO vortex states, that provide considerable advantages to describe the lifting of the macroscopic quantum degeneracy of the energy levels by an arbitrary potential energy or random smooth fluctuations in the Rashba SO parameter. Then, we have solved the equation of motion for the Green's function in this representation, taking advantage of the fact that a mixed phase-space deformation-quantization formulation of the Dyson equation is possible at high magnetic fields. Considering an arbitrary locally flat disorder potential with both random electric fields and Rashba coupling, we have computed the SO vortex Green's function for the electronic drift states and obtained the energy spectrum. From the analytical and controlled nonperturbative expression of the spectrum we have discussed the mechanisms which can participate in the spatial dispersion of the energy levels and analyzed the interplay between the disorder and the fluctuations of the SO coupling. Finally, as an additional illustration of the theory, we have calculated an analytical microscopic expression for the LDoS valid at different temperature regimes. The spatial dependence and linewidth of the LDoS have been used to interpret the scanning tunneling spectroscopy experimental data [11, 86] where spatial correlations between the energy spin-splitting and the disorder potential were previously noticed. Our theoretical model for the experimental results suggests that the spatial fluctuations of the disordered electrostatic landscape are probably more important than the fluctuations of the Rashba SO interaction.

In the last chapter of this first part, we have tackled the problem of describing charge and spin transport properties in the integer quantum Hall regime, when a local equilibrium (or hydrodynamic) transport regime sets in. Using a high-magnetic field expansion of the vortex contribution to the electronic Green's function, we have first computed the local particle, spin and current densities in the form of functionals of the potential energy. From the local nonequilibrium electric current density, we have then obtained the conductivity tensor, in the limit of negligible inelastic scattering in which the longitudinal conductivity vanishes, and have extracted an analytical formula for the (semiclassical) local Hall conductivity. This expression encompasses the mixed non-relativistic / relativistic character of the energy spectrum (2.21): it yields the integer Hall plateaus for any finite value of the Rashba SO parameter (and, for which the spectrum is bounded from below) while it describes the half-integer quantization of the Hall conductivity in a disordered topological insulator surface if the SO coupling is formally set to an infinite value (this is the so-called Dirac limit, in which the spectrum is unbounded and relativistic-like). Using the electron current density obtained at high magnetic fields, we have also shown how to obtain a conserved spin current that cures the unphysical features of the previous definitions (resonances) and removes the ambiguity in the angular momentum flow that created persistent equilibrium spin currents. As a final point, we have connected the microscopic with the macroscopic world in the high temperature regime of the integer quantum Hall effect with SO interaction, deducing that the classical percolation exponent is preserved even in the presence of Rashba SO coupling.

Our analysis opens the door to several future research projects (hopefully to be addressed in the near future):

- A precise quantitative comparison between our analytical formula for the LDoS at low temperatures and the experiments realized InSb surface 2DEGs still remains to be done, since it is necessary to carefully map the potential energy landscape experimentally. In this context, we also hope that our theoretical work will allow a thorough characterization of the Rashba SO coupling at the microscopic level.

- The Dyson equation (3.17), which was solved in the drift-state approximation, can also be considered in the regime where the energy scale related to the local Gaussian curvature of the energy landscape is larger than the thermal energy scale. In this context, numerical studies using simple confining geometries for the potential energy function [101] (such as global parabolic potentials that model semiconductor quantum dots) at zero temperature seem to suggest that in the presence of Rashba and Zeeman couplings the repulsion between the energy levels depends on the asymmetry of the dot. Unfortunately, exact diagonalization methods cannot distinguish whether this is an effect purely related to the degree of anisotropy of the confining potential or to Rashba-Landau level mixing. This question could be addressed within the SO vortex formalism, considering the mixing between the energy levels perturbatively at the level of the SO vortex Green's function.

- Another interesting question to be answered is how the spin relaxation in a 2DEG is affected by the presence of a strong quantizing perpendicular magnetic field that soundly alters the transport regime (from diffusive to quasi-ballistic). At low magnetic fields, it has been theoretically predicted [79] that random Rashba fields, which are always present in real systems, produce memory effects that monotonically increase the spin relaxation rate (dominating the expected decrease from the Dyakonov-Perel mechanism[25]). As a consequence of the quasi-regular electron dynamics at high fields, one may expect important modifications of the spin relaxation time with possible oscillations similar to those found in the longitudinal conductance.

- Finally, it is also possible to use the SO vortex formalism to study the local physics of systems described by similar Hamiltonians to the one considered here. An obvious application is to analyze topological insulators under a perpendicular magnetic field and in the presence of smooth disorder potentials. In this case, we could perform a precise analytical calculation of the LDoS for thin films similar to Ref. [153], and which could be compared to experiments [29] and numerical simulations [231]. The single Dirac cone at the surface of the film can be generalized by adding a warping term in the dispersion relation [232] so that more materials can be treated within simple theoretical models. Similar calculations are also possible in graphene bilayers where the spin degree of freedom is replaced by the pseudospin (valley) index [233].

Dans la première partie de cette thèse, nous avons étudié les propriétés spectrales et de transport des systèmes quantiques désordonnés qui combinent la présence du SO de type Rashba et de l'interaction Zeeman dans le régime de l'effet Hall quantique entier. Pour cela, nous avons généralisé un formalisme de fonctions de Green basé sur des états de vortex cohérents, très pertinent pour décrire les effets du désordre lisse d'origine électrostatique en GE2D, avec l'objectif d'inclure le couplage non-trivial entre les dégrés de liberté orbitaux et de spin à fort champ magnétique. Le formalisme nous

[25]The Dyakonov-Perel spin relaxation mechanism is one the two important relaxation mechanisms in semiconductors with one type of charge carriers. In the presence of SO interaction, the electronic spin precesses around an axis of rotation due an effective momentum-dependent magnetic field. Electron collisions with impurities then change the direction of the momentum and after a few collisions the memory of the original spin direction is lost.

permet d'obtenir des fonctionnelles analytiques controllées et microscopiques pour les observables reliés au spectre d'énergie et au transport [comme la densité d'états locale (LDoS), la densité de particules et de spin ou le courant (électronique ou de moment cinétique) dans différents régimes de température.

Les principaux ingrédients nécessaires pour comprendre les mécanismes microscopiques mis en jeu dans les GE2D avec SO Rashba sous champs magnétiques forts et perpendiculaires ont été présentés dans les deux premiers chapitres de ce manuscrit. Dans le premier chapitre, nous avons introduit le régime de l'effet Hall quantique (entier) à travers d'une soigneuse description de la extraordinaire phénoménologie vue expérimentalement, à la fois dans le cas non-relativiste "standard", rencontré typiquement dans les heterostructures semiconductrices, et dans le cas relativiste ou anormale, caractéristique du graphène et des isolants topologiques. Ensuite, nous avons analysé l'effet du désordre dans les états de dérive électroniques et nous avons esquissé une théorie assez sophistiqué qui fourni un cadre quantique complètement analytique dans lequel il est possible d'étudier d'une manière quantitative ce régime de transport très particulier. Dans le deuxième chapitre, nous avons présenté l'autre composant, c.à. d. l'interaction SO de type Rashba. Nous avons décrit son origine physique, la génération de couplage SO dans les semiconducteurs de basse dimensionalité et discuté profondement les particularités des niveaux d'énergie dans un gaz d'électrons bidimensionnel (avec couplage Rashba et Zeeman) en absence de désordre. Pour la partie finale de cet échauffement, nous avons revisité d'une façon critique la dynamique du spin dans les GE2D sous la forme des courants de spin, en signalant les contradictions de la définition habituelle de l'opérateur de courant de spin à fort champ magnétique. Ces contradictions se manifestent par la présence de résonances dans la conductance de spin Hall dans les GE2D en absence de désordre.

Comme mentionné précédemment, un des succès les plus remarquables de cette thèse est la généralisation de la théorie vortex de l'effet Hall quantique entier, avec l'objectif d'incorporer des paramètres physiques additionnelles comme le spin de l'électron (et son interaction avec le mouvement orbital des électrons produit par la force de Lorentz). Le cadre théorique général a été décrit dans le troisième chapitre de ce manuscrit, où nous avons introduit une base de spineurs appelés états SO vortex qui fournissent des avantages considérables dans la description de la levée de dégénérescence quantique à l'échelle macroscopique. Cette levée de dégénérescence des niveaux d'énergie est produite bien par une énergie potentielle arbitraire ou bien par les fluctuations aléatoires et lisses du paramètre SO Rashba. Ensuite, nous avons résolu l'équation du mouvement pour la fonction de Green dans la représentation SO vortex en profitant du fait que nous travaillons avec une formulation de déformation quantique dans l'espace de phases (ce qui est possible à fort champ magnétique). Si nous considérons un potentiel de désordre arbitraire localement plat (c. à. d. nous négligeons les termes de courbure locale) qui tient compte des champs électriques aléatoires et du couplage Rashba désordonné, il est possible de calculer la fonction de Green SO vortex pour les états de dérive électroniques et obtenir le spectre énergétique. À partir de l'expression analytique, contrôlée et non-perturbative du spectre, nous avons discuté les mécanismes qui peuvent être impliqués dans la dispersion spatiale des niveaux d'énergie et nous avons analysé l'interaction entre le désordre et les fluctuations du couplage SO Rashba. Finalement, et comme une application directe de la théorie, nous avons calculé

une expression analytique et microscopique de la densité détats locale (LDoS) valable pour différents régimes de températures. La dépendance spatiale et l'élargissement des pics de la LDoS ont ensuite été utilisés dans l'interprétation des donnés expérimentales obtenus par spectroscopie tunnel [11, 86]. Ces donnés montraient des corrélations spatiales entre le spin-splitting en énergie et le potentiel de désordre électrostatique. Notre modèle théorique pour les résultats expérimentaux suggère que les fluctuations spatiales du potentiel désordonné d'origine électrostatique sont plus importantes que les fluctuations du couplage SO Rashba.

Dans le dernier chapitre de cette première partie, nous avons attaqué le problème de la description des propriétés de transport de charge et de spin dans le régime de l'effet Hall quantique, où le transport est décrit par un régime d'équilibre locale (hydrodynamique). À partir d'une expansion en gradient de la contribution vortex à la fonction de Green électronique (ce qui est valable à fort champ magnétiques), nous avons calculé la densité de particules, de spin et du courant sous la forme de fonctionnelles locales de l'énergie potentielle. Ensuite, en utilisant la densité de courant électrique hors d'équilibre, nous avons obtenu le tenseur de conductivité local dans la limite où la diffusion inélastique peut être négligée. Dans ce cas, le tenseur est non-diagonale (les composantes diagonales sont nulles) et il est possible d'extraire une formule analytique de la conductivité de Hall pour le régime sémiclassique. Cette expression manifeste le caractère hybride non-relativiste / relativiste du spectre énergétique (2.21) *: on obtient des plateaux typiques de l'effet Hall quantique entier dite "standard" pour n'importe quelle valeur finie du paramètre de SO Rashba (et pour lesquelles le spectre est borné par le bas) tandis qu'on trouve une conductivité de Hall demi-quantifiée typique de la surface bidimensionnelle d'un isolant topologique désordonné si le couplage SO est formellement infinie (ceci est appelé limite de Dirac et dont le spectre relativiste n'est plus borné). Puis, nous avons profité de la formule de la densité de courant à fort champ pour montrer qu'il est plausible d'établir un courant de spin conservé qui résout les problèmes physiques des définitions précédentes (en particulier, les résonances de la conductance de Hall de spin) et permet d'éliminer les ambiguïtés dans le flot de moment cinétique qui produit des courants persistants. Enfin, nous avons connecté le monde microscopique au monde macroscopique dans le régime de haute température de l'effet Hall quantique entier avec interaction SO en déduisant que l'exposant de percolation classique est préservé même en présence de SO de type Rashba.*

Bicomplex Representation for the Fractional Quantum Hall Effect

In the second part of this thesis, we have begun a deep study of the fractional quantum Hall effect, theoretically reconsidering the problem from a novel point of view by taking into account the insights given by the vortex Green's function method. We expect that this new study of strong correlations in the quantum Hall regime will help to increase the current knowledge of these systems, which surprisingly at the present moment are still not completely understood. At the fundamental level, one of our primary goals is to expand the idea that the Landau level index has a topological origin related to the quantization of the magnetic flux to the many-body regime. As such, we expect to find this (topological)

quantum number in the phase of the wave function, which is also a topological defect (a vortex) in higher dimensions, robust to perturbations (disorder and electron-electron interactions).

As an introduction to this part, we have briefly discussed a portion of the vast body of knowledge that has been collected in the last thirty years about the astonishing physical phenomenon of the fractional quantum Hall effect. To this purpose, we have devoted the fifth chapter of this thesis to introduce the main phenomenology related to many-body effects in 2DEGs under perpendicular magnetic fields and very low temperatures (*i.e.* the fractional quantum Hall regime). Afterwards, we have critically reviewed, identifying both the strengths and the shortcomings, the most important theoretical approaches that deal with the computation of the energy gaps and response functions for the most robust odd-denominator fractions: exact numerical diagonalization, trial wave functions (of the Laughlin's and Jain's type), edge state theory and the Chern-Simons (composite fermion) approaches.

In the sixth chapter, we have presented our approach to start looking for the solution of a generalized two-body problem with strong interactions in the presence of single-particle potential energy (disorder, nonequilibrium electric fields, *etc.*). An important fraction of the chapter has been devoted to the presentation and development of the necessary mathematical tools, some of which have been discovered and refined in the course of this thesis work. We have then pointed out how, by performing an extension of the Hilbert space to a non-Euclidean one, we can introduce a new topological representation for the two-body eigenstates of the free electronic Hamiltonian. These new states, so-called bicomplex vortex states, encode topological long-range correlations between the two electrons whose motion is governed by the Lorentz force. The bicomplex vortex states are also generalized coherent states living in a four dimensional space and describe a robust topological defect. Importantly, we have also proved that the set of bicomplex vortex states form an overcomplete semiorthogonal basis in the extended Hilbert space which can be used to project the equation of motion onto this representation. The Dyson equation, together with the matrix elements of the generalized potential energy, that in this scheme includes one-body and two-body contributions, has been presented afterwards. We have discussed the form of the two-particle infinite order bidifferential product governing the dynamics of the Green's function and compared the full equation of motion to the one obtained in the single-body case. A formal solution in the semiclassical limit (infinite magnetic field or vanishing magnetic length) has been obtained in order to show that one needs to take into account the quantum corrections (at finite magnetic field and finite magnetic length) to obtain spectral gaps in the poles of the Green's function. Indeed, in the semiclassical limit, only a continuous shift due to the potential in the energy levels of the pair is obtained. This is equivalent to saying that the degeneracy of the energy levels is lifted only partially (indeed, only with respect to $\mathbf{R}$ but not with respect to the discrete degeneracy quantum number m or its associated auxiliary integer p). Lastly, we have shown that our approach is mathematically consistent, by proving the closure relation by using a non-trivial identity with techniques related the solution of polynomial equations adapting the methods of calculus (umbral calculus).

Nevertheless, the work is still in progress and many open questions remain to be answered. We name here just a few:

- It is clear that, in order to analytically obtain the fractional plateaus in the electron density and the Hall conductance, we need to find the solution to Dyson equation

(6.62) for finite magnetic length. In this case, it is necessary to fully understand the form of the infinite order bidifferential operator associated to the four dimensional guiding center of the pair composite object and given by Eq. (6.63). From the vortex theory of the single-particle integer quantum Hall effect we know that the form of this differential operator is not unique, its expression (and that of the vortex Green's function) determining both the difficulty in finding a solution to the equation of motion and the structure of the full Green's function in the electronic representation. Whenever a solution to the quantum equation of motion is found, the energies and gaps deduced from the poles of the resulting Green's function would be compared to the energies and gaps obtained by other theoretical methods.

- From the local vortex Green's function, we need to perform a change of variables towards the electronic representation if we want to be able to compute all the physically relevant observables. An example of these quantities is the single-particle electron density, which could be obtained from the lesser Green's function after gauging away the degrees of freedom related to one of the electrons that form the composite vortex, or the Hall conductance. At this moment, we do not know how to trace out these degrees of freedom to obtain single-particle observables. Note also that the connection between the local microscopic quantities calculated using the Green's function scheme and the macroscopic global observables measured in experiments can give considerable computational problems that have be solved.

- Another interesting open question is whether (and how) the change of metric caused when using the bicomplex (non-Euclidean) representation alters the well-known theoretical structure within the Landau level and whether we can recover (or not) the results obtained by exact numerical diagonalization and trial wave functions for the spectral gaps. Intuitively, we may think that it would never be possible to recover the "Euclidean energies" from our bicomplex theory as the structure of the Hilbert space has been soundly changed, but a precise proof of this statement is still lacking.

- Finally, other important open questions are to check if the present formalism is capable of reproducing Laughlin's wave function in the appropriate limits, whether the bicomplex wave function is (or not) better than the wave functions obtained by more standard approaches - that is, if the overlap can be enhanced - or if it is possible to describe the incompressible states with the correct quantum numbers (that are related to the filling factors, fractional charge and fractional statistics).

Dans la deuxième partie de cette thèse, nous avons commencé un étude approfondi de l'effet Hall quantique fractionnaire en reconsidérant théoriquement le problème d'un point de vue alternatif, grâce aux idées sur lesquelles la méthode des fonctions de Green vortex est basée. Nous croyons que cet étude des corrélations fortes dans le régime de l'effet Hall quantique permettra d'augmenter les connaissances sur ces systèmes qui ne sont pas encore complètement compris. Dans un premier temps, un des nos objectifs fondamentaux est l'extension au régime de N-corps de l'idée suivante : l'indice des niveaux de Landau présente une origine topologique et est relié à la quantification du flux magnétique dans deux dimensions. À cet égard, nous nous attendons à trouver

un nombre quantique topologique dans la phase non-triviale de la fonction d'onde à plusieurs particules, laquelle représente aussi un défaut topologique (un vortex) qui habite dans un espace multidimensionnel. Ce vortex doit être robuste aux perturbations quelconques comme le désordre ou les interactions électron-électron.

Comme introduction a cette partie, nous avons discuté brièvement une petite portion de l'immense étendue des connaissances, obtenues pendant les derniers trente ans, sur l'incroyable phénomène connu sous le nom d'effet Hall quantique fractionnaire. À cet effet, nous avons dévoué le cinquième chapitre de cette thèse à l'introduction de la principale phénoménologie relative aux effets à N-corps dans les GE2D soumis à très forts champs magnétiques perpendiculaires et à très basses températures (c. à. d. le régime de l'effet Hall quantique fractionnaire). Ensuite, nous avons revisité de façon critique, en identifiant les forces et les faiblesses, les approches théoriques les plus importants qui permettent de calculer les gaps d'énergie ou les fonctions de réponse pour les fractions impaires les plus robustes : diagonalization numérique exacte, fonctions d'onde d'essaie (de type Laughlin et Jain), théorie des états de bord et approche à la Chern-Simons (fermions composites).

Dans le sixième chapitre, nous avons présenté notre approche pour commencer à chercher la solution d'un problème à deux particules généralisé avec des interactions fortes tout en présence d'une énergie potentielle à un corps (qui représente le désordre, les champs électriques hors d'équilibre etc.). Une partie assez importante de ce chapitre a donc été dévoué à la présentation et développement des nouveaux outils mathématiques nécessaires, une partie desquels ont été découverts et raffinés pendant ce travail de thèse. Puis, nous avons signalé comment, en réalisant une extension de l'espace de Hilbert habituel à un espace non-Euclidien, il est possible d'introduire une représentation topologique des états propres de l'Hamiltonien électronique libre à deux corps. Les nouveaux états, appelés états de vortex bicomplexes, encodent les corrélations topologiques à longue portée entre les deux électrons dont le mouvement est dicté par la force de Lorentz. Les états de vortex bicomplexes sont aussi des états cohérents généralisés définis dans un espace des phases à quatre dimensions où ils décrivent un défaut topologique robuste. Une étape clé pour la théorie à été prouvé ensuite car il est possible de démontrer que l'ensemble d'états de vortex bicomplexes forme une base surcomplète et semiorthogonale dans un espace de Hilbert étendu. Par conséquent, il est licite de projeter l'équation du mouvement pour la fonction de Green dans cette représentation. L'équation de Dyson, associée aux éléments de matrice de l'énergie potentielle généralisée (qui dans ce cadre contient des contributions à un et deux corps) sont présentés après cela. Nous avons considéré en détail la forme du produit bidifférentiel et d'ordre infini à deux particules qui contrôle la dynamique de la fonction de Green ; puis, nous avons comparé l'équation de mouvement complète à celle du cas à un corps. Une solution formelle valable dans la limite sémiclassique (champ magnétique infini ou longueur magnétique qui tend vers zéro) a été obtenue pour montrer qu'il faut aller au-délà de cette limite et tenir compte des corrections quantiques (champ et longueur magnétique finies) pour trouver les gaps d'énergie attendus dans les pôles de la fonction de Green. En effet, dans la limite sémiclassique, seulement un déplacement continu produit par l'énergie potentielle (et pas des gaps) apparaît dans les niveaux d'énergie de la paire d'électrons. Ceci est équivalent à avoir une levée partielle de la dégénérescence produite par l'énergie potentielle (concrètement, seulement par rapport à

R *mais pas par rapport à m ou son entier auxiliaire associé p). Finalement, nous avons montré que notre approche est mathématiquement consistante en prouvant la relation de fermeture des états vortex bicomplexes au moyen d'une identité non-triviale. Pour cette identité, nous utilisons des téchniques reliés au calcul umbral où la méthode du calcul est appliqué dans la résolution des équations pôlynomiales.*

Appendices

Appendix A

Overlap and Completeness Relation of the Vortex Representation

We compute in this appendix the overlap (1.44) *and the completeness relation* (1.47) *for the one-body vortex states using (formal) complex notation.*

Nous calculons dans cet annexe le recouvrement (overlap) (1.44) *et la relation de fermeture* (1.47) *pour les états de vortex à une particule en utilisant notation complexe (formelle).*

A.1. Notation

For this appendix, we rewrite the set of quantum numbers as $\nu = \{n, \mathbf{R}\} \equiv \{n, Z\}$ with $n \geq 0$ and $Z = X + iY$. Prior to any calculations, it also seems judicious to measure all the coordinates in natural units of length, $Z = \sqrt{2} l_B$, so that we rescale the variables as $\mathbf{r} = \sqrt{2} l_B \tilde{\mathbf{r}}$ (thus $z = \sqrt{2} l_B \zeta$) and $\mathbf{R} = \sqrt{2} l_B \tilde{\mathbf{R}}$ (so that $Z = \sqrt{2} l_B \mathcal{Z}$). The vortex wave functions (1.43) present then the following compact dimensionless expression

$$\langle \tilde{\mathbf{r}} | n, \mathcal{Z} \rangle = \frac{(\zeta - \mathcal{Z})^n}{\sqrt{\pi n!}} \exp\left(-\frac{|\zeta|^2 + |\mathcal{Z}|^2 - 2\mathcal{Z}\zeta^*}{2} \right). \tag{A.1}$$

A.2. Overlap

The overlap between two vortex states, $|n, \mathcal{Z}\rangle$ and $|n', \mathcal{Z}'\rangle$, can be computed from the scalar product using Eq. (A.1)

$$\begin{aligned} \langle n, \mathcal{Z} | n', \mathcal{Z}' \rangle = \frac{1}{\pi \sqrt{n! n'!}} \exp\left[-\frac{|\mathcal{Z}|^2 + |\mathcal{Z}'|^2}{2} \right] \\ \times \int_{\mathbb{R}^2} d^2\tilde{\mathbf{r}} \, (\zeta^* - \mathcal{Z}^*)^n (\zeta - \mathcal{Z}')^{n'} \exp\left[-|\zeta|^2 + \mathcal{Z}^* \zeta + \mathcal{Z}' \zeta^* \right], \end{aligned} \tag{A.2}$$

fwhere we inserted the resolution of the identity, written as $\int_{\mathbb{R}^2} d^2\tilde{\mathbf{r}}|\tilde{\mathbf{r}}\rangle\langle\tilde{\mathbf{r}}| = \mathbb{1}$. Here, we have to understand that $d^2\tilde{\mathbf{r}} \equiv dx\,dy$ and that the integration can be performed equivalently in the two-dimensional real plane, $\mathbb{R}^2$ or in the complex plane, $\mathbb{C}$, along purely real or imaginary paths (*i.e.* we are not dealing with a path integration but with real integrals in the complex plane). As a first step, we rewrite the exponential factor inside the 2D integral to obtain

$$\langle n, \mathcal{Z}|n', \mathcal{Z}'\rangle = \frac{\langle \mathcal{Z}|\mathcal{Z}'\rangle}{\pi\sqrt{n!n'!}} \int_{\mathbb{R}^2} d^2\tilde{\mathbf{r}}\,(\zeta^* - \mathcal{Z}^*)^n(\zeta - \mathcal{Z}')^{n'} \exp\left[-(\zeta^* - \mathcal{Z}^*)(\zeta - \mathcal{Z}')\right], \quad \text{(A.3)}$$

where $\langle \mathcal{Z}|\mathcal{Z}'\rangle$ is the overlap defined in Eq. (1.45) - but in dimensionless form - which can be expressed as the standard Glauber-Sudarshan overlap for the coherent states [58, 158]

$$\langle \mathcal{Z}|\mathcal{Z}'\rangle \equiv \exp\left[\mathcal{Z}^*\mathcal{Z}' - \frac{|\mathcal{Z}|^2}{2} - \frac{|\mathcal{Z}'|^2}{2}\right]. \quad \text{(A.4)}$$

Next, we note that the complex variable ζ (resp. ζ^*) appears always associated to the vortex position $\mathcal{Z}'$ (resp. $\mathcal{Z}^*$) inside the 2D integral. This suggests that a shift of complex parameters $\mathcal{Z}'$ and $\mathcal{Z}^*$ for each variable ζ and ζ^* can be performed. This step is made rigorous through a formal change of variables from the planar coordinates $(\tilde{x}, \tilde{y})$, which are a pair of real numbers, to the pair (ζ, ζ^*) understood in the Wirtinger sense [234] (therefore $d^2\tilde{\mathbf{r}} \equiv d\zeta^* d\zeta$). In Wirtinger calculus, also known as $\mathbb{CR}$ calculus, we treat ζ and ζ^* as being independent variables (while in $\mathbb{C}$ they are not) so that local operations such as derivatives, ∂_ζ and ∂_{ζ^*}, or translations are well-defined for any complex function generally not purely analytic nor antianalytic. This change of variables can be interpreted as a linear transformation of the integral (A.3) with integration volume $|\det[J(\zeta, \zeta^*)]| = 1/2$. However, we note that integration has only a formal meaning in $\mathbb{CR}$ calculus so that the integral must be performed in the end using polar coordinates (ρ, θ) with $\rho \in [0, +\infty)$ and $\theta \in [0, 2\pi)$ or any other standard method. In this way, the factor of $1/2$ gets reabsorbed by the inverse linear transformation and we recover Eq. (1.44)

$$\langle n, \mathcal{Z}|n', \mathcal{Z}'\rangle = \frac{\langle \mathcal{Z}|\mathcal{Z}'\rangle}{\pi\sqrt{n!n'!}} \int d\zeta^* d\zeta\,(\zeta^*)^n \zeta^{n'} \mathrm{e}^{-|\zeta|^2}, \quad \text{(A.5)}$$

$$= \frac{\langle \mathcal{Z}|\mathcal{Z}'\rangle}{\pi\sqrt{n!n'!}} \int_0^{+\infty} d\rho\,\rho^{n+n'+1}\mathrm{e}^{-\rho^2} \int_0^{2\pi} d\theta\,\mathrm{e}^{i(n'-n)\theta}, \quad \text{(A.6)}$$

$$= \delta_{n,n'}\langle \mathcal{Z}|\mathcal{Z}'\rangle, \quad \text{(A.7)}$$

after the use of the integral representation of the Kronecker delta function

$$\delta_{k,l} = \frac{1}{2\pi} \int_0^{2\pi} d\theta\,\mathrm{e}^{i(k-l)\theta}. \quad \text{(A.8)}$$

A.3. Closure Relation

Let us now consider in detail the calculation of the completeness (closure) relation of the one-body vortex states. Considering the dimensionless expression for the vortex wave

functions given in Eq. (A.1), we have

$$\int_{\mathbb{R}^2} d^2\tilde{\mathbf{R}} \sum_{n=0}^{+\infty} \langle \tilde{\mathbf{r}}'|n,\mathcal{Z}\rangle\langle n,\mathcal{Z}|\tilde{\mathbf{r}}\rangle = \int_{\mathbb{R}^2} \frac{d^2\tilde{\mathbf{R}}}{\pi} \sum_{n=0}^{+\infty} \frac{1}{n!} \left(\zeta^* - \mathcal{Z}^*\right)^n \left(\zeta' - \mathcal{Z}\right)^n \times \exp\left[-\frac{|\zeta|^2 + |\zeta'|^2 + |\mathcal{Z}|^2 - 2\mathcal{Z}^*\zeta - 2\mathcal{Z}(\zeta')^*}{2}\right], \quad \text{(A.9)}$$

where we note $d^2\tilde{\mathbf{R}} = d\mathcal{X}d\mathcal{Y}$. Recognizing the Taylor series which defines the exponential function, we perform the summation over the index n and rewrite the resulting expression in order to obtain

$$\int_{\mathbb{R}^2} d^2\tilde{\mathbf{R}} \sum_{n=0}^{+\infty} \langle \tilde{\mathbf{r}}|n,\mathcal{Z}\rangle\langle n,\mathcal{Z}|\tilde{\mathbf{r}}\rangle = \exp\left[-\frac{|\zeta|^2 + |\zeta'|^2 - 2\zeta^*\zeta'}{2}\right] \times \int_{\mathbb{R}^2} \frac{d^2\tilde{\mathbf{R}}}{\pi} \exp\left[2i\,\mathrm{Im}\,\mathcal{Z}^*(\zeta - \zeta')\right]. \quad \text{(A.10)}$$

To compute the remaining integral, we can take two different paths. The first one, more straightforward, is to calculate the integral directly using cartesian coordinates and take advantage of the fact that it is possible to the product inside the purely imaginary exponential function as $\mathrm{Im}\,\mathcal{Z}^*(\zeta - \zeta') = -\mathcal{X}(\zeta_y - \zeta'_y) - \mathcal{Y}(\zeta_x - \zeta'_x)$ with $\zeta = \zeta_x + i\zeta_y$ and $\mathcal{Z} = \mathcal{X} + i\mathcal{Y}$. This allows us to transform the two-dimensional integral over the full complex plane into two decoupled 1D integrals along the purely real and imaginary axis

$$\int_{\mathbb{R}^2} \frac{d^2\tilde{\mathbf{R}}}{\pi} \exp\left[2i\,\mathrm{Im}\,\mathcal{Z}^*(\zeta - \zeta')\right] = \frac{1}{4\pi} \int_{\mathbb{R}} d\mathcal{X}\, \mathrm{e}^{-i\mathcal{X}'(\zeta_y - \zeta'_y)} \int_{\mathbb{R}} d\mathcal{Y}\, \mathrm{e}^{-i\mathcal{Y}(\zeta_x - \zeta'_x)}, \quad \text{(A.11)}$$

$$= \pi\delta(\zeta'_x - \zeta_x)\delta(\zeta'_y - \zeta_y), \quad \text{(A.12)}$$

$$= \pi\delta^{(2)}(\tilde{\mathbf{r}}' - \tilde{\mathbf{r}}) = \pi\langle\tilde{\mathbf{r}}'|\tilde{\mathbf{r}}\rangle. \quad \text{(A.13)}$$

Here, we used the product property of the Dirac measure in the n-dimensional Euclidean space, $\delta^{(n)}(\boldsymbol{\xi}) = \delta(\xi_1)\delta(\xi_2)\cdots\delta(\xi_n)$ for $\boldsymbol{\xi} = (\xi_1, \xi_2, \ldots, \xi_n)$ (this property holds only when using Cartesian coordinates). Clearly, this relation has to be true for any position in the plane, so that the following closure relation is verified

$$\int \frac{d^2\tilde{\mathbf{R}}}{\pi} \sum_{n=0}^{+\infty} |n,\mathcal{Z}\rangle\langle n,\mathcal{Z}| = \mathbb{1}. \quad \text{(A.14)}$$

Eq. (1.47) can be straightforwardly recovered from Eq. (A.14) by the proper rescaling of the vortex variables.

An alternative way of obtaining the desired closure relation from the integral (A.10) is to directly use polar coordinates. As a first step, we expand the imaginary exponential inside the 2D integral thanks to its analyticity property in the whole complex plane and map the problem from Cartesian to polar coordinates to get

$$\int_{\mathbb{R}^2} \frac{d^2\tilde{\mathbf{R}}}{\pi} \exp\left[2i\,\mathrm{Im}\,\mathcal{Z}^*(\zeta - \zeta')\right] = \frac{1}{\pi} \int_0^{+\infty} d\rho\,\rho \int_0^{2\pi} d\theta \sum_{k=0}^{+\infty} \sum_{l=0}^{+\infty} \frac{\rho^{k+l}}{k!l!} \times \mathrm{e}^{i(k-l)\theta} \left(\zeta'^* - \zeta^*\right)^k \left(\zeta - \zeta'\right)^l. \quad \text{(A.15)}$$

Since the sums are uniformly convergent (for a proof, use Weierstrass M-test) we can interchange the summations and the integration over the compact set for the angular variable and use Eq. (A.8) to obtain

$$\int_{\mathbb{R}^2} \frac{d^2\tilde{\mathbf{R}}}{\pi} \exp\left[2i\,\mathrm{Im}\,\mathcal{Z}^*(\zeta-\zeta')\right] = 2\int_0^{+\infty} d\rho \sum_{k=0}^{+\infty} \frac{(-1)^k}{(k!)^2}\rho^{2k+1}|\zeta-\zeta'|^{2k}, \tag{A.16}$$

$$= \frac{1}{2}\int_0^{+\infty} d\rho'\rho' J_0(\rho'|\zeta-\zeta'|). \tag{A.17}$$

The last line can be derived considering the Taylor series representation of the Bessel function of the first kind

$$J_\nu(x) = \sum_{k=0}^{+\infty} \frac{(-1)^k}{k!\,\Gamma(k+\nu+1)}\left(\frac{x}{2}\right)^{2k+\nu}, \tag{A.18}$$

and the trivial change of variables $\rho = \rho'/2$. It can be proved (see next subsection) that Eq. (A.17) also give a 2D Dirac delta distribution. This is so even if the argument of the Bessel function only depends on the modulus of the complex number $\zeta - \zeta'$ so that we have apparently lost track of one degree of freedom (the phase), with integration being made only along the radial direction. From a geometrical point of view, we can easily be convinced that the 2D character of the Dirac delta distribution appears as a consequence of the Euclidean geometry in the complex plane[1] which implies $|\zeta-\zeta'| = 0 \Leftrightarrow \zeta = \zeta'$ (this is not true, for example, in non-Euclidean spaces such as the hyperbolic plane as we discuss in the second half of this manuscript). As a result, we recover the same completeness relation given in Eq. (A.14) since

$$\int_{\mathbb{R}^2} \frac{d^2\tilde{\mathbf{R}}}{\pi} \exp\left[2i\,\mathrm{Im}\,\mathcal{Z}^*(\zeta-\zeta')\right] = \pi\delta^{(2)}(\tilde{\mathbf{r}}-\tilde{\mathbf{r}}'). \tag{A.19}$$

An additional justification of this formal identification for the 2D Delta distribution function is also given now.

A.3.1. Two-dimensional Dirac delta distribution function

I would like to devote this final subsection to briefly discussion the subtleties of the Dirac delta distribution in two dimensions, regarding Eq. (A.19). We start from the Fourier representation of $\delta^{(2)}(\mathbf{r})$ and transform it to polar coordinates using *explicitly* the expression of the Euclidean dot product

$$\delta^{(2)}(\mathbf{r}) = \int \frac{d^2\mathbf{k}}{(2\pi)^2}\,\mathrm{e}^{i\mathbf{k}\cdot\mathbf{r}} = \int_0^{+\infty} \frac{dk\,k}{(2\pi)^2}\int_0^{2\pi} d\theta\,\exp\left(ik\rho\cos\theta\right). \tag{A.20}$$

From the integral representation of the Bessel function of the first kind

$$J_\nu(x) = \frac{i^{-\nu}}{2\pi}\int_0^{2\pi} d\theta\,\exp\left[i(\nu\theta + x\cos\theta)\right], \tag{A.21}$$

[1]The algebra in $\mathbb{C}$ is equipped with an intrinsic geometry equivalent to the usual Euclidean geometry in $\mathbb{R}^2$. This can be seen in the definition of the modulus of any complex number $|z|^2 = x^2 + y^2 \leftrightarrow \mathbf{r}\cdot\mathbf{r}$ where $\cdot$ represents the Euclidean dot product and $\mathbf{r} = (x, y)$.

we deduce

$$\delta^{(2)}(\mathbf{r}) = \frac{1}{2\pi}\int_0^{+\infty} dk\, kJ_0(k\rho), \tag{A.22}$$

which, up to a factor of $1/\pi$, is the function appearing in Eq. (A.17).

The role of the angular coordinate, θ, in the 2D Dirac delta distribution centered at the origin (A.20) and acting in the functional space over $\mathbb{R}^2$ is very special. This is so because the origin is a singular point of the coordinate transformation from Cartesian to polar coordinates, in which the Jacobian vanishes and θ is undefined [235]. As such, this coordinate is called *ignorable* for $\rho = 0$ and can be integrated out to get

$$\delta^{(2)}(\mathbf{r}) = \frac{\delta(\rho)}{2\pi\rho}, \tag{A.23}$$

which yields the formal identification

$$\frac{\delta(\rho)}{\rho} = \int_0^{+\infty} dk\, kJ_0(k\rho), \tag{A.24}$$

so that

$$\int_0^{+\infty} d\rho\, \rho \int_0^{+\infty} dk\, kJ_0(k\rho) = 1. \tag{A.25}$$

An alternative way of proving Eq. (A.24) is using the closure relation of the Bessel functions of the first kind

$$\int_0^{+\infty} dk\, kJ_\nu(k\rho)J_\nu(k\rho') = \frac{1}{\rho}\delta(\rho - \rho'). \tag{A.26}$$

Taking $\nu = 0$ and $\rho' = 0$ [note that $J_0(0) = 1$ but this does not hold for $\nu > 0$] we recover Eq. (A.24).

As a concluding observation, tracing out the degrees of freedom associated to ignorable coordinates introduces certain symmetries in the functional space under consideration (in the case of 2D polar coordinates the functions must be invariant under rotations around the origin). As a consequence, the functional spaces on the left and right hand-sides of Eq. (A.22) must also be different (we can also understand this point from the different volume elements). However, in Euclidean spaces, we can still make the identification between both sides because the information about the seemingly missing degree of freedom has been concentrated at the singular point of the transformation, in a similar way the information about a complex function integrated in a complex domain is concentrated in the residues of the singularities enclosed by the integration path.

Appendix B

Calculation of the Spin Hall Conductance from Ref. [112]

The purpose of this appendix is to discuss in detail, both qualitatively and quantitatively, the errors in the calculation of the spin Hall conductance performed in Refs. [112, 113, 114]. We also present the correction to the used method, necessary for the calculation of this observable.

L'objectif de cet annexe est de discuter en détail, qualitativement et quantitativement, les erreurs dans le calcul de la composante de Hall de la conductance de spin faites dans les Réfs. [112, 113, 114]. Nous présentons aussi une correction pour la méthode utilisée, capitale pour le calcul approprié de cet observable.

B.1. General Considerations

In this appendix we consider the same Hamiltonian of Refs. [112, 113, 114]

$$\hat{\mathcal{H}} = \hat{\mathcal{H}}_0 + \hat{V}, \tag{B.1}$$

with $\hat{\mathcal{H}}_0$ given by Eq. (2.18) and the function $V(\mathbf{r}) = -e\mathcal{E}y$ describing the potential energy for a constant electric field applied in the $\hat{\mathbf{y}}$ direction, $\boldsymbol{\mathcal{E}} = \mathcal{E}\hat{\mathbf{y}}$. We further consider a magnetic field pointing towards $-\hat{\mathbf{z}}$ (in agreement with S. Q. Shen *et al.*) but take $e = -|e| < 0$ as in the rest of this thesis.

Let us first analyze Eq. (B.1) for $\boldsymbol{\mathcal{E}} = \mathbf{0}$, when we know that the Hamiltonian can be exactly diagonalized. We choose the Landau gauge, $\mathbf{A}(\mathbf{r}) = yB\hat{\mathbf{x}}$, and periodic boundary conditions in the $\hat{\mathbf{x}}$ direction (so that the wave vector $k_x \equiv k$ is a good quantum number and the states are translationally invariant). Introducing the bosonic operators of the harmonic oscillator given in Eq. (1.21), the kinetic term $\hat{\mathcal{H}}_0$ can be rewritten as

$$\hat{\mathcal{H}}_0 = \hbar\omega_c \left\{ \hat{a}_+(k)\hat{a}_-(k) + \frac{1 - Z\sigma_z}{2} + \frac{S}{2}\Big[\hat{a}_-(k)\sigma_- - \hat{a}_+(k)\sigma_+\Big] \right\}. \tag{B.2}$$

Here, we remind that we have, as usual, $\hat{a}_+^\dagger(k) = \hat{a}_-(k)$ for fixed k, $[\hat{a}_-(k), \hat{a}_+(k')] = \delta(k - k')$ for any k, k', $\sigma_\pm = (\sigma_x \pm i\sigma_y)/2$ and we introduced the parameters S and Z

respectively defined in Eqs. (2.22) and (2.23). We have also used $1 \equiv \mathbb{1}$ in order to simplify the notation. The eigenenergies of this Hamiltonian have been already obtained in Sec. 2.2.3 and are given in Eq. (2.21). The eigenstates of Hamiltonian (B.2) are spinors which can be written as[1]

$$\tilde{\Psi}_{n,k,\lambda}(\mathbf{r}) = \langle \mathbf{r}|n,k,\lambda\rangle = \begin{bmatrix} \cos(\theta_n^\lambda)\phi_{n,k}(\mathbf{r}) \\ i\sin(\theta_n^\lambda)\phi_{n-1,k}(\mathbf{r}) \end{bmatrix}, \tag{B.3}$$

where each component has a weight characterized by the angle θ_n^λ defined in Eq. (3.4) and $\phi_{n,k}(\mathbf{r}) = \langle \mathbf{r}|n,k\rangle$ is a Landau wave function, eigenstate of the Hamiltonian (1.11). These eigenfunctions present the following functional expression

$$\phi_{n,k}(\mathbf{r}) = \frac{1}{\sqrt{2^n n!\pi^{1/2} l_B}} \mathrm{e}^{ikx} \exp\left[-\frac{1}{2l_B^2}(y-y_0)^2\right] H_n\left(\frac{y-y_0}{l_B}\right), \tag{B.4}$$

with $y_0 = -kl_B^2$ and $H_n(y)$ a Hermite polynomial of degree n. Note that in this gauge, the moduli of $|\phi_{n,k}(\mathbf{r})|$ are invariant under translations in the $\hat{\mathbf{x}}$ direction and that these eigenstates are not square integrable in the 2D plane.

At this level, we can consider the presence of the constant electric field. For a classical harmonic oscillator, this electric field simply shifts the equilibrium position of the oscillator. In the quantum world, the bosonic operators (1.21) become the operators associated to a forced quantum harmonic oscillator. For a constant electric field, this situation can be taken into account at the operator level by the shifts

$$y \to y' = y - \frac{e\mathcal{E}}{m^*\omega_c^2}, \tag{B.5}$$

$$\hat{a}_-(k) \to \hat{a}'_-(k) = \hat{a}_-(k) - \frac{1}{\sqrt{2}}\frac{l_B}{\hbar}\frac{e\mathcal{E}}{\omega_c}. \tag{B.6}$$

Disregarding contributions quadratic in the electric field, which is assumed to be weak and only lift the macroscopic degeneracy of the Landau levels, it can be proved that the Hamiltonian (B.1) yields

$$\hat{\mathcal{H}} = \hat{\mathcal{H}}'_0 + \hat{\mathcal{H}}', \tag{B.7}$$

where $\hat{\mathcal{H}}'_0$ is given by Eq. (B.2) but expressed in the new shifted operators and

$$\hat{\mathcal{H}}' = \left[\frac{el_B}{2\sqrt{2}} S\sigma_y - \hbar k\frac{c}{B}\right]\mathcal{E}. \tag{B.8}$$

An important point to be addressed here is that the Hamiltonian considered in Refs. [112, 113] and the review [114] is different to this one since the authors forgot to perform the shift in the potential term [*i.e.* the last contribution in Eq. (B.8) is missing]. Moreover, we have to take into account that the electric field $\boldsymbol{\mathcal{E}}$ is defined only at equilibrium, with the only objective of lifting the huge degeneracy of the Landau levels and then be able to apply non-degenerate perturbation theory. Note that, in this case, we cannot consider the use of any linear response technique in this electric field since in the limit $|\boldsymbol{\mathcal{E}}| \to 0$ the Landau levels are again degenerate. To avoid this problem using this method, we have to make instead a distinction between an equilibrium and a nonequilibrium electric field

[1] Note that there is a certain freedom in the way the spinors are written as seen when comparing this expression to Eq. (3.6).

inside the perturbation (before shifting the harmonic oscillator by the equilibrium electric field) so that Eq. (B.8) reads instead

$$\hat{\mathcal{H}}' = \left[\frac{el_B}{2\sqrt{2}} S\sigma_y - \hbar k \frac{c}{B}\right] \mathcal{E}_{\text{eq}} + ey'\mathcal{E}_{\text{neq}}. \tag{B.9}$$

The first part of this expression lifts the degeneracy of the Landau levels (it is allowed then to used non-degenerate perturbation theory in the electric field) while the actual perturbation is given by the second part linear in $\mathcal{E}_{\text{neq}}$. Therefore, it is licit to use a linear response-like approach since we can safely take the limit $\mathcal{E}_{\text{neq}} \to 0$ without affecting the lifting of the degeneracy of the Landau levels.

We turn now to the calculation of the spin current density polarized in the direction $\hat{\mathbf{z}}$ using the operator defined in Eq. (2.26). Focusing on the $\hat{\mathbf{x}}$ component only in Eq. (2.28), since the drift velocity $\mathbf{v}_d \propto \boldsymbol{\mathcal{E}} \times \mathbf{B}$, the spin current density operator reads in this gauge

$$\hat{j}^z_{x,s} = \frac{\hbar}{2}\left(\frac{p_x}{m^*} + \omega_c y' + \frac{e\mathcal{E}_{\text{eq}}}{m^* c}\right)\sigma_z. \tag{B.10}$$

The average spin current density is obtained by summing over all the matrix elements weighted by the distribution function,

$$J^z_{x,s} = \sum_{n,k,\lambda} \left(j^z_{x,s}\right)_{n,k,\lambda} n_{\text{F}}(E_{n,\lambda}), \tag{B.11}$$

where have noted $\left(j^z_{x,s}\right)_{n,k,\lambda}$ the matrix elements of the spin current density operator, $n_{\text{F}}(E)$ the Fermi-Dirac distribution function [given in Eq. (4.15)] and the sum over the quantum numbers is equal to

$$\sum_{n,k,\lambda} = \frac{L_x}{2\pi} \sum_{n=0}^{+\infty} \sum_{\lambda} \int_0^{k_{\max}} dk, \tag{B.12}$$

with $k_{\max} = (2\pi/L_x)n_B$ and n_B the number of states per Landau level. Note that in Eq. (B.10) we have taken into account that the velocity operator in the formula of the spin current density has been shifted and that the electric field appearing in the formula is the equilibrium component. Finally, the spin Hall conductance follows from Eq. (B.11) thanks to the definition $G^s_{\text{H}} \equiv \partial J^z_{x,s}/\partial\mathcal{E}$, that holds for a clean system, in which the integration of the spin current density over the system cross section is trivial.

B.2. Hall Conductance

Before entering into the details of the spin Hall conductance, let us very briefly discuss the result for the [electronic] Hall conductance obtained in Ref. [112]. There, the authors argue that the Hall conductance of the clean system remains unchanged by the presence of Rashba SO interaction. This is partially true at relatively low temperatures where the height of the plateaus (but not the width) is invariant and equal to the conductance quantum e^2/h, as shown in Eq. (4.55). The obtention of this non-trivial result in the presence of a smooth disorder potential is explained in chapter 4 where we show how to eliminate the seemingly present divergencies related to the accidental degeneracies between the pairs of Rashba-Landau energy levels.

B.3. Equilibrium Spin Hall Conductance

We now examine the zero-th order contribution to the spin current density in the framework of perturbation theory. This term can be computed from the diagonal matrix elements of the spin current density operator (B.10)

$$\left(j^z_{x,s}\right)^{(0)}_{n,k,\lambda} = \langle n,k,\lambda|\hat{j}|n,k,\lambda\rangle, \tag{B.13}$$

where we have noted $\hat{j} \equiv \hat{j}^z_{x,s}$. Disregarding all the contributions that are not linear in the (equilibrium) electric field we have

$$\left(j^z_{x,s}\right)^{(0)}_{n,k,\lambda} = \frac{e\mathcal{E}_{\rm eq}}{m^*\omega_c}\langle n,k,\lambda|\sigma_z|n,k,\lambda\rangle = \frac{e\mathcal{E}_{\rm eq}}{m^*\omega_c}\cos(2\theta^\lambda_n), \tag{B.14}$$

where we have used the result

$$\langle n,k,\lambda|\sigma_z|n',k,\lambda'\rangle = \left[\cos(\theta^\lambda_n)\cos(\theta^{\lambda'}_{n'}) - \sin(\theta^\lambda_n)\sin(\theta^{\lambda'}_{n'})\right]\delta_{n,n'}, \tag{B.15}$$

$$= \cos(\theta^\lambda_n + \theta^{\lambda'}_n). \tag{B.16}$$

Finally, introducing the following identity

$$\cos(2\theta^\lambda_n) = \lambda\sqrt{1-\frac{nS^2}{\Delta_n}}, \tag{B.17}$$

the zero-th order spin Hall conductance reads

$$G^{\rm H\,(0)}_s = \frac{e}{4\pi}\sum_{n=0}^{+\infty}\sum_\lambda \lambda n_{\rm F}(E_{n,\lambda})\sqrt{1-\frac{nS^2}{\Delta_n}}, \tag{B.18}$$

which, up to a global minus sign related to the definition of the electron charge, is the result given in Eq. (12) of Ref. [112] or Eq. (15) of Ref. [113]. As it is defined, we stress that this coefficient cannot describe spin transport since the spin current has been generated by an equilibrium electric field. Note also that the spin current density computed in this way can be thought to be related to the density-gradient current introduced in Sec. 4.4.2, as it is a current that appears only for non-vanishing a spin density or spin polarization (4.22). Finally, notice that we have obtained from the zero-th order term in the perturbation expansion the semiclassical spin polarization. Our gradient expansion (see chapter 4) is much more general because it allows us to obtain quantum-mechanical corrections by considering higher order terms in the l_B series.

B.4. Nonequilibrium Spin Hall Conductance

Let us analyze at this point the nonequilibrium contribution to the spin current density. This term appears when considering Landau level mixing in the presence of a nonequilibrium electric field and therefore, can describe transport of spin (so that the spin Hall conductance has a well-defined physical meaning). In order to obtain this quantity, we assume that $\boldsymbol{\mathcal{E}}_{\rm eq}$ has already lifted the degeneracy of the energy levels, so that non-degenerate perturbation theory can be applied (in $\boldsymbol{\mathcal{E}}_{\rm neq}$). We therefore compute the matrix elements

$$\left(j^z_{x,s}\right)^{(1)}_{n,k,\lambda} = \sum_{n',\lambda'}\frac{\langle n',k,\lambda'|ey'\mathcal{E}_{\rm neq}|n,k,\lambda\rangle\langle n,k,\lambda,|\hat{j}|n',k,\lambda'\rangle}{E_{n,\lambda}-E_{n',\lambda'}} + \text{h.c.}, \tag{B.19}$$

where it is implicitly assumed that $n = n' - 1$, $\lambda \neq \lambda'$ and h.c means hermitian conjugate. The only relevant term in the calculation of the matrix elements of the spin current operator $\langle n, k, \lambda, |\hat{j}|n', k, \lambda'\rangle$ given in Eq. (B.10) is the second factor $\hbar\omega_c y'\sigma_z/2$ because, as it can be shown straightforwardly, we have

$$\langle n, k, \lambda|\hat{p}_x\sigma_z|n', k, \lambda'\rangle = \hbar k \cos(\theta_n^{\lambda} + \theta_{n'}^{\lambda'})\delta_{n,n'}. \tag{B.20}$$

That is, the matrix elements of the first factor are diagonal in the Landau level index and, as a consequence, this contribution is automatically excluded from Eq. (B.19). We also disregard all the matrix elements coming from the third term in Eq. (B.10) since they give a current quadratic in the electric field (proportional to $\mathcal{E}_{\rm eq}\mathcal{E}_{\rm neq}$). Taking into account the matrix elements

$$\langle n, k, \lambda|\hat{y}'\sigma_z|n', k, \lambda'\rangle = \sqrt{\frac{\hbar}{2m^*\omega_c}}\Bigg\{ \cos(\theta_n^{\lambda})\cos(\theta_{n'}^{\lambda'})\Big[\sqrt{n'+1}\delta_{n,n'+1} + \sqrt{n'}\delta_{n,n'-1}\Big] - \sin(\theta_n^{\lambda})\sin(\theta_{n'}^{\lambda'})\Big[\sqrt{n'}\delta_{n,n'+1} + \sqrt{n'-1}\delta_{n,n'-1}\Big]\Bigg\}, \tag{B.21}$$

which can be derived from the matrix elements of the position operator of a shifted harmonic oscillator, and following standard computational steps [we introduce Eq. (B.21) into Eqs. (B.19) and (B.11) and evaluate the sum over the Landau levels] we get

$$G_s^{\mathrm{H}\,(1)} = \frac{e}{4\pi}(\hbar\omega_c)\sum_{n=0}^{+\infty}\sum_{\lambda,\lambda'}\frac{n_{\rm F}(E_{n+1,\lambda'}) - n_{\rm F}(E_{n,\lambda})}{E_{n+1,\lambda'} - E_{n,\lambda}} \times \Big[(n+1)\cos^2(\theta_{n+1}^{\lambda'})\cos^2(\theta_n^{\lambda}) - n\sin^2(\theta_{n+1}^{\lambda'})\sin^2(\theta_n^{\lambda})\Big]. \tag{B.22}$$

Several comments are now in order. First, this formula is completely different from Eq. (13) of Ref. [112]. That our calculation has been correctly made can be checked performing the same calculation within the vortex formalism. In that case, we used the method detailed in Sec. 4.4 but for the operator (2.28) instead of the electron current operator. The result for the spin Hall conductivity (which, in a clean system is trivially connected to the spin Hall conductance) is

$$\sigma_{\rm H}^s(\mathbf{r}) = \frac{e}{4\pi}(\hbar\omega_c)\sum_{n=0}^{+\infty}\sum_{\lambda,\lambda'}\frac{n_{\rm F}[\xi_{n+1,\lambda'}(\mathbf{r})] - n_{\rm F}[\xi_{n,\lambda}(\mathbf{r})]}{E_{n+1,\lambda'} - E_{n,\lambda}} \times \Big[(n+1)\cos^2(\theta_n^{\lambda})\cos^2(\theta_{n+1}^{\lambda'}) - n\sin^2(\theta_n^{\lambda})\sin^2(\theta_{n+1}^{\lambda'})\Big], \tag{B.23}$$

where $\xi_{n,\lambda}(\mathbf{r}) = E_{n,\lambda} + V(\mathbf{r})$ and $V(\mathbf{r})$ is an arbitrary (smooth) disorder potential. The second observation to be made is that both formulas (B.22) and (B.23) present resonances whenever two energy levels (n, λ) and (n', λ') become arbitrary close[2]. As such, we can conclude that these resonances appear in the derived expressions not as a result of the method but as an artifact coming from the chosen form for the spin density operator (this

[2]This means that there is an explicit dependence on the SO coupling parameter S in Eq. (B.23), as a difference to the Hall conductivity. This statement can be proved by performing an expansion in powers of S, which can be done analytically up to order $\mathcal{O}(S)^3$.

is not surprising after our discussion in Sec. 2.3.1). A possible solution to this problem, valid in the quantum Hall regime at high magnetic fields, is proposed in Sec. 4.5.3 where, taking advantage of the fact that λ is still a good quantum number, we write the spin current as the difference between two SO-polarized currents. In this way, we automatically choose the proper parametrization in spin space and no resonances, only finite jumps, appear when two energy levels are degenerate. Note also that, physically, these resonances never occur since any non-zero amount of mixing between the two energy levels (due to the disorder, for instance) will always produce an anticrossing due to level repulsion in the spectrum.

Appendix C

Contribution to the electron current density from $g^{(1)}(\mathbf{R};\omega)$

We present in this appendix the details of the calculation of the quantum functionals (4.40) *and* (4.41).

Nous présentons dans cet annexe les détails du calcul des fonctionnelles quantiques (4.40) *et* (4.41).

We start with the spin-resolved U(1) contribution to the drift current density which can be obtained by reporting Eq. (4.10) into Eqs. (4.14) and (4.31). Integration over the energies yields

$$\begin{aligned}\mathbf{j}^{\mathrm{dr}}_{1\sigma}(\mathbf{r}) = \frac{e\hbar}{2m^*}\int \frac{d^2\mathbf{R}}{2\pi l_B^2}\sum_{n=0}^{+\infty}\sum_{\lambda_1,\lambda_2}\sum_{\sigma'=\pm}\frac{l_B}{\sqrt{2}}\sqrt{n_{\sigma'}+1}f_\sigma(\theta_n^{\lambda_1})f_{\sigma'}(\theta_n^{\lambda_1})\\ \times f_\sigma(\theta_{n+1}^{\lambda_2})f_{\sigma'}(\theta_{n+1}^{\lambda_2})\Big[\mathbf{J}_{n_\sigma;n_\sigma+1}(\mathbf{r},\mathbf{R})\partial_+ + \mathbf{J}_{n_\sigma+1;n_\sigma}(\mathbf{r},\mathbf{R})\partial_-\Big]V(\mathbf{R})\\ \times \hbar\omega_c\frac{n_{\mathrm{F}}[\xi_{n+1,\lambda_2}(\mathbf{R})]-n_{\mathrm{F}}[\xi_{n,\lambda_1}(\mathbf{R})]}{\xi_{n+1,\lambda_2}(\mathbf{R})-\xi_{n,\lambda_1}(\mathbf{R})}.\end{aligned} \tag{C.1}$$

Here, the last line contains the difference of the Fermi-Dirac distribution functions evaluated for adjacent Rashba-Landau energy levels [as a consequence of the level mixing induced by the gradients $\partial_\pm V(\mathbf{R})$] and $\mathbf{J}_{n_1;n_2}(\mathbf{r},\mathbf{R})$ is the current kernel (4.32). We also remind that the partial derivatives were defined as $\partial_\pm \equiv \partial_X \pm i\partial_Y$.

Expansion of the bracketed terms shows that the current kernel contribution presents, either diagonal elements of the electronic kernel $F_n(\mathbf{r}-\mathbf{R})$ or terms differing in two Landau levels of the form $F_{n;n\pm2}(\mathbf{r},\mathbf{r},\mathbf{R})$ (that is, both terms give contributions which survive in the semiclassical limit). The latter off-diagonal elements of the electronic kernel satisfy the following identities [130]

$$\sqrt{n+2}\sqrt{n+1}F_{n;n+2}(\mathbf{r},\mathbf{r},\mathbf{R}) = \frac{l_B^2}{2}\sum_{q=0}^{n}(n+1-q)\partial_-^2 F_q(\mathbf{r}-\mathbf{R}), \tag{C.2}$$

$$\frac{l_B^2}{2}\Delta_{\mathbf{r}}\sum_{q=0}^{n}(n+1-q)F_q(\mathbf{r}-\mathbf{R}) = (n+1)F_{n+1}(\mathbf{r}-\mathbf{R}) - \sum_{q=0}^{n}F_q(\mathbf{r}-\mathbf{R}). \tag{C.3}$$

As a result, the bracketed term in Eq. (C.1) can be rewritten in the following way

$$\begin{aligned}
&\frac{l_B^2}{2}\begin{pmatrix}\mathrm{Im}\\ \mathrm{Re}\end{pmatrix}\partial_+ V(\mathbf{R})\sum_{q=0}^{n_\sigma}(n_\sigma+1-q)\partial_-^2 F_q(\mathbf{r}-\mathbf{R}) = \\
&\hat{\mathbf{z}}\times\boldsymbol{\nabla}_{\mathbf{R}}V(\mathbf{R})\left[\sum_{q=0}^{n_\sigma}F_q(\mathbf{r}-\mathbf{R}) - (n_\sigma+1)F_{n_\sigma+1}(\mathbf{r}-\mathbf{R})\right] \\
&+ l_B^2\hat{\mathbf{z}}\times\left[\boldsymbol{\nabla}_{\mathbf{R}}V(\mathbf{R})\cdot\boldsymbol{\nabla}_{\mathbf{r}}\right]\boldsymbol{\nabla}_{\mathbf{r}}\sum_{q=0}^{n_\sigma}(n_\sigma+1-q)F_q(\mathbf{r}-\mathbf{R}).
\end{aligned} \tag{C.4}$$

Using the identity

$$\boldsymbol{\nabla}_{\mathbf{r}}\left[\boldsymbol{\nabla}_{\mathbf{R}}V(\mathbf{R})\cdot\boldsymbol{\nabla}_{\mathbf{r}}F_q(\mathbf{r}-\mathbf{R})\right] = \left[\boldsymbol{\nabla}_{\mathbf{R}}V(\mathbf{R})\cdot\boldsymbol{\nabla}_{\mathbf{r}}\right]\boldsymbol{\nabla}_{\mathbf{r}}F_q(\mathbf{r}-\mathbf{R}), \tag{C.5}$$

we arrive at the final result for the U(1) contribution presented in Eq. (4.40).

We now proceed analogously with the SU(2) contribution, first inserting Eq. (4.10) into Eqs. (4.14) and (4.33) and integrating over the frequencies to obtain

$$\begin{aligned}
\mathbf{j}_{2\sigma}^{\mathrm{dr}}(\mathbf{r}) = \frac{i\alpha e l_B}{\sqrt{2}}\int\frac{d^2\mathbf{R}}{2\pi l_B^2}\sum_{n=0}^{+\infty}\sum_{\lambda_1,\lambda_2}\sum_{\sigma'=\pm}\sqrt{n_{\sigma'}+1} \\
\times f_\sigma(\theta_n^{\lambda_1})f_{\sigma'}(\theta_n^{\lambda_1})f_{-\sigma}(\theta_{n+1}^{\lambda_2})f_{\sigma'}(\theta_{n+1}^{\lambda_2}) \\
\times\Big[F_{n_\sigma;n_{-\sigma}+1}(\mathbf{r},\mathbf{r},\mathbf{R})\partial_+\,(\mp)\,F_{n_\sigma;n_{-\sigma}+1}(\mathbf{r},\mathbf{r},\mathbf{R})\partial_-\Big]V(\mathbf{R})\begin{pmatrix}\sigma\\ i\end{pmatrix} \\
\times\hbar\omega_c\frac{n_{\mathrm{F}}[\xi_{n+1,\lambda_2}(\mathbf{R})] - n_{\mathrm{F}}[\xi_{n,\lambda_1}(\mathbf{R})]}{\xi_{n+1,\lambda_2}(\mathbf{R}) - \xi_{n,\lambda_1}(\mathbf{R})},
\end{aligned} \tag{C.6}$$

where $(\mp)$ means taking $-$ for the $\hat{\mathbf{x}}$ component and $+$ for the $\hat{\mathbf{y}}$ component. As it happened for the SU(2) term in the density-gradient current density, we have to sum over the two spin-projected currents to combine the pairs of electronic kernels between square brackets and obtain a real expression for the current density. Further collecting all the contributions, the SU(2) term is expressed as in Eq. (4.41).

Appendix D

Dictionary of Abstract Algebra

We give to the reader in this appendix a useful map to navigate in the sea of terminology characteristic of the field of abstract algebra and which appears through chapter 6. We mainly focus our attention into the basic definitions and results that justify the existence of a "vector space" over the bicomplex numbers. The whole discussion presented here is essentially based on Refs. [237, 238].

Comme une guide pour le lecteur, nous présentons dans cet annexe une carte utile pour naviguer dans la mer de terminologie caractéristique du domaine de l'algèbre abstraite et qui apparait tout à travers du chapitre 6. Nous nous concentrons dans les définitions basiques et les résultats qui justifient l'existence d'un "espace vectoriel" sur les nombres bicomplexes. L'essentiel des explications présentées ici est inspiré des Réfs. [237, 238].

D.1. Rings and Ideals

D.1.1. Rings

A ring, noted here $\mathcal{R}$, is an important algebraic structure which lies in between the quite flexible notion of group and the more constraining definition of field (which contains, for instance, the well-known sets of real and complex numbers noted respectively $\mathbb{R}$ and $\mathbb{C}$). More precisely, we have the formal definition:

Definition 1 A **ring**[1] is a non-empty set together with two binary operations, usually called addition, noted $+$, and multiplication, noted by either $\cdot$ or a blank space, such that $\forall r, s, t \in \mathcal{R}$

- $(\mathcal{R}, +)$ is an abelian group, *i.e.* the following properties hold:

  1. $r + s = s + t$ (Commutativity),
  2. $(r + s) + t = r + (s + t)$ (Associativity),

[1] One may also encounter the terms ring with unity, unital/unitary ring or ring with identity.

3. $0 + r = r$ (Identity for the addition),
4. $\exists(-r) \in \mathcal{R}$ such that $r + (-r) \equiv r - r = 0$ (Additive inverse).

- $(\mathcal{R}, \cdot)$ is a monoid[2], *i.e.* we have:

1. $(rs)t = r(st)$ (Associativity).
2. $1r = r1 = r$ (Identity for the multiplication)

- The complete distributive law is satisfied:

1. $r(s + t) = rs + rt$ (Left distributivity),
2. $(r + s)t = rt + st$ (Right distributivity).

We note that the multiplication operation in a ring does not have to be commutative. In case it is, we have $rs = sr$ and the ring is called a commutative ring. An example of the latter is the set of integers, $\mathbb{Z}$. However, unlike the familiar integers, non-zero elements of generalized rings can present multiplicative inverses and / or their product can give the identity for the addition. These important properties appear as a consequence of the broad multiplicative structure of the ring and, as a consequence, the corresponding elements verifying them are given special names:

Definition 2 A left zero divisor (respectively right zero divisor) is an element of a ring $r \in \mathcal{R}$ such that $\exists s \in \mathcal{R}$ for which $rs = 0$ (resp. $sr = 0$). A simultaneous left and right zero divisor is simply called a **zero divisor**.

Definition 3 An element $r \in \mathcal{R}$ of a ring is said to be left invertible (resp. right invertible) if $\exists s \in \mathcal{R}$ such that $sr = 1$ (resp. $\exists t \in \mathcal{R}$ such that $rt = 1$). Whenever $s = t \equiv r^{-1}$, this element is said to be **invertible** or to be a **unit**.

The rings whose elements belong (or not) to any of the previous two classes also receive special names:

Definition 4 An **integral domain** is a commutative ring without zero divisors (for example, $\mathbb{Z}$).

Definition 5 A ring in which every non-zero element has a multiplicative inverse, *i.e.* $\forall r \in \mathcal{R} \,|\, r \neq 0$; $\exists r^{-1} \in \mathcal{R}$ such that $rr^{-1} = r^{-1}r = 1$, is a **division ring** or **skew field**. When the ring is also commutative it is called a **field** and is traditionally noted by the letter $\mathbb{K}$. Again, as introduced before, typical examples of this structure are $\mathbb{R}$ and $\mathbb{C}$.

A first important idea that can be extracted from the definitions 2 and 4 is that in an integral domain all the elements present a multiplicative cancellation property related to the lack of zero divisors: if $r, s, t \in \mathcal{R}$ where r is not a zero divisor and $rs = rt$ then, either $r = 0$ or $s = t$ (the proof is trivial). Second, from the definition 5 we have that a field is simply a commutative ring such that each element is a unit. This is highly restraining and imposes that a field has exclusively non-zero divisors, because an element of the ring can not be at the same time a unit and a zero divisor (a field is trivially an integral domain).

We shall finish this subsection with another definition and a theorem:

[2] A monoid is a non-empty set equipped with an associative (closed) binary operation and an identity, typically noted $1 \equiv 1_{\mathcal{R}}$, such that $1 \neq 0$.

Definition 6 We say that an element of a ring, $r \in \mathcal{R}$, is

- nilpotent whenever $r^n = 0$ for $n \in \mathbb{N}$ (n is called the degree of nilpotency),
- idempotent whenever $r^2 = r$.

Theorem 1 Every non-trivial idempotent in a ring, different from 0 or 1, is a zero divisor.

Proof: Straightforward, since $r^2 = r \Rightarrow r(r-1) = 0$. Using an analogous argument, we can also prove that non-zero nilpotent elements of a ring must also be zero divisors.

D.1.2. Ideals

We move at this point to the next important concept of this section, the notion of ideal, which is a fundamental entity in ring theory. We have the following definition:

Definition 7 A subring $\mathcal{I}$ of a ring $\mathcal{R}$ is any non-empty subset, $\mathcal{I} \subset \mathcal{R}$, closed under the natural operations in $\mathcal{R}$. When $\forall r \in \mathcal{R}$ and $x \in \mathcal{I}$ we have $rx \in \mathcal{I}$ (resp. $xr \in \mathcal{I}$) a subring $\mathcal{I}$ is said to be a left ideal (resp. right ideal). Subrings which are simultaneously a left and a right ideal of a ring are simply called **ideals**[3].

The ideals play the same role as normal subgroups do in group theory [239], being invariant subsets of elements of the ring under specific circumstances (automorphisms, which map the ring into itself). They also define a partition of the ring into equivalence classes such that two elements of the ring $r, s \in \mathcal{R}$ are congruent $r \sim s$ if, and only if, $r - s \in \mathcal{I}$ (they are said to be congruent *modulo* $\mathcal{I}$). As such, each class is a set formed by the elements $[r]_{\mathcal{I}} \equiv \{r + i \,|\, i \in \mathcal{I}\}$. The set of all equivalence classes, $\mathcal{R}/\mathcal{I}$, is called quotient ring[4].

There are many types of ideals which can be used to build different kinds of rings. Here, we will mainly focus on the most important ones regarding our task of understanding the ring of bicomplex numbers. One important example of ideals are generated from the elements of the ring. Indeed, given a finite set $\mathcal{I} \in \mathcal{R}$ the elements of $\mathcal{I}$, usually written in tuple notation $(\mathcal{I}) = (i_1, \ldots, i_n)$, are called generators of the ideal $\mathcal{I}$. We say that an ideal is a **principal ideal** if it is generated by a unique element and a ring which is constituted exclusively of principal ideals is called a principal ideal ring. Evidently, the trivial ideal and the complete ring are both principal and generated respectively by 0 and 1.

Definition 8 A proper ideal $\mathcal{P}$ in a ring $\mathcal{R}$ is said to be **prime** if $\forall \mathcal{I}, \mathcal{J} \subset \mathcal{R}$

$$\mathcal{I}\mathcal{J} \subset \mathcal{P} \Rightarrow \mathcal{I} \subset \mathcal{P} \text{ or } \mathcal{J} \subset \mathcal{P}. \tag{D.1}$$

Using the mentioned definition, we can state the following theorems (given without a proof)

[3] We consider here ideals different from the trivial ideal - whose unique element is the zero element of the ring - and the whole ring, which are called proper ideals.

[4] Consider the following simple example: let $\mathbb{Z}$ be the ring of integers and $2\mathbb{Z}$ the (commutative) ring of even integers, which actually is an ideal of the former. The quotient ring $\mathbb{Z}_2 \equiv \mathbb{Z}/(2\mathbb{Z}) = \{\bar{0}, \bar{1}\}$ is the set of integers modulo 2 where $\bar{0}$ represents the even and $\bar{1}$ the odd numbers, *i.e.* which differ from an even number by 1.

Theorem 2 If $\mathcal{P}$ is a proper ideal in a ring $\mathcal{R}$ such that $\forall r, s \in \mathcal{R}$

$$rs \in \mathcal{P} \Rightarrow r \in \mathcal{P} \text{ or } s \in \mathcal{P}, \tag{D.2}$$

then, $\mathcal{P}$ is prime. Conversely, if $\mathcal{P}$ is prime and $\mathcal{R}$ is a commutative ring, the implication (D.2) is always satisfied.

Theorem 3 A proper ideal $\mathcal{P}$ of a commutative ring $\mathcal{R}$ is prime if, and only if, the quotient ring is an integral domain.

We shall finish this section with another important definition and a result.

Definition 9 A proper ideal $\mathcal{I}$ is said to be **maximal** if, for any other proper ideal $\mathcal{J}$ such that $\mathcal{I} \subset \mathcal{J} \subset \mathcal{R}$ is satisfied, then either $\mathcal{I} = \mathcal{J}$ or $\mathcal{J} = \mathcal{R}$. When the two ideals are maximal and we also have $\mathcal{I} \bigcup \mathcal{J} = \mathcal{R}$, both are said to be **comaximal**.

These ideals are always guaranteed to exist in a non-trivial ring. Moreover, we have

Theorem 4 Suppose that $\mathcal{R}$ is a ring which contains an ideal $\mathcal{I}$. Then, for $\mathcal{I}$ maximal and $\mathcal{R}$ commutative, the quotient $\mathcal{R}/\mathcal{I}$ is a division ring. Reciprocally, if the quotient $\mathcal{R}/\mathcal{I}$ is a division ring, then $\mathcal{I}$ is maximal.

D.2. Modules and Algebras

D.2.1. Modules

Intuitively, we can understand the notion of module as the suitable framework of linear algebra over an arbitrary ring of elements. As such, this structure generalizes the idea of vector space but with the scalars allowed to belong to a ring instead of an algebraic field. We note here that, as a difference to vector spaces over fields, a complete classification of all modules for arbitrary rings is still an unsolved problem. Partial results are known for finite-generated modules over integral domains and the so-called free modules (see below). As a result, modules are seemingly more complicated objects than vector spaces, where a basis is not guaranteed to exist, and even if it does, its cardinality is not an invariant.

Definition 10 A (left) **module** over an arbitrary ring $\mathcal{R}$, represented (M, φ_M), is an abelian group M with respect to addition, noted $+$, together with a linear map φ_M, called *scalar multiplication* and noted by a blank space, describing the action of elements of the ring $\mathcal{R}$ on the elements M

$$\begin{aligned} \varphi_M : \mathcal{R} \times M &\to M, \\ (r, m) &\to \varphi_M(r, m) = rm, \end{aligned} \tag{D.3}$$

which is defined for all $r \in \mathcal{R}$, $m \in M$ such that $\forall r, s \in \mathcal{R}$ and $\forall m, n \in M$ such that

1. $r(sm) = (rs)m$ (Associativity),
2. $r(m + n) = rm + rn$ (Distributivity with respect to addition in M),
3. $(r + s)m = rm + sm$ (Distributivity with respect to scalar multiplication).

Elements of M (which, by abuse of notation, denotes the complete module) are usually called vectors.

Let us consider some sweatless examples. The easiest one is a proper ideal of a ring, which is a module over the ring $\mathcal{R}$ itself with the scalar multiplication being the usual multiplication defined in the ring. As a second example, consider the set of square n-dimensional matrices whose entries are elements of a ring, $\mathcal{M}_n(\mathcal{R})$. This is a left module with intrinsic Euclidean metric if we define the module scalar multiplication through the matrix multiplication. Finally [239], consider the ring of real C^1 functions (continuous and at least once differentiable) defined by $f : \mathbb{R}^n \to \mathbf{R}$. These objects are known as scalar fields. We now define the set of n-tuples or vector fields on $\mathbb{R}^n$ by $\mathbf{f}(\mathbf{x}) \equiv [f_1(\mathbf{x}), \ldots, f_n(\mathbf{x})]$ where each component is a scalar field. Under the multiplication rule

$$g(\mathbf{x})\mathbf{f}(\mathbf{x}) = [g(\mathbf{x})f_1(\mathbf{x}), \ldots, g(\mathbf{x})f_n(\mathbf{x})], \tag{D.4}$$

the vector fields define a finite-dimensional module over the C^1 real-valued functions.

Of course, we can restrain the definition of module in the same way as we constrain a ring to be a field:

Definition 11 When $\mathcal{R}$ is a unitary ring, the module built over $\mathcal{R}$ is said to be unitary and we have $1m = m \ \forall m \in M$. If the ring is also division ring, the module is called a left **vector space**.

We also note that we can define, in the same way as above, the right counterpart of the left module: a (unitary) right module over the ring $\mathcal{R}$ is characterized by the map $\varphi'_M : M \times \mathcal{R} \to M$. For commutative rings, there is an isomorphism between any left and right modules over a ring $\mathcal{R}$ if we define $mr \equiv rm \ \forall r \in \mathcal{R}$, $m \in M$ so that we simply speak about (unitary) modules. In what follows we shall assume that all modules over commutative rings are both left and right modules in the previous sense.

After the foundations are laid, we are now in measure of introducing many concepts which will sound familiar to anybody with a basic grasp of linear algebra in vector spaces. First, we establish the existence of an identity element for vector addition, $0_M \equiv \mathbf{0}$. It is straightforward to prove that if $0_\mathcal{R}$ is the additive identity in $\mathcal{R}$ then, $\forall r \in \mathcal{R}$ and $\forall m \in M$

$$0_\mathcal{R} m = \mathbf{0}, \tag{D.5a}$$
$$r\mathbf{0} = \mathbf{0}. \tag{D.5b}$$

As a consequence we identify in the rest of the section $0_\mathcal{R}$, $0 \in \mathbb{Z}$, the trivial module noted $\{\mathbf{0}\}$ and the vector $\mathbf{0}$.

Next, we introduce the notion of **submodule**, which is nothing but a subgroup of a module closed under the restrictive operations that appear in the definitions 10 and 11. Evidently, a submodule has to be a module itself since it inherits all the properties of its father (for the same reasons, a submodule of a unitary module is itself unitary). The usual concepts of linear algebra can now be used for modules, for example:

Definition 12 Let X be a subset of a module M. The intersection of all submodules of M which contain X is called the submodule generated by X. For a finite subset X, the intersection generates the (sub)module N which is said to be **finitely generated**[5] or that X spans N.

[5] In case X is empty it generates the trivial module $\{\mathbf{0}\}$.

Linear independence and basis can be defined at this point in the same way as in vector spaces, which we remind are special cases of modules built over division rings. Of particular importance in module theory are the so-called free modules which are defined by the following theorem (given without a proof):

Theorem 5 Consider $\mathcal{R}$ to be a ring with unity. The following conditions are equivalent:

1. M has a non-empty basis.
2. M is a direct sum of a family of submodules over R, each of which is isomorphic to $\mathcal{R}$, that is,
$$M = \bigoplus_{i \in \Lambda} R, \tag{D.6}$$
where Λ is a set of non-negative integers (not necessarily finite) and R is the module over the ring $\mathcal{R}$ given by the ring itself.

A (unitary) module satisfying any of the previous statements is called a **free module** over the ring $\mathcal{R}$.

The previous theorem yields a constructive way of building a module from a ring $\mathcal{R}$ by defining $\mathcal{R}^n = \{(r_1, \ldots, r_n) \,|\, r_i \in \mathcal{R}\ \forall i = 1, \ldots, n\}$ and making it a module by componentwise addition and multiplication by the elements of ring. We stress that, as a difference to vector spaces, in module theory a submodule of a free module is not necessarily free.

As a final result, we define the analogue of the basis theorem in a module:

Theorem 6 Let $\mathcal{R}$ be a ring and M a free module with a basis, X. Then, every basis of M has the same cardinality than X.

If this theorem holds, M is said to present the **invariant dimension property** with the cardinal of any basis in M called the **rank** of the module. Whenever $\mathcal{R}$ is a division ring, it is well-known that the module always presents this property (since in a vector space all basis have the same number of elements). The same happens when considering a free module over a commutative unital ring, although unfortunately this ceases to be true for modules built over arbitrary rings.

D.2.2. Algebras

Once the scene is set up for linear algebra, the last step is to define the multiplication operation between two arbitrary elements of a module. To that purpose, we have to define the notion of algebra over a ring.

Definition 13 An **algebra**, $\mathcal{A}$, over a ring, $\mathcal{R}$, is a module equipped with a bilinear operation $B(\,\cdot\,,\,\cdot\,) : M \times M \to M$.

That is to say, an algebra is a set of vectors that can be added, multiplied and multiplied by scalars which belong to the underlying ring. When the module is free and it has rank equal to n, the algebra is defined by a set of expressions of the form [205]

$$q = \sum_{k=1}^{n} a_k i_k, \tag{D.7}$$

where the elements $a_k \in \mathcal{R}$ with $k \in \{1, \ldots, n\}$ and $\{i_k\}_{k=1}^n$ is a collection of symbols[6] (called *versors* or *unit basis vectors*). The multiplication $B(q, q') \equiv qq'$ is determined by the table of products

$$i_\alpha i_\beta = \sum_{k=1}^{n} p_{\alpha\beta}^{(k)} i_k, \tag{D.8}$$

where $p_{\alpha\beta}^{(k)} \in \mathcal{R}$ with $\alpha, \beta, k \in \{1, \ldots, n\}$. The algebra $\mathcal{A}$ is completely determined by a choice of the multiplication table, whose coefficients are called structure constants of the algebra. Two algebras are mutually isomorphic if the coefficients appearing in the multiplication table can be made identical by a linear map. Note that, when the module content is to be emphasized, we also write an element of the algebra as a n-tuple $\mathbf{q} = (a_1, \ldots, a_n)$ with the product of two tuples defined accordingly.

Whenever the bilinear operation $B(\,\cdot\,,\,\cdot\,)$ is associative and presents a unity we say that the algebra is a (unitary) associative algebra. Additionally, it can also be commutative and, evidently, the algebra is said to be a commutative algebra. In this case, it is clear that the matrix whose elements are the structure constants is symmetric and we have $i_\alpha i_\beta = i_\beta i_\alpha$. If any non-zero element of the algebra has a multiplicative inverse we say that it is a division algebra. Note that, in a certain way, we can see Eq. (D.7) as a generalization of the fields $\mathbb{K} = \mathbb{R}$, which is a real algebra over itself, or $\mathbb{K} = \mathbb{C}$, which is a two-dimensional commutative division algebra over $\mathbb{R}$. As a consequence, the elements of the algebra $\mathcal{A}$ are called **hypercomplex numbers** [240].

Matrix representation

Any algebra $\mathcal{A}$ also admits a matrix representation [241] where the entries of the matrix belong to a subalgebra $\mathcal{B} \subset \mathcal{A}$. For example, the algebra of the complex numbers $\mathbb{C}$ can be mapped to the algebra of 2×2 matrices with real coefficients, $\mathcal{M}_2(\mathbb{R})$, by the isomorphism

$$z = x + iy \leftrightarrow \mathcal{Z} = \begin{bmatrix} x & -y \\ y & x \end{bmatrix}. \tag{D.9}$$

The properties of the algebra can then be studied from the structure and allowed operations of these matrices. For example, in the case of Eq. (D.9), the sum and products of matrices yield the expected result for the component wise sum and product of two given complex numbers. The determinant of the matrix $\mathcal{Z}$, which is an invariant, can be related to the modulus of the complex number since $|z|^2 = x^2 + y^2 = \det(\mathcal{Z})$.

Calculus over algebras

We would like to end up this appendix with a mathematical justification for the use of algebras $\mathcal{A}$, different than the usual $\mathbb{R}$ or $\mathbb{C}$, as a platform in the quest for a useful and consistent function theory in higher dimensional modules. These results for algebras are certainly not new. Indeed, the two main important theorems which restrict the use of certain algebras for this purpose where formulated more than a hundred years ago. The first one, attributed to Frobënius (1877), states [242]:

[6] When the underlying ring (or one of its subrings) is the set of real numbers, we customarily define $i_1 \equiv 1$.

Theorem 7 Division algebras over the real numbers of dimension higher than two cannot be commutative.

This theorem can be seen as the reason why quaternions, which are a four-dimensional associative division algebra over the real numbers, do not commute. The second fundamental theorem was proved by Scheffers in 1893 [205]:

Theorem 8 Conventional [analytic] differential and integral calculus does not exist over a non-commutative algebra.

The latter theorem justifies why a standard calculus does not exist for quaternions but leaves the door open for (standard) calculus on commutative algebras such as that generated in the bicomplex (commutative quaternion) module.

Appendix E

Coordinate Transformations in the Bicomplex Vortex Representation

We detail in this appendix the necessary steps involved in some of the intermediate calculations related to the change of coordinates from the complex to the bicomplex space.

Dans cet annexe nous détaillons les étapes nécessaires pour comprendre certains calculs intermédiaires relatifs au changement des coordonnées depuis l'espace complexe vers l'espace bicomplexe.

E.1. Jacobian to Polar Coordinates

We briefly mention here how to compute the Jacobian that governs the change of variables between the Cartesian and polar variables in the bicomplex numbers, as defined in Sec. 6.2.2. The calculation is fairly simple: first, the Jacobian matrix is defined as

$$J(\rho, \theta_i, \varphi, \theta_{ij}) = \frac{\partial(t, x, y, z)}{\partial(\rho, \theta_i, \varphi, \theta_{ij})}, \tag{E.1}$$

where each row respectively contains the partial derivatives of the Cartesian variables $\{t, x, y, z\}$ with respect to the polar variables $\{\rho, \theta_i, \varphi, \theta_{ij}\}$. The calculation of the partial derivatives is trivial and yields the following matrix

$$J(\rho, \theta_i, \varphi, \theta_{ij}) = \begin{bmatrix} t/\rho & -x & y & -z \\ x/\rho & t & z & y \\ y/\rho & -z & t & -x \\ z/\rho & y & x & t \end{bmatrix}. \tag{E.2}$$

Note that the Jacobian matrix (E.2) has exactly the same form of the characteristic matrix (6.12) but with the elements of the first column divided by ρ. Therefore, we have

$$\det[J(\rho, \theta_i, \varphi, \theta_{ij})] = \frac{1}{\rho}\det\tilde{M}_q = \rho^3 \tag{E.3}$$

so that the differential coordinate transformation is $d^4q = \rho^3 d\rho\, d\theta_i d\varphi d\theta_{ij}$. This transformation proves useful in the identification of the forbidden zones (zero divisors) in the bicomplex functional space.

E.2. Laplacian Operator

We show in this section how to write the Laplacian operator using bicomplex coordinates. Noting that bicomplex numbers present three different types of (bicomplex) conjugation, we define the linear transformation $\{x_1, y_1, x_2, y_2\} \to \{q, q^{*^i}, q^{*^j}, q^{*^{ij}}\}$ by

$$q = z_1 + jz_2 = x_1 + iy_1 + jx_2 + ijy_2, \tag{E.4a}$$

$$q^{*^i} = z_1^* + jz_2^* = x_1 - iy_1 + jx_2 - ijy_2, \tag{E.4b}$$

$$q^{*^j} = z_1 - jz_2 = x_1 + iy_1 - jx_2 - ijy_2, \tag{E.4c}$$

$$q^{*^{ij}} = z_1^* - jz_2^* = x_1 - iy_1 - jx_2 + ijy_2, \tag{E.4d}$$

where $*$ is the usual complex conjugation [$z_k^* = (x_k + iy_k)^* = x_k - iy_k$ for $k \in \{1, 2\}$] and we remind that $j^2 = +1$ is the hyperbolic unit. The inverse linear transformation $\{q, q^{*^i}, q^{*^j}, q^{*^{ij}}\} \to \{x_1, y_1, x_2, y_2\}$ is given by

$$x_1 = \frac{1}{4}\left(q + q^{*^i} + q^{*^j} + q^{*^{ij}}\right), \tag{E.5a}$$

$$y_1 = \frac{1}{4i}\left(q - q^{*^i} + q^{*^j} - q^{*^{ij}}\right), \tag{E.5b}$$

$$x_2 = \frac{1}{4j}\left(q + q^{*^i} - q^{*^j} - q^{*^{ij}}\right), \tag{E.5c}$$

$$y_2 = \frac{1}{4ij}\left(q - q^{*^i} - q^{*^j} + q^{*^{ij}}\right). \tag{E.5d}$$

Calculation of the derivatives is straightforward using the chain rule. For the Cartesian coordinates given by the set $\{x_1, y_1, x_2, y_2\}$ we get

$$\partial_{x_1} = \partial_q + \partial_{q^{*^i}} + \partial_{q^{*^j}} + \partial_{q^{*^{ij}}}, \tag{E.6a}$$

$$\partial_{y_1} = i\left(\partial_q - \partial_{q^{*^i}} + \partial_{q^{*^j}} - \partial_{q^{*^{ij}}}\right), \tag{E.6b}$$

$$\partial_{x_2} = j\left(\partial_q + \partial_{q^{*^i}} - \partial_{q^{*^j}} - \partial_{q^{*^{ij}}}\right), \tag{E.6c}$$

$$\partial_{y_2} = (ij)\left(\partial_q - \partial_{q^{*^i}} - \partial_{q^{*^j}} + \partial_{q^{*^{ij}}}\right). \tag{E.6d}$$

The derivatives with respect to the components of the set of bicomplex coordinates $\{q, q^{*^i}, q^{*^j}, q^{*^{ij}}\}$ can also be obtained very easily and yield

$$\partial_q = \partial_{x_1} - i\partial_{y_1} + j\partial_{x_2} - (ij)\partial_{y_2}, \tag{E.7a}$$

$$\partial_{q^{*^i}} = \partial_{x_1} + i\partial_{y_1} + j\partial_{x_2} + (ij)\partial_{y_2}, \tag{E.7b}$$

$$\partial_{q^{*^j}} = \partial_{x_1} - i\partial_{y_1} - j\partial_{x_2} + (ij)\partial_{y_2}, \tag{E.7c}$$

$$\partial_{q^{*^{ij}}} = \partial_{x_1} + i\partial_{y_1} - j\partial_{x_2} - (ij)\partial_{y_2}. \tag{E.7d}$$

The second order derivatives with respect to the members of the set $\{x_1, y_1, x_2, y_2\}$ can be computed applying again the chain rule to Eqs. (E.6a)-(E.6d). We find

$$\begin{aligned}
\partial_{x_1}^2 = {} & \partial_q^2 + \partial_{q^{*i}}^2 + \partial_{q^{*j}}^2 + \partial_{q^{*ij}}^2 + 2\partial_q\partial_{q^{*i}} + 2\partial_q\partial_{q^{*j}} + 2\partial_q\partial_{q^{*ij}} \\
& + 2\partial_{q^{*i}}\partial_{q^{*j}} + 2\partial_{q^{*i}}\partial_{q^{*ij}} + 2\partial_{q^{*j}}\partial_{q^{*ij}}\,, \qquad \text{(E.8a)} \\
\partial_{y_1}^2 = {} & -\partial_q^2 - \partial_{q^{*i}}^2 - \partial_{q^{*j}}^2 - \partial_{q^{*ij}}^2 + 2\partial_q\partial_{q^{*i}} - 2\partial_q\partial_{q^{*j}} + 2\partial_q\partial_{q^{*ij}} \\
& + 2\partial_{q^{*i}}\partial_{q^{*j}} - 2\partial_{q^{*i}}\partial_{q^{*ij}} + 2\partial_{q^{*j}}\partial_{q^{*ij}}\,, \qquad \text{(E.8b)} \\
\partial_{x_2}^2 = {} & \partial_q^2 + \partial_{q^{*i}}^2 + \partial_{q^{*j}}^2 + \partial_{q^{*ij}}^2 + 2\partial_q\partial_{q^{*i}} - 2\partial_q\partial_{q^{*j}} - 2\partial_q\partial_{q^{*ij}} \\
& - 2\partial_{q^{*i}}\partial_{q^{*j}} - 2\partial_{q^{*i}}\partial_{q^{*ij}} + 2\partial_{q^{*j}}\partial_{q^{*ij}}\,, \qquad \text{(E.8c)} \\
\partial_{y_2}^2 = {} & -\partial_q^2 - \partial_{q^{*i}}^2 - \partial_{q^{*j}}^2 - \partial_{q^{*ij}}^2 + 2\partial_q\partial_{q^{*i}} + 2\partial_q\partial_{q^{*j}} - 2\partial_q\partial_{q^{*ij}} \\
& - 2\partial_{q^{*i}}\partial_{q^{*j}} + 2\partial_{q^{*i}}\partial_{q^{*ij}} + 2\partial_{q^{*j}}\partial_{q^{*ij}}\,. \qquad \text{(E.8d)}
\end{aligned}$$

Inserting the previous expressions into the definition of the Laplacian operator, $\Delta \equiv \Delta_{\mathbf{r}_1} + \Delta_{\mathbf{r}_2} = \partial_{x_1}^2 + \partial_{y_1}^2 + \partial_{x_2}^2 + \partial_{y_2}^2$, we finally get

$$\Delta = 8\left(\partial_q\partial_{q^{*i}} + \partial_{q^{*j}}\partial_{q^{*ij}}\right). \qquad \text{(E.9)}$$

Note that the obtained form for the Laplacian operator shows that the four independent second order derivatives in the complex space get rearranged into two decoupled pairs of hyperbolic conjugate first order derivatives in the bicomplex space. This is a consequence of the fact that the Laplacian operator is real (in this sense, it does not contain any complex numbers, neither in its definition nor in the spectral decomposition).

Appendix F

Proof of Relation (6.41)

In this appendix, we provide a proof of the useful identity given in Eq. (6.41)*, necessary to compute many integrals in the bicomplex Hilbert space, such as those that appear in the normalization of the two-body wave function, the overlap between two bicomplex vortex states or the modified Voros product which governs the dynamics of the bicomplex Green's function.*

Dans cet annexe, nous fournissons une démonstration d'une identité remarquable, introduite dans l'Éq. (6.41)*, cruciale pour calculer beaucoup d'intégrales dans l'espace de Hilbert bicomplexe. Les intégrales de ce type apparaissent dans la normalisation de la fonction d'onde à deux corps, le recouvrement entre deux états de vortex bicomplexes ou même le produit de Voros modifié qui régit la dynamique de la fonction de Green bicomplexe.*

Our goal in this appendix is to evaluate the following integral

$$I_{n,m;n',m'} = 16 \int \frac{d^4\mathbf{r}}{(2\pi)^2} q^{n'} \left(q^{*^i}\right)^n \left(q^{*^j}\right)^m \left(q^{*^{ij}}\right)^{m'} \exp\left[-\left(qq^{*^i} + q^{*^j} q^{*^{ij}}\right)\right], \tag{F.1}$$

$$= n!m!\,\delta_{n,n'}\delta_{m,m'}. \tag{F.2}$$

and show that the second equality holds. This integral is a generalized version of Eq. (6.41) and can be computed by using a generating function that encodes the non-Euclidean geometry of the bicomplex module in an elementary way. To see how this works, let us consider first the simpler case $n = n' = 0$ and $m = m' = 0$ which corresponds to a real Gaussian integral. The integral can be computed by standard calculus because the hyperbolic unit j is absent (there is no need to use the conformal projection techniques developed in Sec. 6.2.4) and its value, $I_{0,0;0,0} = 1$ acts as a "source" value for the rest of integrals. The presence of the factorials and the Kronecker delta functions can be proved by using the invariance under translations of the integral in the full four dimensional bicomplex space. This is a very general principle and clearly belongs to the class of distance preserving maps in the bicomplex module. In this case, we have

$$16 \int \frac{d^4\mathbf{r}}{(2\pi)^2} \exp\left[-(q-Q)(q-Q)^{*^i} - (q-Q)^{*^j}(q-Q)^{*^{ij}}\right] = 1, \tag{F.3}$$

from which we can derive the identity

$$\frac{4}{\pi^2}\int d^4\mathbf{r}\exp\left[-\left(qq^{*^i}+q^{*^j}q^{*^{ij}}\right)\right]\exp\left(Qq^{*^i}+Q^{*^i}q+Q^{*^j}q^{*^{ij}}+Q^{*^{ij}}q^{*^j}\right)$$
$$=\exp(QQ^{*^i}+Q^{*^j}Q^{*^{ij}}). \quad \text{(F.4)}$$

The left-hand side of this equation is a generating function and its moments with respect to Q, Q^{*^i}, Q^{*^j} and $Q^{*^{ij}}$ (which are generated by taking n, n', m and m' derivatives with respect to the previous parameters and setting all of them simultaneously to zero afterwards) yields Eq. (F.2). The Kronecker delta functions appear as additional constraints on the right-hand side of the identity at the moment of considering $\mathbf{R}=\mathbf{0}$.

Bibliography

[1] R. G. Mani, J. H. Smet, K. v. Klitzing, V. Narayanamurti, W. B. Johnson, and V. Umanskyk, Nature **420**, 646 (2002).

[2] K. Hashimoto, T. Champel, S. Florens, C. Sohrmann, J. Wiebe, Y. Hirayama, R. A. Römer, R. Wiesendanger, and M. Morgenstern, Phys. Rev. Lett. **109**, 116805 (2012).

[3] K. S. Novoselov, A. K. Geim, S. V. Morozov, D. Jiang, M. I. Katsnelson, I. V. Grigorieva, S. V. Dubonos, and A. A. Firsov, Nature **438**, 197 (2005).

[4] C. Brüne, C. X. Liu, E. G. Novik, E. M. Hankiewicz, H. Buhmann, Y. L. Chen, X. L. Qi, Z. X. Shen, S. C. Zhang, and L. Molenkamp, Phys. Rev. Lett. **106**, 126803 (2011).

[5] M. E. Raikh and T. V. Shahbazyan, Phys. Rev. B **47**, 1522 (1993).

[6] M. Flöser, *From Local to Non-Local Transport: Percolation in Quantum Hall Systems / Cross Correlations in Superconducting Hybrid Structures* (PhD thesis, Université de Grenoble, 2012).

[7] T. Champel, *Vortex Theory of the Quantum Hall Effect* (Habilitation Thesis, Université Joseph Fourier, Grenoble, France, 2013).

[8] E. I. Rashba, Fiz. Tverd. Tela (Leningrad) **2**, 1224 (1960) [Sov. Phys. Solid State **2**, 1109 (1960)].

[9] H. C. Koo, J. H. Kwon, J. Eom, J. Chang, S. H. Han, and M. Johnson, Science **325**, 1515 (2009).

[10] J. K. Jain, *Composite Fermions* (Cambridge University Press, Cambridge, 2007).

[11] M. Morgenstern, A. Georgi, C. Straßber, C. R. Ast, S. Becker, and M. Liebmann, Physica E **44**, 1795 (2012).

[12] K. von Klitzing, G. Dorda, and M. Pepper, Phys. Rev. Lett. **45**, 494 (1980).

[13] K. von Klitzing, *25 years of quantum Hall effect: a personal view on the discovery, physics and applications of this quantum effect*, Séminaire Poincaré, 1 (2004).

[14] K. von Klitzing, Rev. Mod. Phys. **58**, 519 (1986).

[15] H. Bachmair, E. O. Göbel, G. Hein, J. Melcher, B. Schumacher, J. Schurr, L. Schweitzer, and P. Warnecke, Physica E **20**, 14 (2003).

[16] W. Poirier, F. Schopfer, J. Guignard, O. Thévenot, and P. Gournay, C. R. Physique **12**, 347 (2011).

[17] F. Schopfer and W. Poirier, MRS Bull. **37**, 1255 (2012).

[18] Y. Zhang, Y. W. Tan, H. Stormer, and P. Kim, Nature **438**, 201 (2005).

[19] K. S. Novoselov, Z. Jiang, Y. Zhang, S. V. Morozov, H. L. Stormer, U. Zeitler, J. C. Maan, G. S. Boebinger, P. Kim, and A. K. Geim, Science **315**, 1379 (2007).

[20] M. O. Goerbig, *Quantum Hall Effects*, arXiv:0909.1998 (2009).

[21] F. Amet, J. R. Wiliams, K. Watanabe, T. Taniguchi, and D. Goldhaber-Gordon, Phys. Rev. Lett. **112**, 196601 (2014).

[22] B. Jeckelmann and B. Jeanneret, Rep. Prog. Phys. **64**, 1603 (2001).

[23] D. C. Tsui, H. L. Stormer, and A. C. Gossard, Phys. Rev. Lett. **48**, 1559 (1982).

[24] C. W. J. Beenakker and H. van Houten, Solid State Phys. **44**, 1 (1991).

[25] N. M. R. Peres, Rev. Mod. Phys. **82**, 2673 (2010).

[26] M. O. Goerbig, Rev. Mod. Phys. **83**, 1193 (2011).

[27] K. S. Novoselov, D. Jiang, F. Schedin, T. J. Booth, V. V. Khotkevich, S. M. Morozov, and A. K. Geim, Proc. Natl. Acad. Sci. U. S. A. **102**, 10451 (2005).

[28] P. Avouris and C. Dimitrakopoulos, Mater. Today **15**, 86 (2012).

[29] T. Hanaguri, K. Igarashi, M. Kawamura, H. Tagaki, and T. Sasagawa, Phys. Rev. B **82**, 081305(R) (2010).

[30] Y. Jiang, Y. Wang, M. Chen, Z. Li, C. Song, K. He, L. Wang, X. Chen, X. Ma, and Q. K. Xue, Phys. Rev. Lett. **108**, 016401 (2010).

[31] E. Abrahams, P. W. Anderson, D. C. Licciardello, and T. V. Ramakrishnan, Phys. Rev. Lett. **42**, 673 (1979).

[32] N. W. Ashcroft and N. D. Mermin, *Solid State Physics* (Saunders, USA, 1976).

[33] E. H. Hall, Am. J. Math. **2**, 287 (1879).

[34] M. M. Fogler, A. Yu. Dobin, V. I. Perel, and B. I. Shklovskii, Phys. Rev. B **56**, 6823 (1997).

[35] M. Flöser, B. A. Piot, C. L. Campbell, D. K. Maude, M. Henini, R. Airey, Z. R. Wasilewski, S. Florens, and T. Champel, New J. Physics **15**, 083027 (2013).

[36] B. Douçot and V. Pasquier, *Physics in a strong magnetic field*, Séminaire Poincaré, 17 (2004).

[37] P. A. M. Dirac, *The Principles of Quantum Mechanics* (Oxford University Press, Oxford, 1981).

[38] S. Kivelson, C. Kallin, D. Arovas, and J. R. Schrieffer, Phys. Rev. B **36**, 1620 (1987).

[39] X. L. Qi and S. C. Zhang, Rev. Mod. Phys. **83**, 1057 (2011).

[40] R. Jackiw, Phys. Rev. D **29**, 2375 (1984).

[41] A. H. MacDonald, *Introduction to the physics of the quantum Hall regime*, edited by E. Akkermans, G. Montambaux, J. L. Pichard, and J. Zinn-Justin, Les Houches Session LXI (Elsevier, Amsterdam, 1995).

[42] K. Hashimoto, C. Sohrmann, J. Wiebe, T. Inaoka, F. Meier, Y. Hirayama, R. A. Römer, R. Wiesendanger, and M. Morgenstern, Phys. Rev. Lett. **101**, 256802 (2008).

[43] R. E. Prange, Phys. Rev. B **23**, 4802 (1981).

[44] B. I. Halperin, Phys. Rev. B **25**, 2185 (1982).

[45] T. Champel and S. Florens, Phys. Rev. B **80**, 161311(R) (2009).

[46] J. T. Chalker and P. D. Coddington, J. Phys. C **21**, 2665 (1988).

[47] B. Kramer, T. Ohtsuki, and S. Kettemann, Phys. Rep. **417**, 211 (2005).

[48] E. Bocquillon, V. Freulon, F. D. Parmentier, J. M. Berroir, B. Plaçais, C. Wahl, J. Rech, T. Jonckheere, T. Martin, C. Grenier, D. Ferraro, P. Degiovanni, and G. Fève, Ann. Phys. **526**, 1 (2013).

[49] M. Büttiker, Phys. Rev. B **38**, 9375 (1988).

[50] M. Z. Hasan and C. L. Kane, Rev. Mod. Phys. **82**, 3045 (2010).

[51] Z. F. Ezawa, *Quantum Hall Effects: Field Theoretical Approach and Related Topics* (World Scientific, Singapore, 2008).

[52] D. Yoshioka, *The Quantum Hall Effect* (Springer, Berlin, 2002).

[53] J. N. Fuchs, F. Piéchon, M. O. Goerbig, and G. Montambaux, Eur. Phys. J. B **77**, 351 (2010).

[54] I. A. Malkin and V. I. Man'ko, Zh. Eksp. Teor. Fiz. **55**, 1014 (1968) [Sov. Phys. JETP **28**, 527 (1969)].

[55] T. Champel and S. Florens, Phys. Rev. B **75**, 245326 (2007).

[56] J. P. Gazeau, *Coherent States in Quantum Physics* (Wiley-VCH, Weinheim, Germany, 2009).

[57] W.-M. Zhang, D. H. Feng, and R. Gilmore, Rev. Mod. Phys. **62**, 867 (1990).

[58] E. C. G. Sudarshan, Phys. Rev. Lett. **10**, 277 (1963).

[59] *Quantum Mechanics in Phase Space: An overview with selected papers*, edited by C. K. Zachos, D. B. Fairlie, and T. L. Curtright, World Scientific Series in 20th Century Physics, Vol. **34** (World Scientific, Singapore, 2005).

[60] C. Zachos, Int. J. Mod. Phys. A **17**, 297 (2002).

[61] F. Bayen, M. Flato, C. Fronsdal, A. Lichnerowicz, and D. Sternheimer, Ann. Phys. **111**, 61 (1978); **111**, 111 (1978).

[62] M. R. Douglas and N. A. Nekrasov, Rev. Mod. Phys. **73**, 977 (2001).

[63] C. Zachos, J. Math. Phys. **41**, 5129 (2000).

[64] S. Galluccio, F. Lizzi, and P. Vitale, Phys. Rev. D **78**, 085007 (2008).

[65] I. Žutic, J. Fabian, and S. Das Sarma, Rev. Mod. Phys. **76**, 323 (2004).

[66] D. D. Awschalom, L. C. Bassett, A. S. Dzurak, E. L. Hu, and J. R. Petta, Science **339**, 1174 (2013).

[67] S. Datta and B. Das, Appl. Phys. Lett. **56**, 665 (1990).

[68] L. Chirolli, D. Venturelli, F. Taddei, R. Fazio, and V. Giovannetti, Phys. Rev. B **85**, 155317 (2012).

[69] T. Nakajima, K. T. Lin, and S. Komiyama, arXiv:1207.7243.

[70] C. Cohen-Tannoudji, B. Diu, and F. Laloë, *Quantum Mechanics* (Wiley, France, 1977).

[71] S. Goudsmit and G.E. Uhlenbeck, Physica **6**, 273 (1926).

[72] *Spin Physics in Semiconductors*, edited by M. I. Dyakonov, Springer Series in Solid-State Sciences, Vol. **157** (Springer-Verlag, Heidelberg, 2008).

[73] R. Winkler, *Spin-Orbit Effect in Two-Dimensional Electron and Hole Systems* (Springer, Berlin, 2003).

[74] Y. A. Bychov and E. I. Rashba, Pis'ma Zh. Eksp. Teor. Fiz. **39**, 66 (1984) [JETP Lett. **39**, 78 (1984)].

[75] G. Dresselhaus, Phys. Rev. **100**, 580 (1955).

[76] J. Nitta, T. Akazaki, H. Takayanagi, and T. Enoki, Phys. Rev. Lett. **78**, 1335 (1997).

[77] E. Ya. Sherman, Phys. Rev. B **67**, 161303 (2003).

[78] M. M. Glazov and E. Ya. Sherman, Phys. Rev. B **71**, 241312(R) (2005).

[79] M. M. Glazov, E. Ya. Sherman, and V. K. Dugaev, Physica E **42**, 2157 (2010).

[80] J. Schliemann, Int. J. Mod. Phys. B **20**, 1015 (2006).

[81] N. A. Sinitsyn, E. M. Hankiewicz, W. Teizer, and J. Sinova, Phys. Rev. B **70**, 081312(R) (2004).

[82] R. de Sousa and S. Das Sarma, Phys. Rev. B **68**, 155330 (2003).

[83] J. B. Miller, D. M. Zumbúhl, C. M. Marcus, Y. B. Lyanda-Geller, D. Goldhaber-Gordon, K. Campman, and A. C. Gossard, Phys. Rev. Lett. **90**, 076807 (2003).

[84] S. D. Ganichev, V. V. Bel'kov, L. E. Golub, E. L. Ivchenko, P. Schneider, S. Giglberger, J. Eroms, J. De Boeck, G. Borghs, W. Wegscheider, D. Weiss, and W. Prettl, Phys. Rev. Lett. **92**, 256601 (2004).

[85] B. A. Bernevig, J. Orenstein, and S. C. Zhang, Phys. Rev. Lett **97**, 236601 (2006).

[86] S. Becker, M. Liebmann, T. Mashoff, M. Pratzer, and M. Morgenstern, Phys. Rev. B **81**, 155308 (2010).

[87] J. H. Bardarson, *Effect of Spin-Orbit Coupling in Quantum Transport* (PhD thesis, Leiden University, 2008).

[88] J. E. Moore, Nature **464**, 194 (2010).

[89] A. P. Schnyder, S. Ryu, A. Furusaki, and A. W. W. Ludwig, Phys. Rev. B **78**, 195125 (2008).

[90] Y. Ando, J. Phys. Soc. Japan **82**, 102001 (2013).

[91] V. L. Grigoryan, A. Matos Abiague, and S. M. Badalyan, Phys. Rev. B **80**, 165320 (2009).

[92] V. L. Grigoryan, Journal of Contemporary Physics (Armenian Academy of Sciences) **45**, 172 (2010).

[93] A. Reynoso, G. Usaj, M. J. Sánchez, and C. A. Balseiro, Phys. Rev. B **70**, 235344 (2004).

[94] Z. Wang, W. Zhang and, P. Zhang, Phys. Rev. B **79**, 235327 (2009).

[95] M. G. Pala, M. Governale, U. Zülicke, and G. Iannaccone, Phys. Rev. B **71**, 115306 (2005).

[96] S. Debald and B. Kramer, Phys. Rev. B **71**, 115322 (2005).

[97] M. S. Kushwaha, Phys. Rev. B **76**, 245315 (2007).

[98] S. Debald and C. Emary, Phys. Rev. Lett. **94**, 226803 (2005).

[99] M. Kushwaha, J. Appl. Phys. **104**, 083714 (2008).

[100] P. Pietiläinen and T. Chakraborty, Phys. Rev. B **73**, 155315 (2006).

[101] S. Avetisyan, P. Pietiläinen, and T. Chakraborty, Phys. Rev. B **85**, 153301 (2012).

[102] S. V. Iordansky, Solid State Commun. **43**, 1 (1982).

[103] R. F. Kazarinov and S. Luryi, Phys. Rev. B **25**, 7626 (1982).

[104] S. A. Trugman, Phys. Rev. B **27**, 7539 (1983).

[105] *The Quantum Hall Effect*, edited by R. E. Prange and S. M. Girvin (Springer, New York, 1987).

[106] G. Vignale, J. Supercond. Nov. Magn **23**, 3 (2010).

[107] J. Sinova, D. Culcer, Q. Niu, N. A. Sinitsyn, T. Jungwirth, and A. H. MacDonald, Phys. Rev. Lett. **92**, 126603 (2004).

[108] O. Chalaev and D. Loss, Phys. Rev B **71**, 245318 (2005).

[109] J. Shi, P. Zhang, D. Xiao, and Q. Niu, Phys. Rev. Lett. **96**, 076604 (2006).

[110] Q. F. Sun and X. C. Xie, Phys. Rev. B **72**, 256602 (2005).

[111] K. Ando and E. Saitoh, Nat. Comm. **3**, 629 (2011).

[112] S. Q. Shen, M. Ma, X. C. Xie, and F. C. Zhang, Phys. Rev. Lett. **92**, 256603 (2004).

[113] S. Q. Shen, Y. J. Bao, M. Ma, X. C. Xie, and F. C. Zhang, Phys. Rev. B **71**, 155316 (2005).

[114] F. C. Zhang and S. Q. Shen, Int. J. Mod. Phys. B **22**, 94 (2008).

[115] Y. J. Bao and S. Q. Shen, Phys. Rev. B **76**, 045313 (2007).

[116] R. Kubo, J. Phys. Soc. Japan 12, 570 (1957).

[117] P. Walters, *An Introduction to Ergodic Theory* (Springer, New York, 1982).

[118] H. L. Stormer, Rev. Mod. Phys. **71**, (1999).

[119] J. Xia, V. Cvicek, J. P. Eisenstein, L. N. Pfeiffer, and K. W. West, Phys. Rev. Lett. **105**, 176807 (2010).

[120] V. Y. Aristov, G. LeLay, P. Soukiassian, K. Hricovini, J. E. Bonnet, J. Osvald, and O. Olsson, Europhys. Lett. **26**, 359 (1994).

[121] D. Hernangómez-Pérez, J. Ulrich, S. Florens, and T. Champel, Phys. Rev. B **88**, 245433 (2013).

[122] T. Champel and S. Florens, Phys. Rev. B **82**, 045421 (2010).

[123] D. B. Chklovskii, B. I. Shklovskii, and L. I. Glazman, Phys. Rev. B **46**, 4026 (1992).

[124] N. R. Cooper and J. T. Chalker, Phys. Rev. B **48**, 4530 (1993).

[125] T. H. Stoof and G. E. W. Bauer, Phys. Rev. B **52**, 12143 (1995).

[126] I. A. Larkin and L. S. Levitov, Physica E **6**, 91 (2000).

[127] A. Manolescu and R. R. Gerhardts, Phys. Rev. B **56**, 9707 (1997).

[128] G. H. Chen and M. E. Raikh, Phys. Rev. B **60**, 4826 (1999).

[129] B. Piot, *Levée de dégénérescence de spin dans le régime Hall quantique* (PhD thesis, Université Joseph Fourier, Grenoble, France, 2006).

[130] T. Champel, S. Florens, and L. Canet, Phys. Rev. B **78**, 125302 (2008).

[131] T. Champel, S. Florens, and M. E. Raikh, Phys. Rev. B **83**, 125321 (2011).

[132] T. Champel and S. Florens, Phys. Rev. B **80**, 125322 (2009).

[133] J. Larson, *Extended Jaynes-Cummings models in cavity quantum electrodynamics* (PhD thesis, The Royal Institute of Technology, Stockholm, Sweden, 2005).

[134] X. F. Wang and P. Vasilopoulos, Phys. Rev. B **67**, 085313 (2003).

[135] X. F. Wang and P. Vasilopoulos, Phys. Rev. B **75**, 075331 (2007).

[136] Z. Li and J. P. Carbotte, Phys. Rev. B **89**, 085413 (2014).

[137] D. K. K. Lee, Phys. Rev. B **50**, 7743 (1994).

[138] C. B. Hanna, D. P. Arovas, K. Mullen, and S. M. Girvin, Phys. Rev. B **52**, 5221 (1995).

[139] Y. Avishai and Y. Meir, Phys. Rev. Lett. **89**, 076602 (2002).

[140] Y. J. Bao, H. B. Zhuang, S. Q. Shen, and F. C. Zhang, Phys. Rev. B **72**, 245323 (2005).

[141] Y. K. Kato, R. C. Myers, A. C. Gossard, and D. D. Awschalom, Science **306**, 1910 (2004).

[142] D. Hernangómez-Pérez, S. Florens, and T. Champel, Phys. Rev. B **89**, 155314 (2014).

[143] A. C. Hirshfeld and P. Henselder, Am. J. Phys. **70**, 537 (2001).

[144] K. Lier and R. R. Gerhardts, Phys. Rev. B **50**, 7757 (1994).

[145] A. Siddiki and R. R. Gerhardts, Phys. Rev. B **70**, 195335 (2004).

[146] J. Fröhlich and U. M. Studer, Rev. Mod. Phys. **65**, t733 (1993).

[147] I. V. Tokatly, Phys. Rev. Lett. **101**, 106601 (2008).

[148] R. Raimondi, P. Schwab, C. Gorini, and G. Vignale, Ann. Phys. **524**, 153 (2012).

[149] M. R. Geller and G. Vignale, Phys. Rev. B **50**, 11714 (1994).

[150] E. J. König, P. M. Ostrovsky, I. V. Protopopov, I. V. Gornyi, I. S. Burmistrov, and A. D. Mirlin, arXiv:1406.5008 (2014).

[151] V. P. Gusynin and S. G. Sharapov, Phys. Rev. Lett. **95**, 146801 (2005).

[152] L. Fu and C. L. Kane, Phys. Rev. B **76**, 045302 (2007).

[153] A. A. Zyuzin and A. A. Burkov, Phys. Rev. B **83**, 195413 (2011).

[154] S. H. Simon and B. I. Halperin, Phys. Rev. Lett. **73**, 3278 (1994).

[155] M. Flöser, S. Florens, and T. Champel, Phys. Rev. Lett. **107**, 176806 (2011).

[156] M. Flöser, S. Florens, and T. Champel, Int. J. Mod. Phys: Conf. Series **11**, 49 (2012).

[157] E. I. Rashba, Phys. Rev. B **68**, 241315(R) (2003).

[158] R. J. Glauber, Phys. Rev. **131**, 2766 (1963).

[159] R. Kubo, J. Phys. Soc. Japan **12**, 570 (1957).

[160] R. B. Laughlin, Phys. Rev. Lett. **50**, 1395 (1983).

[161] H. L. Stormer, D. C. Tsui, and A. C. Gossard, Rev. Mod. Phys. **71**, 298 (1999).

[162] R. Willett, J. P. Eisenstein, H. L. Stormer, D. C. Tsui, A. C. Gossard, and J. H. English, Phys. Rev. Lett. **59**, 1776 (1987).

[163] E. Wigner, Phys. Rev. **102**, 46 (1934).

[164] M. I. Dyakonov in *Recent Trends in the Theory of Physical Phenomena in High Magnetic Fields*, Proceedings of the NATO ARW (Kluwer Academic Publishers, 2003).

[165] W. Pan, H. L. Stormer, D. C. Tsui, L. N. Pfeiffer, K.W. Baldwin, and K.W. West, Phys. Rev. Lett, **88**, 176802 (2002).

[166] R. B. Laughlin, Rev. Mod. Phys. **71**, 863 (1999).

[167] X. G. Wen, Adv. Phys. **44**, 405 (1995).

[168] M. O. Goerbig, *Étude théorique des phases de densité inhomogène dans les systèmes à effet Hall quantique* (PhD thesis, Université Paris Sud, Paris, 2004).

[169] F. D. M. Haldane, Phys. Rev. Lett. **51**, 605 (1983).

[170] F. D. M. Haldane and E. H. Rezayi, Phys. Rev. Lett. **54**, 237 (1985).

[171] D. Yoshioka, B.I. Halperin, and P.A. Lee, Phys. Rev. Lett. **50** 1219, (1983).

[172] K. Výborný, Ann. Phys. **16**, 87 (2007).

[173] N. Shibata and D. Yoshioka, Phys. Rev. Lett. **86**, 5755 (2001).

[174] R. H. Morf, N. d'Ambrumenil, and S. Das Sarma, Phys, Rev. B **66**, 075408 (2002).

[175] H. Li and F. D. M. Haldane, Phys. Rev. Lett. **101**, 010504 (2008).

[176] J. Dubail, N. Read, and E. H. Rezayi, Phys. Rev. B **85**, 115321 (2012).

[177] M. Hermanns, A. Chandran, N. Regnault, and B. Andrei Bernevig, Phys. Rev. B **84**, 121309(R) (2011).

[178] S. M. Girvin and T. Jach, Phys. Rev. B **29** 5617 (1984).

[179] B. I. Halperin, Phys. Rev. Lett. **52**, 1583 (1984).

[180] D. Arovas, J. R. Schrieffer, and F. Wilczek, Phys. Rev. Lett. **53**, 722 (1984).

[181] F. Wilczek, *Fractional Statistics and Anyon Superconductivity* (World Scientific, Singapore, 1990).

[182] C. Nayak, S. H. Simon, A. Stern, M. Freedman, and S. Das Sarma, Rev. Mod. Phys. **80**, 1083 (2008).

[183] J. K. Jain, Phys. Rev. Lett. **63**, 199 (1989).

[184] J. K. Jain, Phys. Rev. B **41**, 7653 (1990).

[185] J. K. Jain, Phys. Today **53** (4), 39 (2000).

[186] D. R. Leadley, R. J. Nicholas, C. T. Foxon, and J. J. Harris, Phys. Rev. Lett. **72**, 1906 (1994).

[187] X. G. Wen, Phys. Rev. B **41**, 12838 (1990).

[188] X. G. Wen, Int. J. Mod. Phys. **B6**, 1711 (1992).

[189] F. M. D. Haldane, J. Phys. C: Solid State Phys., **14**, 2585 (1981).

[190] A. M. Chang, Rev. Mod. Phys. **75**, 1449 (2003).

[191] A. Lopez and E. Fradkin, Phys. Rev. B **44**, 5246 (1991).

[192] S. C. Zhang, H. T. Hansson, and S. Kivelson, Phys. Rev. Lett. **62**, 82 (1989).

[193] S. C. Zhang, Int. J. Mod. Phys. B **6**, 25 (1992).

[194] S. H. Simon in *Composite Fermions*, edited by O. Heinonen (World Scientific, Singapore, 1998).

[195] J. J. Quinn and A. Wójs, J. Phys.: Cond. Matt. **12**, R265 (2000).

[196] B. I. Halperin, P.A. Lee and N. Read, Phys. Rev. B **47**, 7312 (1993).

[197] S. M. Girvin, *The Quantum Hall Effect: Novel Excitations and Broken Symmetries* edited by A. Comtet, T. Jolicoeur, S. Ouvry, and F. David, Les Houches Session LXIX (Springer, France, 1999).

[198] R. Shankar, Ann. Phys. **523**, 751 (2011).

[199] G. Murthy, Phys. Rev. B **64**, 195310 (2001).

[200] G. Murthy and R. Shankar, Phys. Rev. B **59**, 12260 (1999).

[201] R. Shankar, Phys. Rev. B **63**, 085322 (2001).

[202] S. M. Girvin, A. H. MacDonald, and P. Platzman, Phys. Rev. B **33**, 2481 (1986).

[203] I. I. Kogan, Int. J. Mod. Phys. A **9**, 3887 (1994).

[204] Gregory L. Naber, *The Geometry of Minkowski Spacetime: An Introduction to the Mathematics of the Special Theory of Relativity* (Springer, 2nd edition, 2012).

[205] F. Catoni, D. Boccaletti, R. Cannata, V. Catoni, E. Nichelatti and P. Zampetti, *The Mathematics of Minkowski Space-Time: With an Introduction to Commutative Hypercomplex Numbers* (Birkhäuser Verlag, Berlin, 2008).

[206] C. M. Davenport, *A Commutative Hypercomplex Calculus with Applications to Special Relativity* (privately published, Tennessee, 1991).

[207] R. G. Lavoie, L. Marchildon and D. Rochon, Adv. Appl. Clifford Algebras **21**, 561 (2011).

[208] A. V. Smirnov in *Space-Time Structure. Algebra and Geometry*, ed. by D. G. Pavlov, Gh. Atanasiu and V. Balan (Lilia-Print, Moscow, 2007).

[209] R. Séroul, *Programming for Mathematicians* (Springer-Verlag, Berlin, 2000).

[210] S. M. Girvin, *Introduction to the Fractional Quantum Hall Effect*, Séminaire Poincaré, 53 (2004).

[211] R. Mosseri and R. Dandoloff, J. Phys. A: Math. Gen. **34**, 10243 (2001).

[212] D. W. Lyons, Mathematics Magazine **76**, 87 (2003).

[213] S. Adler, *Quaternionic Quantum Mechanics and Quantum Fields* (Oxford University Press, New York, 1995).

[214] M. A. Nielsen and I. L. Chuang, *Quantum Computation and Quantum Information* (Cambridge University Press, Cambridge, 2000).

[215] G. Murthy and R. Shankar, Rev. Mod. Phys. **75**, 1101 (2003).

[216] M. W. Ortalano, S. He, and S. Das Sarma, Phys. Rev. B **55**, 7702 (1997).

[217] G. T. Horowitz, Class. Quantum Grav. **8**, 587 (1991).

[218] A. P. Balachandran, G. Bimonte, G. Marmo, and A. Simoni, Nucl. Phys. B **446**, 299 (1995).

[219] A. D. Shapere, F. Wilczek, and Z. Xiong, arXiv:1210.3545 (2012).

[220] J. C. Baez and J. Dolan, J. Math. Phys. **36**, 6073 (1995).

[221] J. Lurie, in *Current Developments in Mathematics*, Vol **2008**, 129 (Int. Press, Somerville, MA, 2009). (2009).

[222] F. D. M. Haldane, Phys. Rev. Lett. **107**, 116801 (2011).

[223] B. Yang, Z. Papić, E. H. Rezayi, R. N. Bhatt, and F. D. M. Haldane, Phys. Rev. B **85**, 165318 (2012).

[224] X. G. Wu and J. K. Jain, Phys. Rev. B **51**, 1752 (1995).

[225] D. Rochon and S. Tremblay, Adv. Appl. Clifford Algebras **16**, 135 (2006).

[226] S. V. Duzhin and B. D. Chebotarevskii, *Transformation Groups for Beginners* (American Mathematical Society, United States of America, 2004).

[227] F. Catoni and P. Zampetti, Adv. Appl. Clifford Algebras **22**, 23 (2012).

[228] R. P. Boas and R. C. Buck, *Polynomial Expansions of Analytic Functions* (Springer-Verlag, Berlin, 1958).

[229] R. L. Graham, D. E. Knuth, and O. Patashnik, *Concrete Mathematics: A Foundation for Computer Science* (Addison-Wesley Professional, 1994).

[230] S. Roman, *The Umbral Calculus* (Academic Press, London, 1984).

[231] P. Schwab and M. Dzierzawa, Phys. Rev. B **85**, 155403 (2012).

[232] L. Fu, Phys. Rev. Lett. **103**, 266801 (2009).

[233] P. K. Pyatkovskiy, Phys. Rev. B **88**, 205417 (2013).

[234] P. Henrici, *Applied and Computational Complex Analysis* (Wiley, United States, 1986).

[235] S. Hassani, *Mathematical Physics: a modern introduction to its foundations* (Springer, New York, 1999).

[236] I. S. Gradshteyn and I. M. Ryzhik, *Table of Integrals, Series and Products* (Elsevier, USA, 2007).

[237] D. S. Dummit and R. M. Foote, *Abstract Algebra* (Wiley, United States, 2004).

[238] T. W. Hungerford, *Algebra* (Springer, New York, 1980).

[239] P. Szekeres, *A Course in Modern Mathematical Physics: Groups, Hilbert Space and Differential Geometry* (Cambridge University Press, Cambridge, 2004).

[240] I. L. Kantor and A. S. Solodovnikov, *Hypercomplex Numbers: an Elementary Introduction to Algebras* (Springer, New York, 1989)

[241] D. Alfsmann, in Proceedings of European Signal Processing Conference, Florence, Italy, 2006.

[242] T. Y. Lam, *A First Course in Noncommutative Rings* (Springer, New York, 2001).

[243] W. Appel, *Mathématiques pour la physique et les physiciens* (H&K Éditions, Paris, 2008).

List of Publications

Part of the work presented in this thesis has been published in the following articles:

- D. Hernangómez Pérez, J. Ulrich, S. Florens, and T. Champel, *Spectral properties and local density of states of disordered quantum Hall systems with Rashba spin-orbit coupling*, Phys. Rev. B **88**, 245433 (2013).

- D. Hernangómez Pérez, S. Florens, and T. Champel, *Signatures of Rashba spin-orbit interaction in charge and spin properties of quantum Hall systems*, Phys. Rev. B **89**, 155314 (2014).

Remerciements

Il est habituel à ce stade d'un projet comme une thèse de doctorat de jeter un coup d'œil en arrière pour réfléchir sur son parcours et les personnes spéciales, auxquelles on est particulièrement reconnaissant, qui ont affecté à sa trajectoire.

Je tourne d'abord avec gratitude vers mon directeur de thèse, Thierry Champel, qui m'a guidé avec patience et disponibilité pendant mon immersion dans les profondeurs des eaux inconnues et turbulentes de la recherche, tout en me laissant la liberté nécessaire (dont tout bon chercheur a besoin) pour développer mon indépendance et mon esprit scientifique. Je profite de ces lignes pour lui remercier de m'avoir initié au monde de la physique de l'effet Hall quantique et pour avoir su me transmettre fructueusement son intégrité, son envie de connaître et son savoir faire.

Je n'oublie non plus mon co-encadrant et collaborateur Serge Florens avec qui nous avons eu de très jolies et intéressantes discussions ces trois dernières années, soit au bureau ou soit dans la bibliothèque du laboratoire. Je lui suis très reconnaissant pour sa gentillesse dans un monde rude et la pertinence de tous ses commentaires conséquence de son grand talent scientifique. Pour tout ça et les moments partagés avec Thierry et moi, je lui remercie chaleureusement.

Ensuite, je voudrais exprimer ma gratitude à tous les membres du jury qui m'ont fait l'honneur de participer à ma soutenance de thèse : Mark Goerbig et Stéphane Nonnenmacher pour avoir accepté la tâche, pas toujours facile, de juger mon travail de thèse. J'ai apprécié beaucoup leurs remarques et suggestions, qui ont contribué largement á améliorer la qualité de ce manuscrit, et je leur en remercie. Je suis également très reconnaissant à Benoît Douçot pour la pertinence de ses observations sur la partie fractionnaire, Markus Morgenstern for all the (past and hopefully future) discussions about spin-orbit physics et Julia Meyer pour avoir accepté le rôle de présider mon jury. Je remercie énormément Sergey Skipetrov pour avoir accédé à faire partie de mon jury dans un moment de crise, même si le sujet n'était pas trop parmi ses intêrets scientifiques principaux.

Ce travail de thèse à été fait entre 2011 et 2014 au sein du Laboratoire de Physique et Modélisation des Milieux Condensés (LPMMC). J'aimerais souligner que ce projet de recherche à pu être mené à bon port grâce au soutien économique de la Fondation Nanosciences à Grenoble. Un remerciement particulier doit être adressé à Stèphanie Monfront pour l'envoi de chocolats décisifs pour la bonne rédaction de ce manuscrit.

J'aimerais aussi exprimer ma gratitude ici aux membres du LPMMC avec qui j'ai partagé mon quotidien pendant les trois dernières années. Ce laboratoire m'a proportionné

un cadre de travail parfait pour le bon déroulement de ma thèse de doctorat. En particulier, un grand merci à Léonie Canet, Nicolas Rougerie, Vincent Rossetto et Robert Whitney pour leur disponibilité, les divers conseils et toutes les discussions que nous avons eu. Je ne veux non plus omettre les doctorants et postdoctorants que j'ai pu croiser pendant ma période au laboratoire. Manutea Candé, mon persistant collègue de bureau, je te remercie pour ta bonne humeur quotidienne. Florian Cartarius, Marco Cominotti, Manuel Donaire, Sanjoy Datta, Li Jing Jin, and Gianluca Rastelli thanks for the positive atmosphere and the real-world conversations at lunchtime in the canteen H2 and elsewhere. Angelo Di Marco, grazie per un divertente shopping con te a Dresde. Eiji Kawasaki merci pour nos expériences à table, en face d'une assiette d'alléchants ravioles du Dauphiné. Merci pour tout, mon pote ! Bonne courage avec ta thèse maintenant !

Me gustaría también reconocer y dar las gracias en esta página privilegiada a todas las personas que me han influido especialmente, tanto de manera profesional como personal, en estos últimos años. Concretamente, y sólo por citar a las principales, Carmela Calés Bourdet, quien me mostró que el camino que yo debía seguir estaba en el mundo de la Física; Juan-Diego Ania Castañón, por su amistad, por ser un ejemplo como persona para mí y las repetidas oportunidades que me ha proporcionado para iniciarme en el mundo de la investigación; Pedro Corredera Guillén, por ser capaz de hacerme entrar en un laboratorio experimental y con quien es siempre un placer conversar de todo y nada; Héctor Menéndez Benito, por ser un amigo incondicional a pesar de la distancia. For their kindness and many enjoyable discussions I am also deeply indebted to many colleagues: Elio J. König, Fabien Lafont, Rolf Reinthaler, Björn Trauzettel, Evgeny Sherman and Jascha Ulrich. A special note of gratitude goes to Soumya Bera for being a friend (take care now in Germany!). I humbly apologize to everyone that I have unfortunately missed in these acknowledgements.

Asimismo, quiero expresar mi más sincero agradecimiento a aquéllos más cercanos sin cuya contribución o influencia, directa e indirecta, esta tesis nunca hubiese sido posible. Junto a mis hermanos, Olga, Nieves y Diego, mis padres son para mí uno de los baluartes incondicionales de mi vida. Sois los mejores padres que yo podría desear, una fuente continua de cariño y apoyo y nunca podré agradeceros lo suficiente todo lo que hacéis por mí. Sé que estáis tremendamente orgullosos de vuestro primer hijo doctor [a pesar de que tal vez no fuera el tipo de doctor que una vez pensaste que yo sería, Mamá :D]. Finalmente, quiero dedicar este trabajo a mi compañera de la vida, María, mi Sambo Sol de color granate. Eres una constante fuente de felicidad para mí, dándome fuerzas cuando me faltan, estando a mi lado y cuidando de mí siempre. Me siento enormemente afortunado de haberte encontrado en este mundo, mi alma gemela, y es imposible que tenga espacio suficiente aquí para darte las gracias por todo: simplemente gracias por ser tú. Mi Sol, te rencontrer est la plus belle chose qui m'est jamais arrivée, je suis très heureux et je t'aime du plus profond de mon cœur.

Ora tutto é a posto.

Grenoble, Novembre 2014

Abstract

The quantum Hall effect, appearing in disordered two-dimensional electron gases under strong perpendicular magnetic fields and low temperatures, has been a subject of intense research during the last thirty years due to its very spectacular macroscopic quantum transport properties. In this thesis, we expand the theoretical horizon by analytically considering the effects of spin-orbit coupling and strong electron-electron interaction in these systems.

In the first part of the manuscript, we examine the simultaneous effect of Rashba spin-orbit and Zeeman interaction in the integer quantum Hall regime. Under these conditions, we extend a coherent-state vortex Green's function formalism to take into account the coupling between orbital and spin degrees of freedom within the electronic drift states. As a first application of this framework, we analytically compute controlled microscopic nonperturbative quantum functionals, such as the energy spectrum and the local density of states, in arbitrary locally flat electrostatic potential landscapes, which are then analyzed in detail in different temperature regimes and compared to scanning tunnelling experimental data. As a second application, we thoroughly study local equilibrium charge and spin transport properties and derive analytical useful formulas which incorporate the mixed non-relativistic and relativistic character of Rashba-coupled electron gases.

In the second part of this thesis, we deal with the problem of analytically incorporating strong electron-electron interactions in the fractional quantum Hall regime. To this purpose, we consider a generalized two-body problem where both disorder and correlations are combined and introduce a new vortex coherent-state representation of the two-body states that naturally include long-range correlations between the electrons. The novelty of this theory is that correlations are topologically built in through the non-Euclidean metric of the Hilbert space. Next, we show that this kind of vortex states form a basis of an enlarged Hilbert space and derive the equation of motion for the Green's function in this representation. Finally, we check the consistency of our approach for any Landau level of the pair and discuss the necessity of going beyond the semiclassical (infinite magnetic field) approximation to obtain energy gaps within each energy level.

Keywords: Quantum Hall Effects, Vortex, Green's Functions, Rashba Spin-Orbit Coupling, Electron-Electron Interaction, Bicomplex Numbers

Résumé

L'effet Hall quantique, qui apparaît dans les gaz d'électrons bidimensionnels soumis à un fort champ magnétique perpendiculaire et à basses températures, a été un sujet de recherche intense pendant les derniers trente ans, en particulier, à cause des manifestations spectaculaires de la mécanique quantique dans les propriétés de transport à l'échelle macroscopique. Dans cette thèse, on étend l'horizon de la recherche au niveau théorique sur ce sujet en considérant les effets du couplage spin-orbite et l'interaction électron-électron de façon analytique dans ce régime.

Dans la première partie de ce manuscrit, on considère l'effet simultané du couplage spin-orbite de type Rashba et l'interaction Zeeman dans le régime de l'effet Hall quantique entier. Pour cela, on étend un formalisme de fonctions de Green basé sur des états de vortex cohérents avec l'objectif d'inclure le couplage entre les degrés de liberté orbitaux et de spin dans les états de dérive électroniques. Puis, comme première application, on montre comment obtenir analytiquement, nonperturbativement et de manière contrôlée des fonctionnelles quantiques (spectre et densité d'états locale) pour des potentiels électrostatiques arbitraires et localement plats. Les fonctionnelles sont ensuite analysées dans différents régimes de températures et comparées aux données expérimentales obtenues à partir des sondes de spectroscopie locales. Comme seconde mise en pratique du formalisme, on étudie en profondeur les propriétés de transport de charge et de spin dans un régime hydrodynamique d'équilibre local (ou quasi-équilibre) et dérive des expressions analytiques qui incorporent les caractères non-relativiste et relativiste des gaz d'électrons avec couplage spin-orbite de type Rashba.

Dans la deuxième partie de cette thèse, on s'occupe du problème de traiter analytiquement les fortes interactions électron-électron dans le régime de l'effet Hall quantique fractionnaire. A cette fin, on étudie un problème à deux corps généralisé avec du désordre et des corrélations électroniques, en utilisant une nouvelle représentation d'états de vortex cohérents. Des corrélations à longue portée entre les particules sont incorporées de manière topologique à travers la présence d'une métrique non-Euclidienne. Subséquemment, on montre que ces états de vortex forment bien une base d'un espace de Hilbert élargi, puis on dérive l'équation du mouvement pour la fonction de Green. Enfin, on vérifie la consistance de notre théorie pour tout niveau de Landau de paire et on discute la nécessité d'aller au-delà de la limite semiclassique (à champ magnétique infinie) pour obtenir des gaps dans chaque niveau de énergie.

Mots clés : Effet(s) Hall, vortex, fonctions de Green, couplage spin-orbite Rashba, interaction électron-électron, nombres bicomplexes